جامعة سيدي محمد بن عبد الله بفاس
UNIVERSITÉ SIDI MOHAMED BEN ABDELLAH DE FES
كلية العلوم والتقنيات فاس
FACULTÉ DES SCIENCES ET TECHNIQUES DE FÈS

N° d'ordre : 60/2023

Centre des Etudes Doctorales : Sciences et Techniques et Sciences Médicales
Formation Doctorale : Sciences de l'Ingénieur, Sciences Physiques, Mathématiques et Informatique
Discipline : Génie électrique
Spécialité* : Mécatronique et Systèmes Embarqués
Laboratoire : Systèmes Intelligents, Géoressources et Energies Renouvelables

Thèse pour l'obtention de DOCTORAT

Development of new advanced and robust control laws for quadrotor drones: implementation and experimental validation

Préparée par : Mr Hamid HASSANI

Soutenue le 22/07/2023 devant le jury :

Nom et Prénom	Grade	Etablissement	Qualité
Mohammed JORIO	PES	Faculté des Sciences et Techniques de Fès	Président
Adil BROURI	PES	Ecole Nationale Supérieure d'Arts et Métiers de Meknès	Rapporteur
Ismail BOUMHIDI	PES	Faculté des Sciences Dhar El Mehraz de Fès	Rapporteur
Fatima ERRAHIMI	PES	Faculté des Sciences et Techniques de Fès	Rapporteur
Fouad BELMAJDOUB	PES	Faculté des Sciences et Techniques de Fès	Examinateur
Rachid EL BACHTIRI	PES	Ecole Supérieure de Technologie de Fès	Examinateur
Hassan EL MOUSSAOUI	PES	Faculté des Sciences et Techniques de Fès	Examinateur
Anass MANSOURI	PES	Ecole Nationale des Sciences Appliquées de Fès	Directeur de thèse
ALI AHAITOUF	PES	Faculté des Sciences et Techniques de Fès	Co-Directeur de Thèse

Acknowledgements

I would like to warmly thank **Pr. Anass MANSOURI**, Professor at ENSA FEZ, and **Pr. Ali AHAITOUF**, Professor at FST FEZ and director of SIGER laboratory, for granting me the chance to pursue my PhD under their supervision on a very interesting topic. Their wise advice, encouragement, support, and attention to small details have been an invaluable inspiration to me. I would particularly like to thank them for their patience and the time they spent to carefully reading and correcting all my articles.

Sincere thanks to all my professors at the faculty of science and technology in BENI MELLAL and the faculty of science and technology in FEZ for the great knowledge they have imparted to me throughout my way. A big thanks, especially to **Pr. Abdelali ELBDOURI**, for his unreserved help during the preparation of this thesis.

Many thanks to **Pr. Mohammed JORIO**, Professor at FST FEZ, for accepting to be the president of the jury of my thesis, as well as for his advice during the development of this PhD.

I express all my gratitude to **Pr. Adil BROURI**, Professor at ENSAM MEKNES, **Pr. Ismail BOUMHIDI**, Professor at FSDM FEZ, and **Pr. Fatima ERRAHIMI**, Professor at FST FEZ, for accepting to be referees of my work, and for their constructive remarks. I would also like to express my thanks to **Pr. Fouad BELMAJDOUB**, Professor at FST FEZ, **Pr. Rachid EL BACHTIRI**, Professor at EST FEZ, and **Pr. Hassan EL MOUSSAOUI**, Professor at FST FEZ, for accepting to be part of the jury of my thesis and for giving very insightful comments.

I would like to extend my gratitude to all of my colleagues at the SIGER Laboratory for the precious memories. I would like to give special thanks to a group of dear friends, Lhoussain, Latifa, Mohssin, Youssef, Abderrahim, Abdelaziz, Yahia, hicham and Abdelilah, who have added immense value to my life outside of my studies.

I will be eternally thankful to my family, to my parents, brothers and sister for the continuous encouragement and confidence in me through my journey. Without their unlimited sacrifices, it would have been impossible to achieve where I am today. Thank you.

I am grateful to all those who have had faith in me and given me endless support throughout my journey in this life.

Abstract

Over the past years, quadrotors for civilian and military usage have grown in popularity. Ensuring an accurate trajectory tracking for these aircraft is still a challenging task and a main concern of multi-modern researches. The work of this thesis is within this framework and deals with the development of advanced and robust control strategies for quadrotor unmanned aerial vehicles (UAVs) by addressing the challenges related to modeling uncertainties, unmodeled dynamics, and external disturbances. In more details, the main objectives are to study, develop, and experimentally implement several control algorithms for precise desired trajectory tracking. The control system must be able to drive the vehicle towards a variety of predefined trajectories, to deal with the severity of internal and/or external aerodynamic disturbances, and to reduce the influence of uncertainties on the inertial parameters of the quadrotor vehicle.

In order to achieve these goals, robust control algorithms based on finite-time sliding mode theory are developed. First, a robust hybrid control strategy is used to steer the quadrotor behavior. The control system combines the Backstepping Sliding Mode Control (BSMC) with the Nonsingular Fast Terminal Sliding Mode Control (NFTSMC) to perform enhanced tracking under the influence of unknown disturbances and modeling inaccuracies. An adaptive methodology is introduced to improve the robustness of the adopted control technique. Then, a new Supertwisting Nonsingular Terminal Sliding Mode Control (STNTSMC) is developed to ensure that the tracking errors quickly disappear in a very short time. A Disturbance Observer (DO) is incorporated into the control system to estimate the unknown external perturbations and to enhance the system's robustness. The Lyapunov theory is used to verify the closed-loop stability of the synthesized controllers.

The proposed control strategies are tested and evaluated using the Model-Based Design approach (MBD) to assess the achieved performances. Simulations, Processor-In-the-Loop (PIL) tests, and experimental validation on a home-made quadrotor prototype are performed to highlight the efficiency of the developed controllers.

Our results show a net improvement in the motion control and stability of a single quadrotor, paving the way for the next step, setting up networks of communicating drones.

Keywords: Drones; UAVs; Quadrotors; Supertwisting; Hybrid control; Adaptation methodology; Supertwisting nonsingular terminal sliding mode control; Unmodeled dynamics; Unknown disturbances; Uncertainties; Disturbance Observer.

Résumé

Au cours des dernières années, les quadrirotors à usage civil et militaire ont gagné en popularité. Assurer un suivi de trajectoire précis pour ces aéronefs reste une des tâches les plus difficiles. C'est dans ce cadre que se place notre travail et pour atteindre cet objectif, cette thèse porte sur le développement de stratégies de contrôle robustes pour les véhicules aériens sans pilote quadrirotors en abordant les défis liés aux incertitudes de modélisation, aux dynamiques non modélisées et aux perturbations externes. D'une manière plus précise, les principaux objectifs sont d'étudier, de développer et d'implémenter sur une plateforme expérimentale, développée localement, plusieurs algorithmes de contrôle pour un suivi précis des trajectoires souhaitées. Le système de contrôle doit être capable de piloter automatiquement le véhicule le long d'une variété de trajectoires prédéfinies, de faire face à la sévérité des perturbations aérodynamiques internes et/ou externes, et de réduire l'influence des incertitudes sur les paramètres inertiels du véhicule quadrirotor.

Afin d'atteindre les performances souhaitées, des algorithmes de contrôle robustes basés sur la théorie des modes glissants en temps fini ont été développés. Tout d'abord, une stratégie de contrôle hybride robuste est utilisée pour piloter les mouvements du quadrirotor. Cette stratégie regroupe le contrôle backstepping de mode glissant et le contrôle de mode glissant terminal rapide non singulier pour améliorer le suivi des trajectoires sous l'influence de perturbations inconnues et d'incertitude sur le modèle. Une méthodologie d'adaptation est introduite pour améliorer la robustesse de la stratégie de contrôle développée. Ensuite, une nouvelle commande supertwisting de mode glissant terminal non singulier est développée afin de garantir que les erreurs de suivi disparaissent rapidement. Un observateur de perturbations est incorporé au système de contrôle pour estimer les perturbations externes inconnues et renforcer la robustesse du système. La théorie de Lyapunov est utilisée pour vérifier la stabilité en boucle fermée des contrôleurs synthétisés.

Les stratégies de contrôle proposées sont testées et évaluées selon l'approche "Model-Based Design" afin d'évaluer les performances obtenues. Des tests de simulation, des tests utilisant des processeurs dans la boucle et des tests expérimentaux sur un prototype de quadrirotor développé localement sont réalisés pour mettre en évidence l'efficacité des contrôleurs développés.

Nos résultats ont mis en évidence des hautes performances dans le contrôle et la stabilité des drones, ouvrant la voie vers l'étape suivante, la mise en place de réseaux de drones communicants.

Mots-clés : Drones, Quadrirotors ; Supertwisting ; Contrôle hybride ; Méthodologie d'adaptation ; Commande de mode glissant terminal non singulier supertwisting ; Dynamiques non modélisées ; Perturbations inconnues ; Incertitudes ; Observateur de perturbations.

Table of Contents

Acknowledgements **I**

Abstract **I**

Résumé **II**

List of Figures **V**

List of Tables **VIII**

Symbols and abbreviations **IX**

Introduction 1

1 Quadrotor unmanned aerial vehicles: state of the art on advanced control algorithms 5

1.1 Introduction 6
1.2 Classification of Unmanned Aerial Vehicles 6
1.2.1 Common rotary wing aircraft 9
1.3 Overall control framework: Guidance, Navigation and Control system 10
1.3.1 Navigation subsystem 10
1.3.2 Guidance subsystem 12
1.3.3 Control subsystem 13
1.4 Literature review: recent advance in control strategies for quadrotor UAV . . 13
1.4.1 Linear control approaches 14
1.4.1.1 PID 14
1.4.1.2 Optimal Control 18
1.4.2 Nonlinear control approaches 21
1.4.2.1 Backstepping 21
1.4.2.2 Feedback Linearization (FBL) 24
1.4.2.3 Sliding mode controller 25
1.4.2.4 Robust Adaptive Controllers 28
1.4.2.5 Hybrid controllers 31

1.4.3 Inteligent controllers . . . 36
1.4.3.1 Neural networks . . . 36
1.4.3.2 Fuzzy logic . . . 38
1.4.3.3 MPC . . . 39
1.5 Conclusion . . . 39

2 Quadrotor modeling and control architecture 41
2.1 Introduction . . . 42
2.2 System of coordinates and attitude representation . . . 42
2.2.1 System of coordinates . . . 42
2.2.2 Position and Attitude coordinates . . . 43
2.3 Mechanism of flying . . . 44
2.4 Quadrotor's motions . . . 45
2.5 Quadrotor's kinematic . . . 48
2.6 Quadrotor's dynamic . . . 50
2.6.1 Translational dynamic . . . 51
2.6.2 Rotational dynamic . . . 52
2.6.3 State space representation . . . 54
2.7 Control architechures . . . 55
2.8 Conclusion . . . 57

3 Proposed hybrid control strategy for an uncertain quadrotor 59
3.1 Introduction . . . 60
3.2 Preliminary notions on sliding mode control . . . 60
3.2.1 Reaching laws . . . 62
3.3 Controller design and stability analysis . . . 63
3.3.1 Quadrotor attitude controller . . . 63
3.3.1.1 NFTSMC for the quadrotor attitude . . . 64
3.3.1.2 ANFTSMC for the quadrotor attitude . . . 70
3.3.2 Quadrotor position controller . . . 73
3.4 Controller implementation . . . 77
3.4.1 Simulation results for path tracking in nominal conditions . . . 77
3.4.2 Simulation results in the presence of disturbances and uncertainties . . . 86
3.5 Conclusion . . . 92

4 Proposed robust controller based on a disturbance observer 93
4.1 Introduction . . . 94
4.2 Controller design and stability analysis . . . 94
4.2.1 Disturbance observer . . . 95
4.2.2 Disturbance observer-based nonsingular terminal sliding mode control 96
4.2.3 Disturbance observer-based supertwisting nonsingular terminal sliding mode control . . . 101

4.3 Procedure of the processor-in-the-loop testing . . . 103
4.4 Results and discussion . . . 105
4.4.1 Flight Scenario 1: Robustness against disturbances . . . 105
4.4.2 Flight Scenario 2: Robustness against disturbances and uncertain drag coefficients . . . 110
4.4.3 Comparative analysis . . . 115
4.5 Conclusion . . . 117

5 Development of a quadrotor research platform: Experimental validation 118
5.1 Introduction . . . 119
5.2 Experimental setup . . . 119
5.3 Experimental results . . . 123
5.3.1 Stabilization experiments . . . 124
5.3.2 Transient response experiment . . . 125
5.3.3 Attitude regulation . . . 127
5.3.4 Attitude tracking . . . 131
5.4 Conclusion . . . 135

6 Conclusions and Scope for Future Works 136

Appendix 140

References 148

List of Figures

1 Application of quadrotors in power line inspection (a), autonomous exploration (b), surveillance (c) Road traffic monitoring (d) . . . 2

1.1 Aircraft's classification . . . 7
1.2 Common rotary wing UAVs . . . 9
1.3 Structure of Guidance, Navigation and Control system . . . 11
1.4 Classification of control strategies for the quadrotor UAV . . . 14
1.5 Commonly used PID control architecture . . . 15
1.6 Different test bench platforms for the quadrotor aircraft: (a) [28], (b) [29] ,(c) [31], (d) [34] . . . 16
1.7 Different configuration of the PID controller [33] . . . 17
1.8 NLPID compared with conventional PID in three flight scenarios [35] . . . 18
1.9 LQR compared with PID in a trajectory tracking experiment [46] . . . 20
1.10 Trajectory tracking of a quadrotor drone using the BC method [53] . . . 23
1.11 Chattering phenomenon . . . 25
1.12 Comparison of the SIBC, BC and integral BC methods [78] . . . 26
1.13 Main characteristic of SMC variants . . . 29
1.14 General control architecture of an adaptive control law . . . 29
1.15 Block diagram of the of an hybrid controller based on the integral SMC and the BSMC [101]. . . . 31
1.16 Performance of the hybrid controller in a trajectory tracking task [103]. . . . 32
1.17 Block diagram of an hybrid control scheme based on the IBC, BC and integral TSMC [105]. . . . 33
1.18 Time evaluation of the adaptive gains and disturbance estimation [106]. . . . 34
1.19 SMC-based NN flow chart and obtained results [109]. . . . 37
1.20 Block-diagram of the intelligent BC method with fuzzy compensator [112]. . . 38

2.1 Frame axes using the right-hand rule . . . 43
2.2 Euler angles . . . 43
2.3 Generated thrust and moment by a single rotor . . . 44
2.4 Quadrotor's configurations . . . 46
2.5 Possible vertical motions of a quadrotor aircraft . . . 47
2.6 Rotational and the associated translational motions versus rotor speed variation 48

2.7 Dual-Loop control structure 56
2.8 The developed Simulink model 57

3.1 Sliding and reaching phase of the SMC 61
3.2 Proposed hybrid control scheme for a perturbed quadrotor 63
3.3 Proposed ANFTSMC block diagram 71
3.4 Position trajectory tracking 79
3.5 Attitude trajectory tracking (Φ, Θ, Ψ) 80
3.6 Trajectory tracking errors under nominal conditions 81
3.7 generated control torque $(\tau_\Phi, \tau_\Theta, \tau_\Psi)$ 82
3.8 Generated thrust force 83
3.9 Adaptive gains of the attitude controllers 84
3.10 3D trajectory tracking under nominal conditions 85
3.11 Position tracking performance under disturbances/uncertainties 88
3.12 Attitude tracking performance under disturbances/uncertainties 89
3.13 Generated control torques under disturbances/uncertainties 90
3.14 Generated control effort under disturbances/uncertainties 91
3.15 3D trajectory tracking under disturbances/uncertainties 91

4.1 Proposed disturbance observer based-robust tracking control of a quadrotor UAV 95
4.2 Flow chart of the PIL implementation process 104
4.3 Trajectory tracking in the presence of complex disturbances 106
4.4 Attitude tracking in the presence of complex disturbances 107
4.5 Evolution of the tracking errors in the first scenario 108
4.6 Estimation of external disturbances on the quadrotor's position 108
4.7 Estimation of external disturbances on the quadrotor's attitude 109
4.8 Trajectory tracking in the $x - y$ space 110
4.9 Variation of random drag coefficients 111
4.10 Response curves of the quadrotor's position (x, y, z) in the second scenario . 112
4.11 Time response evaluation of the quadrotor's attitude (Φ, Θ, Ψ) in the second scenario 113
4.12 Evolution of the tracking errors in the second scenario 114
4.13 Estimation of external disturbances on the quadrotor's position in the second scenario 114
4.14 Estimation of external disturbances on the quadrotor's attitude in the second scenario 115
4.15 Trajectory tracking in the 3D space 116

5.1 Graphical illustration of the experimental platform 120
5.2 Quadrotor vehicle used in the experimental testing 121
5.3 Bifilar pendulum setup 122
5.4 Experimental platform developed for real testing under wind disturbances . . 123

5.5 Stabilization experiment of the attitude state 124
5.6 Time histories of the control torques in the origin stabilization experiments . 125
5.7 Attitude response for the step input 126
5.8 Tracking performance for regulation task under wind gust 128
5.9 Time histories of the attitude tracking errors in the regulation experiment . . 129
5.10 Time histories of the generated control signals in the regulation experiment . 130
5.11 Attitude response in the tracking experiment 132
5.12 Time evolution of the attitude tracking errors in the tracking experiment . . 133
5.13 Time histories of the generated control signals in the tracking experiment . . 134

List of Tables

1.1 Comparison of different unmanned aircraft 8
1.2 PID controller parameters effects 15
1.3 Linear controllers and their main characteristics. 21
1.4 Commonly used sliding surfaces 28
1.5 Nonlinear controllers and their main characteristics. 35
1.6 Nonlinear controllers and their main characteristics. (Continued) 36
1.7 Intelligent controllers and their main characteristics 39

2.1 Motion control for a quadrotor depending on rotor speed 49

3.1 Comparison in terms of the settling time indicator 78
3.2 Quantitative comparison in terms of ISE index in the first scenario 86
3.3 Quantitative comparison in terms of ISE index in the second scenario 92

4.1 Performance's comparisons in terms of the ISE index 116

5.1 Quadrotor Components 120
5.2 Comparison of the settling-time for the several strategies 127
5.3 Comparison of the ISE performance in the regulation experiment 129
5.4 Comparison of the $IAD\tau$ index in the regulation experiment 131
5.5 RDP % for IADτ index in the regulation experiment 131
5.6 Quantitative comparison in the tracking experiment 134
5.7 RDP % for IADτ index in the tracking experiment 135

6.1 Physical parameters of the quadrotor used in chapter 3 143
6.2 Parameters of the hybrid controller 143
6.3 Physical parameters of the quadrotor used in chapter 4 144
6.4 Parameters of the DO-STNTSMC controller 144

Symbols and abbreviations

List of Symbols

$\{O_B, X_B, Y_B, Z_B\}$	B-frame	43
$\{O_E, X_E, Y_E, Z_E\}$	E-frame	43
$\chi = \{\chi_i,\ i = 1, 2, \ldots, 12\}$	state variable	54
$\ddot{\eta}_B$	Rotational acceleration	54
$\ddot{\zeta}$	Translational acceleration	52
$\delta_B = (p, q, r)^T$	Angular velocities	50
$\dot{\eta}_B = (\dot{\Phi}, \dot{\Theta}, \dot{\Psi})^T$	Attitude rate	50
$\mathcal{R}_{B\to E}$	rotation matrix	50
Ω	rotation speed	45
ρ	Air density	45
τ_Φ,τ_Θ, τ_Ψ	Control torques	54
τ_a	friction torques	54
τ_i	torque due to rotor's thrust	45
τ_{gyro}	Gyroscopic torques	54
$\eta = (\Theta, \Phi, \Psi) \in \mathbb{R}^3$	Euler angles	43
$\zeta = (x, y, z)$	Cartisian position	43
C_Q	drag coefficient	45
C_T	Thrust coefficient	45
$d_\zeta = (d_x, d_y, d_z)^T$	disturbances in the position subsystem	52

$d_\eta = (d_\Phi, d_\Theta, d_\Psi)^T$	disturbances in the attitude subsystem 54
F_a^E	Drag force 52
F_G^E	Gravity force 52
F_{mi}	Thrust force 45
$J = \text{diag}\,(J_x, J_y, J_z)$	inertial parameters 54
$K_h = diag\,(K_\Phi,\ K_\Theta, K_\Psi)$	friction coefficients 54
l	arm length 45
M_i	Drag moment 45
R^{-1}	Skew matrix 50
v^B	Translational velocity in the B-frame 50
v^E	Translational velocity in the E-frame 50

List of abbreviations

AIA	Aerospace Industry Association 6
AB	Adaptive backstepping 33
ASTTSMC	Adaptive Supertwisting TSMC 31
AUVSI	Association for Unmanned Vehicle Systems International 6
BC	Backstepping Control 22
BNITSMC	Backstepping Nonsingular Integral Terminal SMC 124
BSMC	Backstepping Sliding Mode Control I
BSTSMC	Backstepping Supertwisting SMC 124
CCW	counterclockwise 46
CPPRL	Constant Plus Proportional Reaching Law 68
CSMC	Conventional Sliding Mode Control 25
CW	clockwise 46
DO	Disturbance Observer I

DO-STNTSMC	disturbance observer-based supertwisting NTSMC 102
DOF	Degrees of Freedom 44
ESO	Extended State Observer 24
FBL	Feedback Linearization 24
FLC	Fuzzy Logic Control 38
FTSMC	Fast Terminal Sliding Mode Control 27
FTSS	Fast Terminal Sliding Surface 65
GA	Genetic Algorithm 18
GFTSMC	Global Fast Terminal Sliding Mode Control 77
GNC	Guidance, Navigation, and Control 10
GPS	Global Positioning System 6
HFTC	Hybrid finite-time control 32
HOSMO	High-Order Sliding Mode Observer 24
IBC	Integral Backstepping Control 24
ISMC	Integral Fast Terminal Sliding Mode Control 77
LQR	Linear Quadratic Regulator 18
MBD	Model-Based Design I
MPC	Model Predictive Control 38
MST	Modified Supertwisting 27
NFTSMC	Nonsingular Fast Terminal Sliding Mode Control I
NFTSS	Nonsingular Fast Terminal Sliding Surface 67
NN	Neural Networks 36
NPID	NonlinearProportional-Integral-Derivative 18
NTSMC	Nonsingular Terminal Sliding Mode Control 27
NTSTC	Nonsingular Terminal Supertwisting 27
PID	Proportional-Integral-Derivative 14

PIL	Processor-In-the-Loop	I
PSO	Particle Swarm Optimization	18
PWM	Pulse-Width Modulation	10
RBFNN	Radial Basis Function NN	38
SIBC	Saturation Integral Backstepping Control	124
SIBC	saturated integral BC	27
SMC	Sliding Mode Control	25
SOMC	Second-Order SMC	27
ST-SMC	Supertwisting control	27
STNTSMC	Supertwisting Nonsingular Terminal Sliding Mode Control	I
T-S	Takagi-Sugeno	38
TSMC	Terminal Sliding Mode Control	27
TSS	Terminal Sliding Surface	65
UAVs	Unmanned Aerial Vehicles	I
VTOL	Vertical Take-Off and Landing	10

Introduction

UNMANNED aerial vehicles, used both in the military and the civilian sectors, are currently under numerous studies, researches and investigations. They present the only solution for certain problems that can't be solved by autonomous ground and/or underwater vehicles. Additionally, applications that demand hovering flight restrict the use of autonomous aircraft to rotary-wing vehicles like quadrotors. The application domains are numerous and range from surveillance, search and rescue, aerial photography, disaster management, forest monitoring, military war, and aerobatic flights for entertainment. UAVs, especially quadrotors, have served as an interesting aerial research platform for the design and experimental validation of new algorithms for the guidance, state estimation, and control systems since their natural behavior raises various challenges that are not addressed in other robotic systems.

Around the world, UAVs in a variety of shapes and sizes keep emerging in daily activities [1]; but, in the meantime, the challenges associated with the improvement of their flight capabilities are also increasing, especially in terms of robust stabilization and accurate trajectory tracking. The notoriety of these vehicles is deeply related to the quality of the control system. However, the synthesis of an efficient flight control algorithm for unmanned quadrotors remains an ongoing challenge, especially when moving from a basic theoretical model to a practical application in which many sources of uncertainties due to imperfect modeling, inaccuracies in the aerodynamic coefficients, and external disturbances should be considered. Controlling the quadrotor vehicle in the presence of these factors is a big and difficult task as the system can quickly deviate from the targeted path, threaten the system's stability, or even cause the aircraft to crash.

As a consequence, it is necessary to have a control system with strict requirements in terms of accuracy, fast convergence, and robustness. The works developed in this thesis focuses on the development of a practical flight control system for a quadrotor vehicle by considering the problems of underactuation, unmodelled dynamics, parameters inaccuracies, and time-varying/sustained perturbations.

Motivation and research objectives

Recently, quadrotors, whether fully autonomous or remotely piloted, are experiencing a high rate of investment in various application areas. In fact, there have been several attempts to integrate these machines into multiple complex missions, including flying longer distances and carrying payloads [2, 3]. Nowadays, quadrotor-drones are used for medical deliveries, which decreases the delivery time by more than half and reduces contact human-to-human, thus reducing the spread rate of contagious diseases, or viruses transmission such as, the coronavirus [4]. Some governments have used quadrotors to disinfect public spaces without the need of human intervention. In other countries, quadrotors are supplied with speakers and used to give some instructions and raise citizens' awareness of staying at home. Quadrotors have also been adopted as a solution to sustain the quarantine zones and to control their infringement [5]. Figure 1 shows some other uses of unmanned quadrotors in additional applications [6–8]. Nevertheless, as exciting as its advantages seem to be, the nonlinearity, the multivariable dynamic, the inherent open-loop unstable behavior, the coupling in their state variables, and the sudden changes in the control signals make the precise-control of the quadrotor UAV a challenging task [9, 10]. Furthermore,the total number of sensors and electronics needed to perform sophisticated flight missions is important, hence the resulting noise increase. In addition, actuator vibration presents an additional source of parasitic dynamics. Also, in outdoor applications, these vehicles can be easily affected by plant uncertainties and aerodynamic perturbations, which can create unfavorable performance for accurate trajectory tracking [11]. It should be mentioned that disturbances are not always exogenous (external to the natural behavior), but they can be endogenous (sensed when the vehicle mass changes).

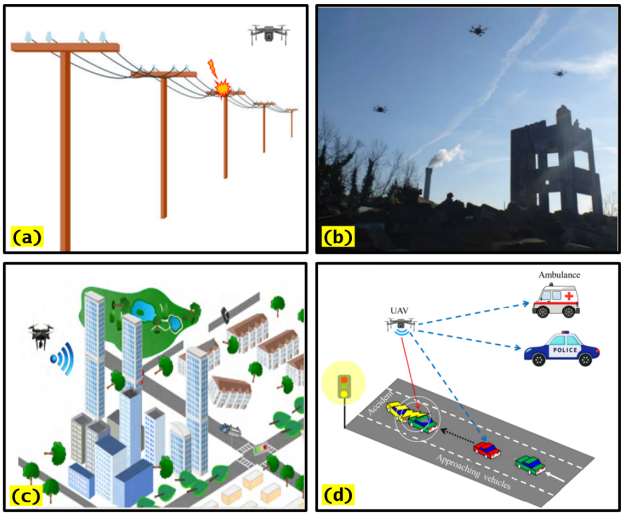

Figure 1: Application of quadrotors in power line inspection (a), autonomous exploration (b), surveillance (c) Road traffic monitoring (d)

In response to the aforementioned difficulties in quadrotor control, this thesis will approach the development of new control laws for stabilization and trajectory tracking of autonomous quadrotors under the influence of wind disturbances and parameter uncertainties. The details of the theoretical design and stability analysis of all proposed controllers are provided. Furthermore, a quadrotor research platform is constructed to evaluate the performance of the control systems in a real-world environment.

This thesis is one of the earliest studies on the tracking control of unmanned quadrotor conducted at SIGER laboratory. Our first objective was to familiarize ourselves with the challenges related to quadrotor control, master this process theoretically and experimentally and apply some new strategies to improve the quadrotor capabilities.

The main contributions of this thesis are as follows:

- An efficient flight controller for attitude tracking is developed based on a nonsingular fast terminal sliding mode control combined with a real-time adaptive methodology. This method offers a number of advantages, such as achieving zero tracking errors in a short finite time, ensuring fast and accurate tracking, and compensating for the impact of severe uncertainties in the model parameters.

- In order to improve the tracking capabilities in the existence of complex perturbations such the modeling errors and system uncertainties, a compound control scheme based on a perturbation estimator combined with an improved supertwisting nonsingular terminal sliding mode control has been developed. Moreover, Processor-In-the-Loop (PIL) implementation on a real autopilot has been performed to confirm the validity of the developed controller.

- A low-cost quadrotor prototype has been developed to validate the feasibility of our controllers. In addition, a set of flight scenarios has been performed to test and evaluate the performance of the control systems under several operational constraints. In addition, comparisons with multiple linear and non-linear controllers are also presented to show the superior performance of the proposed controllers.

Thesis organization

This thesis is formed of six chapters quickly described as follows:

Chapter 1: Quadrotor unmanned aerial vehicles: state of the art on advanced control algorithms
This chapter presents a general overview of unmanned aerial vehicles by stating the features

of each vehicle. The concept of guidance, navigation, and control systems is also introduced. Finally, a literature review on stabilization, regulation, and trajectory tracking of unmanned quadrotors is presented. It covers relevant works related to the control system by a presentation of the advantages, limitations, and major differences between several approaches. The main goal of this part is to give a unified analysis, placing the linear, nonlinear, and robust adaptive controllers into the proper context.

Chapter 2: Quadrotor modeling and control architecture
This chapter describes the quadrotor system as an underactuated mechanical system. Fundamental concepts regarding motion control, reference frames, dynamic equations, state space representation, and control structure are detailed here.

Chapter 3: Proposed hybrid control strategy for an uncertain quadrotor
In this chapter, the development of an adaptive nonlinear controller for the path tracking of an uncertain quadrotor is investigated. The proposed flight control algorithm can drive the drone toward the pre-established path and vanish the tracking errors within a short finite-time. A detailed analysis, in terms of robustness and tracking precision, with multiple control strategies is also conducted to validate the performance of the recommended method.

Chapter 4: Proposed robust controller based on a disturbance observer
This chapter presents the design of a compound control scheme based on an improved super-twisting nonsingular terminal sliding mode control combined with a nonlinear disturbance observer. Processor In the Loop experiments are performed to confirm the validity of the proposed method.

Chapter 5: Development of a quadrotor research platform: Experimental validation
This chapter attempts to fill a gap in the literature and establish a roadmap towards experimental validation of robust attitude flight control systems. For that reason, a quadrotor testbed platform has been constructed to check the validity of our proposed controller. In addition, an automatic tool to implement controllers directly from MATLAB/Simulink code onto real autopilot hardware is presented. Multiple experimental tests are suggested as a method to validate the workability of the flight control system.

Chapter 6: Conclusions and Scope for Future Work
This chapter synthesizes the major findings of this thesis project and gives an overview and suggestions for the envisaged future works.

1 Quadrotor unmanned aerial vehicles: state of the art on advanced control algorithms

1.1 Introduction

Recent technological developments in computation devices, wireless communication systems, sensor miniaturization, and lightweight materials have paved the way for tremendous progress in the capabilities of autonomous aerial vehicles. In addition, with the increasing demands of civilian activities, including disaster monitoring, power line inspection, traffic surveillance, and delivery of goods, the UAV/drone sector is becoming a mainstream industry.

To acquaint the reader with these vehicles, in this chapter we present a general overview of multiple unmanned aerial vehicles with a special focus on the quadrotor UAV. A literature review on control strategies applied for the stabilization and tracking control of the quadrotor UAV is also presented. Hence, section 1.2 gives some introductory notions on UAV classification, including the advantages and limitations of each type. Section 1.3 explains the concept of guidance, navigation, and control systems, starting from the formal architecture to the functional role of each unit. The literature review on flight control systems is finally exposed in section 1.4.

1.2 Classification of Unmanned Aerial Vehicles

Unmanned aerial vehicles have revolutionized the aircraft sector in the last few years. According to the Aerospace Industry Association (AIA), the global civilian drones production revenue will grow from 3.5 to 302 million US dollars in 2023. The Association for Unmanned Vehicle Systems expects the creation of more than 100 000 new jobs in drone sectors by 2025 [12]. UAVs are available in a variety of forms, sizes, and configurations, depending on mission requirements. They range in size from large-scale aircraft with a payload of 15 000 kg to tiny micro-electro-mechanical systems called "smart dust" with a payload of 5 mg [13]. The number of actuators might change from two to four or more. The configurations vary from simple structures with low-cost microprocessors to sophisticated systems with embedded vision, wireless communication, and Global Positioning System (GPS) navigation.

Based on flying principles, several classifications can be considered for UAVs. The common characteristics for aircraft classification are propulsion mode, mechanical design, and the number of actuators, based on which, UAVs can be classified into three principal categories as shown in Figure 1.1 : fixed-wing, rotary-wing, and flapping wing. They are different from each other both structurally and regarding mechanical modeling and control design. Each category exhibits its advantages and its inherent weaknesses.

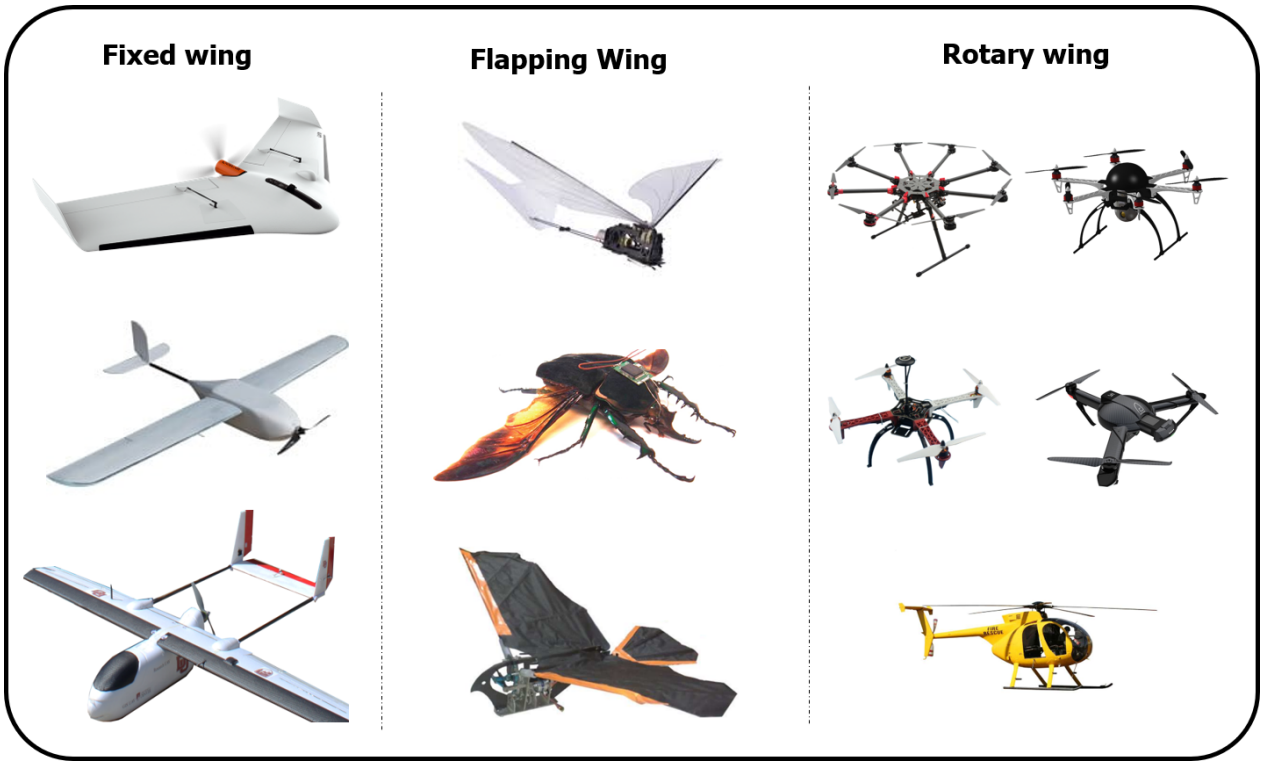

Figure 1.1: Aircraft's classification

The fixed-wing UAVs are the most prevalent type in military applications, owing to their capabilities in flying for wide-range and long endurance at higher speed while consuming less power [14]. They have natural gliding properties without the need for energy and are capable of carrying larger payloads over longer distances. Their propulsion mechanism can be at the front of the fuselage or at the rear. However, these vehicles have the disadvantage of requiring a runway or launcher for takeoff and landing. Furthermore, the vehicle propulsion mechanism provides forward airspeed, which produces the thrust to counteract the weight of the vehicle. Therefore, the fixed-wing aircraft must maintain a constant forward velocity and thus cannot take off or land vertically.

Flapping wing UAVs mimic the natural movement/behaviors of some birds and insects. Most of these UAVs are still in development [15]. The small size and the high maneuverability will enable them to covertly enter locations inaccessible by other vehicles. They can hover, take-off and land vertically, making them ideal for espionage missions. They belong to the class of micro UAVs, which have a very limited payload capability. The mechanical structure of these machines is inspired by birds and insects, which makes the flight dynamics more complex compared to other drones [16, 17].

Rotary wing UAVs are the preferable choice in many civilian applications. Potential uses of these aircraft include surveillance, cinematography, mapping, firefighting, infrastructure

inspection, and precision agriculture... and so on [18]. These applications require vertical and stationary flights, which make the rotary wing aircraft more convenient and properly exploited in these situations. They are capable of low-altitude flights and hovering and do not require a runway to take off or land. However, they are not fast and their endurance is still limited compared to fixed-wing UAVs [19].

The comparison in terms of flight capabilities between the fixed-wing, flapping-wing, and rotary-wing is summarized in Table 1.1. Three distinct degrees of comparison were employed in the comparisons: low (1), medium (2), and high (3). Obviously, rotary-wing UAVs have the highest indicator index. In fact, rotary-wing UAVs with their different configurations are acknowledged as the most promising unmanned flying concept [20].

Table 1.1: Comparison of different unmanned aircraft

Parameter	Fixed-wing	Flapping wing	Rotary-wing
Energy consumption	2	1	1
Payload	3	1	2
Maneuverability	2	3	3
Stationary fly	1	2	3
VTOL	1	2	3
Flight safety	3	1	2
Endurance	2	1	1
Low speed fly	1	2	3
Miniaturization	1	3	3
Civilian application	1	2	3
Military application	3	2	2
Indoor usage	1	3	3

1.2.1 Common rotary wing aircraft

The class of rotary-wing aircraft can be subdivided according to the number of rotors (see Figure 1.2); for instance, Monocopters (1 rotor), Tricopter (3 rotors), Quadrotor (4 rotors), Hexacopter (6 rotors), Octocopter (8 rotors).

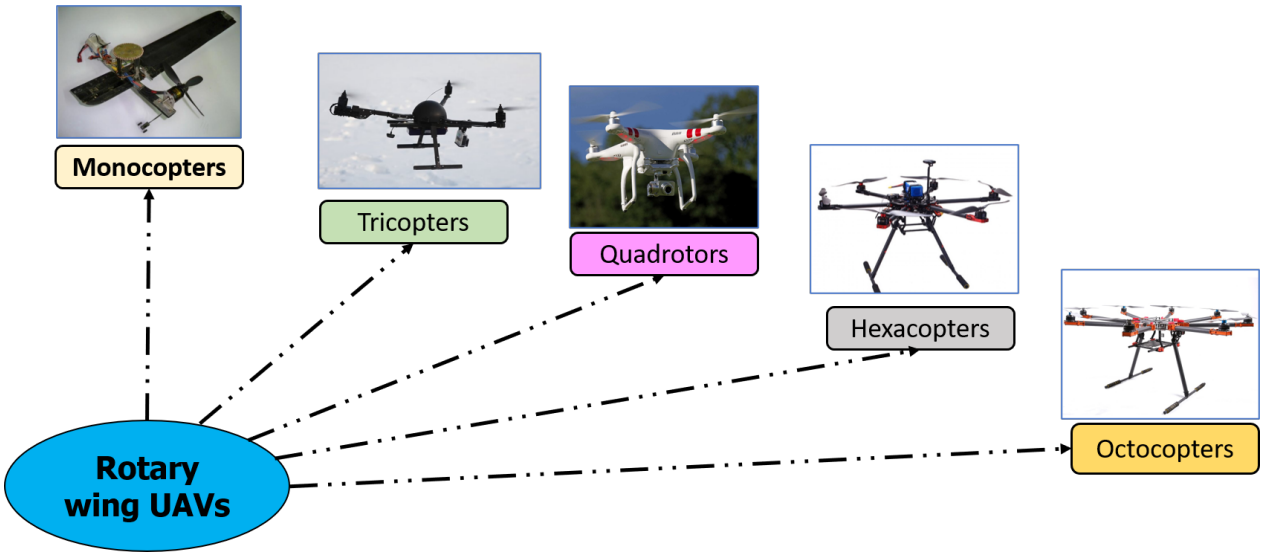

Figure 1.2: Common rotary wing UAVs

Monocopters consist of a main actuator and a single wing to create lift. A flap with a servomotor is used to direct the movements of the vehicle. Although this vehicle was innovatively designed and successfully tested through simulation and experience, the vehicle's operation has a lot of weaknesses, including the weak stability, the imprecise hover, and the ease of collision [21].

Tricopters are made up of three actuators that are evenly separated by 120 degrees from each other, which makes them more suitable for videography. Their small and lightweight structure give them a longer battery life. Tricopters, on the other hand, are less stable with a higher probability of crash in the case of total/partial failure of one actuator.

Quadrotor also known as **quadcopter** is a small-scale unmanned aircraft that has found widespread application in scientific and practical applications. It consists of four identical motors spaced equally around its center of mass. Because of its hover and low-speed flying characteristics, as well as its relative simplicity compared to regular helicopters, it is mostly used for surveillance, reconnaissance, and aerial photography. Quadrotor hover with better stability and higher thrust-to-weight ratio when compared to Monocopters, and Tricopters. They are safe to operate in both outdoor and indoor environments, easy to understand, and have been constructed successfully in a variety of sizes.

Hexacopters compared to quadrotors, tricopters, and monocopters, have better stability even after a single actuator failure. Hexacopters have better lifting capabilities and can transport heavier payloads. But they are more expensive to develop, require more energy from batteries, and are significantly larger than quadrotors.

Octocopters consist of eight propulsion systems that are evenly separated by 45 degrees. In comparison to the other Vertical Take-Off and Landing (VTOL) aircrafts with less actuators, they have the highest stability and can carry greater payloads. However, cost, power consumption, and size limit the use of this kind of aircraft in indoor environments.

Quadrotors offer the greatest advantages in terms of stability, price, structural size, and simplicity of modeling and development. Due to these advantages, they have been extensively researched and are widely used in a variety of domains, which explains the primary motive of this thesis in studying the flight principles, developing dynamic models, exploring prevalent control strategies, and proposing new solutions to improve the flight capabilities against modeling uncertainties and wind disturbances.

1.3 Overall control framework: Guidance, Navigation and Control system

The overall control framework of a quadrotor system is commonly grouped into three parts, which are the Guidance, Navigation, and Control (GNC) [22]. A typical architecture of the GNC system is schematized in Figure 1.3. The GNC system is the pillar of the automatic flight control system, as it allows the vehicle to fulfill the preprogrammed mission autonomously. It helps the aircraft to follow waypoints and to complete other specified tasks such as tracking trajectory, autonomous takeoff and landing, and hovering flight. The navigation subsystem provides real-time localization based on sensors (IMU, GPS, camera ...) mounted on the aerial vehicle. Then, the guidance subsystem generates the feasible trajectory, taking into account some specific tasks such as obstacle avoidance. Afterward, based on the reference path and the real-time localization, the control subsystem generates the appropriate torques and lift forces. These latter are transformed into adequate Pulse-Width Modulation (PWM) signals, allowing the vehicle to perform the programmed maneuvers.

1.3.1 Navigation subsystem

The navigation block is responsible for determining, at a given time, the state of the vehicle as well as the detection of obstacles and targets. Specifically, the navigation tasks are separated into two parts: one for determining the state of the vehicle (**State Estimator**) and the other for acquiring information about the surroundings (**Perception block**).

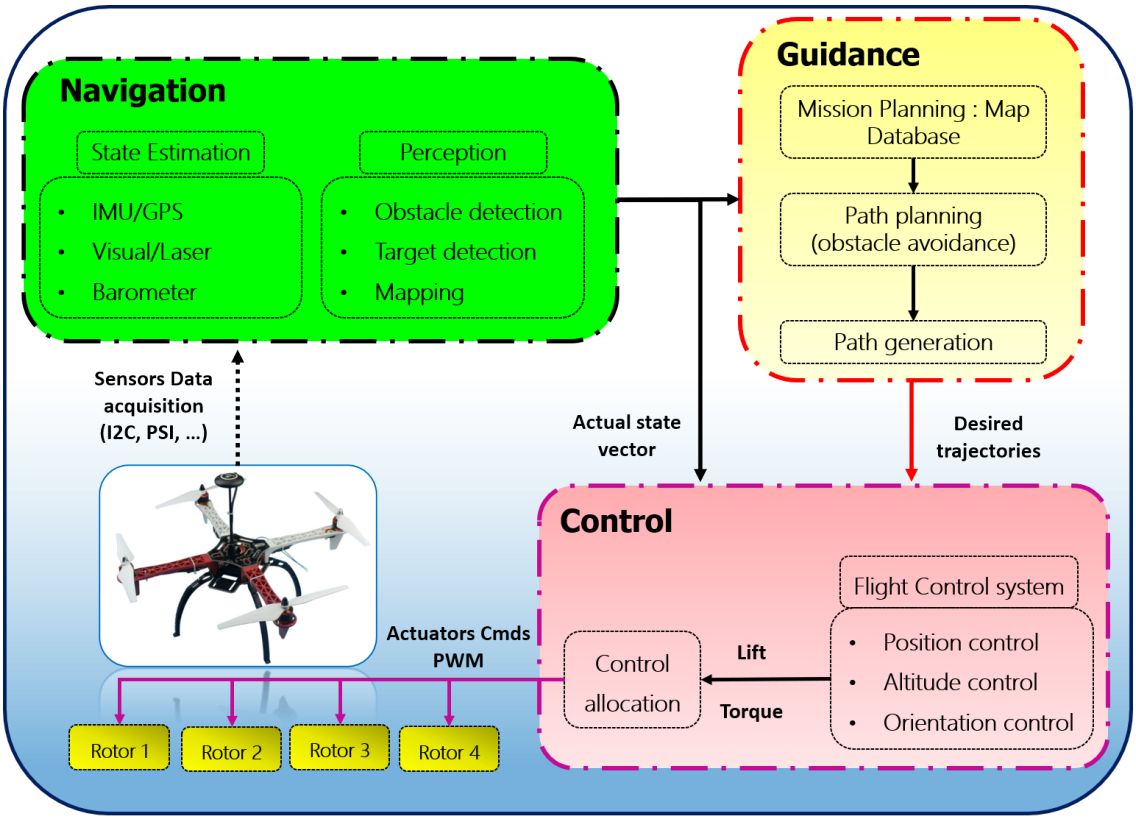

Figure 1.3: Structure of Guidance, Navigation and Control system

- **State estimation**

  The most commonly used sensors for the measurement of the vehicle state are the inertial measurement units (accelerometer, gyroscope, magnetometer), cameras, GPS, barometers, and LIDARs. The provided measurements are directly processed by the state estimator to estimate information about the vehicle's self-motion (orientation, position, velocity, etc.). The recent advances in computer technologies make fusion of data coming from several sensors possible to provide an accurate estimation of the vehicle state. In order to cope with any sensor's noise/failure, some filtering techniques were used, particularly the baseline navigation filters are the Kalman filter and the complementary filter [23].

- **Perception**

  Perception is defined as the capacity to use sensor data to sense the surroundings environment. Vision systems (i.e. cameras) and LIDAR sensors are commonly used to gather data. Typically, the information collected by perception algorithms is used as inputs for the guidance subsystems rather than being directly employed as measure-

ments in the flight controller. The navigation block's data serves a dual purpose: it is used by the control module for controlling motions and by the guidance subsystem for mission planning.

1.3.2 Guidance subsystem

Guidance refers to determining the route that the aircraft must take in order to track a path, follow a target, or arrive to a specified location within the vehicle's operational constraints. Signals from the navigation system, vehicle state, are used as inputs. Then, the guidance block makes the necessary decision, selects the correct maneuvers, and provides the required changes within the targeted trajectories such as velocity, rotation, and acceleration. The generated trajectories are then sent to the control block for motion control. The guidance subsystem groups some specific functions that allow the vehicle to operate either autonomously or manually, reach the desired destination, and perform the assigned missions correctly. These functions are detailed as follows:

- **Mission planning**

  Mission planning plays a key role in the ground control station. It can be defined as the procedure for determining the desired 3D waypoints, and defining the operation mode like landing, takeoff, hovering, altitude tracking, waypoint tracking, and target tracking. The operation mode (flight mode) can be updated either by a human operator directly from the ground control station via a WiFi link or by the Fail-Safe system, which is a set of preprogrammed instructions that command the vehicle when some unexpected behavior occurs [24].

- **Path planning**

  Path planning is deemed as the process that allows the vehicle to identify the most flyable and safest route to facilitate driving the aircraft from one place to another. Generally, the path planning is separated into two parts [25]. The first step is to create a sequence of waypoints directly connected by straight lines. This part is labeled "global path planning". The second step consists of refining the trajectory to be flyable considering the surrounding environment (obstacles) and the operational constraints of the quadrotor. This step is named "local path planning".

- **Trajectory generation**

  Trajectory generation is the process of constructing a physically feasible path for the control loop considering the vehicle's operational constraints (maximum acceleration

and velocity) and the operation mode. To avoid aggressive maneuvers, smooth reference trajectories in 3D space are generated based on the desired velocity and the actual position of the vehicle.

1.3.3 Control subsystem

The control block (autopilot) receives the targeted trajectories from the guidance module and the state of vehicle (attitudes, velocities, and accelerations) from the navigation module. Using this information, it calculates the tracking errors according to the control law; then, it generates the required thrust and torques. These signals are transformed into PWM signals and then transmitted to the actuators, allowing the vehicle to execute the mission entrusted by the guidance module. The control loop includes attitude, altitude, and position control. It is responsible for regulating the vehicle motion, preserving a stable feedback loop, and tracking the pre-established path. As for the control strategies used for the quadrotor system, the literature review is rich with multiple approaches.

Basically, three classes of controls dealing with the command of uncertain and perturbed quadrotor can be outlined; linear, nonlinear, and intelligent approaches.

Linear control techniques such as proportional-integral-derivative control are still broadly applied due to their ease of design and implementation. A common shortcoming of linear controllers is that their application requires model linearization, which may reduce the credibility of the controllers when perturbations arise in the system. Thus, these approaches fail to reach equilibrium and the system becomes unstable. To get better performance, nonlinear controllers are a good choice. These methods can be adopted without linearizing the model dynamics, but assume that the model parameters are fixed and totally known in advance, which is not the case. Practically, quadrotors are susceptible to some uncertainties, also the quadrotor mass and matrix of inertia changes in the flight mission, so controllers with static parameters cannot take these changes into consideration. Intelligent controllers with the ability to adjust the control structure depending on the flight nature are a good solution to steer the quadrotor movement without losing the targeted trajectory.

1.4 Literature review: recent advance in control strategies for quadrotor UAV

Unmanned aerial vehicles have made significant technological advances over the past few years. Aircraft with vertical take-off and landing capabilities are of special relevance since they can be maneuvered quickly, take-off, and land easily. Quadrotors are the best-known example of this kind. An appropriate feedback control system allowing reliable position and

attitude control must be synthesized in order to take advantage of their capabilities. Aiming at a unifying perspective, the most adopted control strategies for quadrotor UAVs are classified into three categories, respectively: those based on model linearization characterized by their simple design procedure and implementation, those based on nonlinear methodologies that take into consideration the nonlinear part of the system, and finally intelligent strategies that offer more adaptiveness with the maneuver under several external conditions. Figure 1.4 shows the decomposition of the control strategies adopted during our investigation.

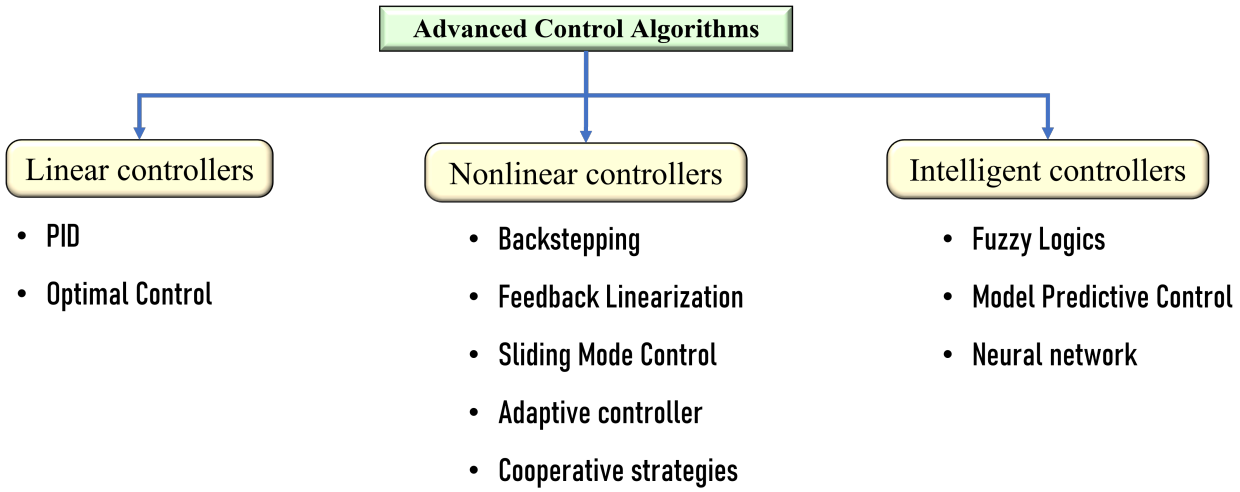

Figure 1.4: Classification of control strategies for the quadrotor UAV

1.4.1 Linear control approaches

1.4.1.1 PID

Even though the area of robot control has seen a remarkable transition and development, the Proportional-Integral-Derivative controller (PID) is still broadly used due to its insight simplicity in both design and implementation. From the point of view of industrial applications, the PID algorithm delivers acceptable accuracy with a good cost/benefit ratio, which is hard to obtain using other advanced control algorithms. Moreover, the simple and functional structure of linear PID controllers has allowed their broad applicability in commercial models. In fact, more than $90-95\%$ of industrial applications are based on simple PID controllers [26].

PID, in principle, combines three control function: proportional (P), integral (I) and derivative (D), and the well-known architecture of this method is shown in Figure 1.5. The PID control law is adopted to reduce the tracking error between the desired state and the measured one. Each parameter of the three control functions has unique effects and should be selected depending on the system to be controlled. Specifically, the proportional term (P-term) improves the response time and reduces the error in the steady state. A large increase

in the P-term produces overshoot and can sometimes destabilize the system. The integral term (I-term) offsets the steady-state error and fastens the response time, but a large value in the I-term may produce some undesired oscillations. The derivative term (D-term) reduces the unwanted oscillation and the overshoots introduced by the I-term whereas a large value of the D-term slows down the system's response and makes it more sensitive to the influence of noise.

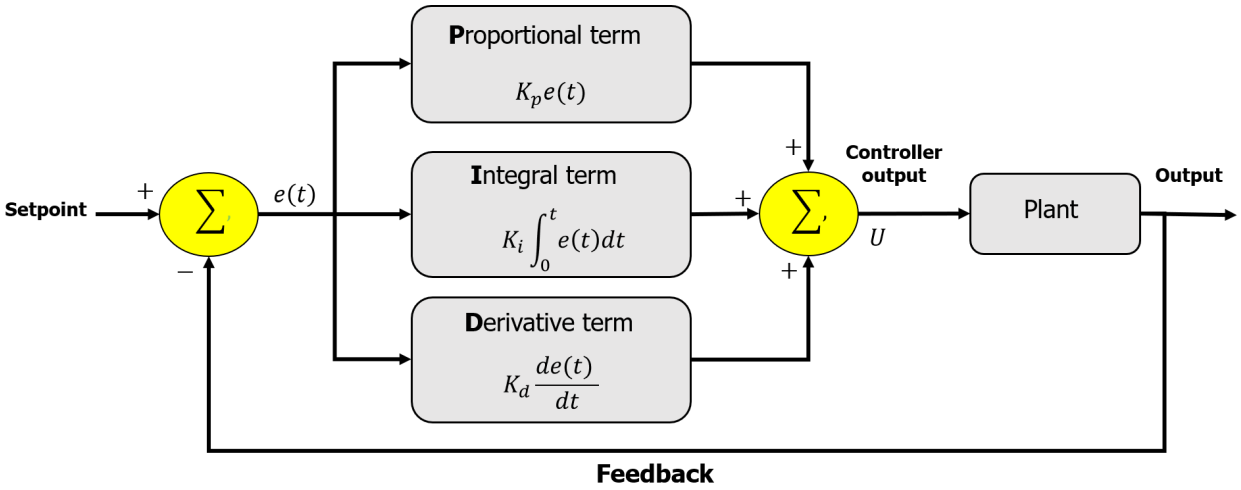

Figure 1.5: Commonly used PID control architecture

Table 1.2 summarizes the impact of each parameters of the PID controller [27].

Table 1.2: PID controller parameters effects

Parameter	Rise time	Overshoot	Settling time	Steady state error
P	Decrease	Increase	Minor decrease	Decrease
I	Decrease	Increase	Increase	Eliminate
D	Minor increase	Decrease	Decrease	No effect

Several research proposals dealing with the stabilization and path following using the concept of PID control algorithms with application to quadrotor aircraft have come up with some exciting and interesting results.

Attitude stabilization plays a dominant role during the flight maneuver as it allows, in addition to the control of the quadrotor orientation, the achievement of the desired horizontal position. In reference [28], the PID control law is applied to stabilize the quadrotor orientation. The model dynamic is linearized locally around the hovering condition; consequently, gyroscopic torques are ignored during the process of designing the flight controller. In addition, a PID controller has also been adopted for each motor to control the speed. The validity

of the designed controller is proven experimentally on a 3 degrees-of-freedom quadrotor test bench, shown in Figure 1.6-(a), exhibiting good performance in hovering flight, especially for the yaw motion. But the stabilization of both roll and pitch rotations was slower and exceeded 5 seconds.

In another work, the PID controller is adopted for the real-time attitude control of a quadrotor aircraft [29]. A kalman filtering technique has also been included for the attitude estimation and sensor noise reduction. As seen in figure 1.6-(b), the authors constructed a test-bed quadrotor platform. The prototype is used to confirm the performance of the proposed PID-based kalman filtering for the roll and pitch rotation. However, the inter-axis interaction cannot be evaluated thorough this test-bed system because the rotation is allowed only in one axis (either the pitch or the roll). In addition, the control of yaw motion is not supported with this prototype.

Bolandi et al. [30] presented an optimal-tuning based PID controller for the quadrotor flight attitude. The control parameters were tuned using an optimization algorithm by considering four cost functions, namely the integral absolute error, the integral time multiply absolute error, the integral square error and integral time multiply square error. The authors stated that the best results were achieved using the integral absolute error cost function. Faster response is achieved in both regulation and tracking tasks. However, the problem of overshoot is noticed in the simulation results.

In another research [31], a quaternion representation with proportional-derivative feedback control is studied. The authors of this work have succeeded in the experimental stabilization of the quadrotor attitude without linearization and while considering the gyroscopic effects due to the body-frame and propeller rotation. A complementary filter was introduced to estimate the vehicle's attitude and to reduce noise. The control system was executed on the test bench shown in Figure 1.6-(c). The results emphasize the ability of the proposed solution to stabilize the aircraft even at large attitude angles.

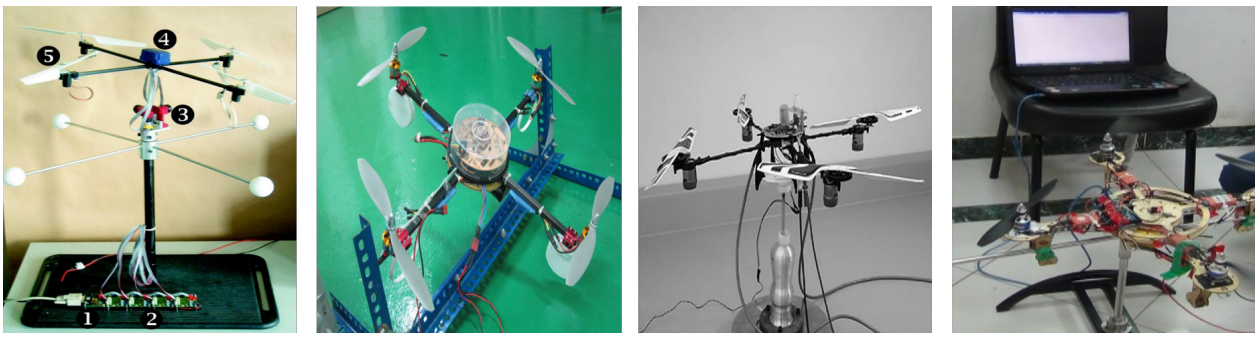

(a) (b) (c) (d)

Figure 1.6: Different test bench platforms for the quadrotor aircraft: (a) [28], (b) [29] ,(c) [31], (d) [34]

Hoffmann et al. [32] deployed a modified PID controller for an autonomous quadrotor. The concept of a PID controller is improved by adding another term based on the feedback of angular acceleration. This term aims to stabilize the angular acceleration in aggressive maneuvers and to overcome the high acceleration influence. Furthermore, an algorithm for trajectory generation is applied and its experimental validations in both indoor and outdoor fights are also presented, providing good accuracy in terms of path following. In reference [33], three control architectures based on the PID controller are presented. The key idea is to alter the three control parameters' in order to change the controller's internal structure. This alteration will have an impact on the tracking performance. The quadrotor is first modeled using the Euler-Lagrange principle, and the three PID configurations' control design processes are then thoroughly explained. Figure 1.7 illustrates the three control structures defined by the authors. From the comparative analysis in terms of the integral square errors (ISE) performance index, the control structure type B has provided the smallest value with 0.77048 compared to 0.90128 for type A and 1 for type C. The authors in [34] confirmed that the modified PID controller (type B) can ensure attitude stabilization in real flight conducted on the quadrotor prototype shown in Figure 1.6-(d).

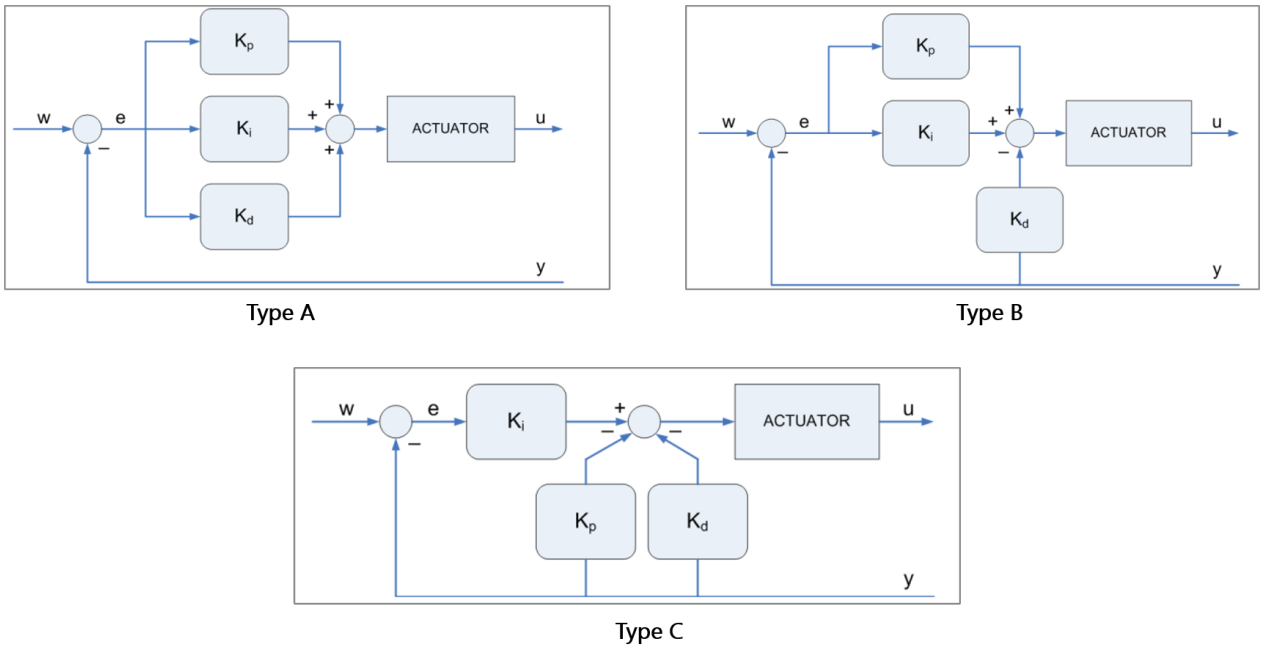

Figure 1.7: Different configuration of the PID controller [33]

Moreno et al.[35] presented a Nonlinear PID controller (NLPID) to ensure the stabilization and tracking control of the quadrotor in the existence of some disturbance in one actuator. A real-time implementation of the proposed algorithm was provided and its comparison with both linear PID and SMC methods is also presented. The experimental results highlight the superiority of the suggested method compared to the other strategies. Similarly, an NLPID controller is introduced in [36] to maintain the stability of the six degrees of freedom and to

force the system outputs to follow the planned trajectory with enhanced accuracy. In order to get better performance, the parameters of the NLPID control law are automatically adjusted using an optimzation algorithm by considering a multi-objective cost function defined as a combination of the integral absolute error and the controller energy. Figure 1.8 depicts the results of tracking multiple complex trajectories using the nonlinear and the linear PID controllers. Clearly, the NLPID could give better tracking performance than the linear PID controller.

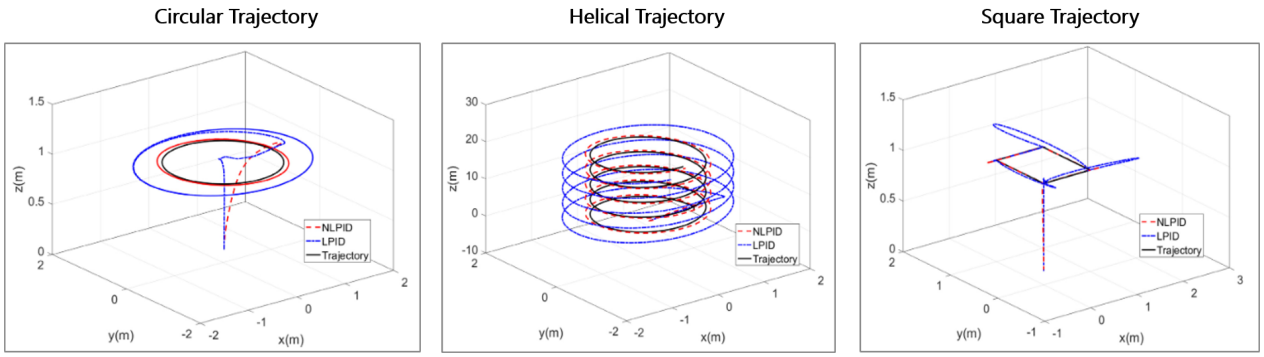

Figure 1.8: NLPID compared with conventional PID in three flight scenarios [35]

More recently, a quadrotor aircraft with tilt-rotors has been designed, modeled, and controlled in order to transform the entire dynamics into a fully actuated system [37]. The design modification in this study allows the achievement of a tilted hover without any translational motion, which is not achievable with a traditional quadrotor. The concept of a conventional PID controller is employed to regulate the quadrotor movements. The results of simulations and experiments are good in terms of stabilization and precision. Within the conducted research on quadrotor control using the PID controller, the controller parameters are either selected empirically or through some tuning strategies. These latter can be classified as traditional methods, such as Ziegler-Nichols [38], or automatic methods based on some optimization algorithms, e.g. Particle Swarm Optimization algorithm, Genetic Algorithm, Gravitational search algorithm, Ant Colony Optimization algorithm, Cuckoo Search algorithm, and the list is not exhaustive [39–42]. After determining the optimal values of the proportional, integral, and derivative gains through a tuning strategy, they are usually kept constant during the testing phase. This means that the optimization process is typically performed only once at the beginning of the test, and the controller gains are then kept fixed at their optimized values throughout the entire testing period.

1.4.1.2 Optimal Control

The Linear Quadratic Regulator (LQR) is an optimal control that operates a dynamic system by minimizing a cost function, known also as quadratic performance index, that depends on the system's states and control signals [43]. It represents the system's performance criteria.

For a dynamics system defined by $\dot{x} = Ax + Bu$ with A and B being the system matrices, the general form of the cost function J is given as [44]

$$\begin{cases} \dot{x} = Ax + Bu \\ J = \int \left(x^T Q x + u^T R u \right) dt \\ u(t) = -K_c x(t) \end{cases} \tag{1.1}$$

Where A and B are the system matrices. Q and R are the the weighting matrices. $u(t)$ and K_c are respectively the optimal control input and control gains.

As shown in Eq. 1.1, the cost function J is defined as the sum of two terms. The first term, $x^T Q x$, measures the cost of state deviation and penalizes deviations of the system state from its desired state. The second term, $u^T R u$, measures the cost of control effort and penalizes high control effort. Together, these terms form a trade-off between minimizing the deviation from the desired state and minimizing the control effort required to achieve it. By adjusting the weighting factors (Q and R), it is possible to adjust the relative importance of these two goals and design a control strategy that achieves the desired performance objectives.

In reference [45], PD, PID, and LQR methods were implemented on a quadrotor system with the target of stabilizing the vehicle attitude. The PD and PID were applied to the quadrotor linearized model, while the LQR control was applied to the complete dynamical model. The performance was satisfactory when only the PD control was used, but a steady state error was noticed during the experimental test. The integral term of the PID controller can reduce this steady state error and speed up the response of the control system. However, the authors of this work claim that this controller will not be able to stabilize the drone in the presence of strong perturbations. On the other hand, the LQR controller achieved a better response during the simulation tests. However, as stated by the authors, the tuning of the LQR control is not easy at all. Moreover, the experimental results were not good, probably due to controller parameters that were not tuned properly.

In a similar work, lui et al.[46] compared the accuracy of the LQR and PID controllers in terms of trajectory tracking. Simulation tests as well as experimental flight test on an Qball-X4 quadrotor have been conducted to evaluate the performance of both controllers. As can be observed from Figure 1.9, results of the LQR controller are better with reduced deviation from the targeted trajectories compared to the PID controller.

In reference [47], the model dynamic of the quadrotor is first derived using the Newton Euler formalism, then linearized to be suitable for the application of linear controllers. The LQR control is designed and applied for the quadrotor attitude regulation. Then, an optimization algorithm has also been used to automatically select the adequate controller

parameters. Two simulation tests were conducted and demonstrated that the vehicle can achieve the steady state in about $3s$.

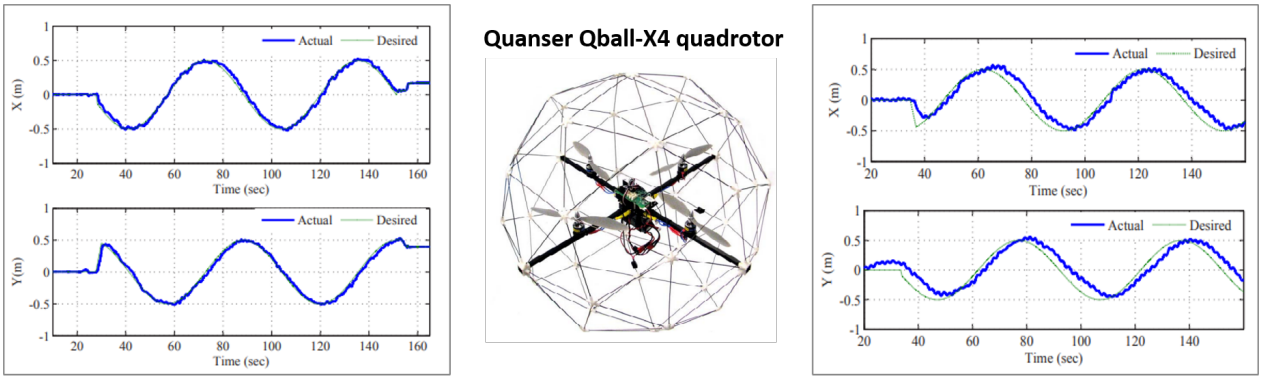

(a): Trajectory tracking using the LQR

(b): Trajectory tracking using the PID

Figure 1.9: LQR compared with PID in a trajectory tracking experiment [46]

In another research, Martins et al. [48] explored the use of LQR control to achieve accurate trajectory tracking of a quadrotor aircraft. To apply the LQR method, they first derived and linearized the aircraft model around the hover condition. A Kalman filter was also used to estimate the attitude of the aircraft. The suggested control approach was validated both in simulation and on a real quadrotor UAV, demonstrating good tracking performance. The results revealed that the simplified dynamic model was sufficient for the nominal flight situation, and that the root mean square errors for trajectory tracking were nearly identical in both simulation and real flight. However, the proposed method was not evaluated under the impact of disturbances and model uncertainties.

In reference [49], the LQR control with gain adjustment is applied for the attitude and position control of the quadrotor vehicle. In that study, the quaternion representation was used to describe the vehicle orientation. In addition, the controller's gains were tuned for two distinct scenarios: when the aircraft is far from the targeted trajectory and when it is already tracking. To achieve fast trajectory tracking when the vehicle is far from the desired path (large tracking errors), the controller's LQR gains are set higher, but this can result in overshoot and undesired oscillations as the vehicle approaches the planned path. To address this issue, the gain adjustment method automatically reduced the controller's gains to smaller values once the tracking errors dropped below some specific thresholds. The authors highlighted that the proposed strategy increases tracking accuracy and reduces overshoot. However, the practicality and robustness of the proposed method were not verified.

Table 1.3 summarizes the advantages and disadvantages of linear approaches.

Table 1.3: Linear controllers and their main characteristics.

Method	Advantages	Disadvantages
PID	- Simple design - Easy to implement -Less energy consumption	- Lack of adaptiveness and robustness -Less disturbance resistance
LQR	-Produce very low steady-state error -Good transition response	- Slow parameters update - Rigorous robustness can't be ensured

Some features of linear control approaches are the simplicity and facility of control development and implementation. Most of these strategies are based on linearized models. However, quadrotor dynamics is nonlinear. In addition, a high inter-axis coupling exists between the vehicle outputs. Obviously, the simplification of the dynamical model can negatively influence the representation of reality and become an additional source of unmodeled uncertainties. In addition, the accuracy of linear strategies would deteriorate significantly when the system departs from its operating point. Also, linear control approaches are inapt to ensure robustness against disturbances. Practically, it is very compulsory to consider the system nonlinearities when designing a flight control system.

1.4.2 Nonlinear control approaches

1.4.2.1 Backstepping

Due to its flexibility and systematic design procedure, the Backstepping Control scheme (BC) has drawn increasing attention among the most commonly used control approaches for quadrotor UAVs. These features effectively reduce the complexity of high-order systems [50]. Furthermore, it offers a good solution to account for nonlinearities. In fact, the BC strategy is more convenient for lower triangle systems (see Eq. 1.2) [51], to which the quadrotor model belongs. The key idea of the BC approach is to subdivide the full control design into a set of sub-controllers identified recursively. The BC design theory relies on the use of some state variables as "virtual controls" to stabilize other variables via state-space representation. This technique entails two steps: in the first, the tracking error and its derivative are defined, then the first Lyapunov function is selected, and a virtual control is introduced to ensure the convergence of the error vector. Afterwards, the tracking error related to the aforementioned virtual control and the augmented Lyapunov function are defined, and finally the control law is extracted in such a way that the Lyapunov function is positive definite and its derivative is negative.

$$\begin{aligned} \dot{x}_1 &= x_1 + f_i(t, x_1) \\ \dot{x}_2 &= x_3 + f_2(t, x_1, x_2) \\ &\cdots \\ \dot{x}_{n-1} &= x_n + f_n(t, x_1, x_2, \cdots, x_{n-1}) \end{aligned} \tag{1.2}$$

With $x = [x_1, x_2, \cdots, x_n]^T \in \mathcal{R}^n$ represent the system state, $f_i(t, x)$ corresponds to the system's nonlinearities.

Motivated by the recursive design procedure of the BC methodology, several successful attempts to apply this method for stability and trajectory tracking purposes have been reported in the literature. Bouabdallah and Siegwart [52] employed the BC approach and the sliding-mode control for the attitude stabilization of a mini indoor quadrotor . The suggested methods were simulated using MATLAB/Simulink software. Subsequently, the control systems were tested on a test bench. According to the results of the comparison, the tracking performance of the SMC is less performant than that of the BC approach due to high frequency oscillations in the control signals.

The backstepping method was successfully employed in other works, as it is simple to implement in real time. For instance, in reference [53], the BC strategy is adopted for the control of the quadrotor's translational and rotational movements. Experimental flight tests were conducted to examine the effectiveness of the adopted approach in path tracking missions. As can be observed in Figure 1.10, the BC method enable the aircraft good tracking accuracy. Moreover, the authors highlighted that the BC strategy can provide lower tracking errors and reduces the integral absolute error index by $8,13\%$ for the x motion and by $12,46\%$ for y motion compared to the proportional-derivative (PD) controller. In a similar research, Rodriguez et al. [54] have presented a study of the position and attitude control of the quadrotor aircraft using the BC method. The control algorithm is first developed using Lyapunov theory and then experimentally validated in a path tracking task. Finally, using the developed BC method, the quadrotor UAV was employed in a flight mission to identify pests in maize crops. The authors reported that the BC strategy improved the flight accuracy, which reduced the number of erroneous images of the crops.

In reference [55], a comparative study in term of attitude/position regulation is conducted between three control algorithms: PID, Sliding mode control and Backstepping. It was found that the PID controller provides slower response and causes high overshoot during attitude stabilization. Also, the PID controller cannot ensure stability when the system operate far from the hovering condition. In term of rapidity, the BC method could guarantees faster response with reduced overshoot. The generated control signals are more smooth compared to the PID and SMC. However, no test of robustness was conducted in that research.

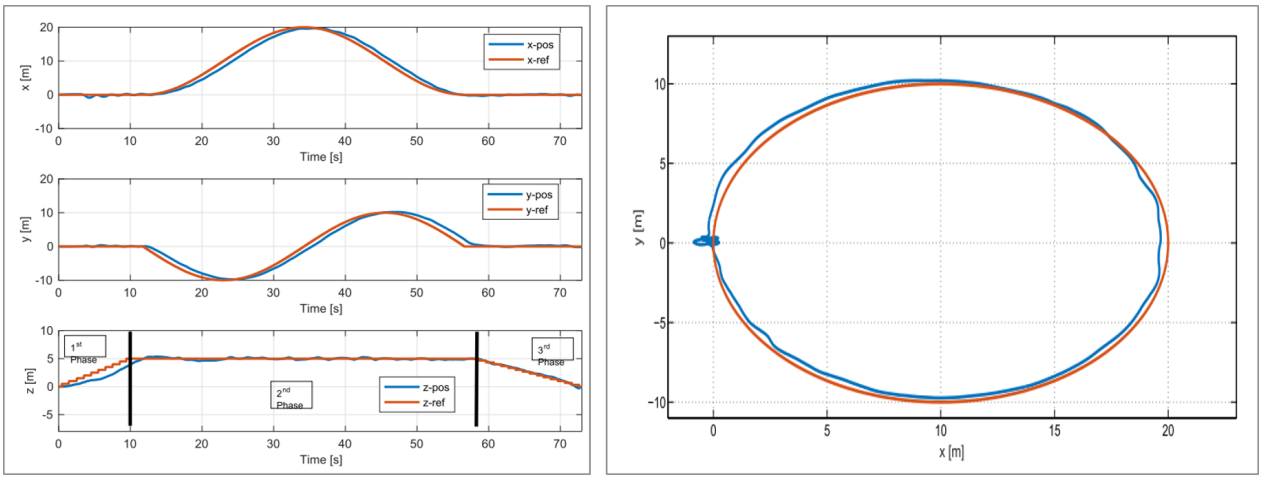

(a): Quadrotor's position during the flight mission

(b): x vs y during the flight mission

Figure 1.10: Trajectory tracking of a quadrotor drone using the BC method [53]

The effectiveness of the BC strategy depends on the correct choice of the controller's gains. However, there is no standard for choosing the appropriate configuration of the BC parameters. To deal with this problem, Rodríguez-Abreo et al. [56] suggested an automated tuning approach for the BC strategy's parameters using the genetic algorithm. Numerical simulations were presented to validate/highlight the outperformance of the proposed method compared to the linear PID controller. The same principle of optimization was adopted in [57] by using the ant colony optimization algorithm. The results demonstrated effective stability and path tracking. Other optimization methods, such as PSO, genetic algorithms, and gravitational search, have been developed to address the problem of choosing the BC parameters; see for examples references [58–60]. Although the BC provided quick tracking of the commanded trajectories, it cannot ensure strong robustness to external perturbations and to model uncertainties, when used alone.

As a solution to improve the robustness of the BC strategy and to eliminate the possible error in the steady state, Integral BC (IBC) is employed in some studies to steer the quadrotor motions during flight [61]. In their research, Xuan-Mung and Hong [62], developed a robust control system for unmanned quadrotors affected by disturbances, uncertainties, and input saturation. The proposed method is based on the BC strategy running in parallel with an Extended State Observer (ESO). The latter estimates the unmeasured states as well as the unknown aerodynamic factors. In comparison to several existing methodologies, the findings showed that the recommended methodology was more accurate, smooth, and robust. Shao et al. [63], developed a backstepping output feedback strategy based on a dual-loop control scheme for the robust tracking control of a quadrotor UAV. The proposed method is applied to the translational and rotational dynamics in the occurrence of disturbances and uncertainties. In addition, a high-order ESO is developed to estimate some unmeasured state as well as the external perturbations. The findings revealed the robustness of this approach in dealing

with external disturbances.

1.4.2.2 Feedback Linearization (FBL)

The fundamental idea behind this approach is to algebraically transform the system nonlinearities, whether completely or partially, into a linearized model by an adequate feedback law [64]. This makes it possible the use of linear controllers. Different from the conventional techniques of linearization, which are based on some linear approximations of the system dynamics, the FBL results from an exact transformation.

The study in [65] investigated the tracking control of a quadrotor aircraft using the FBL approach. The obtained results highlighted the convergence of the velocity and the yaw angle to the reference value. However, disturbances like aerodynamic drag forces and parametric uncertainties were not considered when designing the control. Lee et al. [66] compared the performance of two nonlinear control schemes, namely, the adaptive sliding mode control and the FBL control. Under nominal flight conditions, the FBL method provided satisfactory tracking with fast stabilisation of the quadrotor position and attitude, and without being influenced by the chattering problem. However, considering the influence of noise and parameter uncertainty, the FBL method does not guarantee closed-loop stability, resulting in a divergence of the state variables. They demonstrated that the FBL method cannot not ensure robustness when used alone.

Several proposals have been introduced to provide FBL control with robustness against uncertainties and disturbances. For instance, in reference [67],a flight control system was developed for a quadrotor aircraft to control its position and orientation. To achieve this, the proposed method utilizes an attitude controller to direct the aircraft to the desired orientation, while a position controller is used to track the planned 3D trajectories. The proposed approach incorporates the FBL method and the High-Order Sliding Mode Observer (HOSMO). The suggested method is evaluated by simulation considering some aerodynamic force/torque perturbations. The acquired findings highlight the accuracy of the HOSMO in estimating both unmeasured states and disturbances. The authors demonstrated that this combination ensure system stability in both nominal and perturbed flight tasks. Mokhtari et al. [68] developed a state observer-based FBL controller to ensure the controllability of the quadrotor UAV under wind disturbances and uncertainties in the mass and inertia matrix. They showed that the proposed algorithm can provide satisfactory results even under 20% of uncertainties. In addition, the authors mentioned that the observed gain should be selected carefully as a larger gain may result in additional noise. In another similar work, Aboudonia et al. [69] applied the FBL control in conjunction with a disturbance observer to control a quadrotor aircraft. The simulation tests highlight the capability of the proposed method to reduce the influence of unmodeled dynamics, wind disturbances, and 40% of the loss of efficacy in one actuator. More recently, Eltayeb et al. [70] examined the performance of an adaptive FBL controller in comparison with the conventional FBL controller. The

control scheme is developed to achieve precise tracking of the targeted altitude and attitude trajectories. Under pulse-type disturbances and load change, several flying scenarios were examined in terms of attitude stabilization and trajectory tracking. The obtained results revealed that the adaptive FBL outperformed the traditional FBL.

1.4.2.3 Sliding mode controller

Among all the control strategies for unmanned quadrotors, Sliding Mode Control (SMC) stands out for its strong robustness in the face of model inaccuracies and perturbations. The key idea of the sliding mode theory is to design a sliding surface then extract the control law that can drive and maintain the system state into the predesigned sliding manifold until reaching the equilibrium. One primary limitation of the SMC is the occurrence of the chattering phenomenon, which is a high-frequency vibration around the equilibrium point (see Figure 1.11) [71]. Such a problem results in poor accuracy of the control system, actuator wear and high heat losses. Some ideas have been proposed to avoid this problem or at least reduce its negative impact. The simplest method to surround this phenomenon is to adopt a continuous approximation of the switching law using a saturation function, an hyperbolic tangent function, or a sigmoid function [72].

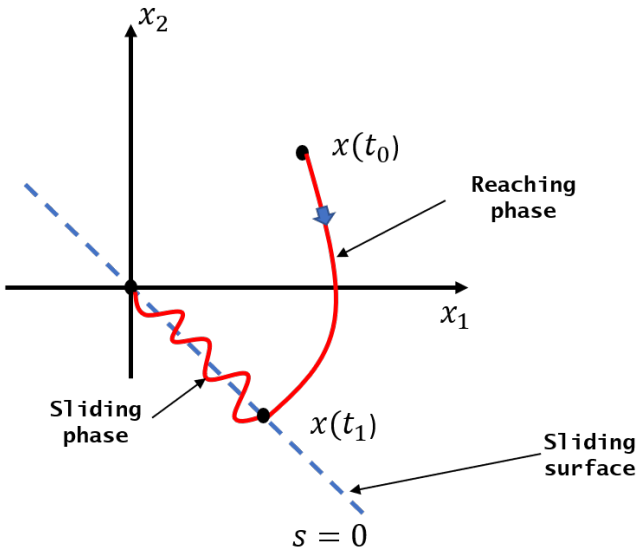

Figure 1.11: Chattering phenomenon

In reference [73], four control methods, namely the PD, BC, inverse dynamics, and SMC, were developed and used to drive the quadrotor's attitude. The comparison in terms of stabilization in the presence of noise highlights the faster transition and reduced tracking error of the SMC method. In another work, Noordin et al. [74] used the SMC for the attitude and altitude control of a quadrotor aircraft subjected to gaussian noise disturbances. Then, they used a saturation function instead of the sign function to reduce the amount of chattering. The accuracy of the proposed controller was assessed via some simulation tests in the pres-

ence of gaussian noise. The results show that the adopted controller can ensure stability and robustness; however, a high level of chattering is noticed in the control signals, which can degrade the performance in real flight. The work reported in [75] investigated the stability and tracking control of a quadrotor vehicle using a control scheme based on the integral SMC method. The simulation results show that the proposed method is robust and quickly eliminates tracking errors. However, the chattering phenomenon cannot be alleviated using this strategy.

In [76], a chattering-free control algorithm based SMC approach is developed for the quadrotor altitude flight. The authors used a continuous high-slope saturation function rather than the conventional sign function, which significantly reduce the chattering influence. Then, a real-time implementation of proposed method was carried out to confirm its performances. From the obtained results, it was clear that the aerial vehicle achieved the desired altitude position in less than 3 seconds. Moreover, during the hovering maneuver, improved flying performances were attained using this approach. Authors of [77] proposed a nonlinear control scheme for the trajectory tracking purpose of a quadrotor aircraft in the presence of perturbations. The proposed method merges two popular algorithms, namely the integral BC and the conventional SMC(CSMC) techniques. Instead of the discontinuous sign function, a saturation function is employed to reduce the chattering impact. Numerical simulations were presented to prove the feasibility of the proposed algorithm, from which the authors highlighted that the proposed method quickly reached the steady state with reduced oscillation compared to PID, LQR, BC and integral BC controllers. In another similar work, Zhou et al.[78] proposed a flight control system based on a saturated integral BC method (SIBC) for the full tracking control of the quadrotor. Simulation as well as experimental outdoor flight were conducted to illustrate the practicality, the accuracy, and the disturbance rejection ability of the suggested method compared to the conventional BC and integral BC techniques. As can be observed in Figure 1.12, the proposed method tracked the desired 3D trajectory with a small deviation. Furthermore, the resulting tracking error was reduced by 80% and 30%, respectively, when compared to the BC method and the integral BC method.

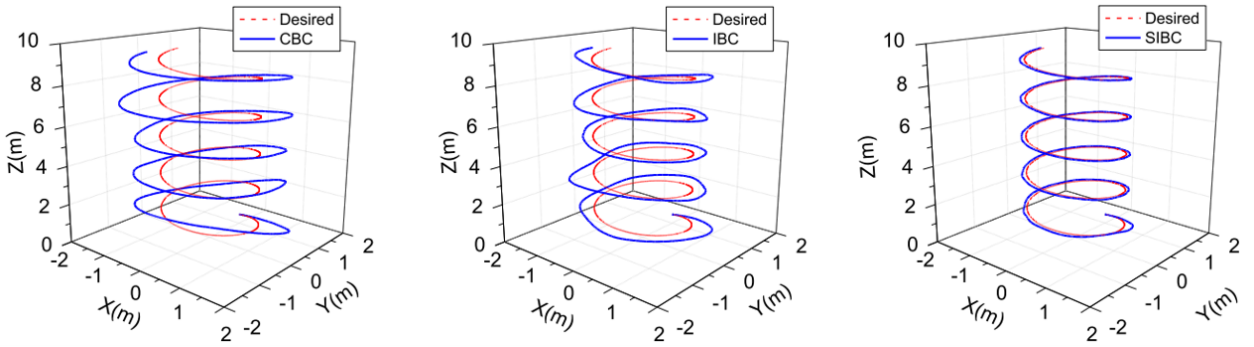

Figure 1.12: Comparison of the SIBC, BC and integral BC methods [78]

When using a continuous approximation of the sign function in the switching control laws, the chattering phenomenon can be reduced, but on the other hand, the system robustness will be degraded. Many solutions have been proposed to mitigate the chattering effect while improving the response time and the system's robustness. The pioneer example of these solutions is the supertwisting (ST) given in Eq. 1.3 [79, 80]. In comparison with the CSMC method, the ST algorithm can offer a smooth response with high tracking precision while lowering the chattering influence without compromising the system's robustness. The chattering mitigation property of the ST algorithm is demonstrated through the continuous nature of its control signals. This is clear from Eq. 1.3, where the sign function is under integration and the term $\beta_1 |S|^{1/2}$ sign is continuous. This characteristic allows the ST algorithm to deliver precise and smooth control signals.

$$U_{ST} = -\beta_1 |S|^{1/2} \operatorname{sign}(S) - \beta_2 \int_0^t \operatorname{sign}(S)\, \mathrm{d}\tau \tag{1.3}$$

With S is the sliding surface. β_1 and β_2 are positive constants.

The ST strategy is among the leading options for controlling quadrotor UAVs. For instance, Munoz et al. [81], developed three control systems based on the ST algorithm for the quadrotor altitude: supertwisting SMC (ST-SMC), Modified Supertwisting SMC (MST-SMC) and Nonsingular Terminal Supertwisting control (NTSTC). To examine the effectiveness of the proposed methods, a detailed theoretical analysis is first presented, followed by an experimental implementation . The obtained results demonstrate the superiority of the MST-SMC, which exhibits the best compromise between algorithm complexity and tracking error. Similarly, Cano-González et al. [82] elaborated a continuous ST-SMC for the tracking control of the quadrotor altitude. The proposed method incorporates a HOSMO to estimate the supposed unmeasured altitude velocity and the unknown disturbances. From the simulation and experimental results, the suggested technique exhibits better performance than the three methods presented in reference [81]. Using the aforementioned techniques [76–83], the robustness and the chattering reduction can be ensured at certain level, but the convergence in short finite-time cannot be obtained.

Multiple strategies have been developed to overcome this issue using some advanced forms of the sliding mode theory. To ensure the convergence in a reasonably finite-time, the Terminal Sliding Mode Control (TSMC) is initially developed [84]. Then, a Fast TSMC (FTSMC) is developed to speed up the convergence when the state is not close to the origin [85, 86]. To guarantee high stability with quick convergence and chattering avoidance, some researchers have developed a global fast dynamic SMC method for a quadrotor [87]. In that work, the Hurwitz method was used to compute the coefficients of the predesigned sliding surfaces. Using this method, the authors demonstrated that the chattering influence is avoided and that the magnitude of the control signals is also reduced. Although these methods realized good tracking, a singularity problem may occur due to the existence of a term with negative fractional power in the sliding surface dynamic (see Table 1.4). Nonsingular TSMC

(NTSMC) [88] can solve this issue but has a slowest convergence speed compared to the FTSMC. Nonsingular FTSMC (NFTSMC) is a robust technique that takes into account all the shortcomings of the CSMC, FTSMC, and NTSMC, then solves them simultaneously, but while preserving their merit and features [89–91].

Table 1.4 provides a summary of the various types of sliding surfaces and their corresponding time derivatives. From the table, it can be concluded that the CSMC method is not prone to singularity issues because it employs a linear sliding surface. On the other hand, the TSMC and FTSMC methods are susceptible to singularity problems because their sliding surface time-derivatives include fractional terms with negative exponents, leading to singularity when the tracking error approaches zero. In contrast, the NTSMC and NFTSMC methods do not suffer from this issue, as their sliding surface time derivatives do not include any singular terms.

Table 1.4: Commonly used sliding surfaces

Method	Sliding surface	Sliding surface dynamics	Remarks
CSMC	$s = \dot{e} + \lambda e, \quad \lambda > 0$	$\dot{s} = \ddot{e} + \lambda \dot{e}$	No singularity
TSMC	$s = \dot{e} + \lambda e^{\nu}$, $\lambda > 0,\ 0 < \nu < 1$	$\dot{s} = \ddot{e} + \lambda \nu e^{\nu-1} \dot{e}$	Singularity will occur when e tends to zero because $\nu - 1 < 0$
FTSMC	$s = \dot{e} + \lambda_1 e + \lambda_2 \lvert e \rvert^{\nu} \operatorname{sgn}(e)$, $\lambda_1, \lambda_2 > 0, 0 < \nu < 1$	$\dot{s} = \ddot{e} + (\lambda_1 + \lambda_2 \nu \lvert e \rvert^{\nu-1}) \dot{e}$	Singularity will occur when e tends to zero because $\nu - 1 < 0$
NTSMC	$s = e + \lambda \lvert \dot{e} \rvert^{\nu} \operatorname{sgn}(\dot{e})$, $\lambda > 0,\ 1 < \nu < 2$	$\dot{s} = \dot{e} + \lambda \nu \lvert \dot{e} \rvert^{\nu-1} \ddot{e}$	No singularity because $\nu - 1 > 0$
NFTSMC	$s = e + \lambda_1 \lvert e \rvert^{\nu_1} \operatorname{sgn}(e) + \lambda_2 \lvert \dot{e} \rvert^{\nu_2} \operatorname{sgn}(\dot{e})$, $\lambda_1, \lambda_2 > 0,\ 1 < \nu_2 < 2,\ \nu_2 < \nu_1$	$\dot{s} = (1 + \lambda_1 \nu_1 \lvert e \rvert^{\nu_1 - 1}) \dot{e} + \lambda_2 \nu_2 \lvert \dot{e} \rvert^{\nu_2 - 1} \ddot{e}$	No singularity because $\nu_1 - 1 > 0$ and $\nu_2 - 1 > 0$

In Figure 1.13 we summarized the main characteristics of the above-reviewed variants of the Slinding Mode Control, SMC.

Although the outstanding features of the aforementioned works involving stability and trajectory tracking, the robustness of these controllers hugely depends on the precise knowledge of the disturbances' upper bound, which is difficult to obtain. As a result, it is necessary to incorporate an adaptive mechanism in order to approximate the value of this constraint.

1.4.2.4 Robust Adaptive Controllers

In order to improve the system's robustness against unmodeled dynamics and to overcome the necessary criteria of the disturbance upper limit prior knowledge, adaptive control laws based on position and velocity tracking errors can be a good solution [92–100]. This type of technique seeks to mitigate the negative effects of model uncertainties by automatically adjusting and changing controller parameters according to the planned trajectory. Figure 1.14 shows the general block diagram of an adaptive control scheme for the quadrotor.

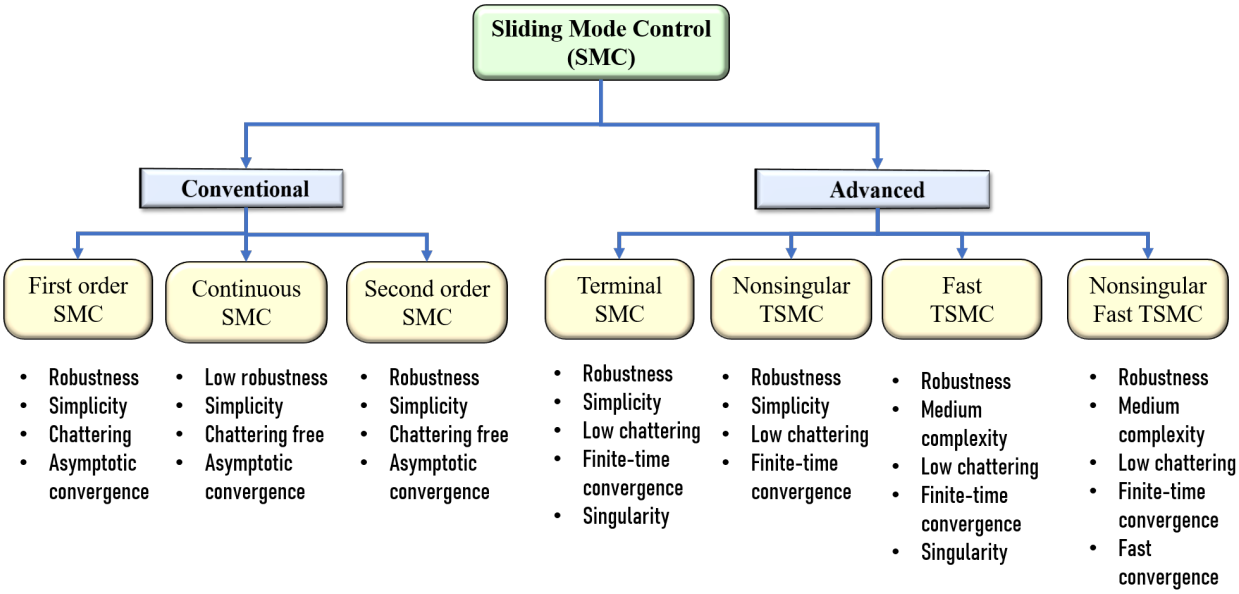

Figure 1.13: Main characteristic of SMC variants

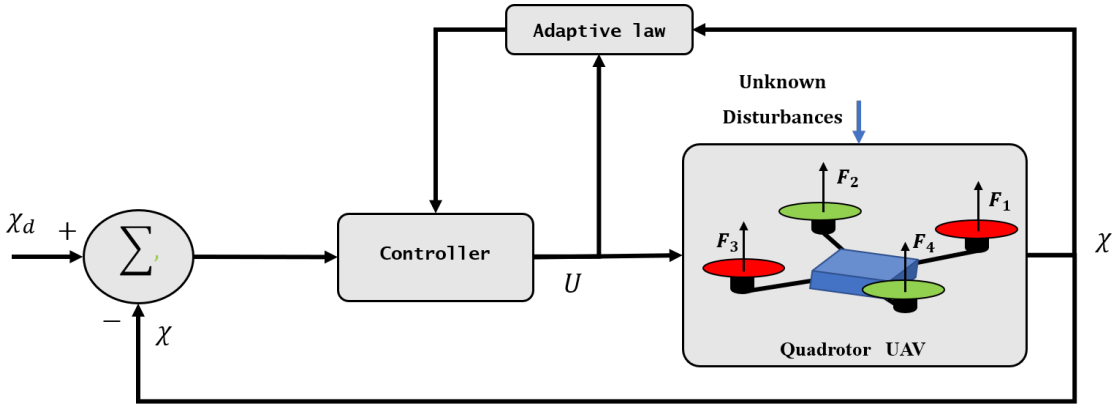

Figure 1.14: General control architecture of an adaptive control law

Thanh et al. [92] investigated the quadrotor's attitude and altitude control in the presence of unknown perturbations. The proposed algorithm is based on an adaptive SOSMC with a PID sliding surface. The adaptive law is used to approximate the upper limit of external perturbations, which enhances the controller's robustness. The obtained results highlight the robustness and the chattering reduction abilities of the proposed controller. Though the method provides robust stabilization in the existence of complex disturbances, the problem of path following was not investigated in this work. In reference [93], an adaptive sliding mode altitude tracking control is developed for a quadrotor UAV subject to the influence of time-varying load. To deal with parameter uncertainties caused by load variation and ground effect, an adaptive rule is introduced. Numerical as well as experimental tests are conducted to examine the performance of the proposed controller compared to the PID con-

troller. The results show the superiority of the adaptive controller with its faster response and robust behavior against load variations. Similarly, Hassani et al. [94] presented a robust control system for the quadrotor's position and attitude based on an adaptive double power reaching law. They compared the proposed controller with both the PID and CSMC in some simulation tests, considering the influence of time-varying disturbances and parameter uncertainties. The finding shows that the developed controller can provide better results with faster response and less tracking errors.

In another study, Basri. [95] developed a robust BSMC with adaptive switching gains for guiding the quadrotor aircraft in the existence of wind disturbances. Rather than the discontinuous sign function, a saturation function is used in the switching control, which further reduces the influence of chattering. Selecting the appropriate BSMC parameters can be challenging since there is no known standard for that purpose. Basri tackled this issue by using a PSO algorithm to automate parameter selection and improve the controller's performance. The author reported that the proposed method reduces the integral absolute error by 75.70% compared to the optimal BC controller. The work in reference [96] presents the development of a robust control system for a quadrotor drone, whose mass is uncertain due to variable loads. The proposed approach uses the sliding mode control (SMC) method, where a linear sliding surface is enhanced by a fractional-order derivative to achieve better performance. In addition, an adaptive control law that utilizes a load-correcting factor is developed to enhance the robustness of the control system. The adaptive control law estimates the variable load in real time and adjusts the generated control inputs accordingly. As a result, stable flight is guaranteed, regardless of changes in the load conditions. Although the aforesaid approaches provided good tracking accuracy, the convergence in finite-time has been ignored in these researches [92–96].

By using an adaptive updating mechanism to approximate the upper limit of the unknown disturbances, an adaptive integral TSMC method is elaborated in [97]. The control scheme is applied for the guidance of the position and orientation of the quadrotor in the existence of state inaccuracies, external disturbances, and measurement noise. Numerical tests validated the performance of the proposed method. As an extension of the last cited article, Mofid et al. [98] designed an adaptive supertwisting integral TSMC for a quadrotor UAV under model uncertainty, wind disturbances, and input delay. The comparison with the adaptive PID controller revealed the outperformance of the suggested method in terms of rapidity, robustness, and chattering alleviation. Experimental tests are also conducted to confirm the practicality of the proposed controller.

An adaptive finite-time controller that combines the integral BC and the FTSMC is proposed for the regulation of the position and orientation of an uncertain quadrotor exposed to wind disturbances [99]. The proposed method presents some improvements in terms of robustness, quick convergence, and tracking precision. However, a term in the sliding surface

dynamics has a negative fractional power (see Table 1.4), which might lead to a singularity problem. In reference [100], the control of the attitude and altitude of the quadrotor is considered by designing two adaptive nonlinear control schemes. To accomplish the tracking control in finite time, an adaptive NTSMC is first developed. Then, an Adaptive Super-twisting TSMC (ASTTSMC) is suggested in order to maintain the property of convergence in a limited time while reducing the chattering impact without compromising the system's robustness. It has been proved that both strategies provided enhanced performance with a superiority of the ASTTSMC in term of chattering avoidance. However, there was no practical validation for this strategy.

1.4.2.5 Hybrid controllers

In order to maintain the advantages of various techniques while removing their drawbacks, cooperative control strategies, also known as hybrid control algorithms, can be used. This results in an improved controller with more features and fewer drawbacks.

In order to tackle the influence of bounded uncertainties and external disturbances, Almakhles [101] divided the quadrotor dynamics into a position and an attitude subsystems. The diagram of the proposed control architecture is shown in Figure 1.15. As can be seen, an integral SMC method is adopted to manage the quadrotor position while a robust BSMC is used for the tracking control of the quadrotor attitude. Simulation experiments are performed to evaluate the performance of the proposed control algorithm. It can be concluded that, in the absence of perturbations, the proposed method allows the drone to reach the desired altitude position in one second with reduced overshoot. In the presence of Gaussian noise and wind perturbations, the vehicle completed the fly mission successfully, but introduced chattering in the control signals. In addition, the tracking errors in the y displacement were considerable compared to the other movements. Specifically, the maximum deviation from the desired trajectories was 0.5 m for the x position, 1.9 m in for the y position, and 0.05 m for the z position.

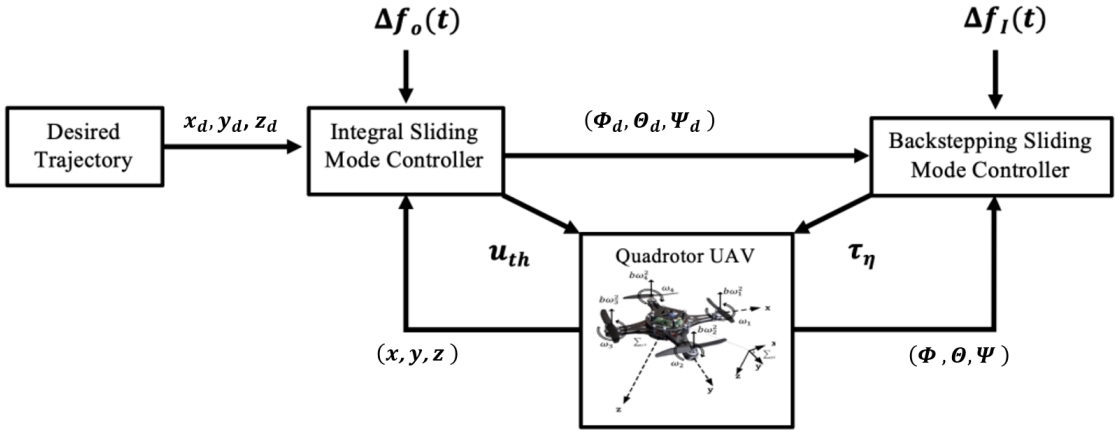

Figure 1.15: Block diagram of the of an hybrid controller based on the integral SMC and the BSMC [101].

In another similar work, Chen et al. [102] developed a robust stabilizer and tracker for the quadrotor aircraft. The solution developed uses a BSMC controller to drive the translational motion and a CSMC method to stabilize the attitude of the vehicle. The robustness of the system is increased by an observer-based fault estimation. In the presence of 45% of uncertainty, Gaussian noise, and actuator faults, the proposed method enables better tracking than the BC controller. The results indicate that the observer accurately estimated constant faults but failed to estimate time-varying faults.

In the work reported in [103], the quadrotor is controlled using a hybrid finite-time control strategy (HFTC). Particularly, the BC technique is utilized to guide the horizontal translation and an adaptive integral SMC is designed for the vertical displacement. In addition, an NTSMC combined with a finite-time disturbance observer is deployed for the attitude subsystem. Simulation experiments under aerodynamic disturbance were conducted, and the results of the proposed method were compared with the conventional SMC and the BC strategy showing good trajectory tracking (see Figure 1.16-a). However, using the BC technique alone to stabilize the horizontal displacement will certainly reduce the system's accuracy when facing complex wind disturbances along the x and y directions. Moreover, as can be seen in Figure 1.16-b the generated control signals are impacted by the chattering influence.

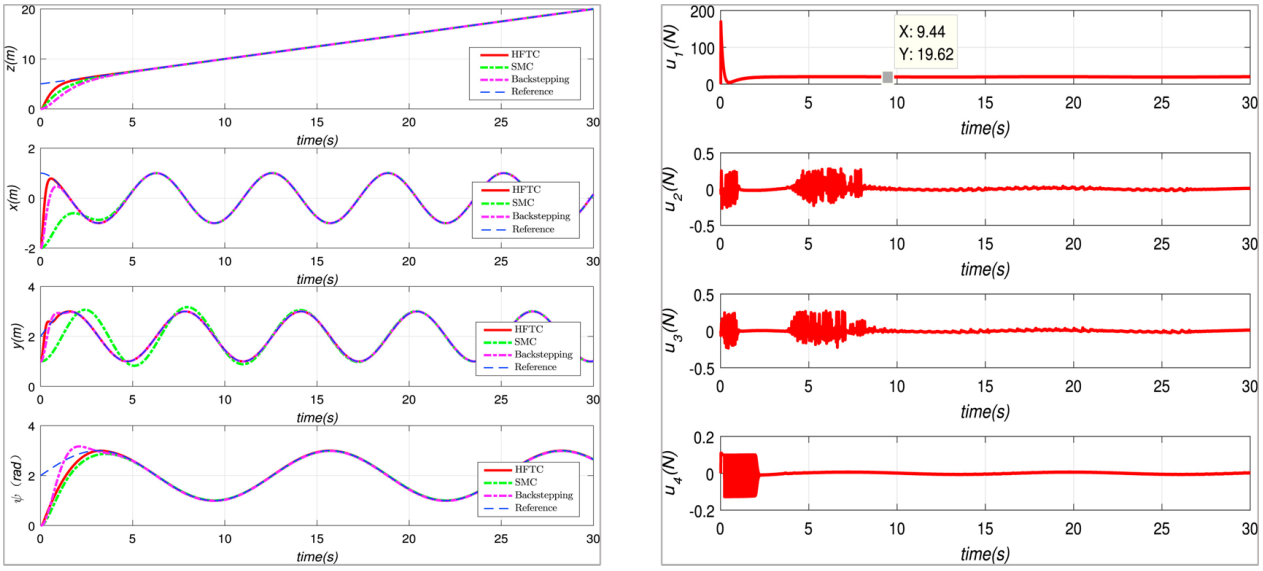

(a): Comparison in term of trajectory tracking

(b): Generated control inputs by the hybrid control

Figure 1.16: Performance of the hybrid controller in a trajectory tracking task [103].

In another paper, Mechali et al. [104] focused on controlling the translational and rotational motions of a quadrotor aircraft using a hybrid control strategy. They first subdivided the full dynamics into a position subsystem and an attitude subsystem. Then, a finite-time

disturbance observer combined with a continuous NTSMC is synthesized for the quadrotor's attitude, while a backstepping integral TSMC combined with an extended state observer is designed for the quadrotor's position. The method was tested through processor in-loop implementation, considering the influence of wind disturbances and model uncertainties (30% in the vehicle's mass and 50% in the matrix of inertia). The obtained results show that the proposed strategy is able to handle uncertainties/disturbances and reduce both steady-state error and chattering phenomena compared to some existing methods. However, the results highlight that this controller achieved the desired altitude by introducing an overshoot.

In reference [105], a hybrid flight control algorithm is developed for an autonomous quadrotor subjected to external disturbances. Figure 1.17 illustrates the block diagram used for the implementation of the proposed hybrid controller. The control design is divided into three parts: a robust integral TSMC-based attitude controller is implemented to provide finite-time stabilization of the vehicle orientation, an adaptive backstepping (AB) controller is applied to control the altitude motion and deal with the mass uncertainty, and a BC method is used to control the horizontal position of the vehicle. Simulation tests are conducted to validate the performance of the suggested strategy during flight tasks affected by sustained disturbances. The findings highlight that the proposed controller can deliver a faster response with reduced deviation from the desired trajectories compared to the BC and SMC methods. However, the influence of time-varying disturbances was not studied in this paper.

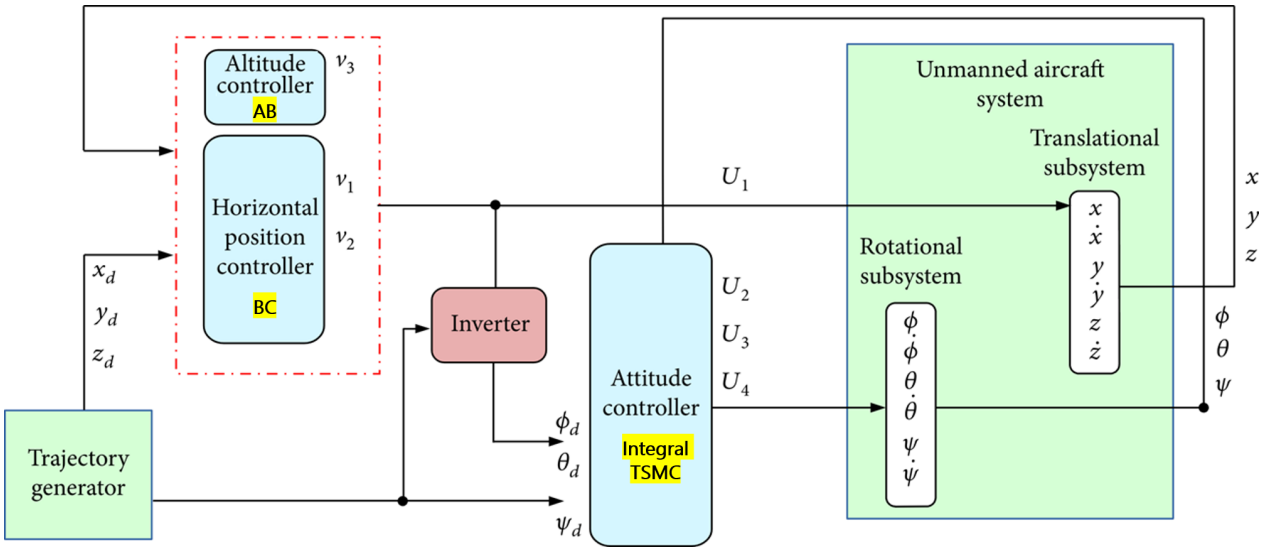

Figure 1.17: Block diagram of an hybrid control scheme based on the IBC, BC and integral TSMC [105].

Modirrousta and Khodabandeh [106] studied the tracking control of the quadrotor aircraft using two sliding mode controllers. First, a backstepping NTSMC with adaptive gains

is applied for the altitude and attitude of the quadrotor to reduce chattering and improve robustness. Second, an integral SMC method combined with a disturbance estimator is used to command the horizontal position of the quadrotor. In addition, adaptive laws are introduced to deal with the unknown bound of external perturbations. Comparative analysis with the PID and BC controllers, emphasized the superior performances of the suggested controller in terms of disturbance rejection. The results shown in Figure 1.18-b, on the other hand, indicated that the observer takes a long duration to estimate the disturbances whenever the vehicle changes directions. Moreover, the values of the adaptive gains are large, which can result in large magnitudes of the control inputs when following trajectories with abrupt changes.

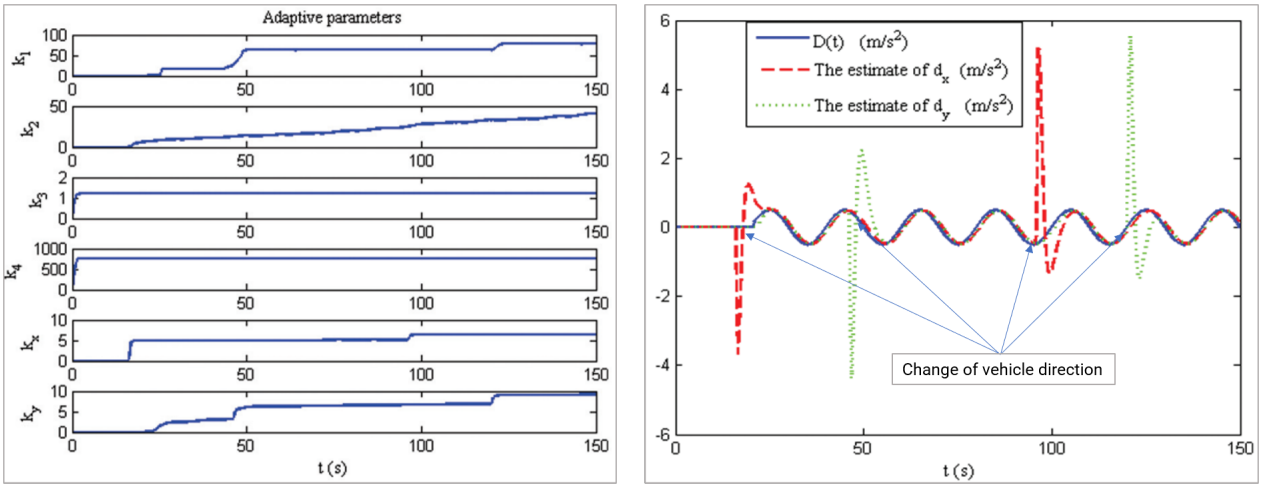

(a): Adaptive gains (b): Disturbances estimation

Figure 1.18: Time evaluation of the adaptive gains and disturbance estimation [106].

Those studies show that, the synergic combination of different control algorithms can provide good results.

Although linear controllers are much simpler to implement, non-linear controllers are known to be conceptually difficult and require more study to understand their operation. Nonlinear controllers offer a significantly larger operating range in which the entire dynamic system can be evaluated and nonlinear aerodynamic effects can be accounted for, whereas linear controllers have a much smaller operating range. These controllers also offer others advantages like robustness, flight accuracy, disturbance rejection, and fast trajectory tracking. However, only a few experimental works are conducted using these strategies. Tables 1.5 and 1.6 summarize the advantages and limitations of the nonlinear controllers.

The comparison in Tables 1.6 and 1.5, as well as the previous discussion about nonlinear controllers, reveal the shortfall of single solution to effectively control and stabilize the quadrotor. However, the NFTSMC and NTSMC controllers are recognized in many studies

to provide fast convergence with good robustness against uncertainties and disturbances. The performance of these methods can be improved by introducing adaptive laws to provide more adaptation during the flight missing. Another improvement is to use some perturbation estimators to effectively compensate for the influence of complex disturbances.

Table 1.5: Nonlinear controllers and their main characteristics.

Method	**Advantages**	**Disadvantages**
Bc	- High accuracy - Fast response - Small overshoot - Good robustness to the known uncertainties	- Large magnitude control signals - Requires the access to the full state - Less adaptiveness - Not robust to unknown uncertainties
FL	- Simple design - Smooth control	- Needs an exact model - High sensitivity to parameter changes - Less adaptiveness - Sensitive to sensors noise
SMC	- Precise path tracking with reduced error - Robust to unmodeled dynamics - Simple structure and easy parameter tuning - Asymptotic convergence	- Its stability depends on the upper limit of external disturbances. - Chattering effect - Considerable energy consumption
SOSMC	- High robustness - Chattering free - Fast response	- Complex structure - Information about external perturbations is required
TSMC	- Invariance to modeling uncertainties - Convergence in finite time - Fast transition	- Slow convergence when the system is far from the origin - Singularity problem - Large control signals
NTSMC	- Convergence in finite time - Singularity free	- Slow convergence when the system is far from the origin - Require information on the perturbation upper bound

Table 1.6: Nonlinear controllers and their main characteristics. (Continued)

Method	Advantages	Disadvantages
NFTSMC	- Robust to the modeling uncertainties \perturbation - Short finite time convergence - Singularity free	- Needs the precise knowledge of the disturbance upper bound
Adaptive controller	- Rapid in convergence and transition - Robust and accurate	- Parameters drift in case of high level of noise - Requires complex adaption laws
Hybrid controller	- Good adaptiveness to the model variation - Robustness	- Computational difficulties

1.4.3 Inteligent controllers

1.4.3.1 Neural networks

Neural Networks (NN) based control for unmanned flying machines is becoming more and more used to compensate for the induced effects of model uncertainties and unknown endogenous/exogenous disturbances.

In reference [107], an adaptive control law using neural network is adopted to control the quadrotor aircraft. The adaptive law is adopted to approximate the unknown limit of the external perturbation, while the NN is used to estimate the unknown uncertainties. Simulation tests under state uncertainties are conducted showing that the suggested method can ensure stability during the flight task. However, the finite-time convergence was not considered in this research. To solve this issue, Özhan and Güzey [108] improved their previous study by adopting a finite-time sliding mode algorithm to control a quadrotor aircraft with a suspended payload. The sliding mode controller is used to guarantee the controllability of all the states, while the NN is used to estimate the uncertain dynamics and reduce chattering. The results highlight the outperformance of the suggested method based on the NN over the conventional and finite-time SMC approaches regarding robustness and chattering mitigation.

In another paper, Razmi. [109] developed an adaptive NN-based flight control for an unmanned quadrotor. In that study, the Newton-Euler principle is used to derive the quadrotor dynamics. Figure 1.19-a highlights the adopted control structure with two main controllers:the lateral, longitudinal, and yaw motions are controlled using a second-order sliding

mode controller, while the adaptive SMC-based NN is introduced for the flight altitude to compensate for the influence of uncertainties in the quadrotor mass. In the presence of 10% uncertainty in the quadrotor mass, a comparative simulation test was performed with the SOSMC. The obtained results demonstrate the proposed method's ability to deal with uncertainty in the quadrotor mass (see Figure 1.19-b). However, the influence of disturbances was not assessed in this paper. In a follow-up to their earlier work, Razmi and Afshinfar [110] presented an adaptive SMC based-NN for the tracking control of a quadrotor UAV. The proposed method was used for all the state variables, unlike their previous work [109]. The parameters of the switching control were estimated online by using NN. Simulation experiments under parametric uncertainties and external disturbances were conducted to check the advantage of the proposed method compared to the SOSMC. Comparative analyses show the superiority of the proposed method, which reduced the settling time by 30.89% and the overshoot by 44.55% and 21.45%, respectively, in the x and y directions.

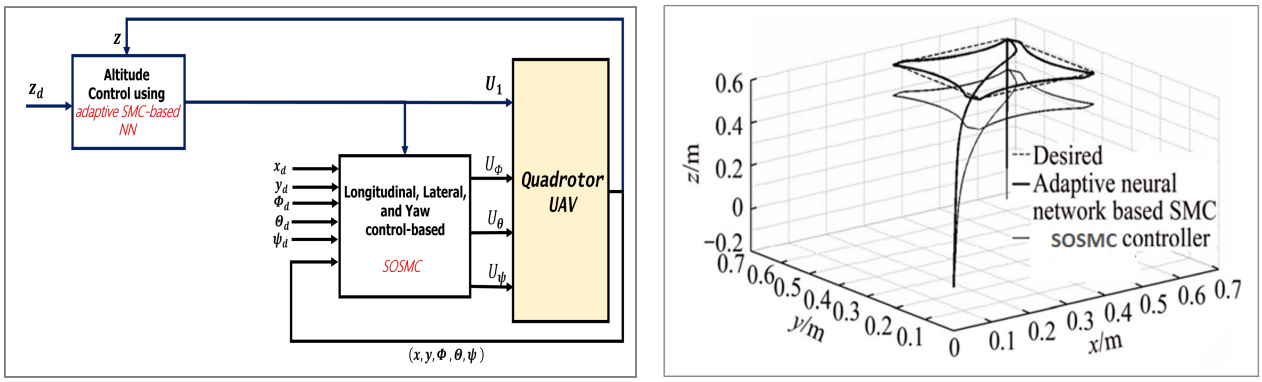

(a): Flow chart of adaptive SMC-based NN for altitude flight control

(b): Comparison of the adaptive SMC-based NN and SOSMC

Figure 1.19: SMC-based NN flow chart and obtained results [109].

In a recent article by Yanez et el.[111] , an adaptive NN-based PID controller is adopted for the stabilization and path tracking of the quadrotor UAV. In that research, NN was used for the real-time adaptation of the PID controller gains, thus improving the performance of the adopted control algorithm. A perturbation estimator is used to estimate the disturbances affecting the vehicle dynamics. These estimations are used within the developed controller, thus improving the robustness of the control system. To validate the proposed method's performance, multiple simulation tests are executed under various operating constraints. The findings show that the proposed method gives a good response to disturbances and mass variations.

In reference [112], a robust position and attitude control is developed for an underactuated quadrotor under wind perturbations. Figure 1.20 shows the proposed flight control system. It uses an optimized BC controller to ensure the full controllability of the quadrotor vehicle.

The Radial Basis Function NN (RBFNN) is incorporated into the control system to approximate the unknown uncertainties and disturbances. Moreover, a fuzzy compensator is used to deal with the approximation error of the RBFNN. The obtained results confirm the performance of the suggested method in terms of robustness and trajectory tracking. However, the finite-time convergence of the tracking errors was not considered in this work, in addition this controller generates large control inputs, which may cause actuator saturation in practice.

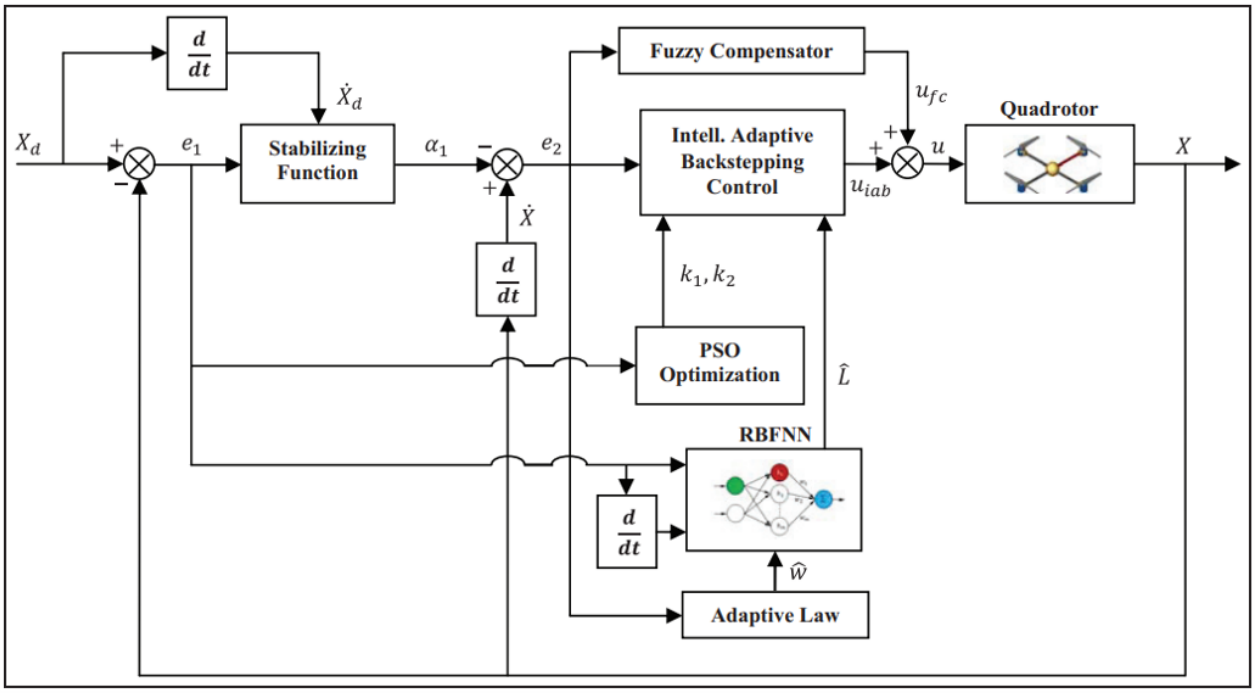

Figure 1.20: Block-diagram of the intelligent BC method with fuzzy compensator [112].

1.4.3.2 Fuzzy logic

Recently, the Fuzzy Logic Control (FLC) has emerged as powerful method to handle the system nonlinearities without the requirement of its precise mathematical model [113]. The fuzzy controller, in particular, has gained popularity on quadrotor system, both as a standalone technique or in combination with other algorithms. Al-Mahturi et al. [114] introduced a robust control system for the quadrotor UAV, where two proportional-derivative controllers combined with an adaptive fuzzy TSMC are used to stabilize the quadrotor and follow the targeted trajectories. Specifically, the PD controllers generate the desired attitude angles, and the TSMC regulates the speed of the rotors, while adaptive fuzzy logic is used to identify the external disturbances. Simulation tests and experimental implementation have been performed to validate the efficacy of the suggested method.

In the literature, three distinct types of fuzzy models [115] are widely used, including

the Mamdani fuzzy model [116], Takagi-Sugeno (T-S) fuzzy model [117] , and type-II fuzzy [114].However, designing the control rules and analyzing the closed system stability is not trivial when using FLC. It also takes a long time to tune the controller's parameters, and may be impacted by some approximation errors [118].

1.4.3.3 MPC

Model Predictive Control (MPC) is a type of advanced control that is used to keep the output at the desired operating conditions and set points. The MPC technique is well adapted to robotic systems involving input, output, and state limitations [119]. This control strategy predicts future control actions based on the history of the control inputs [120].However, there is no guarantee of calculation time when employing this strategy. Furthermore, the MPC controller relies on the model's accuracy; as a result, if the model changes due to some inaccuracies in the inertial parameters, for example, the quadrotor mass, the resultant control input may not be appropriate.

Table 1.7 summarizes the main advantages and limitations of the class of intelligent controllers. Clearly, the main disadvantage is the complexity of these algorithms. Particularly, ANN hugely depends on the training algorithm. Furthermore, the identification of the network structure is not easy at all. In addition, the practical implementation of ANN needs the use of powerful hardware due to the intensive computation.

Table 1.7: Intelligent controllers and their main characteristics

Method	Advantages	Disadvantages
Neural Network	- Adaption - No need of exact model - Good robustness to unknown disturbances	- Necessitates a large amount of data for learning - Computational difficulties
Fuzzy Logic	- Adaption - No need of quadrotor precise model	- Not robust to complex disturbances - Takes longer time for parameter tuning
MPC	- Can deal with constraint in inputs/outputs - Robustness	- Slow transition response - Risk of instability if the prediction model is inaccurate

1.5 Conclusion

In this chapter, we have presented a comprehensive overview of various unmanned aerial vehicles, their main classifications, and widely used rotary-wing aircrafts. An in-depth survey of many nonlinear, adaptive, and intelligent control systems developed for quadrotor control has also been discussed. Each control scheme is thoroughly examined in terms of various

performance indices such as robustness, adaptation for various parametric variations, step response, asymptotic convergence, and finite time convergence. The main remarks highlighted from this literature review are as follows:

- In terms of stability, all the controllers reviewed above can provide closed-loop stability in nominal conditions if the control parameters are correctly configured.

- In terms of robustness, linear controllers are incapable of ensuring the system's robustness in the case of disturbances and uncertainties. On the other hand, nonlinear controllers can offer good robustness but have some limitations. For instance, the SMC can compensate for the impact of disturbances. However, its accuracy is degraded by the chattering problem.

- In terms of complexity, linear control approaches are simpler and easier to develop, which explains their wide use in practice. The complexity of nonlinear controllers differs from one method to another. The BC and SMC, for example, are not so complex. However, they do not provide high accuracy when used alone. NFTSMC and NTSMC can provide good consistency between the robustness and the complexity of the algorithm. Intelligent controllers like NN and FL are more complex compared to linear and nonlinear controllers.

Therefore, it can be concluded that synthesizing an adequate control strategy is not trivial. The hybridization and combination of two or more strategies can provide better flight capabilities in both stabilization and trajectory tracking.

2 Quadrotor modeling and control architecture

Contents

1.1 Introduction 6

1.2 Classification of Unmanned Aerial Vehicles 6

1.2.1 Common rotary wing aircraft 9

1.3 Overall control framework: Guidance, Navigation and Control system 10

1.3.1 Navigation subsystem 10

1.3.2 Guidance subsystem 12

1.3.3 Control subsystem 13

1.4 Literature review: recent advance in control strategies for quadrotor UAV 13

1.4.1 Linear control approaches 14

1.4.2 Nonlinear control approaches 21

1.4.3 Inteligent controllers 36

1.5 Conclusion 39

2.1 Introduction

Quadrotor drones and other types of rotary-wing aircraft share several common characteristics in terms of flight principles, communications, and the control system that could improve the system's autonomy. However, control modules for quadrotor UAVs require careful attention due to their intrinsically unstable nature and the additional degrees of freedom in state space that distinguish them from their equivalents. A reliable mathematical model is then needed for the design of a more precise control scheme for these robots.

The purpose of this chapter is to provide the technical information necessary to model the quadrotor by recalling the basics of motion control, kinematic equations, and dynamical model derivation using the Newton-Euler principle. The obtained model will serve as the basis for the control solution's development, simulation, and implementation. For that, the appropriate state-space representation of the quadrotor vehicle is established. Finally, an effective control structure is presented as a method to realize the control of the quadrotor's six degrees of freedom.

2.2 System of coordinates and attitude representation

In order to study the translational and rotational movements of a quadrotor, it is important to define the appropriate coordinate frames. They are useful for defining the relationship between the dynamical variables, which facilitates the calculations.

2.2.1 System of coordinates

Two frames are considered: an inertial Earth frame $\{O_E, X_E, Y_E, Z_E\}$ (E-frame) and a Body frame $\{O_B, X_B, Y_B, Z_B\}$ (B-frame) fixed to the quadrotor center of mass. Both coordinate frames respect the right-hand rule (see Figure 2.1-b).

The E-frame $\{O_E, X_E, Y_E, Z_E\}$ is used to determine the 3 dimensional position of the aircraft with respect to the Earth's surface. The origin O_E is frequently set to the quadrotor starting location. The X_E-axis is pointing in a particular direction in the horizontal plane, while the Z_E-axis is pointing perpendicular to the ground. The right-hand rule is then used to identify the Y_E axis (see Figure 2.1-a).

The B-frame $\{O_B, X_B, Y_B, Z_B\}$ is fixed to the quadrotor. The center of mass of the quadrotor aircraft is set as the origin O_B of the body frame. The X_B-axis is along the arm with Rotor 1. The Z_B-axis is perpendicular to the X_B-axis and points upward. The Y_B-axis is identified using the right-hand rule.

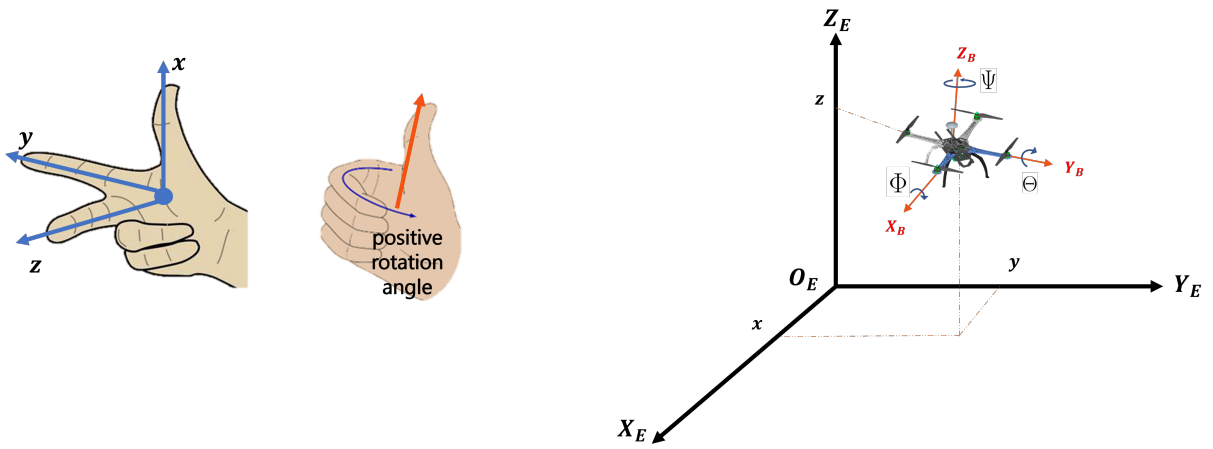

(a): **Right hand rule:** axes orientation and Positive direction of a rotation

(b): Earth $(\boldsymbol{O_E}, \boldsymbol{X_E}, \boldsymbol{Y_E}, \boldsymbol{Z_E})$ and body $(\boldsymbol{O_B}, \boldsymbol{X_B}, \boldsymbol{Y_B}, \boldsymbol{Z_B})$ frames

Figure 2.1: Frame axes using the right-hand rule

2.2.2 Position and Attitude coordinates

The quadrotor translational motion is defined by the Cartesian variables $\zeta = (x, y, z) \in \mathbb{R}^3$ where x, y denotes the state in the horizontal plane, while z is the vertical position.

The orientation of the quadrotor aircraft is represented by three consecutive rotations (see Figure 2.2), known as Euler angles $\eta = (\Phi, \Theta, \Psi) \in \mathbb{R}^3$. These angles reflect the instantaneous orientation of the aircraft in the E-frame.

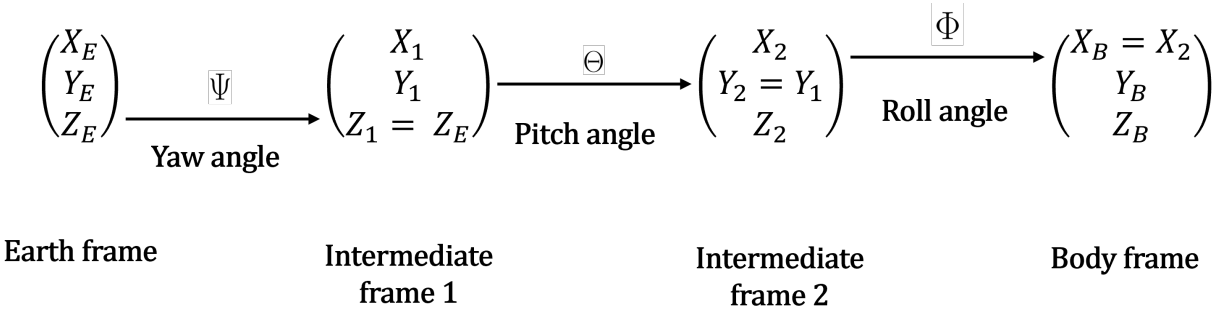

Figure 2.2: Euler angles

- Yaw Ψ: This is a rotation around the Z_E-axis, that correspond to the heading of the aircraft.

- Pitch Θ: This angle defines the rotation around the Y_2-axis.

- Roll Φ: This angle defines the rotation around the X_B-axis.

2.3 Mechanism of flying

A quadrotor is a small rotary-wing aircraft that manages its behavior using four symmetrically positioned propulsion systems (propeller-rotor). To maintain symmetry and avoid overloading one actuator, all electronic components, the microcontroller board, and all sensors are positioned in the middle of the frame. The vehicle takes flight by adjusting the speed of each rotor, resulting in a change in the torque and thrust of the quadrotor system. Specifically, the quadrotor vehicle has six Degrees of Freedom (DOF) to be controlled using only four control inputs. However, neighboring rotors must spin in the opposite direction to counteract the rotational torque of each rotor.

The aircraft's movements are driven by four propellers composed of one or more blades. They present the only sources of aerodynamics. According to the blade element theory, the force and torque created by the propulsion system (propeller + rotor) are determined by the thrust force, the drag moment and the moment due to rotor's thrust [121]. Figure 2.3 shows the force and moments produced by a single rotor.

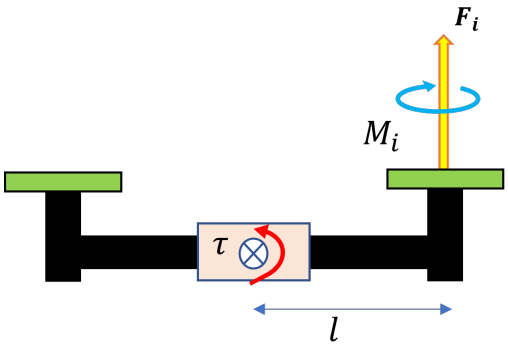

Figure 2.3: Generated thrust and moment by a single rotor

- F_i corresponds to the thrust force, it acts in the z direction, and proportional to the rotor's rotation speed Ω_i. This force can be defined as:

$$F_i = C_T \rho A_p r^2 \Omega_i^2 \tag{2.1}$$

With ρ denotes the air density, r symbolizes the rotor radius, and $A_p = \pi r^2$. C_T represents the thrust coefficient.

Practically, the aerodynamic thrust coefficient can be considered as constant $k_b \approx C_T \rho A_p r^2$. Thus, the thrust force becomes:

$$F_i \approx k_b \Omega_i^2 \tag{2.2}$$

- M_i corresponds to the drag moment, it acts in the same direction of the rotor rotation. This moment can be expressed as:

$$M_i = C_Q \rho A_p r^3 \Omega_i^2 \tag{2.3}$$

With C_Q represents the drag coefficient.

In practice, the aerodynamic drag cofficient can be considered as constant $k_d \approx C_Q \rho A_p r^3$. Thus, the drag moment becomes:

$$M_i \approx k_d \Omega_i^2 \tag{2.4}$$

- τ_i corresponds to the moment created on the quadrotor center of mass due to the rotor thrust. It can be defined as:

$$\tau_i = l F_i \tag{2.5}$$

Where l is the arm length.

2.4 Quadrotor's motions

Within quadrotor UAVs, we differentiate between two configurations: the plus "+" and cross "X" configurations, as shown in Figure 2.4. In the first configuration, roll and pitch motions are obtained by varying the speed of the rotors, which are opposite. For pitching or rolling the quadrotor in cross-configuration, all rotor speeds must be changed. The control of a plus-configuration quadrotor is easy compared to a cross-configuration. That's why the plus-configuration is the most used for acrobatic flying, while the load on the rotors is equitably distributed in the cross configuration [122].

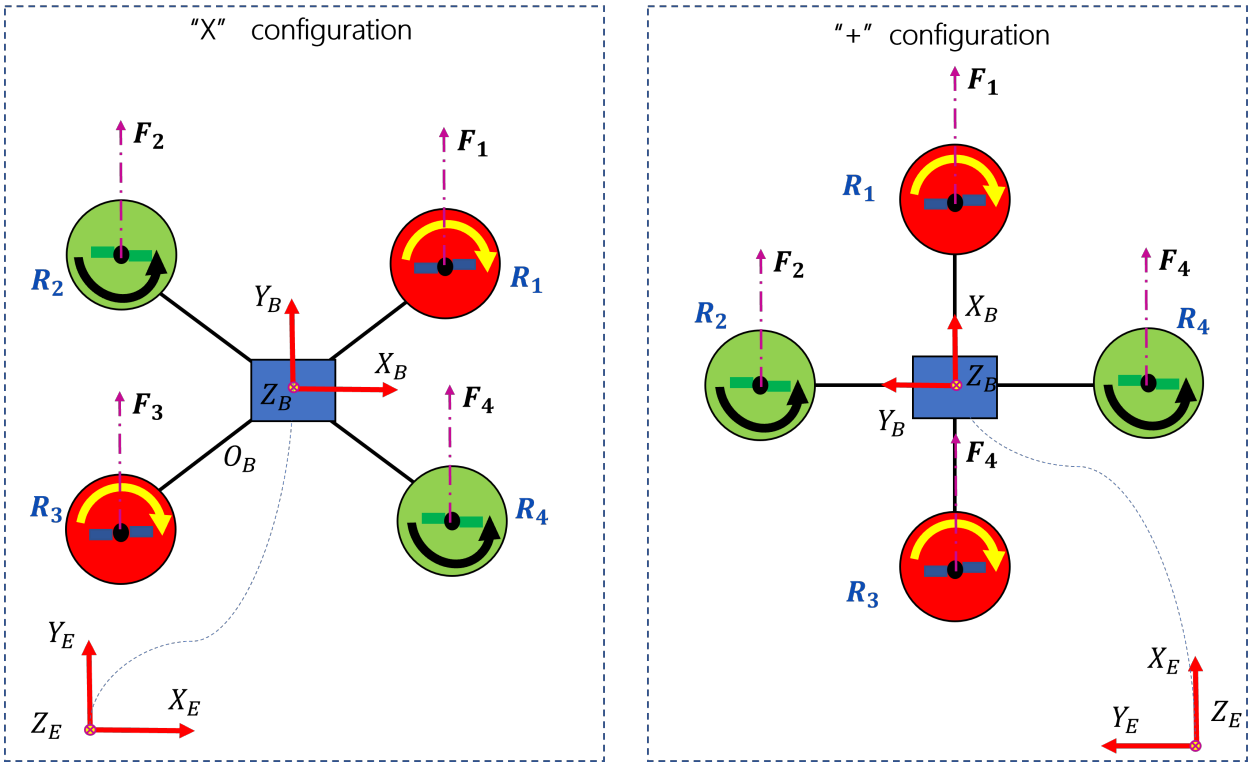

Figure 2.4: Quadrotor's configurations

The intuitive way to understand quadrotor's movement is to analyze how the spinning of the individual rotors influences the motion of the aircraft.

Let's have a look at a + quadrotor with two pairs of rotors: pair 1 (rotors R_1 and R_3) rotate in the clockwise (CW) direction, while pair 2 (rotors R_2 and R_4) rotate in the counterclockwise (CCW) direction. The proper allocation of the four rotor speeds enables the vehicle to reach the prescribed position. Figures 2.5 and 2.6 summarize the basic motions of the quadrotor aircraft. The color and thickness of the arrows on the rotors reflect the rotor's speed, where the dark blue arrow indicates high speed while the light blue arrow indicates low speed. The quadrotor's movement is indicated by the purple arrows.

- The vertical motions of a quadrotor vehicle are depicted in Figure 2.5. Depending on the magnitude of the overall lift force generated by the four propulsion systems, a quadrotor can fly upward, downward, or remain stationary. Specifically, the simultaneous change in angular speeds of all rotors by the same amount results in a change in the lifting forces without any overall moment. Once the total lift force is greater than the quadrotor's weight, the vehicle will move up. Otherwise, the quadrotor will descend. The balance between the thrust and the quadrotor's weight leads to a stationary flight.

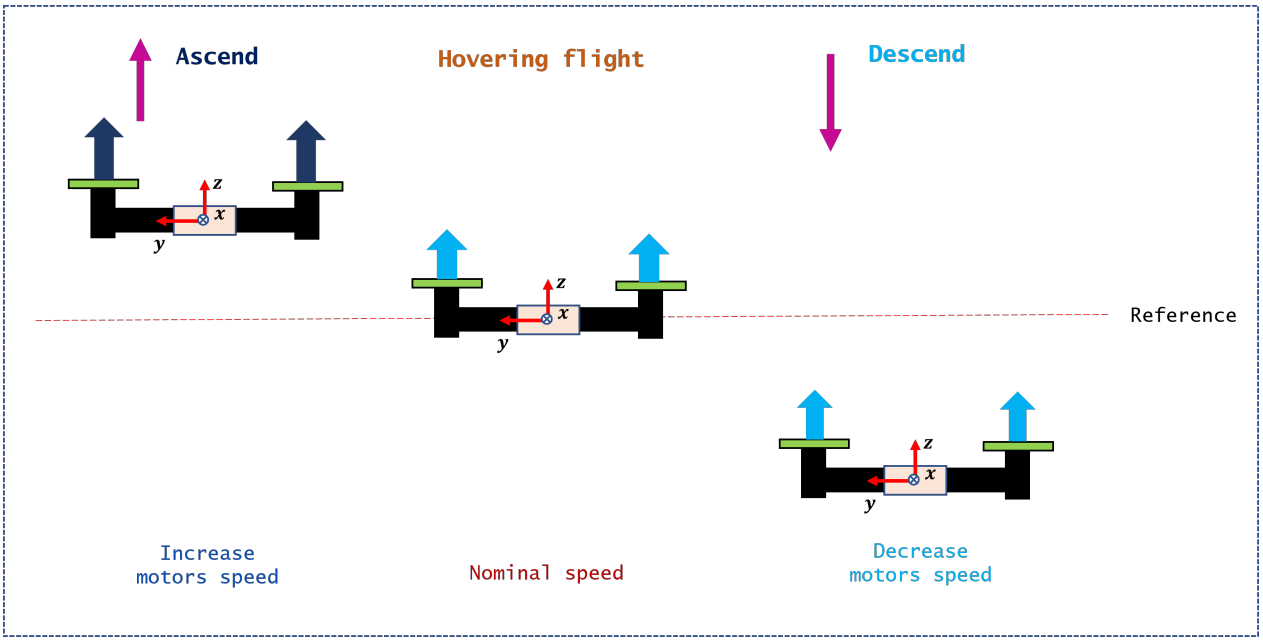

Figure 2.5: Possible vertical motions of a quadrotor aircraft

- Figure 2.6 summarizes the rotational motions and their associated horizontal displacements. Rotational motions are accomplished by applying a speed difference between rotors that are opposite each other. Specifically, rotation around x-axis called roll motion, is achieved by inversely varying the speed of the rotors R_2 and R_4. This rotation is associated with a lateral displacement along y-direction. To control the pitch rotation, rotation around y-axis, we increase (resp. decrease) the speed of rotor R_1 and inversely change the speed of rotor R_3. This motion is coupled with a longitudinal translation along x-direction. The control of heading angle, Yaw rotation, is obtained by varying the average speed between the pair of rotors (R_1,R_3) and(R_2,R_4).

Table 2.1 summarizes the motion control for the quadrotor system based on the speed commands, from which we can see that changing the speed of one rotor will cause either pitch or roll rotation, depending on the selected pair.

From the present analysis, it can be concluded that the vertical displacement as well as the rotational motions are accomplished directly by varying the speed of the four propulsion systems. Whereas, lateral and longitudinal displacement are indirectly governed through roll and pitch rotation.

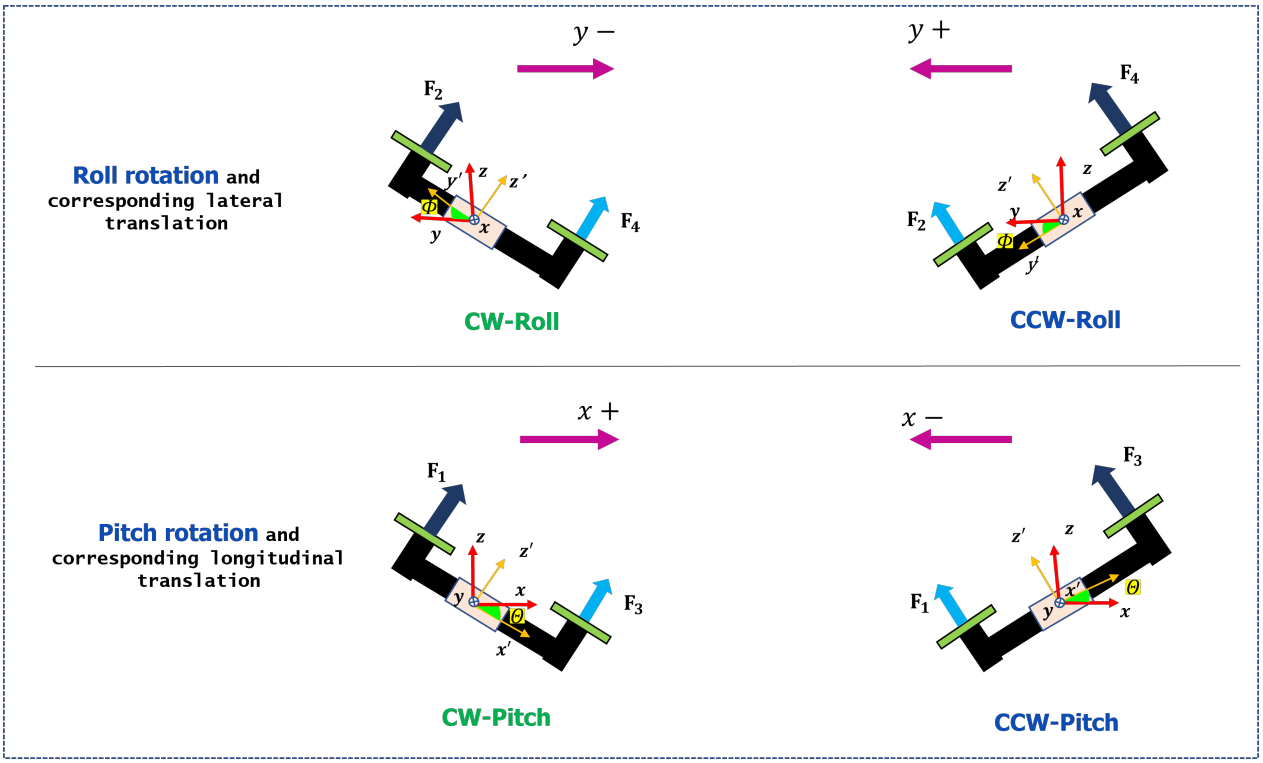

Figure 2.6: Rotational and the associated translational motions versus rotor speed variation

2.5 Quadrotor's kinematic

To formulate the full dynamical model of the quadrotor UAV, we must first define its kinematic which describe the relation existing between the state variables, position and velocity. Then the vehicle dynamic can be expressed as a relation between the rotor forces/torques and the resulting linear and angular accelerations.

Let consider $v^E = [\dot{x}, \dot{y}, \dot{z}]^T \in R^3$ and $v^B = [u, v, w]^T \in R^3$ as the linear velocities of the center of mass in the earth frame and the body frame, respectively. Then, the translational kinematic of the rigid body can be given as follows:

$$v^E = \mathcal{R}_{B \to E} v^B \tag{2.6}$$

Where $\mathcal{R}_{B \to E}$ denotes the orthonormal rotation matrix $(\mathcal{R}^{-1}{}_{B \to E} = \mathcal{R}^T{}_{B \to E})$ from the B-frame to the E-frame. Particularly, starting from the B-frame, the required sequence of rotations is given by rotation around the x-axis, then the y-axis and finally the z-axis. In order to go from the E-frame to the B-frame, an opposite rotation sequence shall be considered starting by a rotation around the z-axis, then the y-axis and finally the x-axis.

Table 2.1: Motion control for a quadrotor depending on rotor speed

Motion	Pair 1	Pair 2	Difference
Hover	$\Omega_1 = \Omega_3$	$\Omega_2 = \Omega_4$	$(\Omega_1 + \Omega_3) = (\Omega_2 + \Omega_4)$
CW-Roll	$\Omega_1 = \Omega_3$	$\Omega_2 > \Omega_4$	N/A
CW-Pitch	$\Omega_1 > \Omega_3$	$\Omega_2 = \Omega_4$	N/A
CW-Yaw	$\Omega_1 = \Omega_3$	$\Omega_2 = \Omega_4$	$(\Omega_1 + \Omega_3) > (\Omega_2 + \Omega_4)$
CCW-Roll	$\Omega_1 = \Omega_3$	$\Omega_2 < \Omega_4$	N/A
CCW-Pitch	$\Omega_1 < \Omega_3$	$\Omega_2 = \Omega_4$	N/A
CCW-Yaw	$\Omega_1 = \Omega_3$	$\Omega_2 = \Omega_4$	$(\Omega_1 + \Omega_3) < (\Omega_2 + \Omega_4)$

The rotation matrix $\mathcal{R}_{B\to E}$ can be defined as follows:

$$\begin{aligned}\mathcal{R}_{B\to E} =& \mathcal{R}_z(\Psi)\,\mathcal{R}_y(\Theta)\,\mathcal{R}_x(\Phi)\\ =& \begin{pmatrix} C_\Psi & -S_\Psi & 0\\ S_\Psi & C_\Psi & 0\\ 0 & 0 & 1\end{pmatrix}\begin{pmatrix} C_\Theta & 0 & S_\Theta\\ 0 & 1 & 0\\ -S_\Theta & 0 & C_\Theta\end{pmatrix}\begin{pmatrix} 1 & 0 & 0\\ 0 & C_\Phi & -S_\Phi\\ 0 & S_\Phi & C_\Phi\end{pmatrix}\\ =& \begin{pmatrix} C_\theta C_\Psi & S_\Phi S_\Theta C_\Psi - C_\Phi S_\Psi & C_\Phi S_\Theta C_\Psi + S_\Phi S_\psi\\ C_\Theta S_\Psi & S_\Phi S_\Theta S_\Psi + C_\Phi C_\Psi & C_\Phi S_\Theta S_\Psi - S_\Phi C_\Psi\\ -S_\Theta & S_\Phi C_\Theta & C_\Phi C_\Theta\end{pmatrix}\end{aligned} \tag{2.7}$$

With $\sin(\bullet)$ and $\cos(\bullet)$ are noted $S_{(\bullet)}$ and $C_{(\bullet)}$, respectively.

Consider $\delta_B = (p, q, r)^T \in \mathbb{R}^3$ and $\dot{\eta}_E = (\dot{\Phi}, \dot{\Theta}, \dot{\Psi})^T \in \mathbb{R}^3$ as the angular velocities in the B-frame and the Euler angles derivative known also as attitude rate in the E-frame, respectively. As already stated, the sequence of rotation from the B-frame to the E-frame start by a rotation around x-axis. This means the rotational velocity $\dot{\Phi}$ around X_E is the equivalent of the rotational velocity p around X_B. Then, the rotational velocity q is obtained after a rotation around x axis. Which means q can be obtained by multiplying $\dot{\Theta}$ by the inverse of $\mathcal{R}_x(\Phi)$. Finally, the angular velocity r results from two successive rotations around x and y axes. Therefore, r can be obtained by multiplying $\dot{\Psi}$ by the inverse of $(\mathcal{R}_y(\Theta)\mathcal{R}_x(\Phi))$.

With respect to the above discussion, the rotational kinematic representing the relation between the angular velocities δ_B and the angular velocities $\dot{\eta}_E$ can be obtained as follows :

$$
\begin{aligned}
\delta_B = \begin{pmatrix} p \\ q \\ r \end{pmatrix} &= \begin{pmatrix} \dot{\Phi} \\ 0 \\ 0 \end{pmatrix} + \mathcal{R}_x(\Phi)^{-1} \begin{pmatrix} 0 \\ \dot{\Theta} \\ 0 \end{pmatrix} + (\mathcal{R}_y(\Theta)\mathcal{R}_x(\Phi))^{-1} \begin{pmatrix} 0 \\ 0 \\ \dot{\Psi} \end{pmatrix} \\
&= \begin{pmatrix} \dot{\Phi} \\ 0 \\ 0 \end{pmatrix} + \begin{pmatrix} 0 \\ \dot{\Theta}C_\Phi \\ -\dot{\Theta}S_\Phi \end{pmatrix} + \begin{pmatrix} -\dot{\Psi}S_\Theta \\ \dot{\Psi}S_\Phi C_\Theta \\ \dot{\Psi}C_\Phi C_\Theta \end{pmatrix} = \begin{pmatrix} \dot{\Phi} - \dot{\Psi}S_\Theta \\ \dot{\Theta}C_\phi + \dot{\Psi}S_\phi C_\Theta \\ \dot{\Psi}S_\Phi C_\Theta - \dot{\Theta}S_\phi \end{pmatrix} \\
&= \begin{pmatrix} 1 & 0 & -S_\Theta \\ 0 & C_\Phi & S_\Phi C_\Theta \\ 0 & -S_\Phi & C_\Phi C_\Theta \end{pmatrix} \times \begin{pmatrix} \dot{\Phi} \\ \dot{\Theta} \\ \dot{\Psi} \end{pmatrix} \\
&= R^{-1}\dot{\eta}_E
\end{aligned}
\tag{2.8}
$$

Therefore, the relation between the euler angle derivative and rotational velocities in the B-frame is obtained as follows [123]:

$$
\dot{\eta}_E = \begin{pmatrix} \dot{\Phi} \\ \dot{\Theta} \\ \dot{\Psi} \end{pmatrix} = \begin{pmatrix} 1 & S_\Phi tan\Theta & C_\Phi tan\Theta \\ 0 & C_\Phi & -S_\Phi \\ 0 & S_\Phi/C_\Theta & C_\Phi/C_\Theta \end{pmatrix} \begin{pmatrix} p \\ q \\ r \end{pmatrix} \tag{2.9}
$$

2.6 Quadrotor's dynamic

The commonly used approaches to model the quadrotor dynamics are the Newton-Euler principle [124] and Euler Lagrange methodology [125, 126]. Newtonian method is the most popular approach which uses the famous Newton's law, while the Lagrangian method is based on the exploitation of the system energy [127]. Several researches' proposals have deeply presented the mathematical modeling of the quadrotor system. Some of them, consider all the physics phenomena including the thrust force resulting from the propellers rotation, drag effect, weight, air friction and the gyroscopic effect induced by both the propellers spinning and the body rotation, which make the obtained model more realistic. Other researchers linearize the dynamic to reduce the system complexity and make the use of classical control laws possible. In this case, the obtained model is valid at certain level, but when a disturbance occurs on the system the credibility of the model becomes invalid.

The quadrotor system is modeled based on the following assumptions [128]

1. The quadrotor structure is supposedly symmetrical and rigid.
2. Propellers are rigid.
3. The generated forces and torque are proportional to the rotor's angular speed.
4. The total thrust force $\sum_{i=1}^{4} F_i$, symbolized also by U_1, is positive and the quadrotor doesn't flip during the maneuver.

   - Pitch and Roll angles: $-\frac{\pi}{2} < \Phi, \Theta < \frac{\pi}{2}$
   - Heading angle: $-\pi < \Psi < \pi$
   - Thrust force: $U_1 > 0$

5. The rotorcraft angular movements are supposedly small, thus, ($C_\Phi = C_\Theta = 1$) and ($S_\Phi = S_\Theta = 0$). It follow from this assumption and Eq. 2.9 that the time derivative of the Euler angles and the angular velocities δ_B are equal $\dot{\eta}_E \simeq \delta_B$.

2.6.1 Translational dynamic

The translational dynamics of the quadrotor system in the E-frame can be given as:

$$m\ddot{\zeta}_E = F_G^E + \mathcal{R}_{B\to E}\ F_m^B + F_a^E + d_\zeta \tag{2.10}$$

Where d_ζ denotes the aerodynamic disturbances. F_G^E, F_m^B and F_a^E are respectively: the gravity force, the total lift force in the body frame and the drag force. These forces are defined as follows:

$$\begin{cases} F_G^E = (0, 0, -mg)^T \\ F_m^B = \left(0, 0, \sum_{i=1}^{4} F_i\right)^T \\ F_a^E = -K_i(\dot{x}, \dot{y}, \dot{z})^T \end{cases} \tag{2.11}$$

Where g is the gravity force, m is the total mass of the vehicle, $F_i = k_p {\Omega_i}^2$ is the lift force with k_p being the thrust coefficient and Ω_i the speed of rotor i.$K_i = diag\,(K_x, K_y, K_z)\,\epsilon\mathbb{R}^{3x3}$ are the friction coefficients.

With respect to Eq. 2.10 and Eq. 2.11, the equations of the translational motion can be calculated as:

$$\begin{aligned} m\ddot{\zeta} &= \sum \mathcal{F} \\ &= -mg \begin{pmatrix} 0 \\ 0 \\ 1 \end{pmatrix} + \mathcal{R}_B^{\mathbf{E}} \begin{pmatrix} 0 \\ 0 \\ k_b \left(\Omega_1^2 + \Omega_2^2 + \Omega_3^2 + \Omega_4^2\right) \end{pmatrix} - \begin{pmatrix} K_x \dot{x} \\ K_y \dot{y} \\ K_z \dot{z} \end{pmatrix} + \begin{pmatrix} d_x \\ d_y \\ d_z \end{pmatrix} \end{aligned} \tag{2.12}$$

Thereafter, we obtain

$$\begin{cases} \ddot{x} = \frac{U_1}{m}(C_\Phi S_\Theta C_\Psi + S_\Phi S_\Psi) - \frac{K_x}{m}\dot{x} + d_x \\ \ddot{y} = \frac{U_1}{m}(C_\Phi S_\Theta S_\Psi - S_\Phi C_\Psi) - \frac{K_y}{m}\dot{y} + d_y \\ \ddot{z} = \frac{U_1}{m}(C_\Phi C_\Theta) - g - \frac{K_z}{m}\dot{z} + d_z \end{cases} \tag{2.13}$$

The control input U_1 is defined as:

$$U_1 = k_b \left(\Omega_1^2 + \Omega_2^2 + \Omega_3^2 + \Omega_4^2\right) \tag{2.14}$$

2.6.2 Rotational dynamic

The quadrotor rotational dynamics are also derived using the Newton– Euler principle as follows:

$$\ddot{\eta}_E = -\dot{\eta}_E \wedge (J\eta_E) + \tau_{\text{pro}}^B - \tau_{\text{gyro}}^B + \tau_a^B + d_\eta \tag{2.15}$$

Where $d_\eta = (d_\Phi, d_\Theta, d_\Psi)^T \in \mathbb{R}^3$ denotes the additive disturbances acting on the rotational dynamics of the quadrotor. $J = \text{diag}\,(J_x, J_y, J_z) \in \mathbb{R}^3$ symbolize the inertia matrix. $\tau_{pro}^B, \tau_{gyro}^B, \tau_a^B$ correspond to the rotor torque, the gyroscopic torque due to the propeller's rotation and the friction torque. They are defined as follows:

$$\begin{cases} \tau_{\text{pro}}^B = (\tau_\Phi, \tau_\theta, \tau_\Psi)^T \\ \tau_{\text{gyro}}^B = \dot{\eta}_B \wedge J_r \left(0, 0, \sum_{i=1}^{4} (-1)^{i+1} \Omega_i\right)^T \\ \tau_a^B = -K_h \left(\dot{\Phi}^2, \dot{\Theta}^2, \dot{\Psi}^2\right)^T \end{cases} \tag{2.16}$$

Where τ_Φ,τ_Θ and τ_Ψ are the control torque for the roll, pitch and yaw rotation, respectively. J_r is the rotor inertia and $K_h = diag\,(K_\Phi,\ K_\Theta, K_\Psi)\,\epsilon\mathbb{R}^{3x3}$ are the friction coefficients.

The torques due to the rotor thrust are defined as:

$$\begin{pmatrix} \tau_\Phi \\ \tau_\Theta \\ \tau_\Psi \end{pmatrix} = \begin{pmatrix} K_b\ell\,(\Omega_2^2 - \Omega_4^2) \\ K_b\ell\,(\Omega_3^2 - \Omega_1^2) \\ K_d\,(\Omega_2^2 + \Omega_4^2 - \Omega_1^2 - \Omega_3^2) \end{pmatrix} \tag{2.17}$$

By expanding Eq. 2.15 with respect to the above analysis, the rotational dynamic of the quadrotor can be calculated as:

$$\begin{aligned} \begin{bmatrix} J_x & 0 & 0 \\ 0 & J_y & 0 \\ 0 & 0 & J_z \end{bmatrix} \begin{bmatrix} \ddot{\Phi} \\ \ddot{\Theta} \\ \ddot{\Psi} \end{bmatrix} = - \begin{bmatrix} \dot{\Phi} \\ \dot{\Theta} \\ \dot{\Psi} \end{bmatrix} \times \begin{bmatrix} J_x & 0 & 0 \\ 0 & J_y & 0 \\ 0 & 0 & J_z \end{bmatrix} \begin{bmatrix} \dot{\Phi} \\ \dot{\Theta} \\ \dot{\Psi} \end{bmatrix} - \begin{bmatrix} J_r\Omega\dot{\Theta} \\ -J_r\Omega\dot{\Phi} \\ 0 \end{bmatrix} + \begin{bmatrix} \tau_\Phi \\ \tau_\Theta \\ \tau_\Psi \end{bmatrix} \\ - \begin{bmatrix} K_\Phi\dot{\Phi}^2 \\ K_\Theta\dot{\Theta}^2 \\ K_\Psi\dot{\Psi}^2 \end{bmatrix} + \begin{bmatrix} d_\Phi \\ d_\Theta \\ d_\Psi \end{bmatrix} \end{aligned} \tag{2.18}$$

Then, after some calculations, we obtain

$$\begin{cases} \ddot{\Phi} = \dot{\Theta}\dot{\Psi}\left(\frac{J_y - J_z}{J_x}\right) - \frac{J_r}{J_x}\dot{\Theta}\Omega + \frac{\tau_\Phi}{J_x} - \frac{K_\Phi}{J_x}\dot{\Phi}^2 + d_\Phi \\ \ddot{\Theta} = \dot{\Phi}\dot{\Psi}\left(\frac{J_z - J_x}{J_y}\right) + \frac{J_r}{J_y}\dot{\Phi}\Omega + \frac{\tau_\Theta}{J_y} - \frac{K_\Theta}{J_y}\dot{\Theta}^2 + d_\Theta \\ \ddot{\Psi} = \dot{\Phi}\dot{\Theta}\left(\frac{J_x - J_y}{J_z}\right) + \frac{\tau_\Psi}{J_z} - \frac{K_\Psi}{J_z}\dot{\Psi}^2 + d_\Psi \end{cases} \tag{2.19}$$

With $\Omega = \Omega_1 - \Omega_2 + \Omega_3 - \Omega_4$

By using Eq. 2.13 and Eq. 2.19 , the complete dynamic model of the aerial vehicle is writing as follows:

$$\begin{cases} \ddot{\Phi} = \dot{\Theta}\dot{\Psi}\left(\frac{J_y - J_z}{J_x}\right) - \frac{J_r}{J_x}\dot{\Theta}\Omega + \frac{\tau_\Phi}{J_x} - \frac{K_\Phi}{J_x}\dot{\Phi}^2 + d_\Phi \\ \ddot{\Theta} = \dot{\Phi}\dot{\Psi}\left(\frac{J_z - J_x}{J_y}\right) + \frac{J_r}{J_y}\dot{\Phi}\Omega + \frac{\tau_\Theta}{J_y} - \frac{K_\Theta}{J_y}\dot{\Theta}^2 + d_\Theta \\ \ddot{\Psi} = \dot{\Phi}\dot{\Theta}\left(\frac{J_x - J_y}{J_z}\right) + \frac{\tau_\Psi}{J_z} - \frac{K_\Psi}{J_z}\dot{\Psi}^2 + d_\Psi \\ \ddot{x} = \frac{U_1}{m}(C_\Phi S_\Theta C_\Psi + S_\Phi S_\Psi) - \frac{K_x}{m}\dot{x} + d_x \\ \ddot{y} = \frac{U_1}{m}(C_\Phi S_\Theta S_\Psi - S_\Phi C_\Psi) - \frac{K_y}{m}\dot{y} + d_y \\ \ddot{z} = \frac{U_1}{m}(C_\Phi C_\Theta) - g - \frac{K_z}{m}\dot{z} + d_z \end{cases} \tag{2.20}$$

Using Eq. 2.17 and Eq. 2.14, the relationship between the control inputs $(U_1, \tau_\Phi, \tau_\Theta, \tau_\Psi)$ and the angular speeds is given as follows:

$$\begin{pmatrix} U_1 \\ \tau_\Phi \\ \tau_\Theta \\ \tau_\Psi \end{pmatrix} = \begin{pmatrix} k_\mathrm{p} & k_\mathrm{p} & k_\mathrm{p} & k_\mathrm{p} \\ 0 & k_\mathrm{p} l & 0 & -k_\mathrm{p} l \\ -k_\mathrm{p} l & 0 & k_\mathrm{p} l & 0 \\ -k_\mathrm{d} & k_\mathrm{d} & -k_\mathrm{d} & k_\mathrm{d} \end{pmatrix} \begin{pmatrix} \Omega_1^2 \\ \Omega_2^2 \\ \Omega_3^2 \\ \Omega_4^2 \end{pmatrix} \tag{2.21}$$

The control effort U_1 is mainly used to drive the robot along the vertical axis. The control torque τ_Θ is used to govern the pitch rotation and the longitudinal movement (x- displacement). τ_Φ is used to steer the roll rotation and the lateral movement (y-displacement). τ_Ψ is used to control the heading angle.

2.6.3 State space representation

The model of the aerial robot can be described by a second order nonlinear system which has the following form:

$$\dot{\chi} = \mathrm{A}(\chi) + \mathrm{B}(\chi)\mathcal{U} + d \tag{2.22}$$

With $\chi = \{\chi_1, \chi_2, \chi_3, \chi_4, \chi_5, \chi_6, \chi_7, \chi_8, \chi_9, \chi_{10}, \chi_{11}, \chi_{12}\}$ stands for the vehicle state variables given by $\left\{\Phi, \dot{\Phi},\ \Theta, \dot{\Theta}, \Psi, \dot{\Psi}, x, \dot{x}, y, \dot{y}, z, \dot{z}\right\}$, $\mathrm{A}(\chi)$and $\mathrm{B}(\chi) \neq 0$ are nonlinear functions. $\mathcal{U}$ corresponds to the control inputs. d represents the additive disturbances which is assumed to be bounded $|d| < \mathfrak{D}$.

Using the state space representation, the quadrotor dynamics given by Eq. 2.20 can be rewriting as:

$$\begin{cases} \dot{\chi}_1 = \chi_2 \\ \dot{\chi}_2 = \rho_{1\Phi}\chi_4\chi_6 + \rho_{2\Phi}\chi_4 + \rho_{3\Phi}\chi_2^2 + B_\Phi\tau_\Phi + d_\Phi \\ \dot{\chi}_3 = \chi_4 \\ \dot{\chi}_4 = \rho_{1\Theta}\chi_2\chi_6 + \rho_{2\Theta}\chi_2 + \rho_{3\Theta}\chi_4^2 + B_\Theta\tau_\Theta + d_\Theta \\ \dot{\chi}_5 = \chi_6 \\ \dot{\chi}_6 = \rho_{1\Psi}\chi_2\chi_4 + \rho_{2\Psi}\chi_6^2 + B_\Psi\tau_\Psi + d_\Psi \\ \dot{\chi}_7 = \chi_8 \\ \dot{\chi}_8 = \dfrac{U_1}{m}\nu_x + \rho_x\chi_8 + d_x \\ \dot{\chi}_9 = \chi_{10} \\ \dot{\chi}_{10} = \dfrac{U_1}{m}\nu_y + \rho_y\chi_{10} + d_y \\ \dot{\chi}_{11} = \chi_{12} \\ \dot{\chi}_{12} = \dfrac{U_1}{m}\left(C_{\chi_1}C_{\chi_3}\right) - g + \rho_z\chi_{12} + d_z \end{cases} \tag{2.23}$$

With $\{\nu_x, \nu_y\}$, are auxiliary control signals used to ensure the control of vehicle in the horizontal plan $x - y$.

$$\begin{cases} \nu_x = \frac{U_1}{m}\left(C_{\chi_1}S_{\chi_3}C_{\chi_5} + S_{\chi_1}S_{\chi_5}\right) \\ \nu_y = \frac{U_1}{m}\left(C_{\chi_1}S_{\chi_3}S_{\chi_5} - S_{\chi_1}C_{\chi_5}\right) \end{cases} \tag{2.24}$$

Where, $\rho_{1\Phi} = \frac{(J_y - J_z)}{J_x}$,$\rho_{2\Phi} = -\frac{J_r}{J_x}\mho$,$\rho_{3\Phi} = -\frac{K_\Phi}{Jx}$, $\rho_{1\Theta} = \frac{(J_z - J_x)}{J_y}$, $\rho_{2\Theta} = \frac{J_r}{J_y}\mho$, $\rho_{3\Theta} = -\frac{K_\Theta}{Jy}$, $\rho_{1\Psi} = \frac{(J_x - J_y)}{J_z}$, $\rho_{2\Psi} = -\frac{K_\Psi}{J_z}$, $\rho_x = -\frac{K_x}{m}$, $\rho_y = -\frac{K_y}{m}$, $\rho_z = -\frac{K_z}{m}$, $\mathrm{B}_\Phi = \frac{1}{J_x}$, $B_\theta = \frac{1}{J_x}$, $\mathrm{B}_\Psi = \frac{1}{J_z}$

2.7 Control architechures

The highly nonlinear dynamics, time-varying behavior of the quadrotor system, inaccuracies in the aerodynamic coefficients, changes in the vehicle mass, and the unknown disturbances due to windy gusts, are all factors that make controlling quadrotor difficult. In addition, the problem of underactuation, due to the presence of fewer control inputs $\{U_1, \tau_\Phi, \tau_\Theta, \tau_\Psi\}$ than the number of DOF $\{\chi_1, \chi_3, \chi_5, \chi_7, \chi_9, \chi_{11}\}$, further complicate the design of an adequate feedback control.

The most practical method to solve this problem is known as "*hierarchical control strategy*", "*cascade feedback strategy*" or "*dual-loop control architecture*" [129]. It is based on separating the vehicle dynamic into two loops (see Figure 2.7); including an inner-loop and an outer-loop that correspond to the attitude subsystem and the position subsystem, respectively [130]. Based on this separation we can differentiate two types of control: attitude control and position control. Attitude control consists of orienting the aircraft in the desired direction. This loop regulates the orientation of the quadrotor (Φ, Θ, Ψ) and generates the appropriate control torques ($\tau_\Phi, \tau_\Theta, \tau_\Psi$). The purpose of the position control is to generate the adequate thrust and the virtual controls. These signals are used to calculate the desired Euler angles (Φ_d, Θ_d) as references to the inner loop (the desired Ψ_d is directly provided by the drone user or a trajectory generator program) which make the aircraft reach a desired location.

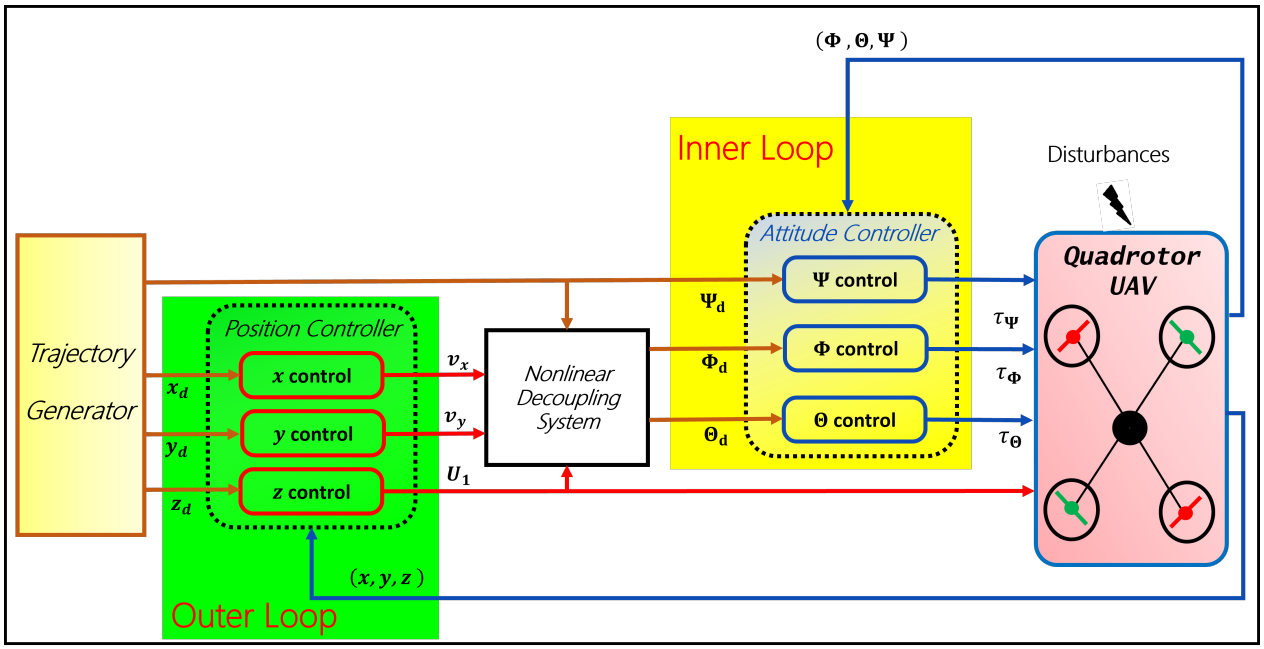

Figure 2.7: Dual-Loop control structure

From Eq. 2.24, the desired roll and pitch angles required to drive the vehicle toward the desired horizontal position $x - y$ are given as:

$$\begin{cases} \Theta_d = \arctan\left(\frac{\nu_x \mathrm{C}_{\Psi_d} + \nu_y \mathrm{S}_{\Psi_d}}{U_z}\right) \\ \Phi_d = \arctan\left(\mathrm{C}_{\theta_d}\left(\frac{\nu_x \mathrm{S}_{\Psi_d} - \nu_y \mathrm{C}_{\Psi_d}}{U_z}\right)\right) \end{cases} \tag{2.25}$$

With $U_z = (C_\Phi C_\Theta)\,\frac{U_1}{m}$.

Figure 2.8 illustrates the overall simulation environment realized on Matlab/simulink based on the dual loop control architecture. As can be seen, the desired position (x_d, y_d, z_d) and heading angle Ψ_d are considered the targeted trajectories. They can be configured directly by the drone user via the ground control station. Specifically, the position controller represented by the "z controller" and "x-y controller" provides the adequate thrust force U_1 and virtual controls (ν_x, ν_y). Then, starting from the position controller's outputs, the desired roll (Φ_d) and pitch (Θ_d) angles can be calculated through the nonlinear linear decoupling system (Eq. 2.25). The attitude controller is used to drive the vehicle's orientations toward their desired values. In this way, all six DOFs can be controlled effectively if the control algorithm is properly selected.

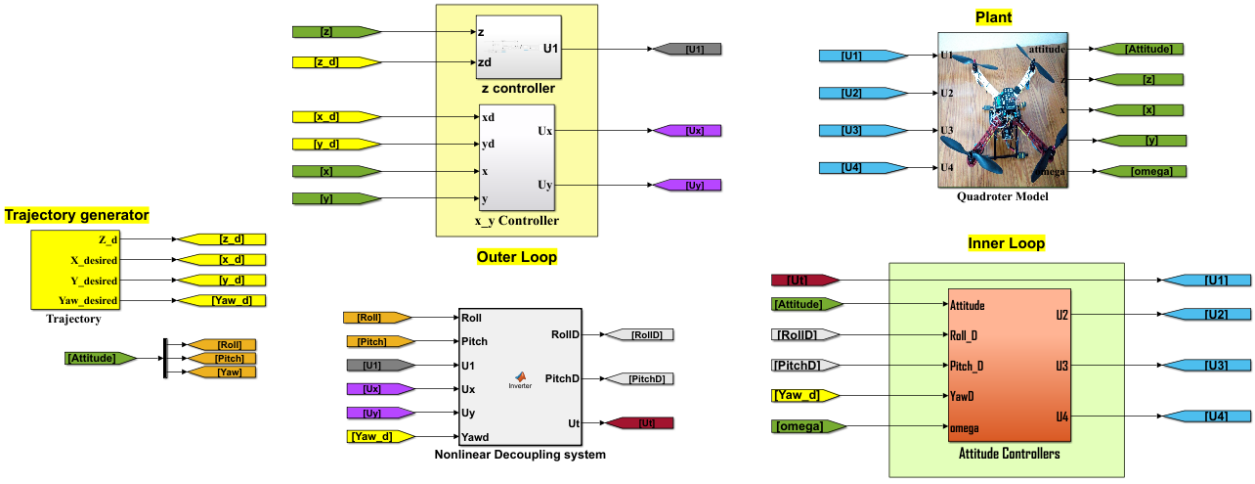

Figure 2.8: The developed Simulink model

It should be stated that within the control design and simulation phases, the linear velocities are assumed to be measurable by on-board sensors. Furthermore, the vehicle's orientation and angular velocities are expected to be obtained via an inertial measurement unit.

2.8 Conclusion

The objective of this chapter was to provide an overview of the key mathematical principles needed to understand and begin dynamic modeling of a disturbed quadrotor. Fundamental concepts regarding motion control of the quadrotor vehicle were first presented. The main forces and torques acting on the vehicle motions were introduced, and then the full dynamical model was derived by considering the influence of external disturbances. The resulting model highlights the presence of nonlinearities and high coupling between vehicle motions. The

appropriate state-space representation was also established. This representation will be used as the baseline for the control design, simulation, and implementation. Finally, the control architecture used to solve the problem of underactuation is thoroughly explained. Moreover, some insights on the developed simulation platform were also presented.

3 Proposed hybrid control strategy for an uncertain quadrotor

Contents

2.1 Introduction 42
2.2 System of coordinates and attitude representation 42
2.2.1 System of coordinates 42
2.2.2 Position and Attitude coordinates 43
2.3 Mechanism of flying 44
2.4 Quadrotor's motions 45
2.5 Quadrotor's kinematic 48
2.6 Quadrotor's dynamic 50
2.6.1 Translational dynamic 51
2.6.2 Rotational dynamic 52
2.6.3 State space representation 54
2.7 Control architechures 55
2.8 Conclusion 57

3.1 Introduction

Without control theory, the technological evolution of robotic system would never be the same. Substantial effort has been conducted in this field in order to achieve accurate and improved control performances. However, there is always the possibility of enhancing the capabilities of the flight control system even more. As it was stated earlier, due the multivariable structure, the strongly nonlinear dynamics, and the harsh operational constraints of the quadrotor system, a significant level of uncertainty is expected. It's evident that accurate control of drones is a priority. This requirement is justified by the fact that unexpected quadrotor behaviors or failures caused by inadequate control could compromise not only the mission of the drone, but also the safety of humans. In this chapter, a robust hybrid control strategy is developed to deal with the challenge related to external disturbances and modeling uncertainties. Based on a finite time sliding mode controller, a novel robust adaptive control scheme is designed to stabilize the quadrotor's attitude despite the impact of external disturbances. Additionally, the backstepping SMC is used for the tracking control of the quadrotor position.

The content of this chapter is structured as follows: In section 3.2, some preliminary notions on the sliding mode control design are presented. In section 3.3 two control strategies are developed for the control purpose of the quadrotor position and attitude. Simulation results and comparative analysis are addressed in section 3.4. Section 3.5 conclude the chapter.

3.2 Preliminary notions on sliding mode control

Sliding mode control (SMC), owing to its impressive robustness in the face of unknown disturbances and uncertainties, is recognized as an efficient method for designing robust control laws for uncertain and or perturbed nonlinear system. The SMC can be viewed as a composition of two control parts: reaching law and equivalent control. The first one forces the state trajectories to achieve the predefined sliding surface, whereas the second part maintains the system state into the selected sliding hyperplane until reaching equilibrium [131].

For a second-order nonlinear system, the sliding surface can be defined as:

$$S(t) = e_2 + ce_1 \tag{3.1}$$

Where e_1 and $e_2 = \dot{e}_1$ defines respectively the position and velocity tracking errors. c is a positive scalar.

As soon as the sliding surface is attained ($S = 0$), the tracking errors (e_1, e_2) will converge to zero as long as they remain on the sliding surface. The principle of sliding mode theory regarding the sliding and reaching phases is highlighted in Figure 3.1. As can be

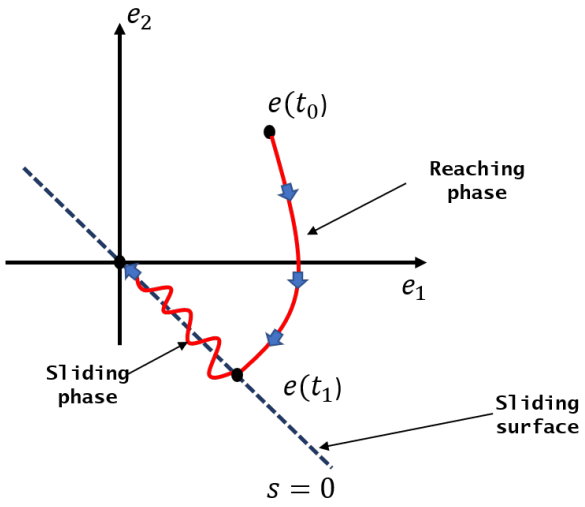

Figure 3.1: Sliding and reaching phase of the SMC

seen, in the reaching phase, the tracking errors (e_1, e_2) are attracted to the sliding surface. Within the sliding phase, the errors slide on the sliding surface until reaching the equilibrium.

After designing the sliding surface, it is important to define the control law that can drive the tracking error to reach the sliding surface. For that purpose , let's consider the following lyapunov function:

$$V_L = \frac{1}{2}S^2 \tag{3.2}$$

To ensure stability, the lyapunov function time derivative must satisfy the following condition:

$$\dot{V}_L = \dot{S}S \quad < 0 \tag{3.3}$$

Satisfying Eq. 3.3 means that $\dot{S} \quad < 0$ if $S \quad > 0$ and $\dot{S} \quad > 0$ if $S \quad < 0$. In order to ensure these conditions, $\dot{S}$ known as reaching law (or switching control) can be selected as:

$$\dot{S} = U_{sw} = -K sign(S) \tag{3.4}$$

Where K is a positive constant, $sign(S)$ is the standard signum function it is defined as:

$$\text{sign}(S(t)) = \begin{cases} 1, & \text{if } S(t) > 0 \\ 0, & \text{if } S(t) = 0 \\ -1, & \text{if } S(t) < 0 \end{cases} \tag{3.5}$$

It should be noted that higher value of K may cause chattering, high oscillations in the vicinity of the sliding surface, while low values slow down the reaching phase.

Considering the sliding phase and reaching phase, the overall control law based on the sliding mode theory can be defined as:

$$U = U_{eq} + U_{sw} \tag{3.6}$$

Where U_{eq} is the equivalent control, it can be derived by setting $\dot{S}(t) = 0$. It is responsible for ensuring the sliding of the tracking errors along the sliding surface. U_{sw} is the switching control that ensures reachability of the predefined sliding surface in a short time.

3.2.1 Reaching laws

In the literature, several reaching laws have been defined, considering the reaching phase speed. The following is a summary of these reaching laws [132]:

- Constant rate reaching law

$$\dot{S} = -Ksign(S) \tag{3.7}$$

  By integrating the above equation with respect to time, we obtain the reaching time $T_r = \frac{|S(0)|}{K}$, which is the time needed for the tracking errors to reach the sliding surface. To speed up the reaching phase, K should be increased however this can results in high chattering.

- Constant plus proportional reaching law

$$\dot{S} = -K_1 sign(S) - K_2 S \tag{3.8}$$

  With K_1 and K_2 are positive scalars. The term $K_2 S$ is added to fasten reaching when S is large. Using Eq. 3.8, the reaching time is $T_r = \frac{1}{K_1} ln(\frac{K_2|S(0)|+K_1}{K_1})$.

- Power reaching law

$$\dot{S} = -K|S|^a sign(S) \tag{3.9}$$

  With $0 \quad < a \quad < 1$. Using this reaching law, the tracking errors can reach the sliding surface within a time $T_r = \frac{|S(0)|^{(1-a)}}{(1-a)K}$.

3.3 Controller design and stability analysis

The proposed control strategy is based on two sub-controllers "an attitude controller and a position controller" as shown in Figure 3.2. Here, the attitude control system is based on the adaptive nonsingular fast terminal SMC that is synthesized to ensure finite-time convergence of the tracking errors by controlling the quadrotor's orientation. The inputs of this controller is the desired Euler angles $(\Phi_d, \Theta_d, \Psi_d)$ and the outputs are the adequate roll, pitch, and yaw torques $(\tau_\Phi, \tau_\Theta, \tau_\Psi)$. The backstepping SMC method is designed for the quadrotor's position to realize accurate control of the horizontal and vertical movements. This controller has as inputs the targeted position trajectories (x_d, y_d, z_d) and as outputs, it produces the thrust force U_1 and the appropriate virtual controls (ν_x, ν_y) that are used to calculate the desired roll and pitch angles for the attitude controller.

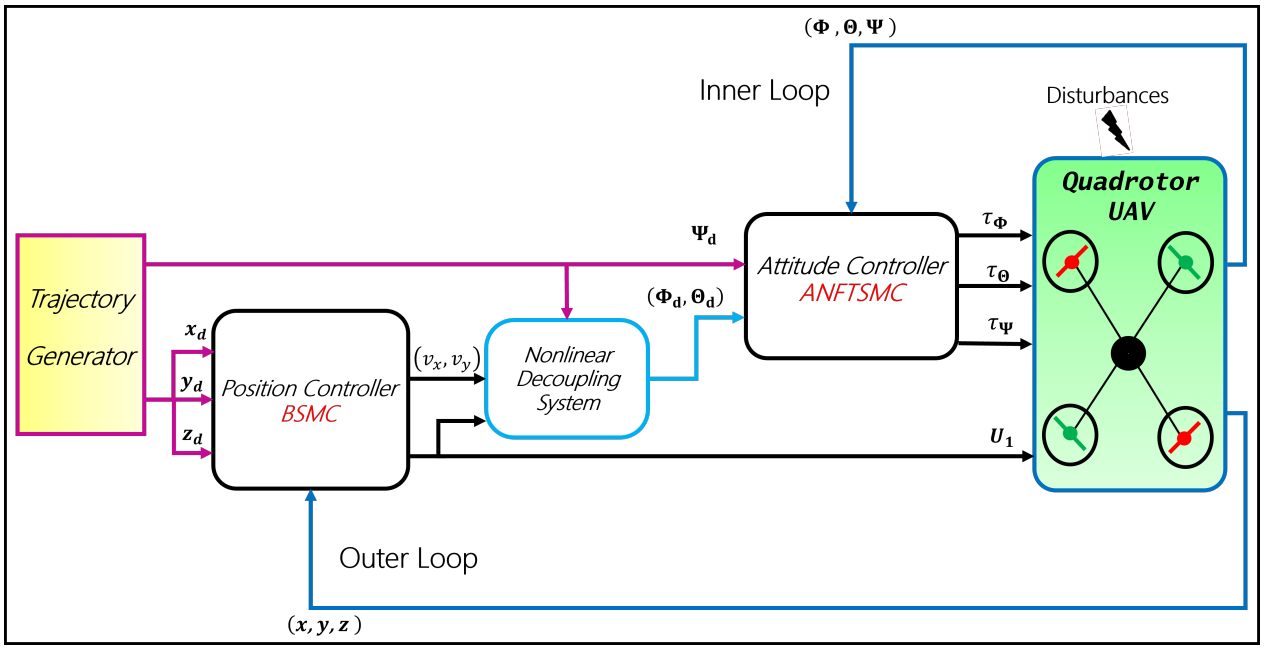

Figure 3.2: Proposed hybrid control scheme for a perturbed quadrotor

3.3.1 Quadrotor attitude controller

The lateral and longitudinal movements can be controlled by managing accurately the roll and pitch rotations, which reflects the importance of the attitude controller. We then proposed our adaptive nonsingular fast terminal SMC method.

From Eq. 2.23, the quadrotor attitude dynamics can be represented in the state space as follows:

$$\begin{pmatrix} \dot{\chi}_2 \\ \dot{\chi}_4 \\ \dot{\chi}_6 \end{pmatrix} = \begin{pmatrix} \rho_{1\Phi}\chi_4\chi_6 + \rho_{2\Phi}\chi_4 + \rho_{3\Phi}\chi_2^2 + \mathrm{B}_\Phi\tau_\Phi \\ \rho_{1\Theta}\chi_2\chi_6 + \rho_{2\Theta}\chi_2 + \rho_{3\Theta}\chi_4^2 + \mathrm{B}_\Theta\tau_\Theta \\ \rho_{1\Psi}\chi_2\chi_4 + \rho_{2\Psi}\chi_6^2 + \mathrm{B}_\Psi\tau_\Psi \end{pmatrix} + \begin{pmatrix} d_\Phi \\ d_\Theta \\ d_\Psi \end{pmatrix} \tag{3.10}$$

Where $d_\hbar$ corresponds to the external torques acting on the quadrotor system:

$$|d_h| < \xi_\hbar \tag{3.11}$$

$\xi_\hbar$ represents the upper limit of the external perturbation and uncertainty, it is given as [133]

$$\xi_\hbar = a_{1\hbar} + a_{2\hbar}\left|e_\hbar\right| + a_{3\hbar}\left|\dot{e}_\hbar\right|^2 \tag{3.12}$$

$a_{1\hbar}$, $a_{2\hbar}$ and $a_{3\hbar}$ are unknown positive scalars. $e_\hbar(\hbar = \Phi, \Theta, \Psi)$ and $\dot{e}_\hbar(\hbar = \Phi, \Theta, \Psi)$ are respectively the position and velocity tracking errors related to the attitude motion. Their expressions are as follows:

$$\begin{bmatrix} e_\Phi \\ e_\Theta \\ e_\Psi \end{bmatrix} = \begin{bmatrix} \Phi_d - \chi_1 \\ \Theta_d - \chi_3 \\ \Psi_d - \chi_5 \end{bmatrix} \quad , \begin{bmatrix} \dot{e}_\Phi \\ \dot{e}_\Theta \\ \dot{e}_\Psi \end{bmatrix} = \begin{bmatrix} \dot{\Phi}_d - \chi_2 \\ \dot{\Theta}_d - \chi_4 \\ \dot{\Psi}_d - \chi_6 \end{bmatrix} \tag{3.13}$$

3.3.1.1 NFTSMC for the quadrotor attitude

The traditional sliding surface based on the tracking error can be represented as follows:

$$S = ce_\hbar + \dot{e}_\hbar \tag{3.14}$$

Where c is a positive constant. Suppose that t_0 is the time when the system reaches the sliding surface ($S = 0, \dot{e}_\hbar = -ce_\hbar$) and t_s is the time when the system achieves the final states ($e_\hbar(t_s) = 0$). The time t_s spent by the system when moving from the reaching phase $S = 0$ to the final state is obtained by integrating Eq. 3.14 between instants t_0 and t_s.

$$t_s = t_0 + \frac{1}{K}\left(\ln(e_\hbar(t_0) - \ln(e_\hbar(t_0 + t_s))\right) \tag{3.15}$$

Knowing that the final states is characterized by zero error ($e_\hbar(t_s) = 0$), we can deduce that the traditional sliding mode control cannot converges to the final states in a finite-time ($t_s \to \infty$).

In order to ensure a finite-time convergence of the tracking error, a nonlinear sliding surface known as terminal sliding surface (TSS) is proposed by some authors as follows:

$$St_\hbar = \dot{e}_\hbar + \beta_\hbar sig(e_\hbar)^{\left(\frac{p_\hbar}{q_\hbar}\right)} \tag{3.16}$$

Where $sig(e_\hbar)^{\left(\frac{p_\hbar}{q_\hbar}\right)} = |e_\hbar|^{\left(\frac{p_\hbar}{q_\hbar}\right)} sign\,(e_\hbar)$ with sign is the sign function defined in Eq 3.5. This term was mainly added to ensure a convergence in finite-time. This can be demonstrated easily, considering $e_\hbar(t_0) \neq 0$ and when $St = 0$. On the sliding surface $St = 0$, Eq. 3.16 can be rewriting as:

$$\dot{e}_\hbar = \frac{de_\hbar}{dt} = -\beta_\hbar sig(e_\hbar)^{\left(\frac{p_\hbar}{q_\hbar}\right)} \tag{3.17}$$

We can apply separation of variables and integrate both sides to obtain:

$$\int_{e_\hbar(t_0)}^{e_\hbar(t_s)} \frac{de_\hbar}{\beta_\hbar sig(e_\hbar)^{\left(\frac{p_\hbar}{q_\hbar}\right)}} = -\int_{t_0}^{t_s} dt \tag{3.18}$$

The integration of Eq. 3.18, gives:

$$t_s = t_0 + \frac{|e_\hbar(t_0)|^{\left(1-\frac{p_\hbar}{q_\hbar}\right)}}{\beta_\hbar\left(1-\frac{p_\hbar}{q_\hbar}\right)} \tag{3.19}$$

We can deduce from Eq. 3.19 that the terminal sliding surface 3.16 allows finite-time convergence of tracking errors. As $0 < \frac{p_\hbar}{q_\hbar} < 1$, the convergence rate of the TSS will be faster in the vicinity of zero ($|e_\hbar| < 1$). However, if the error state is far from the equilibrium $|e_\hbar| >> 1$ the convergence speed will be slow.

In order to speed up the convergence especially when the system state is so far from the equilibrium, a Fast Terminal Sliding Surface (FTSS) is designed as:

$$\bar{s}_{\hbar,\ \hbar=(\Phi,\Theta,\Psi)} = \dot{e}_\hbar + \alpha_\hbar e_\hbar + \beta_\hbar sig(e_\hbar)^{\left(\frac{p_\hbar}{q_\hbar}\right)} \tag{3.20}$$

With $\alpha_\hbar$ and $\beta_\hbar$ are positive constant, $p_\hbar$ and $q_\hbar$ are a positive odd integers satisfying the condition $p_\hbar < q_\hbar$.

Remark 3.3.1 *The FTSS is a combination of the linear sliding surface (Eq. 3.14) and the terminal sliding surface (Eq. 3.16). When the system state reach the sliding surface ($\bar{s}_\hbar = 0$), Eq. 3.20 becomes:*

$$\dot{e}_\hbar = -\alpha_\hbar e_\hbar - \beta_\hbar |e_\hbar|^{\left(\frac{p_\hbar}{q_\hbar}\right)} sign\,(e_\hbar) \tag{3.21}$$

When the error state is far from the equilibrium, the subitem $\alpha_\hbar e_\hbar$ dominate over $\beta_\hbar |e_\hbar|^{\left(\frac{p_\hbar}{q_\hbar}\right)} sign\,(e_\hbar)$ (because $0 < \frac{p_\hbar}{q_\hbar} < 1$). This means, the FTSS operate as a linear sliding surface which allow

a fast convergence rate. When closer to the equilibrium, the term $\beta_\hbar \left|e_\hbar\right|^{\left(\frac{p_\hbar}{q_\hbar}\right)} sign\left(e_\hbar\right)$ *dominates, and the FTSS behave as a terminal sliding surface which allow faster convergence. Thereby, the FTSS can guarantee the fast convergence either the system is far away or near to the sliding surface.*

Theorem 3.3.1 *Using the sliding surface Eq. 3.20, the finite time convergence is guarantee.*

Proof: To demonstrate theorem 3.3.1, suppose that the system states reach the sliding surface, then $\bar{s}_\hbar = 0$. Based on Eq. 3.21 and using the separation of variables, we obtain:

$$\frac{de_\hbar}{-\alpha_\hbar e_\hbar - \beta_\hbar \left|e_\hbar\right|^{\left(\frac{p_\hbar}{q_\hbar}\right)} sign\left(e_\hbar\right)} = dt \tag{3.22}$$

The integration of Eq. 3.22 between t_0 and t_s gives:

$$\int_{e_\hbar(t_0)}^{e_\hbar(t_s)} \frac{de_\hbar}{-\alpha_\hbar e_\hbar - \beta_\hbar \left|e_\hbar\right|^{\left(\frac{p_\hbar}{q_\hbar}\right)} sign\left(e_\hbar\right)} = \int_{t_0}^{t_s} dt \tag{3.23}$$

Then, after some calculations (see appendix A), we obtain

$$t_s = t_0 + \frac{1}{\alpha_\hbar\left(1 - \frac{p_\hbar}{q_\hbar}\right)} \ln \frac{\alpha_\hbar \left|e_\hbar(t_0)\right|^{\left(1-\frac{p_\hbar}{q_\hbar}\right)} + \beta_\hbar}{\beta_\hbar} \tag{3.24}$$

Therefore, the attainability of the sliding manifold in a finite-time is ensured.

Remark 3.3.2 *The convergence time of the FTSS given in Eq. 3.24 is less than the convergence convergence time of the TSS given by Eq. 3.19. The comparison details is given in appendix A*

The major problem with the TSS and FTSS is the singularity problem. To identify the root cause of this problem, consider, for example, the FTSS given in Eq. 3.20, whose derivative is calculated as:

$$\dot{\bar{s}}_\hbar = \ddot{e}_\hbar + \left(\alpha_\hbar + \beta_\hbar \frac{p_\hbar}{q_\hbar} |e_\hbar|^{\left(\frac{p_\hbar - q_\hbar}{q_\hbar}\right)}\right) \dot{e}_\hbar \tag{3.25}$$

Because $\frac{p_\hbar - q_\hbar}{q_\hbar} < 0$, the term $sig(e_\hbar)^{\left(\frac{p_\hbar - q_\hbar}{q_\hbar}\right)}$ will produces singularity when $e_\hbar \to 0$ and $\dot{e}_\hbar \neq 0$, since $\lim_{e_\hbar \to 0} \operatorname{sig}\left(e_\hbar\right)^{\left(\frac{p_\hbar - q_\hbar}{q_\hbar}\right)} \to \infty$. This singularity can result in an infinite control signal, leading to the destabilization of the control system.

Inspired by the work proposed in [134] and the FTSS given in Eq. 3.20, a nonsingular fast terminal sliding surface (NFTSS) is considered to ensure fast convergence while avoiding the singularity problem. The proposed NFTSS is designed as follows:

$$\sigma_\hbar = \dot{e}_\hbar + \alpha_\hbar e_\hbar + \beta_\hbar \, \varpi_\hbar \left(e_\hbar\right) \tag{3.26}$$

With

$$\varpi_h \left(e_h\right) = \begin{cases} \operatorname{sig}\left(e_h\right)^{\left(\frac{p_\hbar}{q_\hbar}\right)} & \text{if } \bar{s}_h = 0 \text{ or } \bar{s}_h \neq 0, |e_h| > \varrho_h \\ l_1 e_h + l_2 \operatorname{sig}\left(e_h\right)^2 & \text{if } \bar{s}_h \neq 0, |e_h| < \varrho_h \end{cases} \tag{3.27}$$

Where $\bar{s}_\hbar = \dot{e}_\hbar + \alpha_\hbar e_\hbar + \beta_\hbar sig(e_\hbar)^{\left(\frac{p_\hbar}{q_\hbar}\right)}$.

The constants (l_1, l_2) in Eq. 3.27 are defined as follows:

$$\begin{aligned} l_1 &= \left(2 - \frac{p_\hbar}{q_\hbar}\right) \varrho_\hbar^{\left(\frac{p_\hbar}{q_\hbar} - 1\right)} \\ l_2 &= \left(\frac{p_\hbar}{q_\hbar} - 1\right) \varrho_\hbar^{\left(\frac{p_\hbar}{q_\hbar} - 2\right)} \end{aligned} \tag{3.28}$$

The constants l_1 and l_2 are selected as Eq. 3.28 to ensure that the function $\varpi_h(e_h)$ (Eq. 3.27) and its temporal derivative are both continuous. Which means, $\lim_{e_h \to \varrho_\hbar^+} \varpi_h(e_h) = \lim_{e_h \to \varrho_\hbar^-} \varpi_h(e_h)$, $\lim_{e_h \to -\varrho_\hbar^+} \varpi_h(e_h) = \lim_{e_h \to -\varrho_\hbar^-} \varpi_h(e_h)$, $\lim_{e_h \to \dot{\varrho}_\hbar^+} \dot{\varpi}_h(e_h) = \lim_{e_h \to \varrho_\hbar^-} \dot{\varpi}_h(e_h)$, $\lim_{e_h \to -\varrho_\hbar^+} \dot{\varpi}_h(e_h) = \lim_{e_h \to -\varrho_\hbar^-} \dot{\varpi}_h(e_h)$.

The first-time derivative of the NFTSS $\sigma_\hbar$ is given by:

$$\dot{\sigma}_\hbar = \ddot{e}_\hbar + \alpha_\hbar \dot{e}_\hbar + \beta_\hbar \dot{\varpi}_\hbar \left(e_\hbar\right) \tag{3.29}$$

With

$$\dot{\omega}_h \left(e_h\right) = \begin{cases} \frac{p_\hbar}{q_\hbar} \left|e_h\right|^{\left(\frac{p_\hbar - q_\hbar}{q_\hbar}\right)} \dot{e}_\hbar & \text{if } \bar{s}_h = 0 \text{ or } \bar{s}_h \neq 0, |e_h| > \varrho_h \\ l_1 \dot{e}_h + 2 l_2 \left|e_h\right| \dot{e}_h & \text{if } \bar{s}_h \neq 0, |e_h| < \varrho_h \end{cases} \tag{3.30}$$

The singularity problem which previously appears in the subitem $sig(e_\hbar)^{\left(\frac{p_\hbar - q_\hbar}{q_\hbar}\right)}$ when $e_\hbar \to 0$ and $\dot{e}_\hbar \neq 0$ is solved using the proposed sliding surface.

Based on Eq. 3.29 the NFTSS time derivative for the attitude subsystem becomes:

$$\begin{bmatrix} \dot{\sigma}_\Phi \\ \dot{\sigma}_\Theta \\ \dot{\sigma}_\Psi \end{bmatrix} = \begin{bmatrix} \ddot{e}_\Phi + \alpha_\Phi \dot{e}_\Phi + \beta_\Phi \dot{\varpi}_\Phi \left(e_\Phi\right) \\ \ddot{e}_\Theta + \alpha_\Theta \dot{e}_\Theta + \beta_\Theta \dot{\varpi}_\Theta \left(e_\Theta\right) \\ \ddot{e}_\Psi + \alpha_\Psi \dot{e}_\Psi + \beta_\Psi \dot{\Phi}_\Psi \left(e_\Psi\right) \end{bmatrix} \tag{3.31}$$

Considering Eq. 3.10 and by replacing the 2nd time derivative of the tracking errors $(\ddot{e}_\Phi, \ddot{e}_\Theta, \ddot{e}_\Psi)$, Eq. 3.31 becomes:

$$\begin{aligned} \dot{\sigma}_\Phi =& \ddot{\Phi}_d - \dot{\chi}_2 + \alpha_\Phi \dot{e}_\Phi + \beta_\Phi \dot{\varpi}_\Phi \left(e_\Phi\right) \\ =& \ddot{\Phi}_d - \rho_{1\Phi}\chi_4\chi_6 - \rho_{2\Phi}\chi_4 - \rho_{3\Phi}\chi_2^2 - \mathrm{B}_\Phi \tau_\Phi + d_\Phi + \alpha_\Phi \dot{e}_\Phi + \beta_\Phi \dot{\varpi}_\Phi \left(e_\Phi\right) \\ \dot{\sigma}_\Theta =& \ddot{\Theta}_d - \dot{\chi}_4 + \alpha_\Theta \dot{e}_\Theta + \beta_\Theta \dot{\varpi}_\Theta \left(e_\Theta\right) \\ =& \ddot{\Theta}_d - \rho_{1\Theta}\chi_2\chi_6 - \rho_{2\Theta}\chi_2 - \rho_{3\Theta}\chi_3^2 - \mathrm{B}_\Theta \tau_\Theta + d_\Theta + \alpha_\Theta \dot{e}_\Theta + \beta_\Theta \dot{\varpi}_\Theta \left(e_\Theta\right) \\ \dot{\sigma}_\Psi =& \ddot{\Psi}_d - \dot{\chi}_6 + \alpha_\Psi \dot{e}_\Psi + \beta_\Psi \dot{\Phi}_\Psi \left(e_\Psi\right) \\ =& \ddot{\Psi}_d - \rho_{1\Psi}\chi_2\chi_4 - \rho_{2\Psi}\chi_6^2 - \mathrm{B}_\Psi \tau_\Psi + d_\Psi + \alpha_\Psi \dot{e}_\Psi + \beta_\Psi \dot{\varpi}_\Psi \left(e_\Psi\right) \end{aligned} \tag{3.32}$$

In order to ensure the reachability of the designed NFTSS, the Constant Plus Proportional Reaching Law (CPPRL) defined in Eq. 3.8 is adopted and designed as follows [72]:

$$\dot{\sigma}_\hbar = -\kappa_\hbar \sigma_\hbar - \xi_\hbar tanh\left(\sigma_\hbar\right) \tag{3.33}$$

Where $\kappa_\hbar$ is a non-zero positive constant, the gain $\xi_\hbar$ represents the disturbance upper bound given in Eq. 3.12.

Using Eq. 3.32, Eq. 3.33 and Eq. 3.12 the attitude control equations are obtained as:

$$\tau_\Phi = \frac{1}{\mathrm{B}_\Phi} \begin{bmatrix} \ddot{\Phi}_d - \rho_{1\Phi}\chi_4\chi_6 - \rho_{2\Phi}\chi_4 - \rho_{3\Phi}\chi_2^2 + \alpha_\Phi \dot{e}_\Phi \\ +\beta_\Phi \dot{\varpi}_\Phi \left(e_\Phi\right) + \kappa_\Phi \sigma_\Phi + \\ \left(a_{1\Phi} + a_{2\Phi}\left|e_\Phi\right| + a_{3\Phi}\left|\dot{e}_\Phi\right|^2\right) \tanh\left(\sigma_\Phi\right) \end{bmatrix} \tag{3.34}$$

$$\tau_\Theta = \frac{1}{\mathrm{B}_\Theta} \begin{bmatrix} \ddot{\Theta}_d - \rho_{1\Theta}\chi_2\chi_6 - \rho_{2\Theta}\chi_2 - \rho_{3\Theta}\chi_3^2 + \alpha_\Theta \dot{e}_\Theta \\ +\beta_\Theta \dot{\varpi}_\Theta \left(e_\Theta\right) + \kappa_\Theta \sigma_\Theta + \\ \left(a_{1\Theta} + a_{2\Theta}\left|e_\Theta\right| + a_{3\Theta}\left|\dot{e}_\Theta\right|^2\right) \tanh\left(\sigma_\Theta\right) \end{bmatrix} \tag{3.35}$$

$$\tau_\Psi = \frac{1}{\mathrm{B}_\Psi} \begin{bmatrix} \ddot{\Psi}_d - \rho_{1\Psi}\chi_2\chi_4 - \rho_{2\Psi}\chi_6^2 + \alpha_\Psi \dot{e}_\Psi \\ +\beta_\Psi \dot{\varpi}_\Psi \left(e_\Psi\right) + \kappa_\Psi \sigma_\Psi + \\ \left(a_{1\Psi} + a_{2\Psi}\left|e_\Psi\right| + a_{3\Psi}\left|\dot{e}_\Psi\right|^2\right) \tanh\left(\sigma_\Psi\right) \end{bmatrix} \tag{3.36}$$

Theorem 3.3.2 *Considering the Φ-subsystem and the NFTSS Eq. 3.26, if the control equation is designed as Eq. 3.34 then the finite-time zeroing of the roll tracking error is guaranteed.*

Proof: Consider the lyapunov function for the Φ-subsystem as follows:

$$V_\Phi = \frac{1}{2}\sigma_\Phi^2 \tag{3.37}$$

The derivative of V_Φ is,

$$\begin{aligned}\dot{V}_\Phi =&\sigma_\Phi \dot{\sigma}_\Phi \\ =&\sigma_\Phi \left(\ddot{\Phi}_d - \rho_{1\Phi}\chi_4\chi_6 - \rho_{2\Phi}\chi_4 - \rho_{3\Phi}\chi_2^2 - \mathrm{B}_\Phi\tau_\Phi + d_\Phi + \alpha_\Phi \dot{e}_\Phi + \beta_\Phi \dot{\varpi}_\Phi\left(e_\Phi\right)\right)\end{aligned} \tag{3.38}$$

Inserting Eq. 3.34 into Eq. 3.38, we get,

$$\dot{V}_\Phi = \sigma_\Phi \left(-\kappa_\Phi\sigma_\Phi + d_\Phi - (a_{1\Phi} + a_{2\Phi}\left|e_\Phi\right| + a_{3\Phi}\left|\dot{e}_\Phi\right|^2)tanh(\sigma_\Phi\ )\right) \tag{3.39}$$

Therefore,

$$\begin{aligned}\dot{V}_\Phi =& -\kappa_\Phi\sigma_\Phi^2 + d_\Phi\sigma_\Phi - \left(a_{1\Phi} + a_{2\Phi}\left|e_\Phi\right| + a_{3\Phi}\left|\dot{e}_\Phi\right|^2\right)\left|\sigma_\Phi\right| \\ \leq& -\kappa_\Phi\sigma_\Phi^2 + \left|d_\Phi\right|\left|\sigma_\Phi\right| - \left(a_{1\Phi} + a_{2\Phi}\left|e_\Phi\right| + \ a_{3\Phi}\left|\dot{e}_\Phi\right|^2\right)\left|\sigma_\Phi\right| \\ \leq& -\kappa_\Phi\sigma_\Phi^2 + \left(\left|d_\Phi\right| - \left(a_{1\Phi} + a_{2\Phi}\left|e_\Phi\right| + \ a_{3\Phi}\left|\dot{e}_\Phi\right|^2\right)\right)\left|\sigma_\Phi\right|\end{aligned} \tag{3.40}$$

Using Eq. 3.11 we have,

$$\dot{V}_\Phi \leq 0 \tag{3.41}$$

Based on the lyapunov criteria, the stability of the roll movement is guarantee.

Theorem 3.3.3 *Considering the quadrotor attitude Eq. 3.10 and the NFTSS Eq. 3.26, if the control equations are designed as Eq. 3.34, Eq. 3.35, and Eq. 3.36 then overall stability of the quadrotor's attitude is ensured.*

Proof: To demonstrate the overall closed-loop stability of the quadrotor's attitude, let's consider the following lyapunov function:

$$V_{att} = \frac{1}{2}\sigma_\Phi^2 + \frac{1}{2}\sigma_\Theta^2 + \frac{1}{2}\sigma_\Psi^2 \tag{3.42}$$

The derivative of V_{att} is given as:

$$\begin{aligned}\dot{V}_{att} =&\dot{V}_\Phi + \dot{V}_\Theta + \dot{V}_\Psi \\ =&\sigma_\Phi\dot{\sigma}_\Phi + \sigma_\Theta\dot{\sigma}_\Theta + \sigma_\Psi\dot{\sigma}_\Psi\end{aligned} \tag{3.43}$$

Thereafter, using similar calculus as in Eq. 3.40, $\dot{V}_{att}$ satisfies the following inequality:

$$\dot{V}_{att} \leq -\kappa_{\Phi}\sigma_{\Phi}^{2} + \left(|d_{\Phi}| - \left(a_{1\Phi} + a_{2\Phi}\,|e_{\Phi}| + a_{3\Phi}\,|\dot{e}_{\Phi}|^{2}\right)\right)|\sigma_{\Phi}| - \kappa_{\Theta}\sigma_{\Theta}^{2} + (|d_{\Theta}| - (a_{1\Theta} + a_{2\Theta}\,|e_{\Theta}| + a_{3\Theta}\,|\dot{e}_{\Theta}|^{2}\Big)\Big)|\sigma_{\Theta}| - \kappa_{\Psi}\sigma_{\Psi}^{2} + \left(|d_{\Psi}| - \left(a_{1\Psi} + a_{2\Psi}\,|e_{\Psi}| + a_{3\Psi}\,|\dot{e}_{\Psi}|^{2}\right)\right)|\sigma_{\Psi}| \tag{3.44}$$

Using Eq. 3.11 we have,

$$\dot{V}_{att} \leq 0 \tag{3.45}$$

Consequently, the closed-loop stability of the attitude subsystem is guaranteed.

3.3.1.2 ANFTSMC for the quadrotor attitude

Quadrotor attitude is generally affected by unstructured dynamics such as high coupling, nonlinearity, exogenous perturbations, and parameter uncertainties. Moreover, the disturbance/uncertainty upper limit is not known in advance and changes depending on the disturbance type. An adaptive control law is then proposed to continuously approximate this limit.

The quadrotor attitude control equations based on the Adaptive NFTSMC are given as:

$$\tau_{\Phi} = \frac{1}{\mathrm{B}_{\Phi}}\begin{bmatrix} \ddot{\Phi}_{d} - \rho_{1\Phi}\chi_{4}\chi_{6} - \rho_{2\Phi}\chi_{4} - \rho_{3\Phi}\chi_{2}^{2} + \alpha_{\Phi}\dot{e}_{\Phi} \\ +\beta_{\Phi}\dot{\varpi}_{\Phi}\left(e_{\Phi}\right) + \kappa_{\Phi}\sigma_{\Phi} + \hat{\xi}_{\Phi}\tanh\left(\sigma_{\Phi}\right) \end{bmatrix} \tag{3.46}$$

$$\tau_{\Theta} = \frac{1}{\mathrm{B}_{\Theta}}\begin{bmatrix} \ddot{\Theta}_{d} - \rho_{1\Theta}\chi_{2}\chi_{6} - \rho_{2\Theta}\chi_{2} - \rho_{3\Theta}\chi_{3}^{2} + \alpha_{\Theta}\dot{e}_{\Theta} \\ +\beta_{\Theta}\dot{\varpi}_{\Theta}\left(e_{\Theta}\right) + \kappa_{\Theta}\sigma_{\Theta} + \hat{\xi}_{\Theta}\tanh\left(\sigma_{\Theta}\right) \end{bmatrix} \tag{3.47}$$

$$\tau_{\Psi} = \frac{1}{\mathrm{B}_{\Psi}}\begin{bmatrix} \ddot{\Psi}_{d} - \rho_{1\Psi}\chi_{2}\chi_{4} - \rho_{2\Psi}\chi_{6}^{2} + \alpha_{\Psi}\dot{e}_{\Psi} \\ +\beta_{\Psi}\dot{\varpi}_{\Psi}\left(e_{\Psi}\right) + \kappa_{\Psi}\sigma_{\Psi} + \hat{\xi}_{\Psi}\tanh\left(\sigma_{\Psi}\right) \end{bmatrix} \tag{3.48}$$

Where $\hat{\xi}_{\hbar}, \hbar = (\Phi, \Theta,\ \Psi)$ is the estimation of $\xi_{\hbar}, \hbar = (\Phi, \Theta,\ \Psi)$. It's expression can be defined as follows:

$$\begin{cases} \hat{\xi}_{\Phi} = \hat{a}_{1\Phi} + \hat{a}_{2\Phi}\,|e_{\Phi}| + \hat{a}_{3\Phi}\,|\dot{e}_{\Phi}|^{2} \\ \hat{\xi}_{\Theta} = \hat{a}_{1\Theta} + \hat{a}_{2\Theta}\,|e_{\Theta}| + \hat{a}_{3\Theta}\,|\dot{e}_{\Theta}|^{2} \\ \hat{\xi}_{\Psi} = \hat{a}_{1\Psi} + \hat{a}_{2\Psi}\,|e_{\Psi}| + \hat{a}_{3\Psi}\,|\dot{e}_{\Psi}|^{2} \end{cases};\begin{cases} \dot{\hat{a}}_{1\hbar} = \Gamma_{1\hbar}\,|\sigma_{\hbar}| \\ \dot{\hat{a}}_{2\hbar} = \Gamma_{2\hbar}\,|e_{\hbar}|\,|\sigma_{\hbar}| \\ \dot{\hat{a}}_{3\hbar} = \Gamma_{3\hbar}\,|\dot{e}_{\hbar}|^{2}\,|\sigma_{\hbar}| \end{cases} \tag{3.49}$$

$\Gamma_{1\hbar}$, $\Gamma_{2\hbar}$ and $\Gamma_{3\hbar}$ are small positive constants. The parameters $\hat{a}_{1\hbar}$, $\hat{a}_{2\hbar}$ and $\hat{a}_{3\hbar}$ are approximated using the position and velocity tracking errors.

The proposed ANFTSMC synoptic scheme for the quadrotor attitude is illustrated in Figure 3.3. The control design starts by defining the NFTSS (Eq. 3.26) based on the position and velocity tracking errors given in Eq. 3.13. Then the estimation of the controller

gains is performed using the proposed adaptive control law (Eq. 3.49), and finally the ultimate control equations (Eq. 3.46, Eq. 3.47 and Eq. 3.48) are calculated and then used to command and drive the attitude motions of the quadrotor aircraft. It should be noted that the proposed ANFTSMC method can be used for other systems, not only the quadrotor UAV.

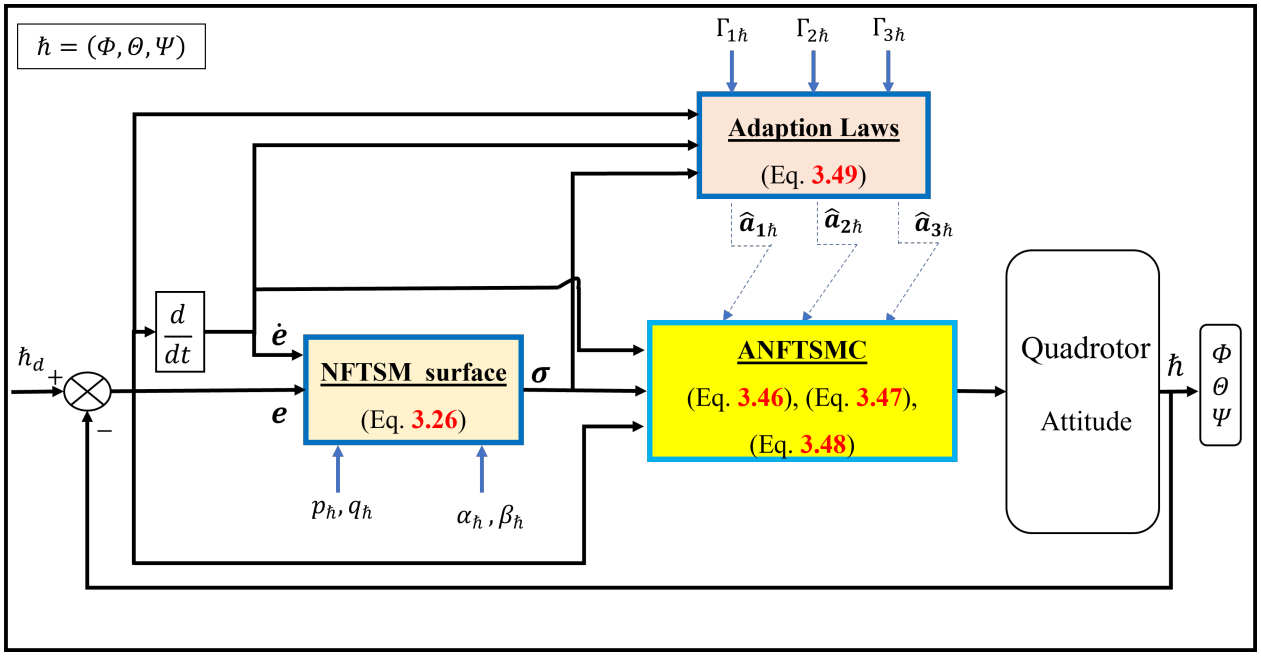

Figure 3.3: Proposed ANFTSMC block diagram

Theorem 3.3.4 *Consider the Φ-subsystem and the NFTSS Eq. 3.26, if the input command τ_Φ is constructed as in Eq. 3.46, and the adaptive control law is selected as Eq. 3.49, then the zeroing of the roll tracking error is guaranteed.*

Proof: For the roll motion, we consider the Lyapunov candidate function as:

$$V = \frac{1}{2}(\sigma_\Phi^2 + \frac{\breve{a}_{1\Phi}^2}{\Gamma_{1\Phi}} + \frac{\breve{a}_{2\Phi}^2}{\Gamma_{2\Phi}} + \frac{\breve{a}_{3\Phi}^2}{\Gamma_{3\Phi}}) \tag{3.50}$$

With $\breve{a}_{i\Phi} = a_{i\Phi} - \hat{a}_{i\Phi}, (i = 1, 2, 3)$ is the adaptation error and $\hat{a}_i$ is the estimate of a_i.

$$\dot{V} = -\kappa_\Phi \sigma_\Phi^2 + d_\Phi \sigma_\Phi - \left(\hat{a}_{1\Phi} + \hat{a}_{2\Phi}\left|e_\Phi\right| + \hat{a}_{3\Phi}\left|\dot{e}_\Phi\right|^2\right)\left|\sigma_\Phi\right| - \frac{\breve{a}_{1\Phi}\dot{\hat{a}}_{1\Phi}}{\Gamma_{1\Phi}} - \frac{\breve{a}_{2\Phi}\dot{\hat{a}}_{2\Phi}}{\Gamma_{2\Phi}} - \frac{\breve{a}_{3\Phi}\dot{\hat{a}}_{3\Phi}}{\Gamma_{3\Phi}} \tag{3.51}$$

Then,

$$\dot{V} = -\kappa_\Phi \sigma_\Phi^2 + d_\Phi \sigma_\Phi - \left(a_{1\Phi} + a_{2\Phi}\left|e_\Phi\right| + a_{3\Phi}\left|\dot{e}_\Phi\right|^2\right)\left|\sigma_\Phi\right| + \breve{a}_{1\Phi}\left(\left|\sigma_\Phi\right| - \frac{\dot{\hat{a}}_{1\Phi}}{\Gamma_{1\Phi}}\right) + \breve{a}_{2\Phi}\left(\left|e_\Phi\right|\left|\sigma_\Phi\right| - \frac{\dot{\hat{a}}_{2\Phi}}{\Gamma_{2\Phi}}\right) + \breve{a}_{3\Phi}\left(\left|\dot{e}_\Phi\right|^2\left|\sigma_\Phi\right| - \frac{\dot{a}_{3\Phi}}{\Gamma_{3\Phi}}\right) \tag{3.52}$$

Using Eq. 3.49, we obtain,

$$\dot{V} = -\kappa_\Phi \sigma_\Phi^2 + \left(\left|d_\Phi\right| - \left(a_{1\Phi} + a_{2\Phi}\left|e_\Phi\right| + a_{3\Phi}\left|\dot{e}_\Phi\right|^2\right)\right)\ \left|\sigma_\Phi\ \right| \qquad \leq 0 \tag{3.53}$$

Based on the Lyapunov stability condition, the stability of the roll rotation is guarantee.

Theorem 3.3.5 *Consider the attitude dynamics Eq. 3.10 and the NFTSS Eq. 3.20, if the control torques are computed as Eq. 3.46, Eq. 3.47 and Eq. 3.48, and the adaptive control laws are selected as Eq. 3.49, then the attitude tracking errors converge to the origin in a finite-time.*

Proof: To prove theorem 3.3.5, consider the following lyapunov function,

$$V_{Att} = \frac{1}{2}(\sigma_\Phi^2 + \frac{\breve{a}_{1\Phi}^2}{\Gamma_{1\Phi}} + \frac{\breve{a}_{2\Phi}^2}{\Gamma_{2\Phi}} + \frac{\breve{a}_{3\Phi}^2}{\Gamma_{3\Phi}}) + \frac{1}{2}(\sigma_\Theta^2 + \frac{\breve{a}_{1\Theta}^2}{\Gamma_{1\Theta}} + \frac{\breve{a}_{2\Theta}^2}{\Gamma_{2\Theta}} + \frac{\breve{a}_{3\Theta}^2}{\Gamma_{3\Theta}}) + \frac{1}{2}(\sigma_\Psi^2 + \frac{\breve{a}_{1\Psi}^2}{\Gamma_{1\Psi}} + \frac{\breve{a}_{2\Psi}^2}{\Gamma_{2\Psi}} + \frac{\breve{a}_{3\Psi}^2}{\Gamma_{3\Psi}}) \tag{3.54}$$

Deriving V_{Att} with respect to time, we obtain

$$\begin{aligned}\dot{V}_{Att} = &-\kappa_\Phi \sigma_\Phi^2 + d_\Phi \sigma_\Phi - \left(\hat{a}_{1\Phi} + \hat{a}_{2\Phi}\left|e_\Phi\right| + \hat{a}_{3\Phi}\left|\dot{e}_\Phi\right|^2\right)\left|\sigma_\Phi\right| - \frac{\breve{a}_{1\Phi}\dot{\hat{a}}_{1\Phi}}{\Gamma_{1\Phi}} - \frac{\breve{a}_{2\Phi}\dot{\hat{a}}_{2\Phi}}{\Gamma_{2\Phi}} - \frac{\breve{a}_{3\Phi}\dot{\hat{a}}_{3\Phi}}{\Gamma_{3\Phi}} \\ &- \kappa_\Theta \sigma_\Theta^2 + d_\Theta \sigma_\Theta - \left(\hat{a}_{1\Theta} + \hat{a}_{2\Theta}\left|e_\Theta\right| + \hat{a}_{3\Theta}\left|\dot{e}_\Theta\right|^2\right)\left|\sigma_\Theta\right| - \frac{\breve{a}_{1\Theta}\dot{\hat{a}}_{1\Theta}}{\Gamma_{1\Theta}} - \frac{\breve{a}_{2\Theta}\dot{\hat{a}}_{2\Theta}}{\Gamma_{2\Theta}} - \frac{\breve{a}_{3\Theta}\dot{\hat{a}}_{3\Theta}}{\Gamma_{3\Theta}} \\ &- \kappa_\Psi \sigma_\Psi^2 + d_\Psi \sigma_\Psi - \left(\hat{a}_{1\Psi} + \hat{a}_{2\Psi}\left|e_\Psi\right| + \hat{a}_{3\Psi}\left|\dot{e}_\Psi\right|^2\right)\left|\sigma_\Psi\right| - \frac{\breve{a}_{1\Psi}\dot{\hat{a}}_{1\Psi}}{\Gamma_{1\Psi}} - \frac{\breve{a}_{2\Psi}\dot{\hat{a}}_{2\Psi}}{\Gamma_{2\Psi}} - \frac{\breve{a}_{3\Psi}\dot{\hat{a}}_{3\Psi}}{\Gamma_{3\Psi}}\end{aligned} \tag{3.55}$$

Using Eq. 3.11 and Eq. 3.49, and with respect to the calculation details given in Eq. 3.52, the first-time derivative of V_{Att} satisfies

$$\dot{V}_{Att} \leq 0 \tag{3.56}$$

Thereafter, the overall stability of the attitude dynamics is guaranteed.

3.3.2 Quadrotor position controller

In this part, we shall present a backstepping sliding mode controller (BSMC) for the quadrotor position. The design of the proposed BSMC is conducted sequentially as follows:

Let's consider the position tracking errors and their temporal derivative as follows:

$$\begin{cases} e_x = x_d - \chi_7 \\ e_y = y_d - \chi_9 \\ e_z = z_d - \chi_{11} \end{cases} ; \begin{cases} \dot{e}_x = \dot{x}_d - \chi_8 \\ \dot{e}_y = \dot{y}_d - \chi_{10} \\ \dot{e}_z = \dot{z}_d - \chi_{12} \end{cases} \tag{3.57}$$

The 1^{rst} Lyapunov functions and its derivative are designed as:

$$\begin{cases} V_x = \frac{1}{2}e_x^2 \\ V_y = \frac{1}{2}e_y^2 \\ V_z = \frac{1}{2}e_z^2 \end{cases} ; \begin{cases} \dot{V}_x = e_x\dot{e}_x = e_x\left(\dot{x}_d - \chi_8\right) \\ \dot{V}_y = e_y\dot{e}_y = e_y\left(\dot{y}_d - \chi_{10}\right) \\ \dot{V}_z = e_z\dot{e}_z \ = e_z\left(\dot{z}_d - \chi_{12}\right) \end{cases} \tag{3.58}$$

Defining the sliding surface for the quadrotor position:

$$\begin{cases} S_x = \chi_8 - \gamma_x \ \ = \chi_8 - \dot{x}_d - K_{x1}e_x \\ S_y = \chi_{10} - \gamma_y = \chi_{10} - \dot{y}_d - K_{y1}e_y \\ S_z = \chi_{12} - \gamma_z = \chi_{12} - \dot{z}_d - K_{z1}e_z \end{cases} \tag{3.59}$$

γ_x,γ_y and γ_z are virtual inputs introduced to stabilize the tracking errors e_x,e_y and e_z. K_{x1}, K_{y1} and K_{z1} are positive constants to be selected depending on the controlled system .

The 2nd lyapunov functions for the quadrotor translational subsystem are selected as:

$$\begin{bmatrix} V_{xx} \\ V_{yy} \\ V_{zz} \end{bmatrix} = 1/2 \begin{bmatrix} e_x^2 + S_x^2 \\ e_y^2 + S_y^2 \\ e_z^2 + S_z^2 \end{bmatrix} \tag{3.60}$$

Taking the derivative of Eq. 3.60 we get:

$$\begin{aligned} \dot{V}_{xx} &= -\,e_x\left(S_x + K_{x1}e_x\right) + S_x\left(\nu_x + \rho_x\chi_8 - \ddot{x}_d + K_{x1}\left(S_x + \ K_{x1}e_x\right)\right) \\ \dot{V}_{yy} &= -\,e_y\left(S_y + K_{y1}e_y\right) + S_y\left(\nu_y + \rho_y\chi_{10} - \ddot{y}_d + K_{y1}\left(S_y + \ K_{y1}e_y\right)\right) \\ \dot{V}_{zz} &= -\,e_z\left(S_z + K_{z1}e_z\right) + S_z\left(\frac{U_1}{m}\left(C_{\chi_1}C_{\chi_3}\right) - g + \rho_z\chi_{12} - \ddot{z}_d + \ K_{z1}\left(S_z + K_{z1}e_z\right)\right) \end{aligned} \tag{3.61}$$

Based on Eq. 3.61, the equivalent control equations for the quadrotor position are obtained as:

$$\begin{cases} \nu_{xeq} = e_x + \ddot{x}_d - \rho_x \chi_8 - K_{x1}\left(S_x + K_{x1} e_x\right) - K_{x2} S_x \\ \nu_{yeq} = e_y + \ddot{y}_d - \rho_y \chi_{10} - K_{y1}\left(S_y + K_{y1} e_y\right) - K_{y2} S_y \\ U_{1eq} = \frac{m}{C_{x_1} C_{x_3}}\left(e_z + \ddot{z}_d + g - \rho_z \chi_{12} - K_{z1}\left(S_z + K_{z1} e_z\right) - K_{z2} S_z\right) \end{cases} \tag{3.62}$$

Where K_{x2}, K_{y2} and K_{z2} are positive scalars.

The switching control for the quadrotor's position are designed as follows:

$$\begin{cases} \nu_{xsw} = -\xi_x sign\left(S_x\right) \\ \nu_{ysw} = -\xi_y sign\left(S_y\right) \\ U_{1sw} = -\dfrac{m}{C_{x_1} C_{x_3}} \xi_z sign\left(S_z\right) \end{cases} \tag{3.63}$$

Hence, the quadrotor position control equations based on the BSMC control law are given by:

$$\begin{aligned} \nu_x =& \nu_{xeq} + \nu_{xsw} \\ =& e_x + \ddot{x}_d - \rho_x \chi_8 - K_{x1}\left(S_x + K_{x1} e_x\right) - K_{x2} S_x - \xi_x sign\left(S_x\right) \\ \nu_y =& \nu_{yeq} + \nu_{ysw} \\ =& e_y + \ddot{y}_d - \rho_y \chi_{10} - K_{y1}\left(S_y + K_{y1} e_y\right) - K_{y2} S_y - \xi_y sign\left(S_y\right) \\ U_1 =& U_{1eq} + U_{1sw} \\ =& \frac{m}{C_{x_1} C_{x_3}}\left(e_z + \ddot{z}_d + g - \rho_z \chi_{12} - K_{z1}\left(S_z + K_{z1} e_z\right) - K_{z2} S_z - \xi_z sign\left(S_z\right)\right) \end{aligned} \tag{3.64}$$

Theorem 3.3.6 *Using the obtained control equation Eq. 3.64, the quadrotor position is stable.*

Proof: To analyze the stability of the position subsystem, we consider the following Lyapunov function:

$$\begin{aligned} V_{Pos} =& V_{xx} + V_{yy} + V_{zz} \\ =& \frac{1}{2}\left(e_x^2 + S_x^2\right) + \frac{1}{2}\left(e_y^2 + S_y^2\right) + \frac{1}{2}\left(e_z^2 + S_z^2\right) \end{aligned} \tag{3.65}$$

Tacking the derivative of V_{Pos} we get,

$$\dot{V}_{Pos} = \dot{V}_{xx} + \dot{V}_{yy} + \dot{V}_{zz} \tag{3.66}$$

Based on Eq. 3.61 and Eq. 3.64, the time derivative of V_{Pos} becomes:

$$\begin{aligned}\dot{V}_{Pos} = &- \sum_{\hbar=x,y,z} \left(K_{\hbar 1} e_{\hbar}^2 + K_{\hbar 2} S_{\hbar}^2 + \xi_{\hbar} \left|S_{\hbar}\right|\right) \\ \leq &0\end{aligned} \tag{3.67}$$

Thereby, the position stability is ensured.

After defining the position and attitude controllers separately, the stability of the overall system must be verified when integrating the two controllers for the closed-loop system. The following theorem is then introduced.

Theorem 3.3.7 *The designed control signals Eq. 3.46, Eq. 3.47, Eq. 3.48, and Eq. 3.64 applied to the quadrotor dynamics ensure the overall stability of the quadrotor aircraft*

Proof: Consider the following lyapunov function for the quadrotor subsystem defined as:

$$V_{Full} = V_{Att} + V_{Pos} \tag{3.68}$$

The first-time derivative of V_{Full} gives,

$$\dot{V}_{Full} = \dot{V}_{Att} + \dot{V}_{Pos} \tag{3.69}$$

Using Eq. 3.56 and Eq. 3.67, we obtain,

$$\dot{V}_{Full} \leq 0 \tag{3.70}$$

Therefore, from the above analysis, the overall closed-loop stability is ensured. This completes the proof.

The proposed hybrid control strategy is described in Algorithm 1.

Algorithm 1 Hybrid flight control system algorithm

Given
Define quadrotor's parameters: $m, J_x, J_y, J_z, l, g, K_\zeta, K_\eta$
Define quadrotor's dynamics: ζ, η
Define the parameters of the position and attitude controllers: $K_{\zeta 1}, K_{\zeta 2}, \xi_\zeta, \alpha_\eta, \beta_\eta, \nu_\eta, \Gamma_{i\eta}$
while (1) **do**
Position controller
acquire real and desired vertical and horizontal position (x, x_d, y, y_d, z, z_d)
Calculate tracking errors (e_x, e_y, e_z)
Calculate tracking errors time's derivative $(\dot{e}_x, \dot{e}_y, \dot{e}_z)$
Calculate the sliding variable(S_x, S_y, S_z)
Calculate the equivalent control $(\nu_{eqx}, \nu_{eqy}, U_{1eq})$
Calculate the switching control $(\nu_{swx}, \nu_{swy}, U_{1sw})$
Calculate the desired Roll and Pitch angles using Eq. 2.25
Attitude controller
acquire real and desired attitude angles $(\Phi, \Phi_d, \Theta, \Theta_d, \Psi, \Psi_d)$
Calculate tracking errors $(e_\Phi, e_\Theta, e_\Psi)$
Calculate tracking errors time's derivative $(\dot{e}_\Phi, \dot{e}_\Theta, \dot{e}_\Psi)$
Calculate the sliding variable$(\sigma_\Phi, \sigma_\Theta, \sigma_\Psi)$
Calculate the equivalent control $(\tau_{eq\Phi}, \tau_{eq\Theta}, \tau_{eq\Psi})$
Calculate $(\hat{a}_{1i}, \hat{a}_{2i}, \hat{a}_{3i})$ the estimated value of the parameter (a_{1i}, a_{2i}, a_{3i})
Calculate the switching control $(\tau_{sw\Phi}, \tau_{sw\Theta}, \tau_{sw\Psi})$
end while

3.4 Controller implementation

In this section, the model dynamics of the quadrotor UAV described in chapter 2 is implemented on MATLAB/Simulink (R2020a version) and used to examine the effectiveness of the proposed control strategies. The modeling phase was performed following MAB (MathWorks® Advisory Board) guidelines [135], which facilitate the integration and deployment of the developed code to the hardware without problems. Moreover, all the simulations are performed on a machine with an Intel core i7 processor and 8 GB of RAM memory, 2.70 GHz.

Note: The physical parameters of the quadrotor system as well as the control strategy are given in appendix B.

Two flight tests were performed to check the accuracy of the suggested control method.

- The first test concerns the problem of tracking trajectories under nominal conditions (without disturbances). A square trajectory is adopted in this case. A comparison in terms of position and attitude tracking is performed with the robust Integral Sliding Mode Control (ISMC) [136], and the nonlinear backstepping technique [137].

- The second test is conducted to demonstrate the ability of the proposed control scheme to compensate for the influence of time-varying external perturbations and parameter uncertainties. A comparison regarding the controller's robustness is also conducted with the second-order sliding mode control (2-SMC) [138], the Global Fast Dynamic Sliding Mode Control (GFDSMC) [87].

3.4.1 Simulation results for path tracking in nominal conditions

In this flight scenario the accuracy of the proposed controller in trajectory tracking is tested. The desired trajectory is a square path and the initial conditions of the quadrotor state variables is selected as:

$$\{ x_i, y_i, z_i, \Phi_i, \Theta_i, \Psi_i\} = \{0,\ 0,\ 0,\ 0,\ 0,\ 0\} \tag{3.71}$$

The flight test results using the three compared flight controllers are shown in Figures 3.4-3.10. The targeted and current trajectories of the aircraft attitude and position are plotted in Figures 3.4 and 3.5. From Figure 3.4, we can observe that the position state variables $\{x, y, z\}$ have reached their reference values $\{x_d, y_d, z_d\}$ rapidly compared to the other methods. Also, the attitude state variables (orientations) are effectively stabilized as shown in Figure 3.5.

It should be stated that the adopted dual-loop control architecture has successfully solved the problem of underactuation. Using this structure, all six degrees of freedom

$(x, y, z, \Phi, \Theta, \Psi)$ are stabilized and converge to their steady states in a short time. Specifically, the proposed controller enables the aircraft to achieve the reference trajectories in a few seconds (1.2835 s for x, 1.2886 s for y, and 0.5828 s for z displacement (see Table 3.1)), which is better than the other methods.

Table 3.1: Comparison in terms of the settling time indicator

	BS	ISMC	Proposed method
x	2.6763	1.4706	**1.2835**
y	2.6463	1.4792	**1.2886**
z	0.8105	0.6852	**0.5828**

Furthermore, the proposed method considerably reduces the influence of the coupling between longitudinal and lateral displacements. This can be noticed in figure 3.4, for example, at $t = 10$ s the vehicle is driven from $x = 0.5$ m to $x = 1$ m; this movement is performed by a pitch rotation (Θ); however, due to the influence of the coupling, a roll (Φ) movement is also performed (see figure 3.4, $t = 10$ s). A small change in the roll angle results in a y-displacement. As shown in the enlarged area of the y-displacement (figure 3.4, $t = 10$ s), the proposed strategy compensated for the influence of the coupling, whereas on the other hand, the ISMC and BS controllers were affected by this variation, resulting in a large deviation from the y_d value.

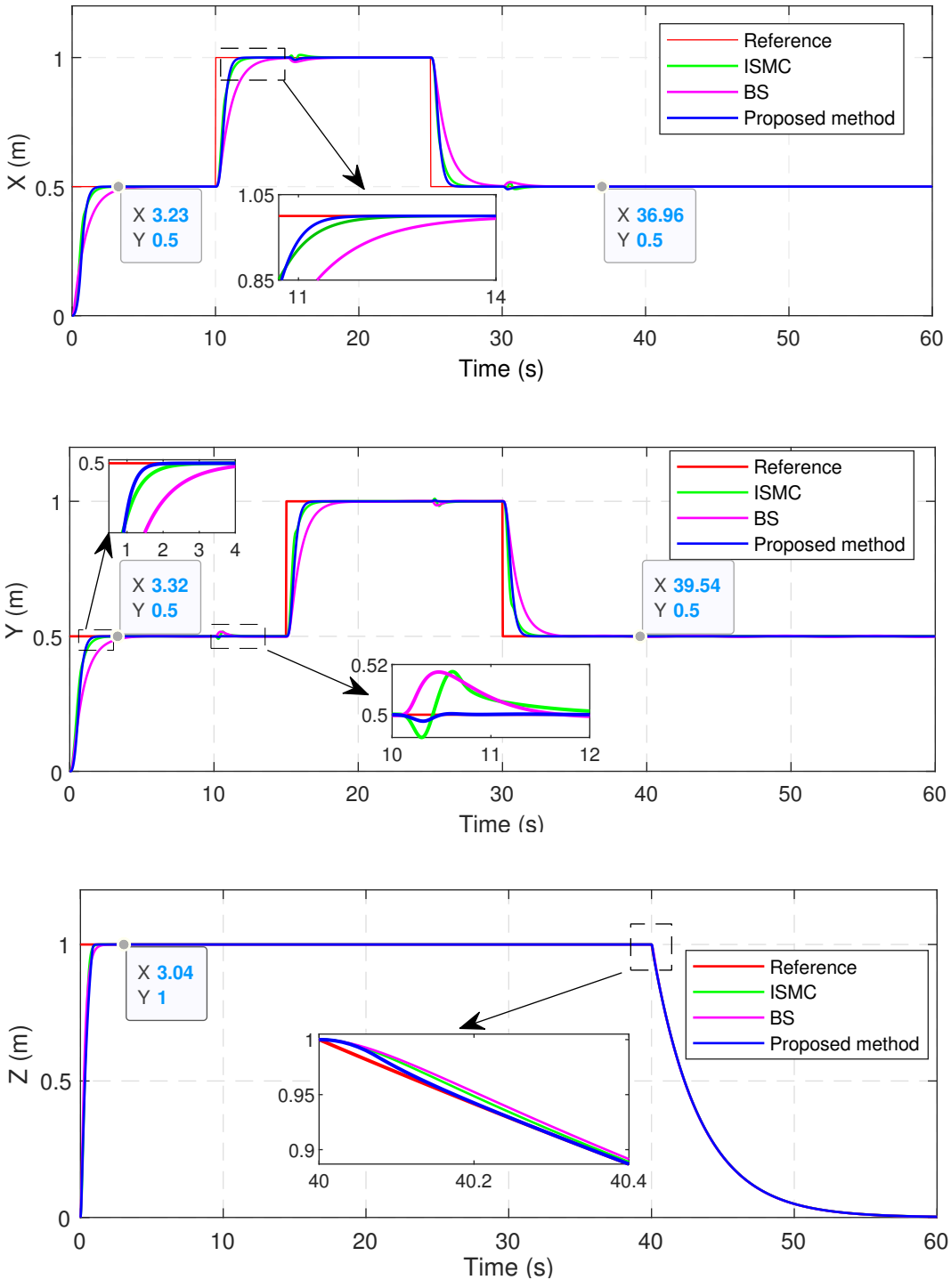

Figure 3.4: Position trajectory tracking

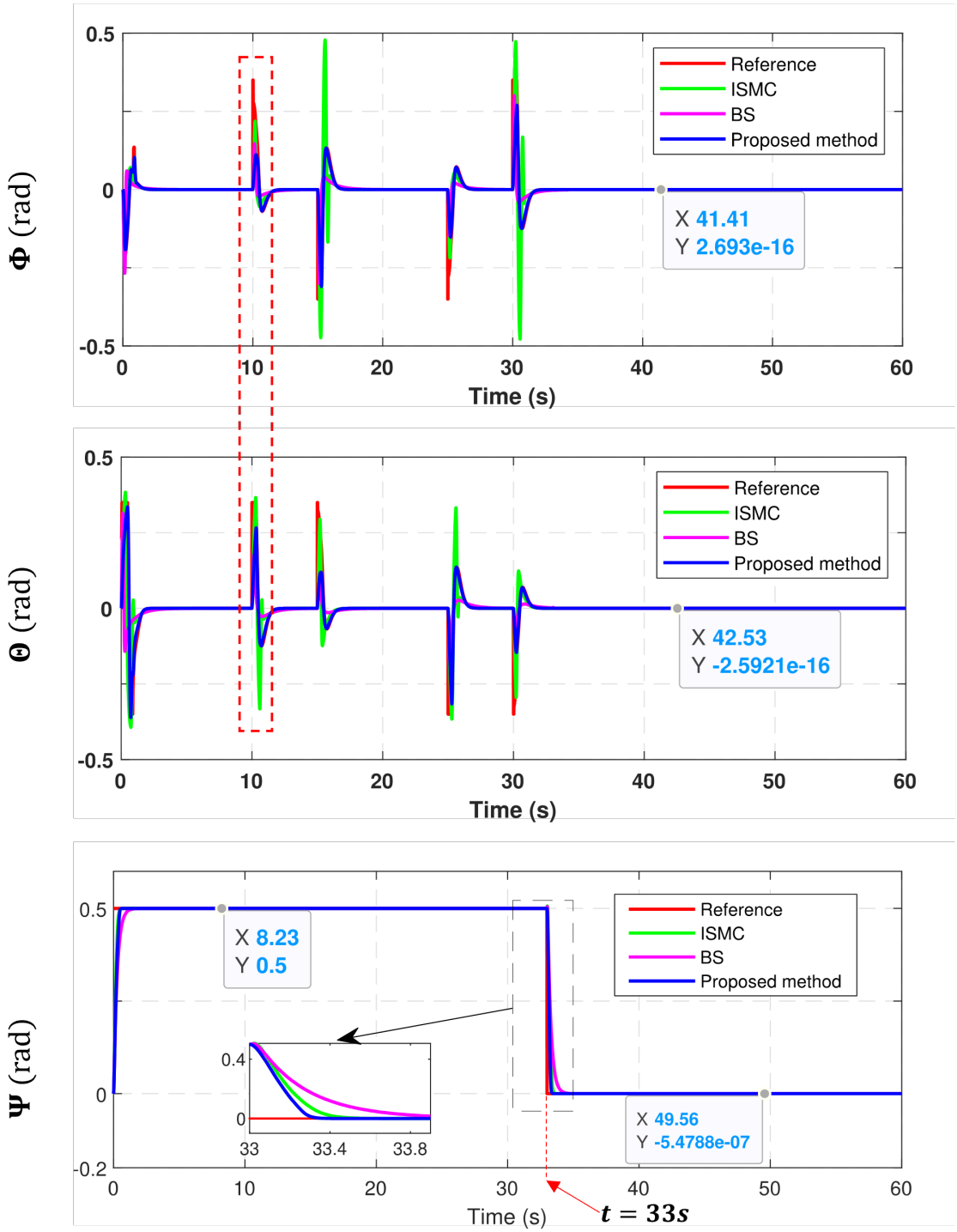

Figure 3.5: Attitude trajectory tracking (Φ, Θ, Ψ)

The time evolution of the position tracking errors are shown in Figure 3.6. As can be observed, the zeroing of the tracking errors can be achieved by the three compared controllers. However, a deeper look at this figure and the zoomed area of Figure 3.4 reveals that, when compared to the other strategies (ISMC and BS controllers), the proposed control approach

is more accurate. Specifically, the tracking errors of the proposed controller converge rapidly compared to the other methods.

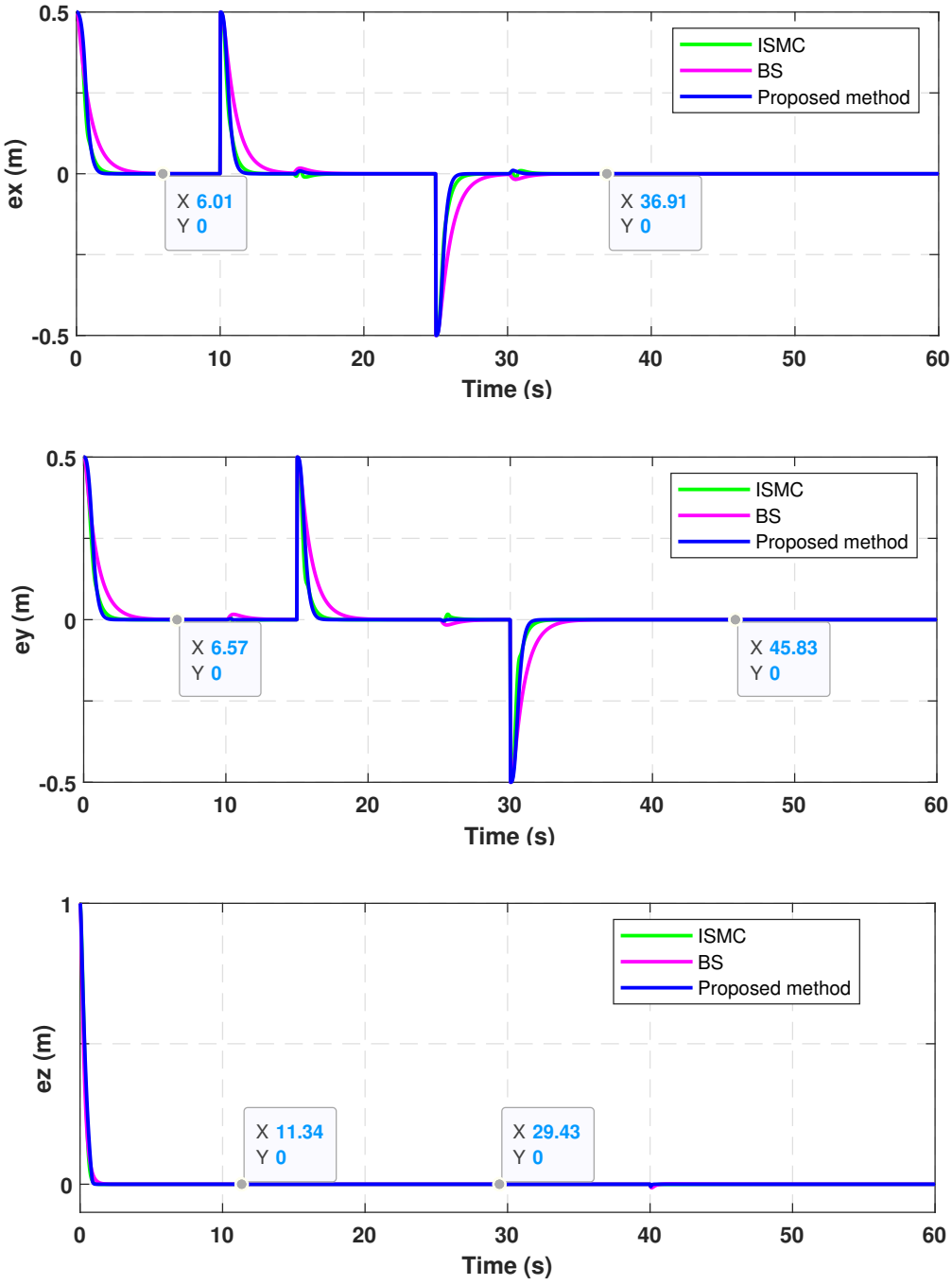

Figure 3.6: Trajectory tracking errors under nominal conditions

Figures 3.7 and 3.8 display the control torques ($\tau_\Phi, \tau_\Theta, \tau_\Psi$) and effort ($U_1$) that enabled the quadrotor to successfully complete the assigned flight task. It should be stated that during

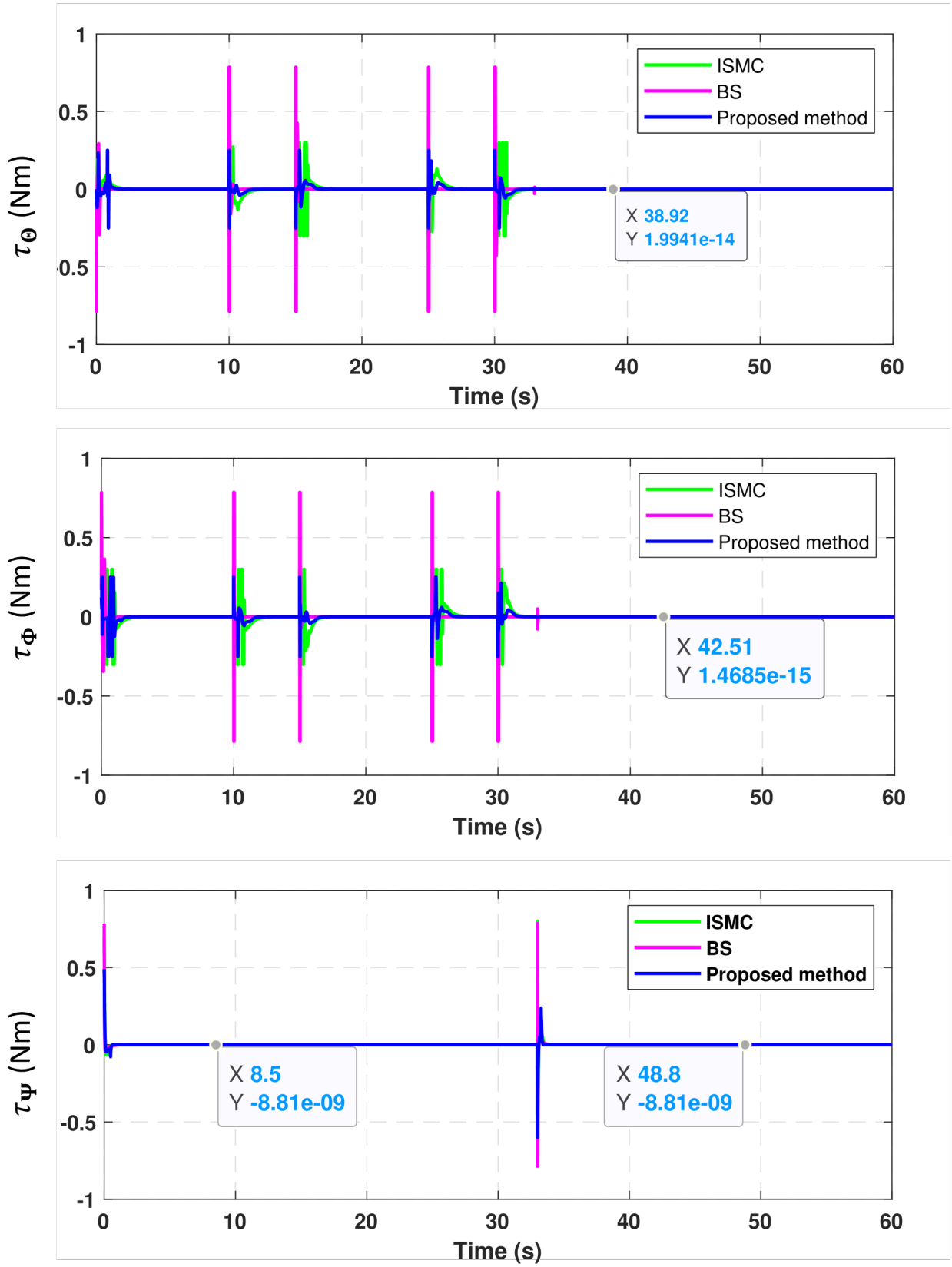

Figure 3.7: generated control torque $(\tau_\Phi, \tau_\Theta, \tau_\Psi)$

a stable flight (hovering flight with no change in the vehicle directions), for example between $t = 5\ s$ and $t = 10\ s$, where the aircraft position is maintained at $(x_d, y_d, z_d) = (0.5, 0.5, 1)$ m, the value of the thrust force will be equal to $mg = 4.905$, and the control torques must be equal to zero. From Figure 3.7 and 3.8 it can be noticed that the proposed controller provides smooth and appropriate control signals. They converge to their equilibrium values $(4.905, 0, 0, 0)$ even under multiple sudden changes in the targeted trajectories, which means flight is more stable.

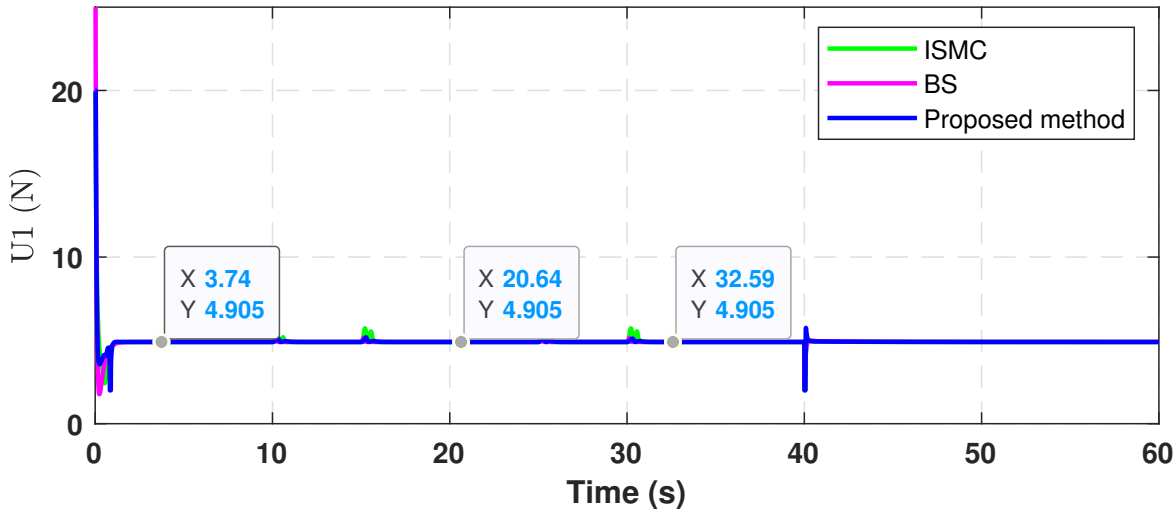

Figure 3.8: Generated thrust force

The estimations of the attitude control parameters are displayed in Figure 3.9. It can be seen that these values change in accordance with the nature of flight, which means good and accurate adaptability to the flight scenario. Specifically, whenever the reference trajectory changes, the controller parameters change in such a way to make the quadrotor response more accurate. For an easy illustration, take the yaw displacement as an example. The desired trajectory for this motion changes its value in two instants: "$t = 0\ s$ and $t = 33\ s$ (see Figure 3.5). The yaw parameters are also changed in these instants, which permit the vehicle to achieve its desired value. Because of the coupling between the horizontal displacements (x and y displacement) and the rotational displacement (pitch and roll motions), we can see that whenever the vehicle changes the x or y direction (instants $t = 0\ s$, $t = 10\ s$, $t = 15\ s$, $t = 25\ s$ and $t = 30s$) the roll and pitch parameters are also updated to ensure adequate rotational motions.

The 3D representation of the quadrotor motions is highlighted in Figure 3.10. As can be seen, the UAV has successfully performed the requested manoeuvre. Moreover, the 3D trajectory traced by the aircraft coincides well with the programmed trajectory.

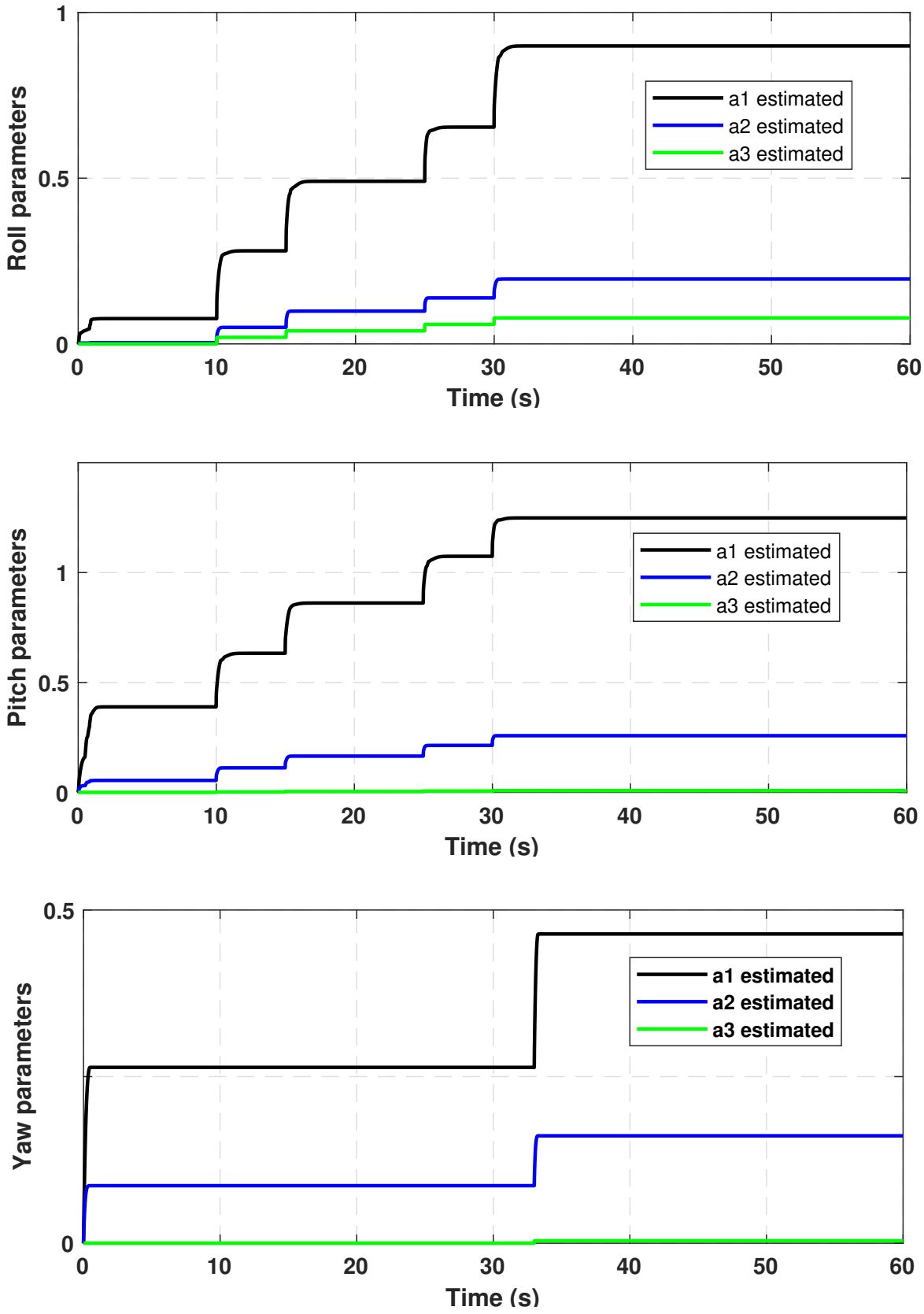

Figure 3.9: Adaptive gains of the attitude controllers

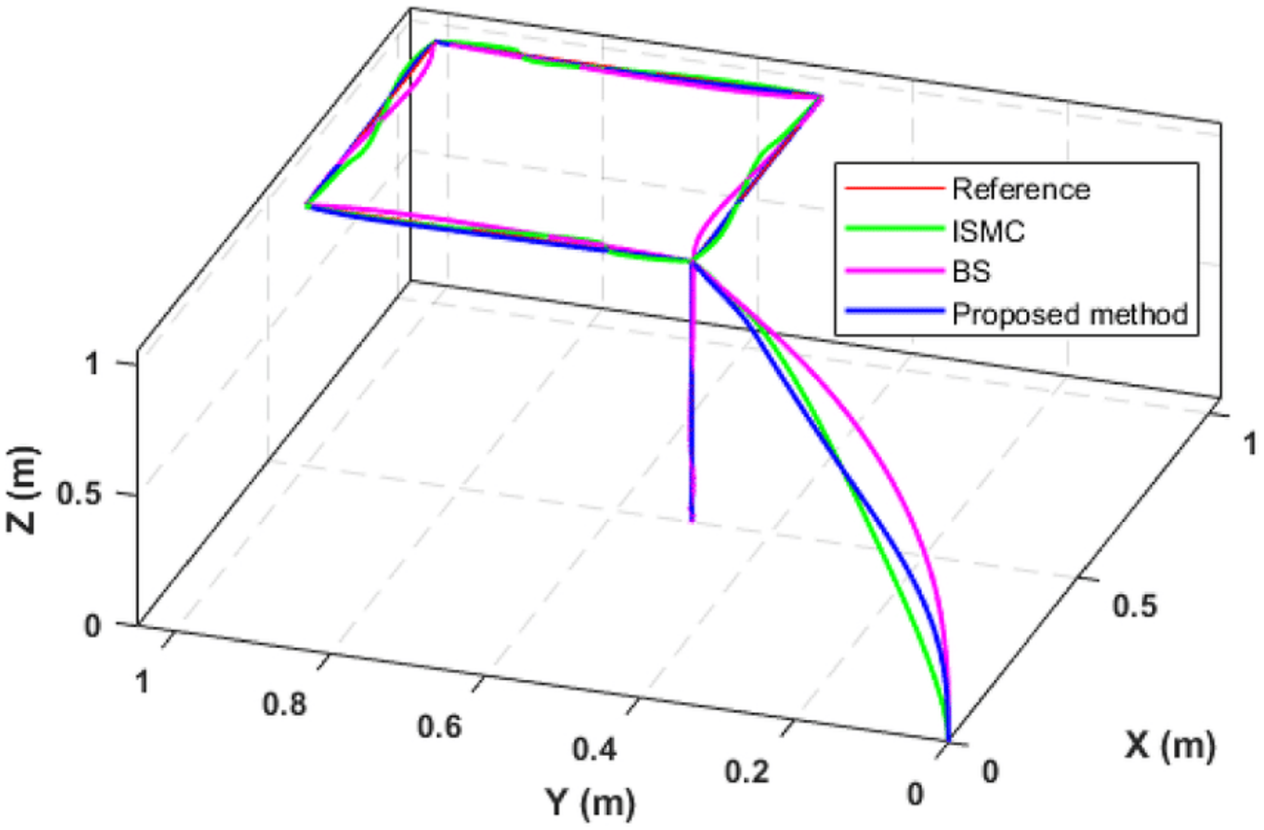

Figure 3.10: 3D trajectory tracking under nominal conditions

In order to clearly display the difference in the flight performances between the three compared methods, a comparison is suggested in terms of the Integral Square Error (ISE) performance index, which is expressed as:

$$ISE = \int_0^{t_f} e^2(t)\, dt \tag{3.72}$$

Where e corresponds to the tracking error, and t_f symbolizes the final simulation time.

The findings of this comparative analysis are reported in Table 3.2. Clearly, the proposed control scheme provides better results, and this can be seen from the smallest value of the ISE in all the conducted tests. Tacking the x displacement as an example, the proposed method is the best one with the lower value of the ISE($ISE = 0.3514$) compared to the BS ($ISE = 0.4344$), and the ISMC($ISE = 0.4084$).

Table 3.2: Quantitative comparison in terms of ISE index in the first scenario

Controller		BC	ISMC	Proposed method
Scenario 1	x	0.4344	0.4084	**0.3514**
	y	0.4379	0.3985	**0.3440**
	z	0.1821	0.2201	**0.1755**
	Ψ	0.0789	0.0602	**0.0452**

In order to highlight the achieved percentage of ISE reduction by the proposed controller, the relative percentage difference (RPD) introduced in [139] is used, it is defined as:

$$RPD_{\text{method}}\,\% = \frac{|ISE_{\text{method}} - ISE_{\text{proposed}}|}{ISE_{\text{method}}} 100 \tag{3.73}$$

The obtained results confirm the superior performance of the proposed strategy compared to the ISMC and BS methods. Specifically, the ISE performance index has decreased by (19.17%) compared to the BS control and by (15.74%) compared to the ISMC.

3.4.2 Simulation results in the presence of disturbances and uncertainties

The robustness against disturbances in the presence of model uncertainties is critical for autonomous quadrotor because the aerodynamic influence, the inertia matrix, and the aircraft mass are extremely hard to identify precisely. To check the effectiveness of the suggested method against model parameter uncertainties, we suppose that the inertial parameters, mass and matrix of inertia, are uncertain. Thus, 30% of uncertainty in these parameters is considered. Specifically, within the present flight test the quadrotor inertial parameters are considered as:

$$\begin{aligned} m &= m_0 \pm 0.3 m_0 \\ J &= J_0 \pm 0.3 J_0 \end{aligned} \tag{3.74}$$

Where m_0 and J_0 are the nominal values of the vehicle mass and matrix of inertia. m and J represent the actual mass and matrix of inertia in the presence of uncertainty.

The targeted path considered in this scenario is a set of several stretches with multiple time-varying trajectories and various change of direction which is a serious challenge in real flight. These trajectories are configured as follows:

$$x_d = \begin{cases} 0.25\cos\left(\frac{2\pi}{15}t\right) m & 0 < t \leq 15 \\ -0.8750 + 0.075tm & 15 < t \leq 25 \\ 1m & 25 < t \leq 35 \\ -2.5 - 0.1t \quad m & 35 < t \leq 45 \\ -3.0015 + 0.0667tm & 45 < t \leq 60 \end{cases} ; \quad y_d = \begin{cases} 0.25\sin\left(\frac{2\pi}{15}t\right) \quad m & 0 < t \leq 15 \\ 0 \quad m & 15 < t \leq 25 \\ -2.5 + 0.1t \quad m & 25 < t \leq 35 \\ 1 \quad m & 35 < t \leq 60 \end{cases}$$

$$z_d = \begin{cases} 0.4 + 0.04tm & 0 < t \leq 15 \\ 1 \quad m & 15 < t \leq 45 \\ \exp(-0.2t + 9)m & 45 < t \leq 60 \end{cases} ; \quad \Psi_d = \begin{cases} 0.5 \quad \text{rad} \\ 0 \quad \text{rad} \end{cases} \tag{3.75}$$

The initial conditions of the quadrotor's position and attitude are chosen as:

$$\{x_i, y_i, z_i, \Phi_i, \Theta_i, \Psi_i\} = \{-0.2,\ -0.2,\ 0,\ 0,\ 0,\ 0\} \tag{3.76}$$

The following sinusoidal external disturbances are also considered to verify the anti-disturbance capability of the proposed control strategy.

$$\begin{aligned} d_\Phi = d_\Theta = d_\Psi &= 1.5\ \cos(\pi t) \qquad rad/s^2 \\ d_x = d_y = d_z &= 0.01\cos(\pi t) \qquad m/s^2 \end{aligned} \tag{3.77}$$

The results of path following under time-varying disturbances and parameter uncertainties are illustrated from Figures 3.11 to 3.15. As shown in Figure 3.11, the three controllers enabled the aircraft to accomplish the mission; however, the figure shows a clear difference in the flight performance. Using the proposed method, the quadrotor achieved the targeted trajectory quickly compared to the other methods. Moreover, in terms of robustness, the suggested method compensated for the impact of disturbances and realized accurate tracking of the desired trajectories.

The uncertainties related to the mass of the quadrotor have a direct impact on the vertical motion. As can be seen from the z-displacement (Figure 3.11), the proposed method is capable of counteracting this factor and allows the vehicle to accurately track the desired vertical position. On the other hand, the 2-SMC is not able to overcome the influence of the mass uncertainty, which causes the largest deviation from the desired z-position. The GFDSMC can reduce the impact of disturbances/uncertainties; however, a slow convergence is observed in the response of this controller.

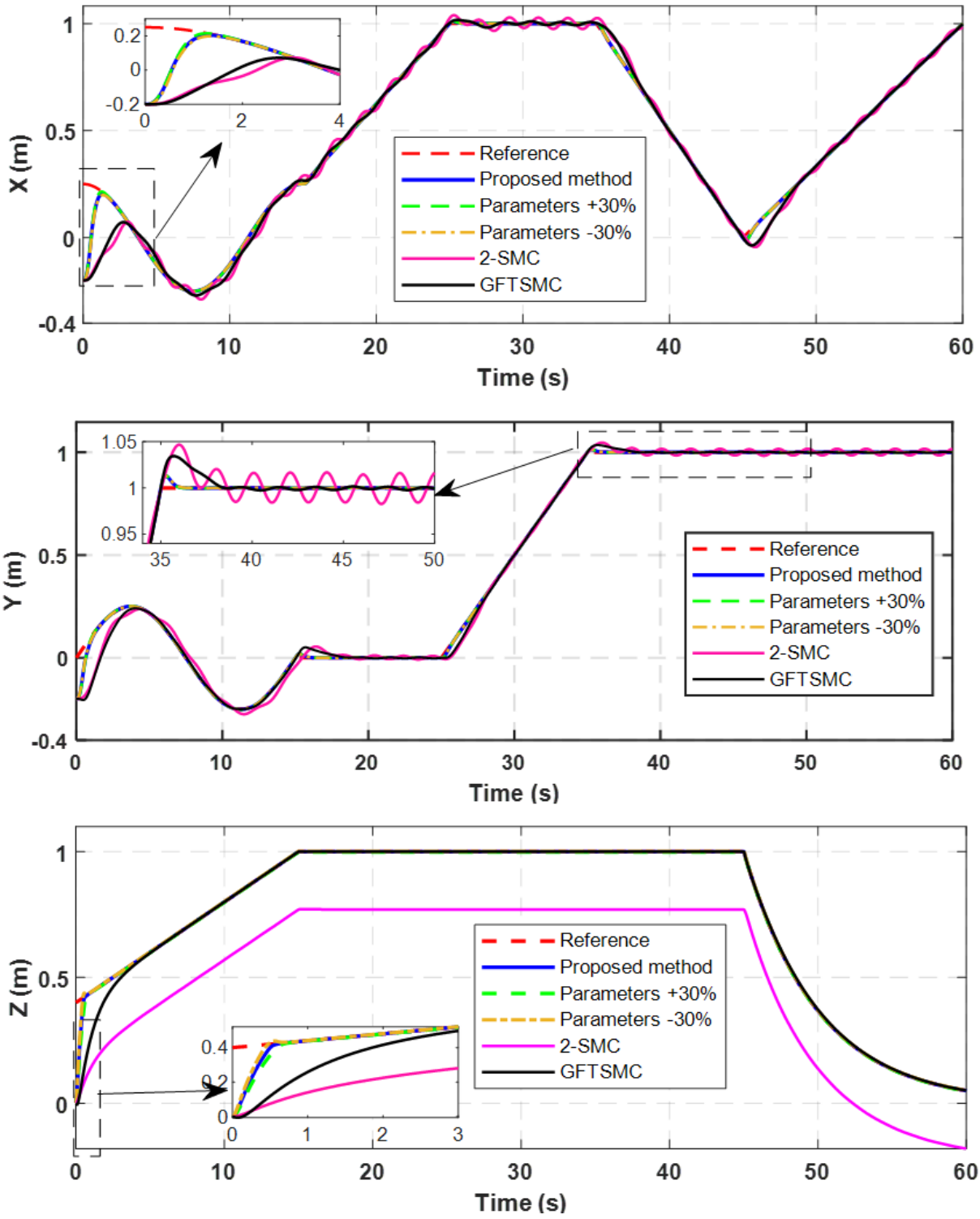

Figure 3.11: Position tracking performance under disturbances/uncertainties

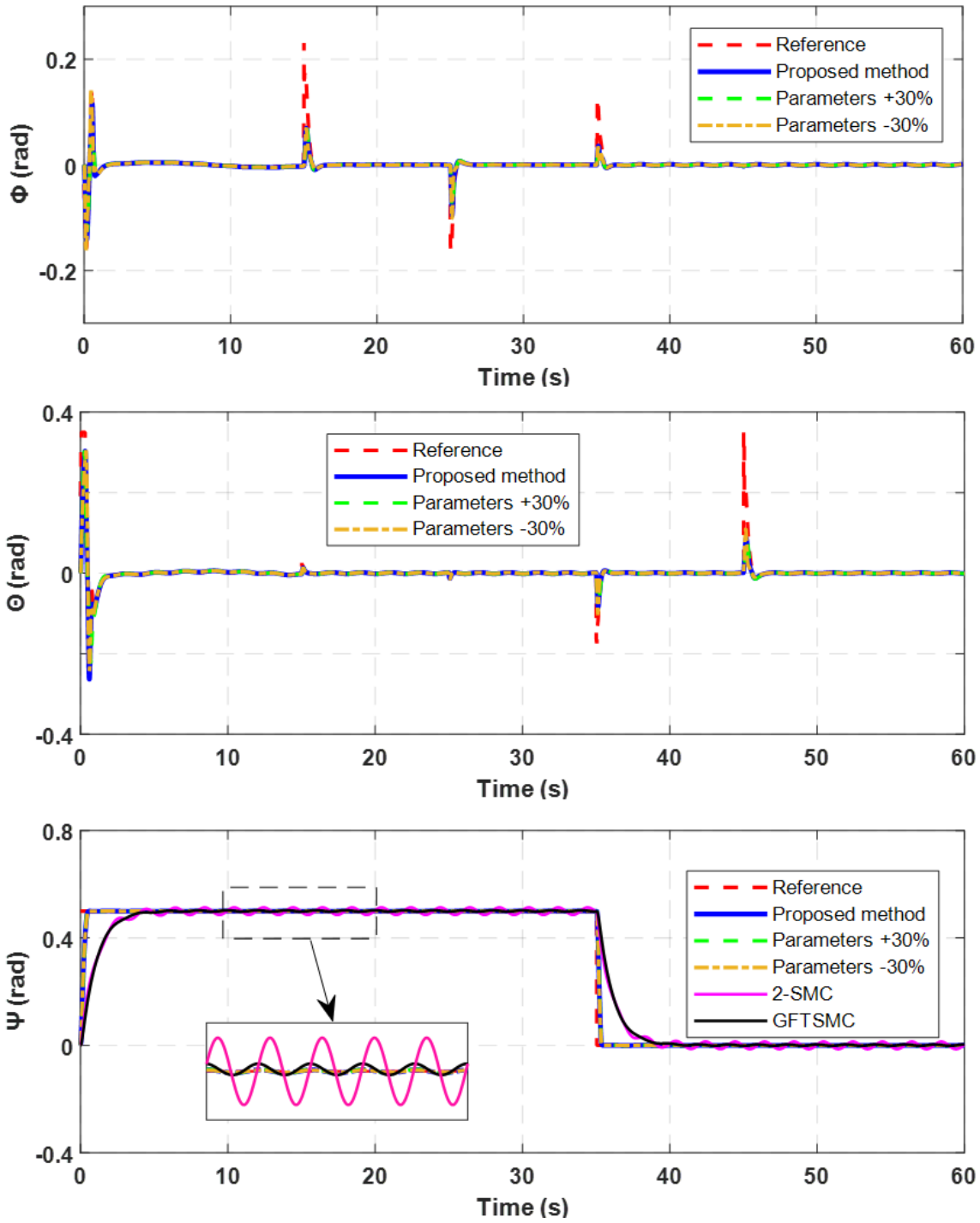

Figure 3.12: Attitude tracking performance under disturbances/uncertainties

As seen in Figure 3.12, the desired orientations $(\Phi_d, \Theta_d, \Psi_d)$ are quickly tracked by the proposed controller, indicating improved flight stability with accurate tracking and good compensation of the influence of disturbances and uncertainties. Moreover, the magnitude

of the attitude angles ($-\pi/2 < \Phi, \Theta < \pi/2$) is small enough to be practically feasible and closely aligns with real quadrotor flight. From the yaw rotation (Ψ), it can be seen that the developed controller reduces the impact of disturbances/uncertainties and shortens the time required to maintain this movement compared to the other methods.

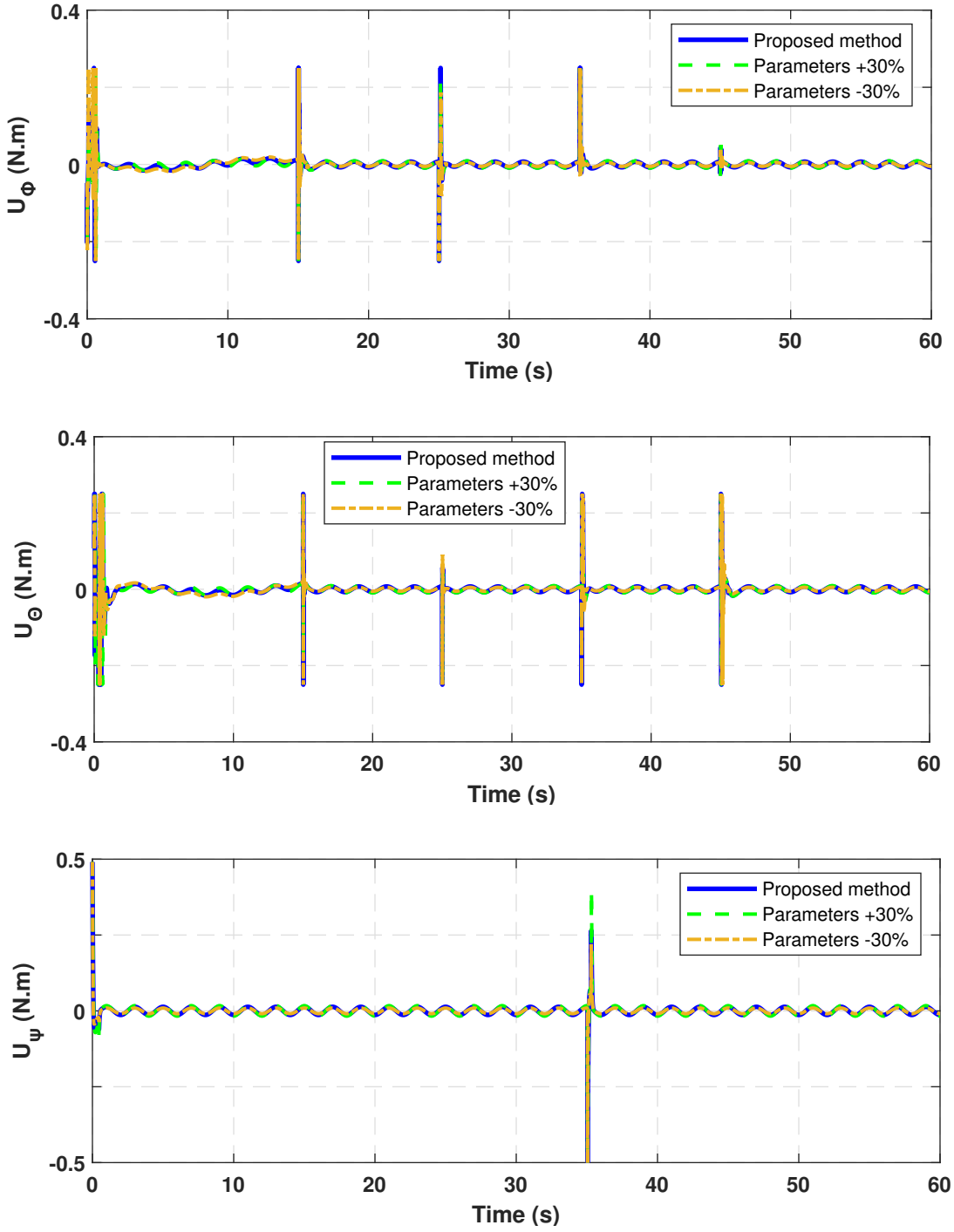

Figure 3.13: Generated control torques under disturbances/uncertainties

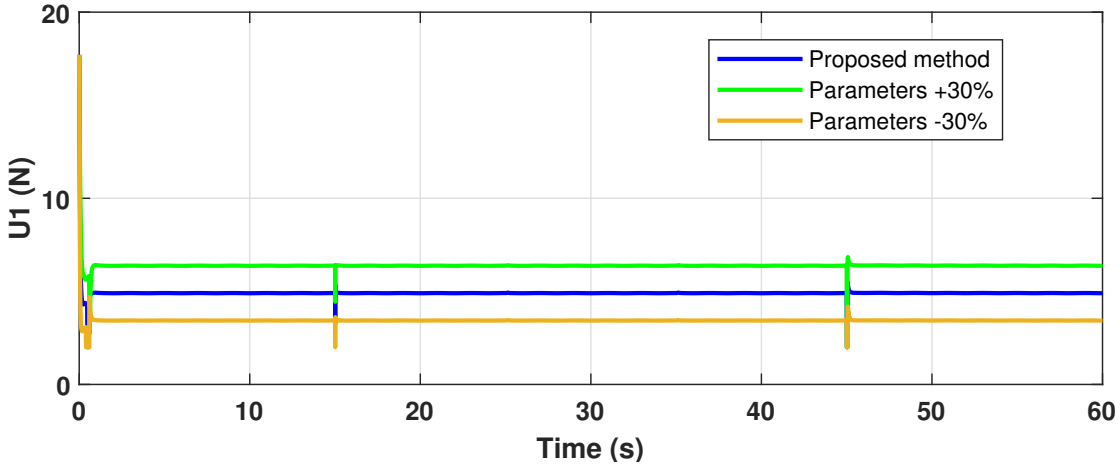

Figure 3.14: Generated control effort under disturbances/uncertainties

The control torques and effort that permit the drone to successfully track the targeted 3D path are respectively shown in Figure 3.13 and Figure 3.14. It can be seen that these signals are smooth without chattering influence.

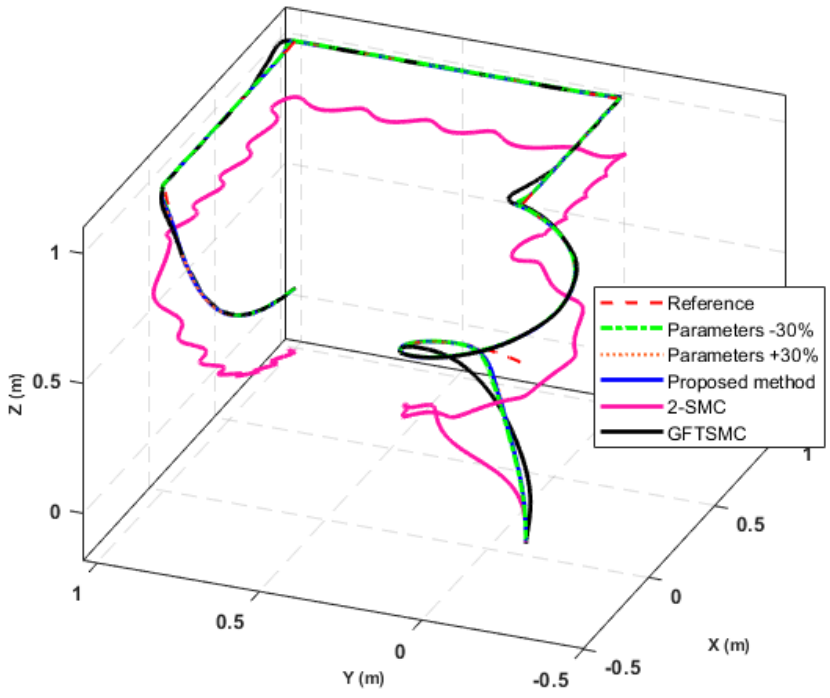

Figure 3.15: 3D trajectory tracking under disturbances/uncertainties

Figure 3.15 illustrates the 3D representation of the reference and actual path under the

influence of unmodeled dynamics. Starting from an initial state of the quadrotor's position far from the desired path, the developed BSMC-ANFTSMC method can drive the aircraft to accomplish the expected flight. Even with 30% of uncertainty in the quadrotor mass and matrix of inertia, the resulting trajectories are almost the same.

In order to further highlight the major differences in the tracking performance between the compared controllers, a comparison in terms of the ISE performance index is suggested. The obtained results are grouped in Table 3.3. As can be noticed, the suggested method provided improved performances with better accuracy, as can be seen from the smallest value of the ISE index. Specifically, the ISE index of the proposed controller has been reduced considerably by (95.05%) compared to the 2-SMC method and by (71.21%) compared to the GFDSMC method. These numerical results reveal the accuracy of the proposed control scheme in both stabilization and trajectory tracking.

Table 3.3: Quantitative comparison in terms of ISE index in the second scenario

Controller		2-SMC	GFDSMC	Proposed method
Scenario 2	x	0.3051	0.1837	**0.0924**
	y	0.1127	0.0941	**0.0187**
	z	3.2724	0.1132	**0.0272**
	Ψ	0.2618	0.2890	**0.0575**

3.5 Conclusion

In this chapter, the problem of quadrotor path tracking in the existence of severe uncertainties in the inertial parameter is investigated. An adaptive nonsingular fast terminal sliding mode control is adopted to efficiently steer the quadrotor orientation, while the backstepping approach is incorporated with the sliding mode technique and used to control the position of the quadrotor system. The simulation experiments, with and without external disturbances, exhibit a remarkable improvement in the response time, the chattering avoidance, and the system robustness. Finally, from the quantitative comparison, it has been asserted that the proposed control law is superior to the BS, the ISMC, the 2-SMC, and the GFTSMC controllers.

4 Proposed robust controller based on a disturbance observer

Contents

3.1 Introduction 60

3.2 Preliminary notions on sliding mode control 60

3.2.1 Reaching laws 62

3.3 Controller design and stability analysis 63

3.3.1 Quadrotor attitude controller 63

3.3.2 Quadrotor position controller 73

3.4 Controller implementation 77

3.4.1 Simulation results for path tracking in nominal conditions 77

3.4.2 Simulation results in the presence of disturbances and uncertainties 86

3.5 Conclusion 92

4.1 Introduction

Quadrotor drones are highly maneuverable aerial robots that are vulnerable to a wide range of undesired aerodynamic factors such as unavoidable modelling errors, unmodeled dynamics, and exogenous disturbances. The impact of these factors becomes important for consideration during the design of the control system. To achieve the desired control objectives in a harsh-disturbed area, a disturbance estimator should be used. In this chapter a novel nonlinear control scheme based on a disturbance observer is developed. It consists of a disturbance observer, a nonsingular terminal SMC (NTSMC), and a supertwisting algorithm (ST). First, the DO is used to estimate the unknown disturbances/uncertainties that affect the vehicle dynamics. Second, a NTSMC is designed to obtain finite-time stability of the vehicle state. Finally, the ST algorithm is employed to ensure the reachability of the sliding surface while reducing the chattering influence.

The rest of this chapter is organized as follows: In section 4.2, the proposed control strategy is designed to realize finite time reaching of the targeted trajectories. In section 4.4 processor in the loop test are conducted to validate the performance of the suggested controller in comparison with some existing strategies. Section 4.5 conclude the chapter.

4.2 Controller design and stability analysis

The control structure of the proposed method is schematically illustrated in Figure 4.1. As can be observed, a hierarchical control structure with two sub-controllers is adopted to deal with the problem of underactuation. Specifically, a position controller is synthesized to drive the aircraft toward the desired locations (x_d, y_d, z_d) by providing adequate control signals (U_1, ν_x, ν_y). For the vehicle orientation, an attitude controller is used to timely track the reference attitude angles. This controller generates the roll, pitch, and yaw torques $(\tau_\Phi, \tau_\Theta, \tau_\Psi)$. The technique used in both controllers integrates the STNTSMC and the DO, which allows an effective elimination of the disturbance influence without being impacted by the chattering influence.

The advantages of the suggested controller can be summarized as follows:

- Unlike our previous contribution presented in chapter 3 in which the finite-time convergence is ensured only for the attitude control, a robust control strategy with finite time convergence property is developed for both the position and attitude control of the quadrotor UAV.
- The proposed controller can provide a real-time approximation of external disturbances.
- Precise tracking of multiple desired trajectories can be achieved by the proposed controller.

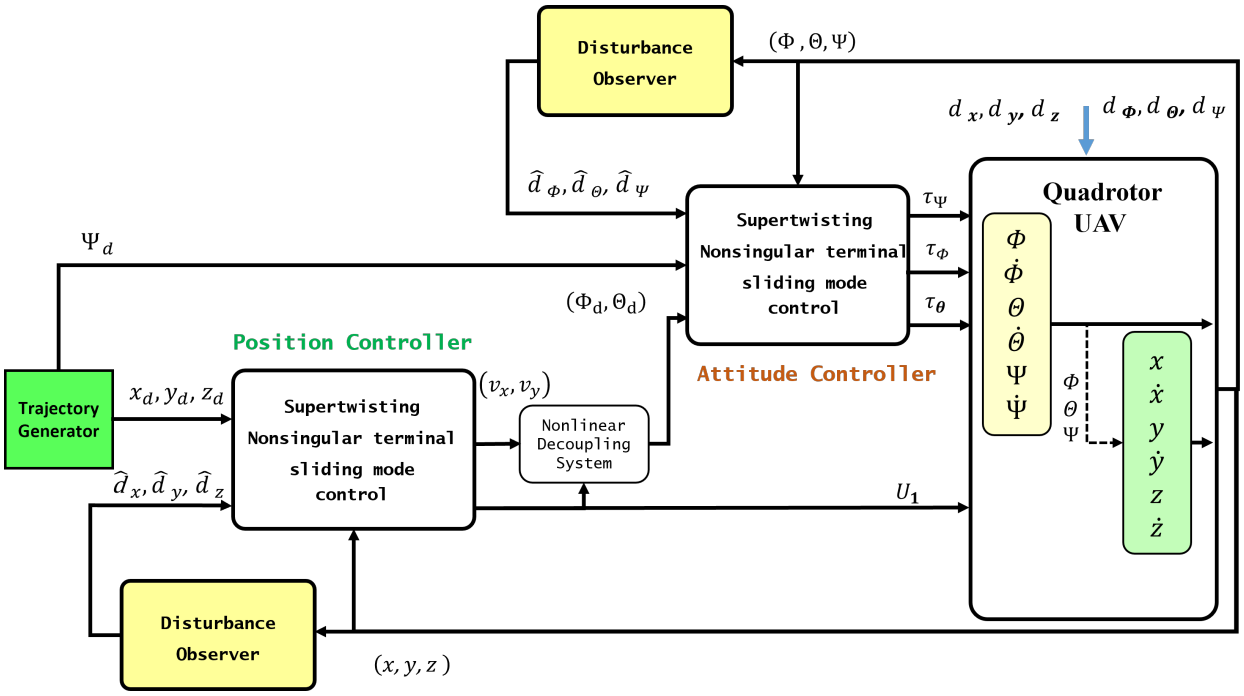

Figure 4.1: Proposed disturbance observer based-robust tracking control of a quadrotor UAV

The design of the proposed controller will be decomposed into three steps. We first start by designing a disturbance observer to have an estimation of the unknown disturbances. Then, based on these estimations, a nonsingular terminal sliding mode control will be derived to ensure closed-loop stability and finite-time convergence of tracking errors. At the final step, the supertwisting algorithm will be introduced to enhance the system's robustness and reduces the chattering influence.

4.2.1 Disturbance observer

Considering the vehicle dynamics exposed to additive disturbances (Eq. 2.23), a disturbance observer can be designed as [140, 141]

$$\begin{cases} \dot{Z}_i = -L_i Z_i - L_i \left(L_i \chi_{i+1} + A_i(\chi) + B_i(\chi) \mathcal{U}_i \right) \\ \hat{d}_i = Z_i + L_i \chi_{i+1} \end{cases} \tag{4.1}$$

Where L_i and Z_i symbolize the observer gain and the observer's internal state, respectively. $\chi_{i+1} = \left\{ \dot{\Phi},\ \dot{\Theta}, \dot{\Psi}, \dot{x}, \dot{y}, \dot{z} \right\}$ correspond to the vehicle's angular and translational velocities. $\hat{d}_i$ represents the estimation of the disturbance. It is assumed that these disturbances are continuous and varies slowly, which means $\dot{d}_i = 0$.

Theorem 4.2.1 *If the observer gain L_i is properly selected, the disturbance's estimation $\hat{d}_i$ will track the additive disturbance d_i asymptotically [140, 142].*

Proof. Let's define the estimation error as:

$$e_{di} = \hat{d}_i - d_i \tag{4.2}$$

The derivative of Eq. 4.2 gives

$$\begin{aligned} \dot{e}_{di} =& \dot{\hat{d}}_i - \dot{d}_i \\ =& \dot{Z} + L\dot{\chi}_{i+1} \end{aligned} \tag{4.3}$$

By invoking Eq. 4.1 in Eq. 4.3,one obtains

$$\begin{aligned} \dot{e}_{di} =& - L_i Z_i - L_i \left(L_i \chi_{i+1} + A_i(\chi) + B_i(\chi)\mathcal{U}_i\right) + L_i \left(A_i(\chi) + B_i(\chi)\mathcal{U}_i + d_i\right) \\ =& - L \left(\hat{d}_i - d_i\right) = -L e_{di} \end{aligned} \tag{4.4}$$

It follow from Eq. 4.4 that the error of observation e_{di} will vanish asymptotically for any $L_i > 0$. Thus, the disturbances can be correctly estimated, that is $\hat{d}_i \equiv d_i$

4.2.2 Disturbance observer-based nonsingular terminal sliding mode control

The proposed controller uses the nonsingular terminal sliding mode control to achieve a finite time convergence of the tracking errors, while avoiding the singularity problem.

Let's start by defining the tracking errors for the attitude and position of the quadrotor UAV. For the quadrotor model given in Eq. 2.23, the state errors are defined as:

$$\begin{cases} e_\Phi = \chi_1 - \Phi_d \\ e_\Theta = \chi_3 - \Theta_d \\ e_\Psi = \chi_5 - \Psi_d \end{cases} ; \quad \begin{cases} e_x = \chi_7 - \chi_d \\ e_y = \chi_9 - y_d \\ e_z = \chi_{11} - z_d \end{cases} \tag{4.5}$$

In order to achieve fast finite-time convergence for the position and attitude dynamics, nonsingular terminal sliding surfaces are selected as follows [143].

$$\begin{cases} \sigma_\Phi = e_\Phi + \kappa_\Phi \left|\dot{e}_\Phi\right|^{\gamma_\Phi} \text{sign}\left(\dot{e}_\Phi\right) \\ \sigma_\Theta = e_\Theta + \kappa_\Theta \left|\dot{e}_\Theta\right|^{\gamma_\Theta} \text{sign}\left(\dot{e}_\Theta\right) \\ \sigma_\Psi = e_\Psi + \kappa_\Psi \left|\dot{e}_\Psi\right|^{\gamma_\Psi} \text{sign}\left(\dot{e}_\Psi\right) \end{cases} \tag{4.6}$$

$$\begin{cases} \sigma_x = e_x + \kappa_x \left|\dot{e}_x\right|^{\gamma_x} \operatorname{sign}\left(\dot{e}_x\right) \\ \sigma_y = e_y + \kappa_y \left|\dot{e}_y\right|^{\gamma_y} \operatorname{sign}\left(\dot{e}_y\right) \\ \sigma_z = e_z + \kappa_z \left|\dot{e}_z\right|^{\gamma_z} \operatorname{sign}\left(\dot{e}_z\right) \end{cases} \tag{4.7}$$

Where $\kappa_\hbar$ are positive constants, and $1 < \gamma_\hbar < 2$.

The first-time derivative of the sliding surfaces can be given by:

$$\begin{cases} \dot{\sigma}_\Phi = \dot{e}_\Phi + \kappa_\Phi \gamma_\Phi \left|\dot{e}_\Phi\right|^{\gamma_\Phi - 1} \ddot{e}_\Phi \\ \dot{\sigma}_\Theta = \dot{e}_\Theta + \kappa_\Theta \gamma_\Theta \left|\dot{e}_\Theta\right|^{\gamma_\Theta - 1} \ddot{e}_\Theta \\ \dot{\sigma}_\Psi = \dot{e}_\Psi + \kappa_\Psi \gamma_\Psi \left|\dot{e}_\Psi\right|^{\gamma_\Psi - 1} \ddot{e}_\Psi \end{cases} \tag{4.8}$$

$$\begin{cases} \dot{\sigma}_x = \dot{e}_x + \kappa_x \gamma_x \left|\dot{e}_x\right|^{\gamma_x - 1} \ddot{e}_x \\ \dot{\sigma}_y = \dot{e}_y + \kappa_y \gamma_y \left|\dot{e}_y\right|^{\gamma_y - 1} \ddot{e}_y \\ \dot{\sigma}_z = \dot{e}_z + \kappa_z \gamma_z \left|\dot{e}_z\right|^{\gamma_z - 1} \ddot{e}_z \end{cases} \tag{4.9}$$

Substituting the second-time derivative of the tracking errors into equations 4.8 and 4.9, we obtain:

$$\begin{cases} \dot{\sigma}_\Phi = \dot{e}_\Phi + \kappa_\Phi \gamma_\Phi \left|\dot{e}_\Phi\right|^{\gamma_\Phi - 1} \left(\rho_{1\Phi}\chi_4\chi_6 + \rho_{2\Phi}\chi_4 + \rho_{3\Phi}\chi_2^2 + \mathrm{B}_\Phi\tau_\Phi + \widehat{d}_\Phi - \ddot{\Phi}_\mathrm{d}\right) \\ \dot{\sigma}_\Theta = \dot{e}_\Theta + \kappa_\Theta \gamma_\Theta \left|\dot{e}_\Theta\right|^{\gamma_\Theta - 1} \left(\rho_{1\Theta}\chi_2\chi_6 + \rho_{2\Theta}\chi_2 + \rho_{3\Theta}\chi_3^2 + \mathrm{B}_\Theta\tau_\Theta + \widehat{d}_\Theta - \ddot{\Theta}_\mathrm{d}\right) \\ \dot{\sigma}_\Psi = \dot{e}_\Psi + \kappa_\Psi \gamma_\Psi \left|\dot{e}_\Psi\right|^{\gamma\Psi - 1} \left(\rho_{1\Psi}\chi_2\chi_4 + \rho_{2\Psi}\chi_6^2 + \mathrm{B}_\Psi\tau_\Psi + \widehat{d}_\Psi - \ddot{\Psi}_\mathrm{d}\right) \end{cases} \tag{4.10}$$

$$\begin{cases} \dot{\sigma}_x = \dot{e}_x + \kappa_x \gamma_x \left|\dot{e}_x\right|^{\gamma_x - 1} \left(\frac{U_1}{m}\left(C_{\chi_1}S_{\chi_3}C_{\chi_5} + S_{\chi_1}S_{\chi_5}\right) + \rho_x\chi_8 + \hat{d}_x - \ddot{x}_d\right) \\ \dot{\sigma}_y = \dot{e}_y + \kappa_y \gamma_y \left|\dot{e}_y\right|^{\gamma_y - 1} \left(\frac{U_1}{m}\left(C_{\chi_1}S_{\chi_3}S_{\chi_5} - S_{\chi_1}C_{\chi_5}\right) + \rho_y\chi_{10} + \hat{d}_y - \ddot{y}_d\right) \\ \dot{\sigma}_z = \dot{e}_z + \kappa_z \gamma_z \left|\dot{e}_z\right|^{\gamma_z - 1} \left(\frac{U_1}{m}\left(C_{\chi_1}C_{\chi_3}\right) - g + \rho_z\chi_{12} + \hat{d}_z - \ddot{z}_d\right) \end{cases} \tag{4.11}$$

Where $\hat{d}_\hbar$ is the estimate of $d_\hbar$.

Sliding mode theory articulates on the design of a feedback control law that ensure that the system's states reach the adopted sliding surface and remain on it until reaching the equilibrium. Specifically, the structure of the control law is:

$$U = U_{eq} + U_{sw} \tag{4.12}$$

Where U_{eq} is the equivalent control that ensures the stability when the system is on the sliding surface ($\sigma_\hbar = 0$), and U_{sw} is the switching control that ensures the reachability of the predesigned sliding surface.

The equivalent control law can be obtained by forcing $\dot{\sigma}_\hbar = 0$; then, the control equations for the attitude and position are respectively given by the following equations:

$$\begin{cases} \tau_{\Phi eq} = \frac{1}{\mathrm{B}_\Phi}\left(\ddot{\Phi}_d - \rho_{1\Phi}\chi_4\chi_6 - \rho_{2\Phi}\chi_4 - \rho_{3\Phi}\chi_2^2 - \widehat{d}_\Phi - \frac{|\dot{e}_\Phi|^{2-\gamma_\Phi}}{k_\Phi\gamma_\Phi}\operatorname{sign}(\dot{e}_\Phi)\right) \\ \tau_{\Theta eq} = \frac{1}{\mathrm{B}_\Theta}\left(\ddot{\Theta}_d - \rho_{1\Theta}\chi_2\chi_6 - \rho_{2\Theta}\chi_2 - \rho_{3\Theta}\chi_3^2 - \widehat{d}_\Theta - \frac{|\dot{e}_\Theta|^{2-\gamma_\Theta}}{k_\Theta\gamma_\Theta}\operatorname{sign}(\dot{e}_\Theta)\right) \\ \tau_{\Psi eq} = \frac{1}{\mathrm{B}_\Psi}\left(\ddot{Z}_d - \rho_{1\Psi}\chi_2\chi_4 - \rho_{2\Psi}\chi_6^2 - \widehat{d}_\Psi - \frac{|\dot{e}_\Psi|^{2-\gamma_\Psi}}{k_\Psi\gamma_\Psi}\operatorname{sign}(\dot{e}_\Theta)\right) \end{cases} \tag{4.13}$$

$$\begin{cases} \nu_{xeq} = \ddot{x}_d - \rho_x\chi_8 - \widehat{d}_x - \frac{|\dot{e}_x|^{2-\gamma_x}}{k_x\gamma_x}\operatorname{sign}(\dot{e}_x) \\ \nu_{yeq} = \ddot{y}_d - \rho_y\chi_{10} - \widehat{d}_y - \frac{|\dot{e}_y|^{2-\gamma_y}}{ky\gamma_y}\operatorname{sign}(\dot{e}_y) \\ U_{1eq} = \frac{m}{c_{\chi_1}c_{\chi_3}}\left(\ddot{z}_d + g - \rho_z\chi_{12} - \widehat{d}_z - \frac{|\dot{e}_z|^{2-\gamma_z}}{k_z\gamma_z}\operatorname{sign}(\dot{e}_z)\right) \end{cases} \tag{4.14}$$

In order to reduce the effect of disturbances and parameter variations, a switching control based on the constant plus proportional reaching law is designed as:

$$\begin{cases} \tau_{\Phi sw} = \frac{1}{\mathrm{B}_\Phi}\left(-b_{1\Phi}\sigma_\Phi - b_{2\Phi}\operatorname{sign}(\sigma_\Phi)\right) \\ \tau_{\Theta sw} = \frac{1}{\mathrm{B}_\Theta}\left(-b_{1\Theta}\sigma_\Theta - b_{2\theta}\operatorname{sign}(\sigma_\Theta)\right) \\ \tau_{\Psi sw} = \frac{1}{\mathrm{B}_\Psi}\left(-b_{1\Psi}\sigma_\Psi - b_{2\Psi}\operatorname{sign}(\sigma_\Psi)\right) \end{cases} \tag{4.15}$$

$$\begin{cases} \nu_{xsw} = -b_{1x}\sigma_x - b_{2x}\operatorname{sign}(\sigma_x) \\ \nu_{ysw} = -b_{1y}\sigma_y - b_{2y}\operatorname{sign}(\sigma_y) \\ U_{1sw} = \frac{1}{\mathrm{B}_z}\left(-b_{1z}\sigma_z - b_{2z}\operatorname{sign}(\sigma_z)\right) \end{cases} \tag{4.16}$$

$b_{1\hbar}$ and $b_{2\hbar}$ are positive constants.

Using equations 4.13, 4.14, 4.15, and 4.16, the disturbance observer based nonsingular terminal SMC for the quadrotor attitude and position can be formulated as,

$$\begin{cases} \tau_\Phi = \frac{1}{\mathrm{B}_\Phi}\left(\ddot{\Phi}_d - \rho_{1\Phi}\chi_4\chi_6 - \rho_{2\Phi}\chi_4 - \rho_{3\Phi}\chi_2^2 - \widehat{d}_\Phi - \frac{|\dot{e}_\Phi|^{2-\gamma_\Phi}}{k_\Phi\gamma_\Phi}\operatorname{sign}(\dot{e}_\Phi) - b_{1\Phi}\sigma_\Phi - b_{2\Phi}\operatorname{sign}(\sigma_\Phi)\right) \\ \tau_\Theta = \frac{1}{\mathrm{B}_\Theta}\left(\ddot{\Theta}_d - \rho_{1\Theta}\chi_2\chi_6 - \rho_{2\Theta}\chi_2 - \rho_{3\Theta}\chi_3^2 - \widehat{d}_\Theta - \frac{|\dot{e}_\Theta|^{2-\gamma_\Theta}}{k_\theta\gamma_\Theta}\operatorname{sign}(\dot{e}_\Theta) - b_{1\theta}\sigma_\Theta - b_{2\Theta}\operatorname{sign}(\sigma_\Theta)\right) \\ \tau_\Psi = \frac{1}{\mathrm{B}_\Psi}\left(\ddot{\Psi}_d - \rho_{1\Psi}\chi_2\chi_4 - \rho_{2\Psi}\chi_6^2 - \widehat{d}_\Psi - \frac{|\dot{e}_\Psi|^{2-\gamma^\Psi}}{k_\Psi\gamma_\Psi}\operatorname{sign}(\dot{e}_\Psi) - b_{1\Psi}\sigma_\Psi - b_{2\Psi}\operatorname{sign}(\sigma_\Psi)\right) \end{cases} \tag{4.17}$$

$$\begin{cases} \nu_x = \ddot{x}_d - \rho_x \chi_8 - \widehat{d}_x - \frac{|\dot{e}_x|^{2-\gamma_x}}{k_x \gamma_x} \operatorname{sign}(\dot{e}_x) - b_{1x}\sigma_x - b_{2x} \operatorname{sign}(\sigma_x) \\ \nu_y = \ddot{y}_d - \rho_y \chi_{10} - \widehat{d}_y - \frac{|\dot{e}_y|^{2-\gamma_y}}{k_y \gamma_y} \operatorname{sign}(\dot{e}_y) - b_{1y}\sigma_y - b_{2y} \operatorname{sign}(\sigma_y) \\ U_1 = \frac{m}{c_{\chi 1} c_{\chi 3}} \left(\ddot{z}_d + g - \rho_z \chi_{12} - \widehat{d}_z - \frac{|\dot{e}_z|^{2-\gamma_z}}{k_z \gamma_z} \operatorname{sign}(\dot{e}_z) - b_{1z}\sigma_z - b_{2z} \operatorname{sign}(\sigma_z) \right) \end{cases} \tag{4.18}$$

Theorem 4.2.2 *Consider the roll subsystem. If the control equations are constructed as Eq. 4.17, then the finite-time convergence is ensured.*

Proof. To prove the stability of the investigated system when using the established control law given by Eq. 4.17, the Lyapunov theory will be used. For this reason, let's consider the following Lyapunov function:

$$V_\Phi = \frac{1}{2}\, \sigma_\Phi^2 \tag{4.19}$$

The derivative of V_Φ is given by:

$$\begin{aligned} \dot{V}_\Phi &= \sigma_\Phi \dot{\sigma}_\Phi \\ &= \sigma_\Phi \left(\dot{e}_\Phi + \kappa_\Phi \gamma_\Phi \left| \dot{e}_\Phi \right|^{\gamma_\Phi - 1} \left(\rho_{1\Phi} \chi_4 \chi_6 + \rho_{2\Phi} \chi_4 + \rho_{3\Phi} \chi_2^2 + \mathrm{B}_\Phi \tau_\Phi + d_\Phi - \ddot{\Phi}_\mathrm{d} \right) \right) \end{aligned} \tag{4.20}$$

By substituting the control signal τ_Φ by it's expression given in Eq. 4.17, the derivative of V gives

$$\begin{aligned} \dot{V}_\Phi = \sigma_\Phi \Big(\dot{e}_\Phi + \kappa_\Phi \gamma_\Phi \left| \dot{e}_\Phi \right|^{\gamma_\Phi - 1} \Big(\rho_{1\Phi} \chi_4 \chi_6 + \rho_{2\Phi} \chi_4 + \rho_{3\Phi} \chi_2^2 + \ddot{\Phi}_d - \rho_{1\Phi} \chi_4 \chi_6 - \rho_{2\Phi} \chi_4 - \rho_{3\Phi} \chi_2^2 - \widehat{d}_\Phi \\ - \frac{|\dot{e}_\Phi|^{2-\gamma_\Phi}}{k_\Phi \gamma_\Phi} \operatorname{sign}(\dot{e}_\Phi) - b_{1\Phi}\sigma_\Phi - b_{2\Phi} \operatorname{sign}(\sigma_\Phi) + d_\Phi - \ddot{\Phi}_\mathrm{d} \Big) \Big) \end{aligned} \tag{4.21}$$

After simplification, $\dot{V}_\Phi$ becomes:

$$\begin{aligned} \dot{V}_\Phi &\leq \sigma_\Phi \kappa_\Phi \gamma_\Phi \left| \dot{e}_\Phi \right|^{\gamma_\Phi - 1} \left(-b_{1\Phi}\sigma_\Phi - b_{2\Phi} sign(\sigma_\Phi) \right) \\ &\leq \kappa_\Phi \gamma_\Phi \left| \dot{e}_\Phi \right|^{\gamma_\Phi - 1} \left(-b_{1\Phi}\sigma_\Phi^2 - \ b_{2\Phi} \left| \sigma_\Phi \right| \right) \\ &\leq 0 \end{aligned} \tag{4.22}$$

As the Lyapunov function V_Φ is positive defined and its first-time derivative $\dot{V}_\Phi$ is negative; then, the closed-loop system stability of the quadrotor UAV is ensured.

In order to prove that the convergence is ensured in finite time, Eq. 4.22 can be rewritten as follows:

$$\dot{V}_\Phi = \frac{dV_\Phi}{dt} \leq -2\kappa_\Phi\gamma_\Phi \left|\dot{e}_\Phi\right|^{\gamma_\Phi - 1} b_{1\Phi} V_\Phi - \sqrt{2}\kappa_\Phi\gamma_\Phi \left|\dot{e}_\Phi\right|^{\gamma_\Phi - 1} b_{2\Phi} V_\Phi^{1/2} \tag{4.23}$$

Let's define $m_{1\Phi} = 2\kappa_\Phi\gamma_\Phi \left|\dot{e}_\Phi\right|^{\gamma_\Phi - 1} b_{1\Phi}$ and $m_{2\Phi} = \sqrt{2}\kappa_\Phi\gamma_\Phi \left|\dot{e}_\Phi\right|^{\gamma_\Phi - 1} b_{2\Phi}$, then Eq. 4.23 becomes

$$\frac{dV_\Phi}{dt} \leq -m_1 V_\Phi - m_2 V_\Phi^{1/2} \tag{4.24}$$

Using the separation of variables, we get

$$dt \leq \frac{-dV_\Phi}{m_{1\Phi} V_\Phi + \sqrt{2} m_{2\Phi} V_\Phi^{\frac{1}{2}}} = \frac{-V_\Phi^{-1/2} dV_\Phi}{m_{1\Phi} V_\Phi^{\frac{1}{2}} + m_{2\Phi}} = \frac{-2dV_\Phi^{1/2}}{m_{1\Phi} V_\Phi^{\frac{1}{2}} + m_{2\Phi}} \tag{4.25}$$

Consider t_s the time from the initial state error $(e_\Phi(t_0) \neq 0, V_\Phi(t_0) \neq 0)$ to $(e_\Phi(t_s) = 0, V(t_s) = 0)$. The integration of Eq. 4.25 is calculated as

$$\int_{t_0}^{t_s} dt \leq \int_{V_\Phi(t_0)}^{V_\Phi(t_s)} \frac{-2dV_\Phi^{1/2}}{m_{1\Phi} V_\Phi^{1/2} + m_{2\Phi}} = \frac{-2}{m_{1\Phi}} \int_{V_\Phi(t_0)}^{V_\Phi(t_s)} \frac{dV_\Phi^{1/2}}{V_\Phi^{1/2} + \frac{m_{2\Phi}}{m_{1\Phi}}} \tag{4.26}$$

Known that $\int_{A_0}^{A_1} \frac{dX}{X+c} = [\ln(X+c)]_{A_0}^{A_1}$, then Eq. 4.26 gives

$$t_s \leq t_0 + \frac{2}{m_{1\Phi}} \ln\left(\frac{m_{1\Phi} V_\Phi(t_0)^{1/2} + m_{2\Phi}}{m_{2\Phi}}\right) \tag{4.27}$$

Therefore, convergence in a finite period is guaranteed.

The stability of the overall closed-loop system can be proved using the same procedure provided in theorem 4.2.2.

Theorem 4.2.3 *Considering the overall quadrotor dynamics, if the control equations are designed as Eq. 4.17 and Eq. 4.18, then overall closed-loop stability of the quadrotor's system is ensured.*

Proof: Consider the following lyapunov function:

$$V_F = \frac{1}{2}\sigma_\Phi^2 + \frac{1}{2}\sigma_\Theta^2 + \frac{1}{2}\sigma_\Psi^2 + \frac{1}{2}\sigma_x^2 + \frac{1}{2}\sigma_y^2 + \frac{1}{2}\sigma_z^2 \tag{4.28}$$

Differentiating V_F, we obtain

$$\dot{V}_F = \sigma_\Phi \dot{\sigma}_\Phi + \sigma_\Theta \dot{\sigma}_\Theta + \sigma_\Psi \dot{\sigma}_\Psi + \sigma_x \dot{\sigma}_x + \sigma_y \dot{\sigma}_y + \sigma_z \dot{\sigma}_z \tag{4.29}$$

Considering the sliding surface dynamics (Eq. 4.10 and Eq. 4.11), it follow

$$\begin{aligned}
\dot{V}_F = {} & \sigma_\Phi \left(\dot{e}_\Phi + \kappa_\Phi \gamma_\Phi \left| \dot{e}_\Phi \right|^{\gamma_\Phi - 1} \left(\rho_{1\Phi} \chi_4 \chi_6 + \rho_{2\Phi} \chi_4 + \rho_{3\Phi} \chi_2^2 + \mathrm{B}_\Phi \tau_\Phi + d_\Phi - \ddot{\Phi}_\mathrm{d} \right) \right) \\
& + \sigma_\Theta \left(\dot{e}_\Theta + \kappa_\Theta \gamma_\Theta \left| \dot{e}_\Theta \right|^{\gamma_\Theta - 1} \left(\rho_{1\Theta} \chi_2 \chi_6 + \rho_{2\Theta} \chi_2 + \rho_{3\Theta} \chi_3^2 + \mathrm{B}_\Theta \tau_\Theta + \widehat{d}_\Theta - \ddot{\Theta}_\mathrm{d} \right) \right) \\
& + \sigma_\Psi \left(\dot{e}_\Psi + \kappa_\Psi \gamma_\Psi \left| \dot{e}_\Psi \right|^{\gamma_\Psi - 1} \left(\rho_{1\Psi} \chi_2 \chi_4 + \rho_{2\Psi} \chi_6^2 + \mathrm{B}_\Psi \tau_\Psi + \widehat{d}_\Psi - \ddot{\Psi}_\mathrm{d} \right) \right) \\
& + \sigma_x \left(\dot{e}_x + \kappa_x \gamma_x \left| \dot{e}_x \right|^{\gamma_x - 1} \left(\frac{U_1}{m} \left(C_{\chi_1} S_{\chi_3} C_{\chi_5} + S_{\chi_1} S_{\chi_5} \right) + \rho_x \chi_8 + \hat{d}_x - \ddot{x}_d \right) \right) \\
& + \sigma_y \left(\dot{e}_y + \kappa_y \gamma_y \left| \dot{e}_y \right|^{\gamma_y - 1} \left(\frac{U_1}{m} \left(C_{\chi_1} S_{\chi_3} S_{\chi_5} - S_{\chi_1} C_{\chi_5} \right) + \rho_y \chi_{10} + \hat{d}_y - \ddot{y}_d \right) \right) \\
& + \sigma_z \left(\dot{e}_z + \kappa_z \gamma_z \left| \dot{e}_z \right|^{\gamma_z - 1} \left(\frac{U_1}{m} \left(C_{\chi_1} C_{\chi_3} \right) - g + \rho_z \chi_{12} + \hat{d}_z - \ddot{z}_d \right) \right)
\end{aligned} \tag{4.30}$$

By substituting the control signals (Eq. 4.17 and Eq. 4.18) in Eq. 4.30, $\dot{V}_F$ becomes:

$$\begin{aligned}
\dot{V}_F \leq {} & \sigma_\Phi \kappa_\Phi \gamma_\Phi \left| \dot{e}_\Phi \right|^{\gamma_\Phi - 1} \left(-b_{1\Phi} \sigma_\Phi - b_{2\Phi} sign\left(\sigma_\Phi \right) \right) + \sigma_\Theta \kappa_\Theta \gamma_\Theta \left| \dot{e}_\Theta \right|^{\gamma_\Theta - 1} \left(-b_{1\Theta} \sigma_\Theta - b_{2\Theta} sign\left(\sigma_\Theta \right) \right) \\
& + \sigma_\Psi \kappa_\Psi \gamma_\Psi \left| \dot{e}_\Psi \right|^{\gamma_\Psi - 1} \left(-b_{1\Psi} \sigma_\Psi - b_{2\Psi} sign\left(\sigma_\Psi \right) \right) + \sigma_\mathrm{x} \kappa_x \gamma_x \left| \dot{e}_x \right|^{\gamma_x - 1} \left(-b_{1x} \sigma_x - b_{2x} sign\left(\sigma_x \right) \right) \\
& + \sigma_y \kappa_y \gamma_y \left| \dot{e}_y \right|^{\gamma_y - 1} \left(-b_{1y} \sigma_y - b_{2y} sign\left(\sigma_y \right) \right) + \sigma_z \kappa_z \gamma_z \left| \dot{e}_z \right|^{\gamma_z - 1} \left(-b_{1z} \sigma_z - b_{2z} sign\left(\sigma_z \right) \right)
\end{aligned} \tag{4.31}$$

After simplification, we obtain

$$\begin{aligned}
\dot{V}_F \leq {} & \kappa_\Phi \gamma_\Phi \left| \dot{e}_\Phi \right|^{\gamma_\Phi - 1} \left(-b_{1\Phi} \sigma_\Phi^2 - \ b_{2\Phi} \left| \sigma_\Phi \right| \right) + \kappa_\Theta \gamma_\Theta \left| \dot{e}_\Theta \right|^{\gamma_\Theta - 1} \left(-b_{1\Theta} \sigma_\Theta^2 - \ b_{2\Theta} \left| \sigma_\Theta \right| \right) \\
& + \kappa_\Psi \gamma_\Psi \left| \dot{e}_\Psi \right|^{\gamma_\Psi - 1} \left(-b_{1\Psi} \sigma_\Psi^2 - \ b_{2\Psi} \left| \sigma_\Psi \right| \right) + \kappa_x \gamma_x \left| \dot{e}_x \right|^{\gamma_x - 1} \left(-b_{1x} \sigma_x^2 - \ b_{2x} \left| \sigma_x \right| \right) \\
& + \kappa_y \gamma_y \left| \dot{e}_y \right|^{\gamma_y - 1} \left(-b_{1y} \sigma_y^2 - \ b_{2y} \left| \sigma_y \right| \right) + \kappa_z \gamma_z \left| \dot{e}_z \right|^{\gamma_z - 1} \left(-b_{1z} \sigma_z^2 - \ b_{2z} \left| \sigma_z \right| \right) \\
& \leq 0
\end{aligned} \tag{4.32}$$

Following the above analysis, the closed-loop stability of the quadrotor dynamics is assured. This convergence will also be guaranteed in a finite time defined by $t_{\hbar s} \leq t_{\hbar 0} + \frac{2}{m_{1\hbar}} \ln \left(\frac{m_{1\hbar} V_\hbar (t_{\hbar 0})^{1/2} + m_{2\hbar}}{m_{2\hbar}} \right)$.

4.2.3 Disturbance observer-based supertwisting nonsingular terminal sliding mode control

In order to improve the robustness and to compensate for the effect of disturbances while reducing the chattering influence, a combination of the supertwisting algorithm with the NTSMC is established. Thus, the resulting disturbance observer-based supertwisting NTSMC

(DO-STNTSMC) for the quadrotor system is designed as follows:

$$U = U_{NTSMC} + U_{ST} \tag{4.33}$$

Where U_{NTSMC} is the NTSMC control laws given by Equations 4.17 and 4.18. U_{ST} symbolizes the supertwisting algorithm defined in ref [144] as:

$$U_{ST} = -\beta_{1\hbar} \left|\sigma_{\hbar}\right|^{\frac{1}{2}} \operatorname{sign}\left(\sigma_h\right) - \beta_{2\hbar} \int_0^t \operatorname{sign}\left(\sigma_{\hbar}\right) d\tau \tag{4.34}$$

With $\beta_{1\hbar}$ and $\beta_{2\hbar}$ are positive constants.

Using Eqs. 4.17, 4.18 and 4.34, the proposed control laws can then be formulated as:

$$\begin{aligned}
\tau_{\Phi} &= \frac{1}{\mathrm{B}_{\boldsymbol{\Phi}}} \begin{pmatrix} \ddot{\Phi}_d - \rho_{1\Phi}\chi_4\chi_6 - \rho_{2\Phi}\chi_4 - \rho_{3\Phi}\chi_2^2 - \widehat{d}_{\Phi} - \frac{\left|\dot{e}_{\Phi}\right|^{2-\gamma_{\Phi}}}{k_{\Phi}\gamma_{\Phi}} \operatorname{sign}\left(\dot{e}_{\Phi}\right) - b_{1\Phi}\sigma_{\Phi} \\ -b_{2\Phi} \operatorname{sign}\left(\sigma_{\Phi}\right) - \beta_{1\Phi} \left|\sigma_{\Phi}\right|^{\frac{1}{2}} \operatorname{sign}\left(\sigma_{\Phi}\right) - \beta_{2\Phi} \int_0^t \operatorname{sign}\left(\sigma_{\Phi}\right) d\tau \end{pmatrix} \\
\tau_{\Theta} &= \frac{1}{\mathrm{B}_{\Theta}} \begin{pmatrix} \ddot{\Theta}_d - \rho_{1\Theta}\chi_2\chi_6 - \rho_{2\Theta}\chi_2 - \rho_{3\Theta}\chi_3^2 - \widehat{d}_{\Theta} - \frac{\left|\dot{e}_{\Theta}\right|^{2-\gamma_{\Theta}}}{k_{\Theta}\gamma_{\Theta}} \operatorname{sign}\left(\dot{e}_{\Theta}\right) - b_{1\Theta}\sigma_{\Theta} \\ -b_{2\Theta} \operatorname{sign}\left(\sigma_{\Theta}\right) - \beta_{1\Theta} \left|\sigma_{\Theta}\right|^{\frac{1}{2}} \operatorname{sign}\left(\sigma_{\Theta}\right) - \beta_{2\Theta} \int_0^t \operatorname{sign}\left(\sigma_{\Theta}\right) d\tau \end{pmatrix} \\
\tau_{\Psi} &= \frac{1}{\mathrm{B}_{\boldsymbol{\Psi}}} \begin{pmatrix} \ddot{\Psi}_d - \rho_{1\Psi}\chi_2\chi_4 - \rho_{2\Psi}\chi_6^2 - \widehat{d}_{\Psi} - \frac{\left|\dot{e}_{\Psi}\right|^{2-\gamma^{\Psi}}}{k_{\Psi}\gamma_{\Psi}} \operatorname{sign}\left(\dot{e}_{\Psi}\right) - b_{1\Psi}\sigma_{\Psi} \\ -b_{2\Psi} \operatorname{sign}\left(\sigma_{\Psi}\right) - \beta_{1\Psi} \left|\sigma_{\Psi}\right|^{\frac{1}{2}} \operatorname{sign}\left(\sigma_{\Psi}\right) - \beta_{2\Psi} \int_0^t \operatorname{sign}\left(\sigma_{\Psi}\right) d\tau \end{pmatrix}
\end{aligned} \tag{4.35}$$

$$\begin{aligned}
\nu_x =& \ddot{x}_d - \rho_x\chi_8 - \widehat{d}_x - \frac{\left|\hat{e}_x\right|^{2-\gamma_x}}{k_x\gamma_x} \operatorname{sign}\left(\dot{e}_x\right) - b_{1x}\sigma_x - b_{2x} \operatorname{sign}\left(\sigma_x\right) - \beta_{1x} \left|\sigma_x\right|^{\frac{1}{2}} \operatorname{sign}\left(\sigma_x\right) \\
& - \beta_{2x} \int_0^t \operatorname{sign}\left(\sigma_x\right) d\tau \\
\nu_y =& \ddot{y}_d - \rho_y\chi_{10} - \widehat{d}_y - \frac{\left|\dot{e}_y\right|^{2-\gamma_y}}{k_y\gamma_y} \operatorname{sign}\left(\dot{e}_y\right) - b_{1y}\sigma_y - b_{2y} \operatorname{sign}\left(\sigma_y\right) - \beta_{1y} \left|\sigma_y\right|^{\frac{1}{2}} \operatorname{sign}\left(\sigma_y\right) \\
& - \beta_{2y} \int_0^t \operatorname{sign}\left(\sigma_y\right) d\tau \\
U_1 =& \frac{m}{c_{\chi_1} c_{\chi_3}} \begin{pmatrix} \ddot{z}_d + g - \rho_z\chi_{12} - \widehat{d}_z - \frac{\left|\dot{e}_z\right|^{2-\gamma_z}}{k_z\gamma_z} \operatorname{sign}\left(\dot{e}_z\right) - b_{1z}\sigma_z - b_{2z} \operatorname{sign}\left(\sigma_z\right) \\ -\beta_{1z} \left|\sigma_z\right|^{\frac{1}{2}} \operatorname{sign}\left(\sigma_z\right) - \beta_{2z} \int_0^t \operatorname{sign}\left(\sigma_z\right) d\tau \end{pmatrix}
\end{aligned} \tag{4.36}$$

Remark 4.2.1 *It should be mentioned that the selection of the controller gains plays a dominant role in the flight performance. An effective way to configure the controller parameters is to start by adjusting the parameters of the attitude controller separately. Then, we keep these gains and we configure the parameters of the position controller. Finally, we keep the best controller gains, which ensure the best consistency in the flight performance.*

The control strategy developed in this chapter is described in Algorithm 2.

Algorithm 2 DO-Supertwisting Nonsingular Terminal SMC algorithm

Given
Define quadrotor's parameters: $m, J_x, J_y, J_z, l, g, K_\zeta, K_\eta$
Define quadrotor's dynamics: ζ, η
Define the parameters of the position and attitude controllers: $\kappa_\eta, \kappa_\zeta, \gamma_\eta, \gamma_\zeta, b_{1\eta}, b_{2\eta}, b_{1\zeta}, b_{2\zeta}, \beta_{1\eta}, \beta_{2\eta}, \beta_{1\zeta}, \beta_{2\zeta}$
while (1) **do**
Position controller
acquire real and desired vertical and horizontal position (x, x_d, y, y_d, z, z_d)
Calculate tracking errors (e_x, e_y, e_z)
Calculate tracking errors time's derivative $(\dot{e}_x, \dot{e}_y, \dot{e}_z)$
Calculate the sliding variable$(\sigma_x, \sigma_y, \sigma_z)$
Calculate $(\hat{d}_x, \hat{d}_y, \hat{d}_z)$ the estimated value of the external disturbances (d_x, d_y, d_z)
Calculate the equivalent control $(\nu_{eqx}, \nu_{eqy}, U_{1eq})$
Calculate the switching control $(\nu_{swx}, \nu_{swy}, U_{1sw})$
Calculate the ultimate control (ν_x, ν_y, U_1)
Calculate the desired Roll and Pitch angles using Eq. 2.25
Attitude controller
acquire real and desired attitude $(\Phi, \Phi_d, \Theta, \Theta_d, \Psi, \Psi_d)$
Calculate tracking errors $(e_\Phi, e_\Theta, e_\Psi)$
Calculate tracking errors time's derivative $(\dot{e}_\Phi, \dot{e}_\Theta, \dot{e}_\Psi)$
Calculate the sliding variable$(\sigma_\Phi, \sigma_\Theta, \sigma_\Psi)$
Calculate $(\hat{d}_\Phi, \hat{d}_\Theta, \hat{d}_\Psi)$ the estimated value of the external disturbances $(d_\Phi, d_\Theta, d_\Psi)$
Calculate the equivalent control $(\tau_{eq\Phi}, \tau_{eq\Theta}, \tau_{eq\Psi})$
Calculate the switching control $(\tau_{sw\Phi}, \tau_{sw\Theta}, \tau_{sw\Psi})$
Calculate the ultimate control $(\tau_\Phi, \tau_\Theta, \tau_\Psi)$
end while

4.3 Procedure of the processor-in-the-loop testing

The proposed flight control system was validated by adopting an effective verification and validation (V&V) method known as model-based design testing. At first, the quadrotor model (Eq. 2.23) as well as the proposed control system (Equations 4.35 and 4.36) are developed and implemented on MATLAB/Simulink. In this phase, the controller model as well as the quadrotor model are both programmed using Simulink's blocks, then tested in simulation. This step is referred to as Model-in-the-Loop (MIL) testing. In the second step, the suggested controller's code is then generated, connected with the quadrotor model, and tested once again in the simulation environment (this test is known as Software-in-the-Loop testing). The third step corresponds to the Processor-in-the-Loop testing (PIL), in which the quadrotor model is simulated on the host PC while the suggested controller's code is executed on the embedded microprocessor.

Processor-in-the-loop implementation (PIL) is a powerful method to verify the efficiency of a control scheme on a real hardware board, while the studied model is software [145]. The PIL test checks the functionality of the embedded code on a real microprocessor. Figure 4.2 highlights the procedure of the PIL experiments used to verify the feasibility of the proposed method.

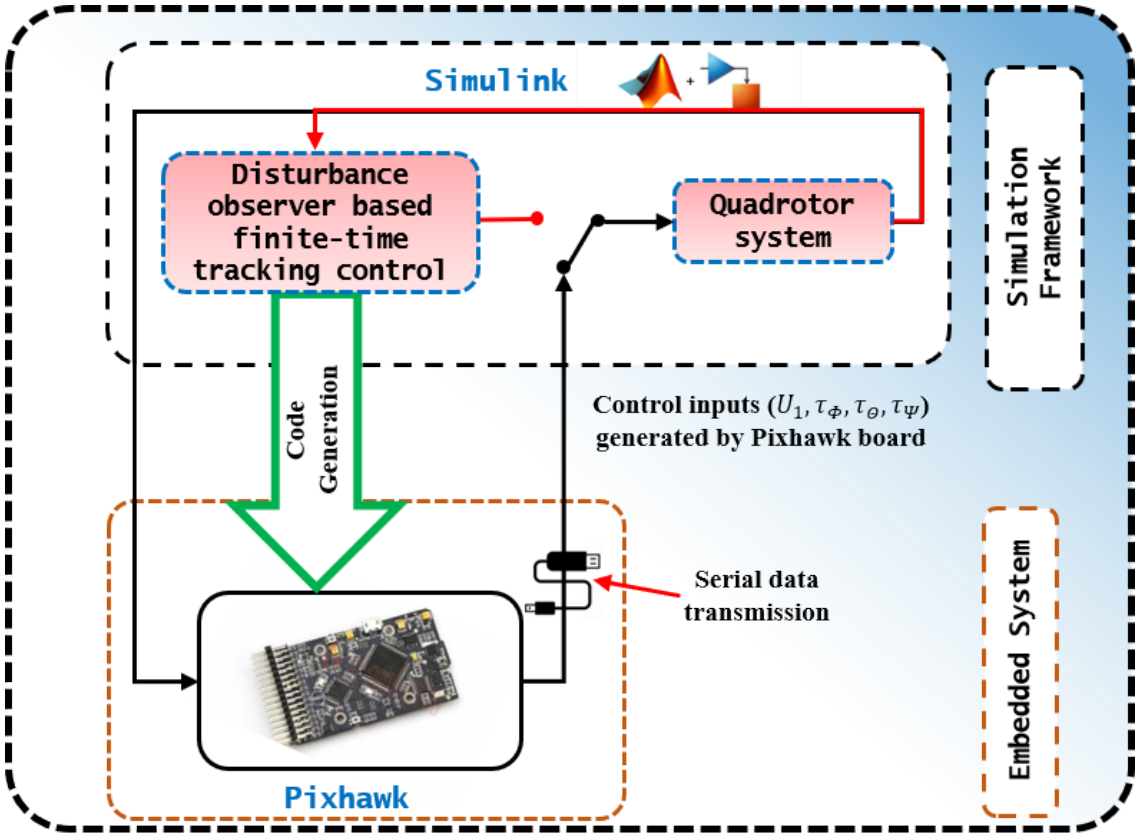

Figure 4.2: Flow chart of the PIL implementation process

To execute the PIL testing, the MATLAB toolbox "*Support Package for PX4 Autopilots* " has been used [146]. This toolbox automates the generation of C++ code directly from a MATLAB/Simulink program, as well as its deployment to the target hardware. Using a USB cable, this toolbox also permits connectivity between the Pixhawk board and MATLAB/Simulink for test visualization and monitoring. During the PIL experiments, the generated code will run in the platform hardware while the disturbed quadrotor model is simulated in MATLAB/ Simulink. Specifically, the control inputs $(U_1, \tau_\Phi, \tau_\Theta, \tau_\Psi)$ computed by the autopilot board are transmitted back to MATLAB/ Simulink to control the vehicle's behaviors. The PIL testing checks the functionality of the embedded code on a real microprocessor board.

The Pixhawk (PX4) autopilot hardware [147] is used to implement and execute control algorithms. It is an open-source autopilot based on an STM 32-bit STM32F427 Cortex® M4, 256KB SRAM, 180MHz, ARM®, 2MB flash. The Pixhawk autopilot has a built-in real-time operating system to assure basic functions including algorithm execution, low-level drivers and multi-thread scheduling. Moreover, the board integrate an MEAS MS5607 barometer. Besides, an inertial measurement unit (IMU) embedded in the autopilot board serves to sense the instantaneous orientation (Φ, Θ, Ψ) as well as the angular rate $(\dot{\Phi}, \dot{\Theta}, \dot{\Psi})$. The IMU incorporates an ST Micro LSM303D 14-bit accelerometer/magnetometer, MPU 6000 3-axis accelerometer/gyroscope, ST Micro L3GD20H 16-bit gyroscope. Furthermore, the autopilot board can communicate with other components using I2C, SPI, CAN and UART protocols.

4.4 Results and discussion

In this section, processor-in-the-loop tests are performed to validate the feasibility and superior performance of the suggested approach over the existing nonsingular terminal sliding mode control (NTSMC). The parameters of the proposed controller are given in appendix B.

To verify the merits and performance of the proposed approach, two flight scenarios for the path following are carried out. In the first scenario, the aircraft is asked to follow a square path under the influence of time-varying disturbances, while in the second one, the vehicle is mandated to follow an eight-shaped trajectory. In this latter, in addition to the influence of disturbances, a random variation of the drag coefficients in the position and attitude is also considered.

4.4.1 Flight Scenario 1: Robustness against disturbances

In this flight test, the drone is commanded to track a square path under the influence of disturbances. The initial conditions of the vehicle's state are $(x_i, y_i, z_i) = (0, 0, 0)\ m$, $(\Phi_i, \Theta_i, \Psi_i) = (0, 0, 0)\, rad$.

The results of path tracking obtained by the PIL implementations of the proposed control scheme in comparison with conventional NTSMC are illustrated in Figure 4.3-4.8. The actual and targeted trajectories in the presence of additive disturbances are displayed in Figure 4.3. From this figure, it can be noticed that, in comparison with the NTSMC strategy, the proposed method can provide significantly enhanced tracking performance. From the zoomed area in Figure 4.3, it is clear that the suggested control scheme remarkably attenuates the impact of external perturbations and tracks accurately the targeted trajectories with reduced tracking errors. Attitude response is illustrated in Figure 4.4. As can be observed, the roll Φ and pitch Θ angles follow their desired values even in case of continuous changes of the targeted horizontal paths (x and y), whereas the heading angle Ψ precisely tracks its desired time-varying trajectory, regardless of the influence of external disturbances.

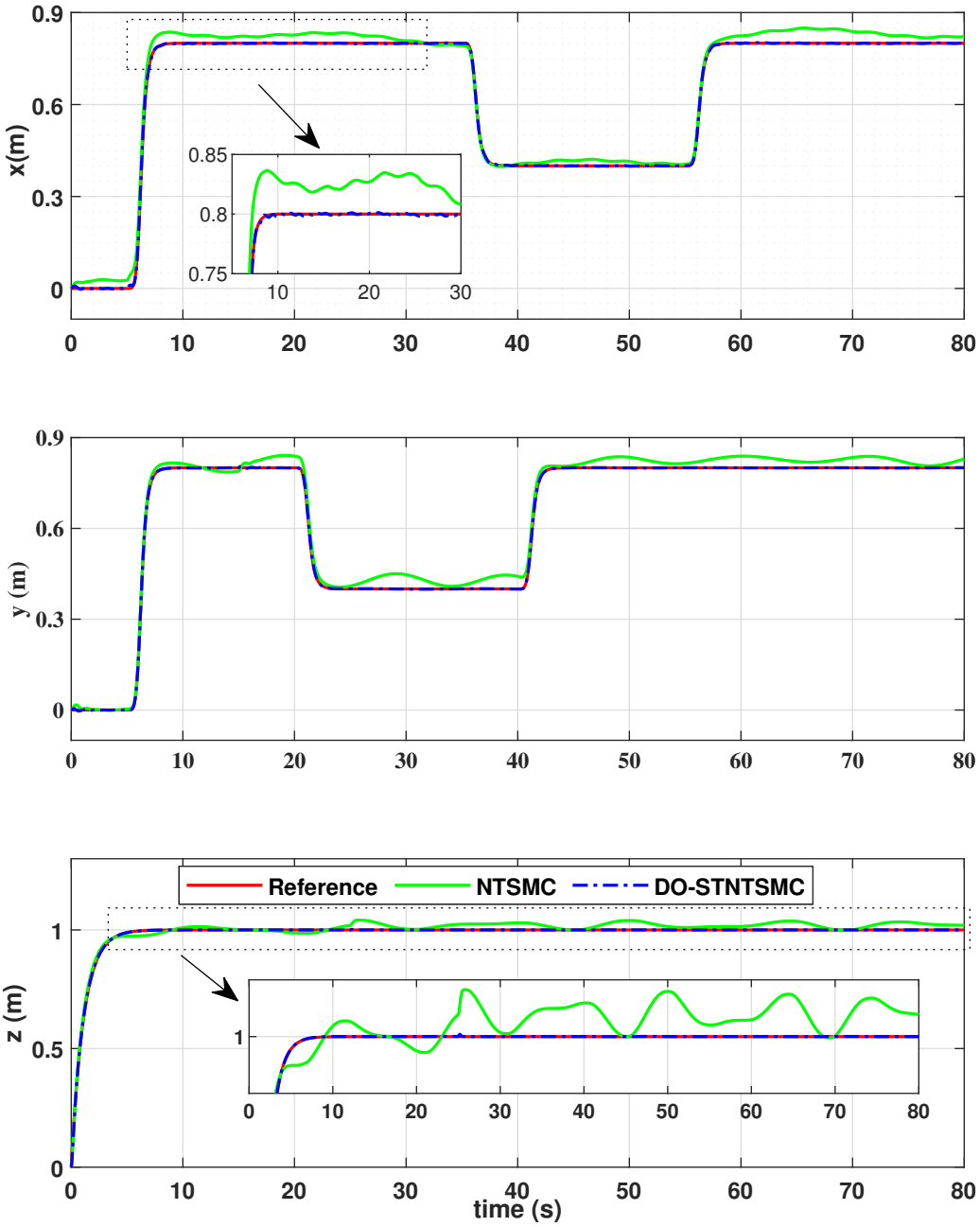

Figure 4.3: Trajectory tracking in the presence of complex disturbances

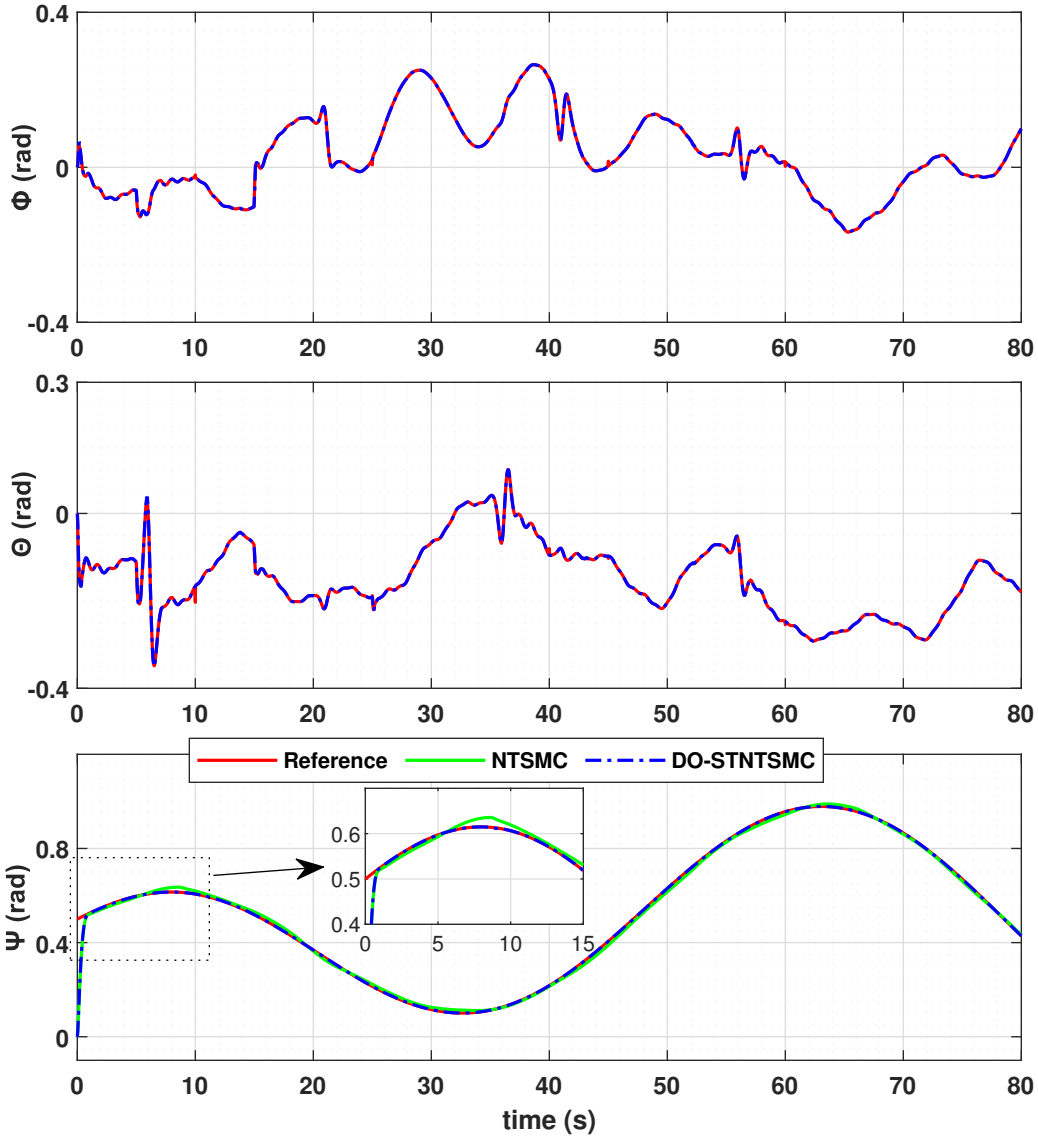

Figure 4.4: Attitude tracking in the presence of complex disturbances

The accuracy of the proposed method is evaluated in more detail on the basis of the tracking errors between the commanded and real trajectories. Figure 4.5 summarizes the comparison in terms of the tracking errors between the proposed method and the NTSMC method. It can be observed that the errors converge to zero within a short period compared to the other strategy.

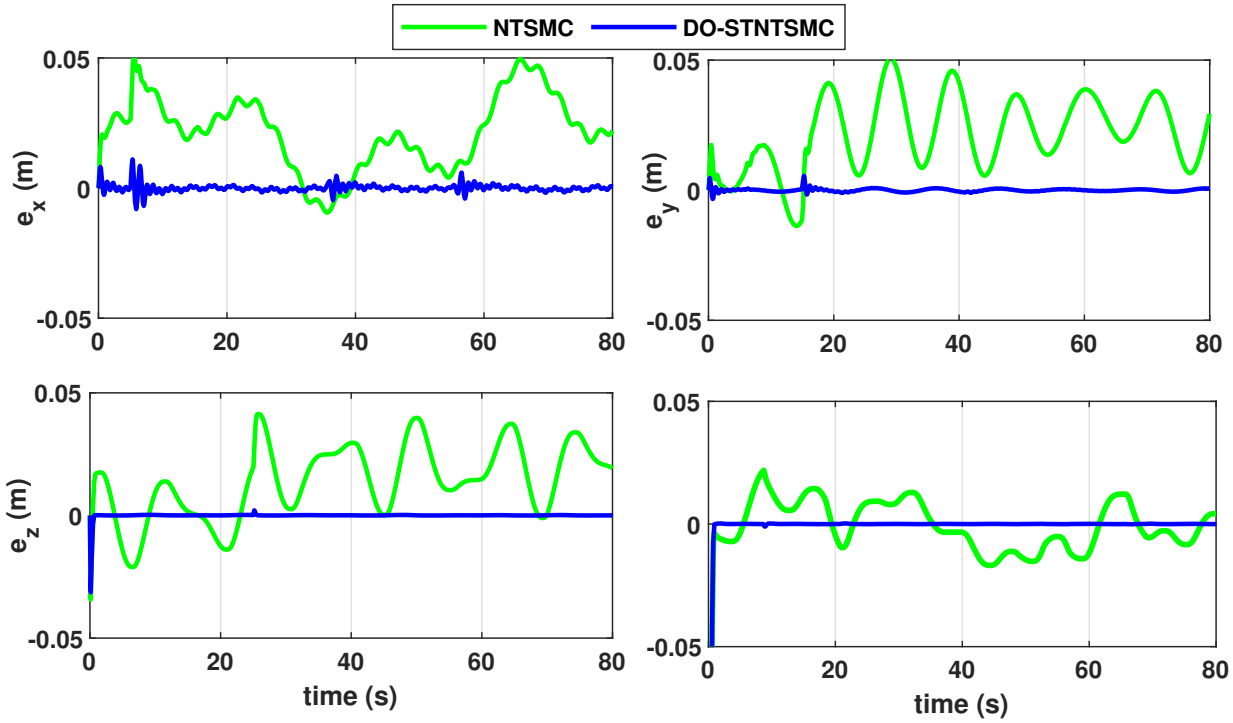

Figure 4.5: Evolution of the tracking errors in the first scenario

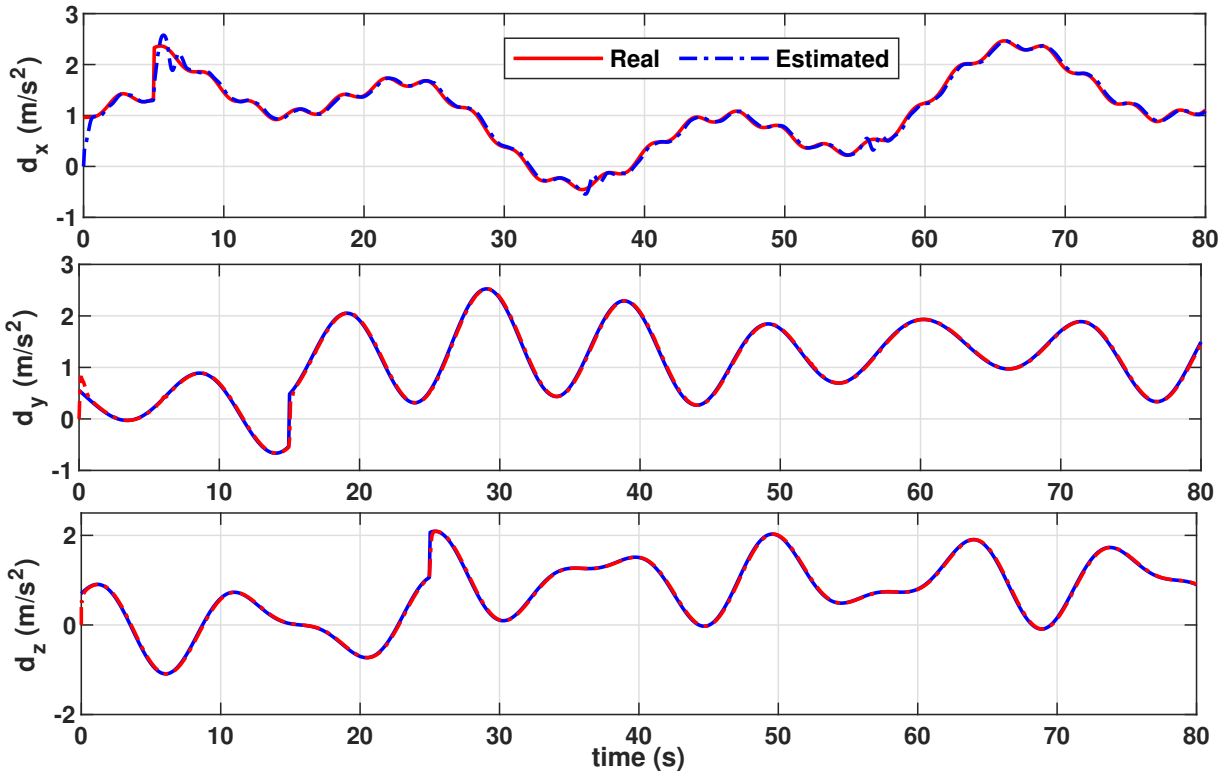

Figure 4.6: Estimation of external disturbances on the quadrotor's position

Figures 4.6 and 4.7 show the real and estimated disturbances, respectively, in the position and attitude dynamics. It can be observed that the adopted disturbance observer provided accurate estimation of the external disturbances. Specifically, the disturbances estimation accurately follow the real disturbances.

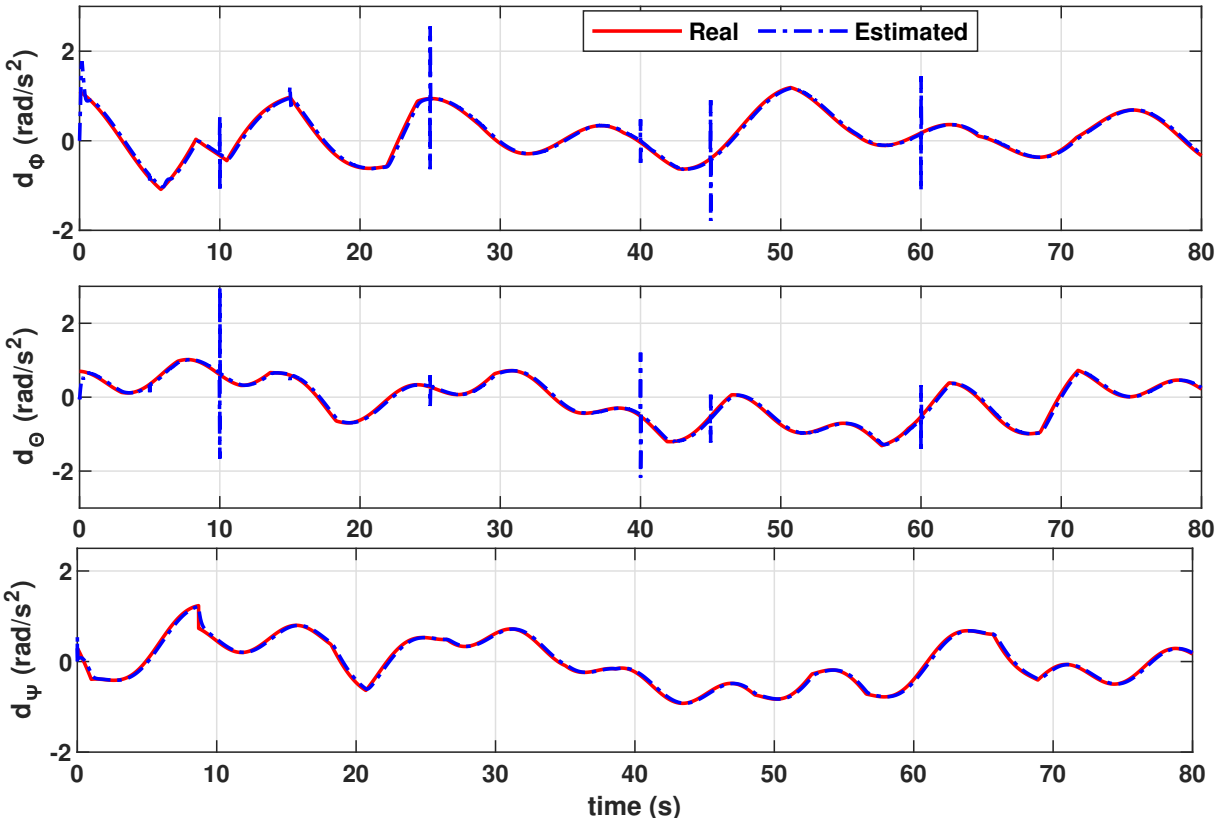

Figure 4.7: Estimation of external disturbances on the quadrotor's attitude

The way in which the drone tracks the prescribed path in the $x-y$ plane for the investigated controllers is illustrated in Figure 4.8. The results indicate that by using the suggested method, the reference path can be tracked in a more precise and efficient way compared to the other method.

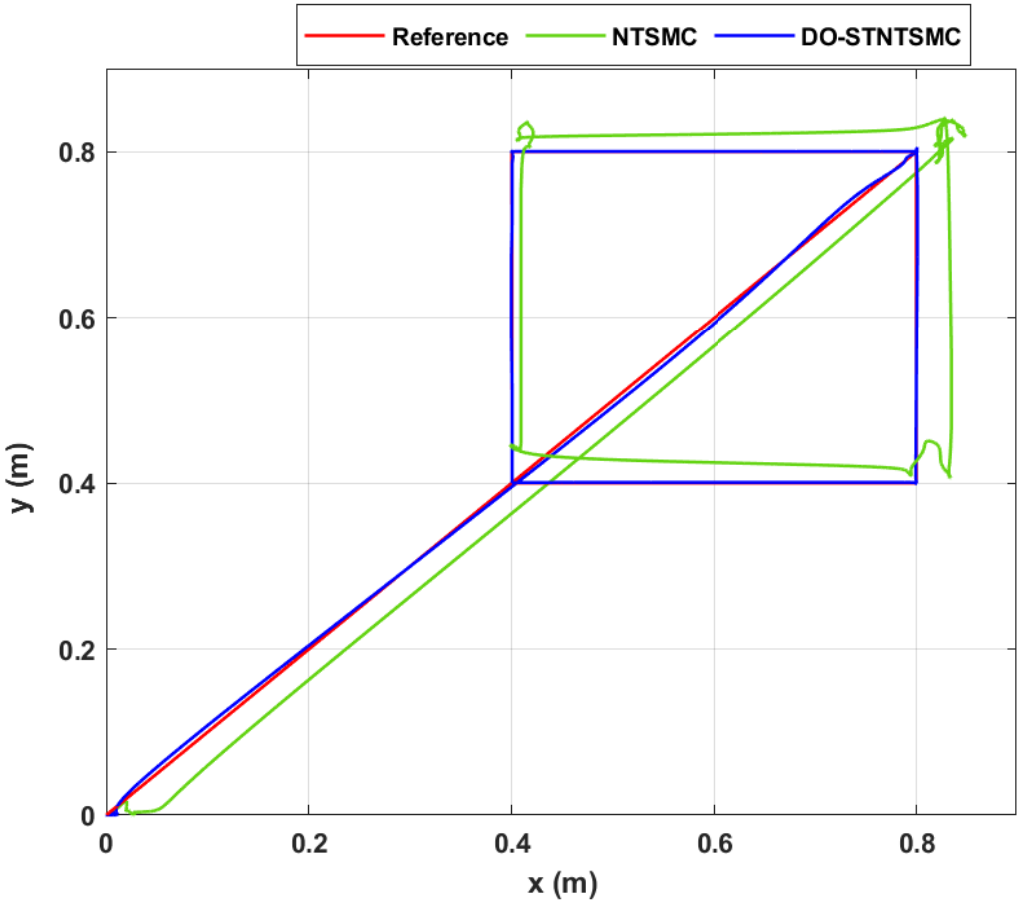

Figure 4.8: Trajectory tracking in the $x - y$ space

The obtained results confirm that the developed control system can effectively drive the quadrotor vehicle during the flight mission. Moreover, better robustness against external disturbances has been achieved by the proposed controller.

4.4.2 Flight Scenario 2: Robustness against disturbances and uncertain drag coefficients

In this scenario, the flight test is conducted under the influence of disturbances. In addition, a random variation of the drag coefficients for the translational and rotational motions is also considered to simulate real outdoor flight. The profile of the drag coefficients is illustrated in Figure 4.9. Within the conducted PIL test, these parameters are generated using a MATLAB function that provides a random variation between -0.01 and 0.01.

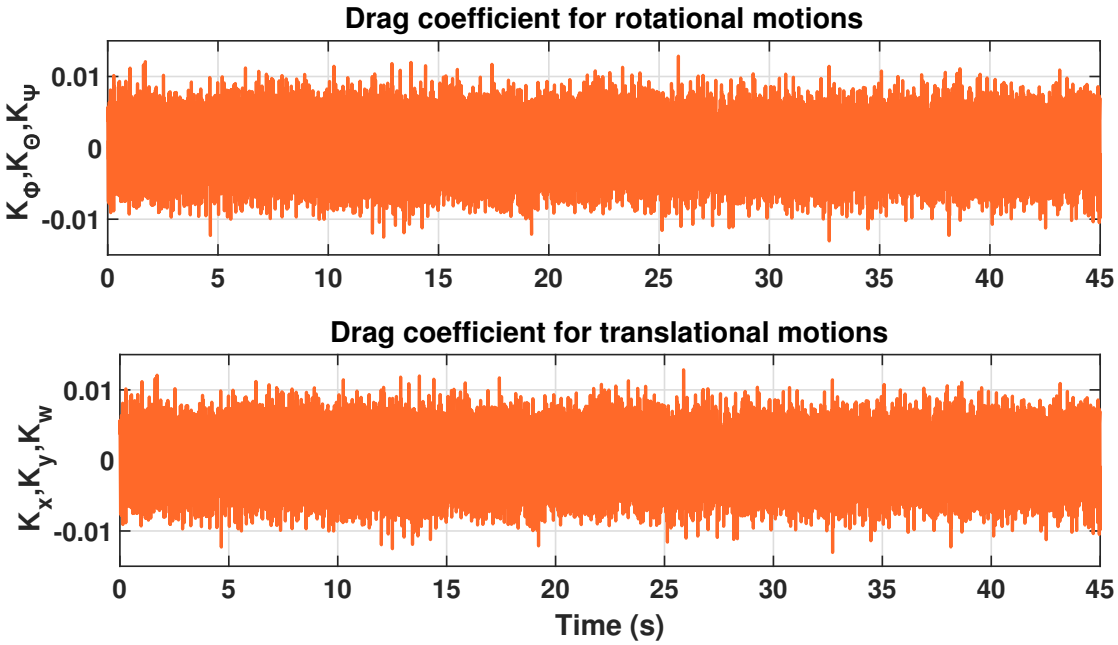

Figure 4.9: Variation of random drag coefficients

The flight mission consists of tracking an eight-shaped trajectory while encountering complex external disturbances. The desired time-varying trajectories of the position and heading angle are given as follows:

$$
\begin{aligned}
x_d &= \begin{cases} 0 & m \quad t \in [0, 10] \\ 2[1 - \cos(0.2(t-10))] & m \quad t \in [0, 50] \end{cases} \\
y_d &= \begin{cases} 0 & m \quad t \in [0, 10] \\ 2\sin(0.4(t-10)) & m \quad t \in [10, 50] \end{cases} \\
z_d &= 5 \text{ m} \\
\Psi_d &= 0 \text{ rad}
\end{aligned}
\tag{4.37}
$$

The results of PIL implementation are given from Figure 4.10 to Figure 4.15. It can be seen that the proposed control scheme succeeded in maintaining the position and orientation of the quadrotor system in stable states.

The reference and actual trajectories of the quadrotor's position are displayed in Figure 4.10, from which we can observe that the proposed DO-STNTSMC method effectively drives the vehicle toward the planned path more accurately compared to the other method. Note that the proposed controller is able to successfully compensate for the negative impact of time-varying disturbances and uncertain drag coefficients; since, the trajectory described by the quadrotor with the proposed flight controller is much closer to the desired trajectory. The time history of the quadrotor orientation (Φ, Θ, Ψ) is depicted in Figure 4.11. It can be concluded that the proposed controller ensures the accurate tracking of the desired attitude angles.

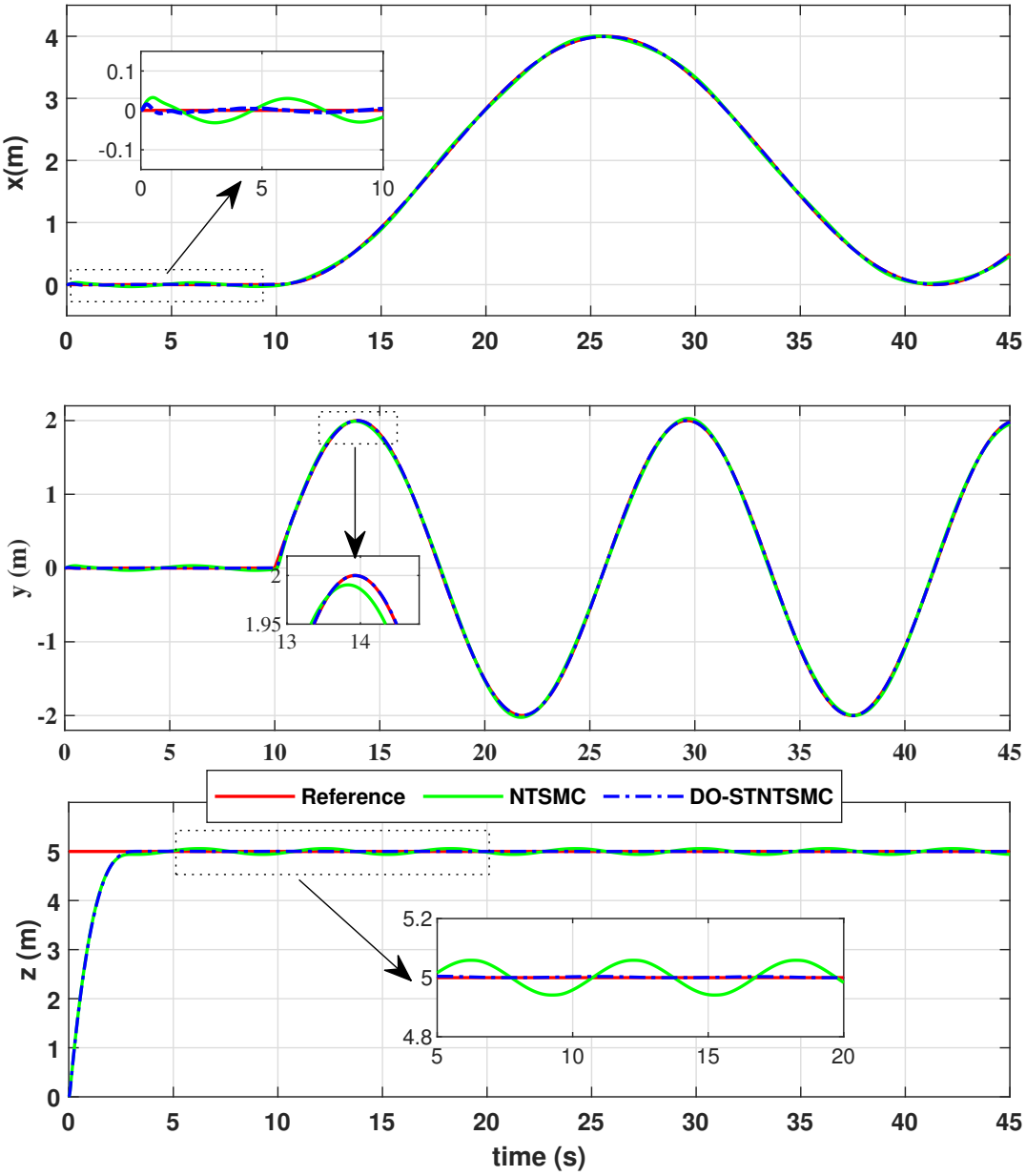

Figure 4.10: Response curves of the quadrotor's position (x, y, z) in the second scenario

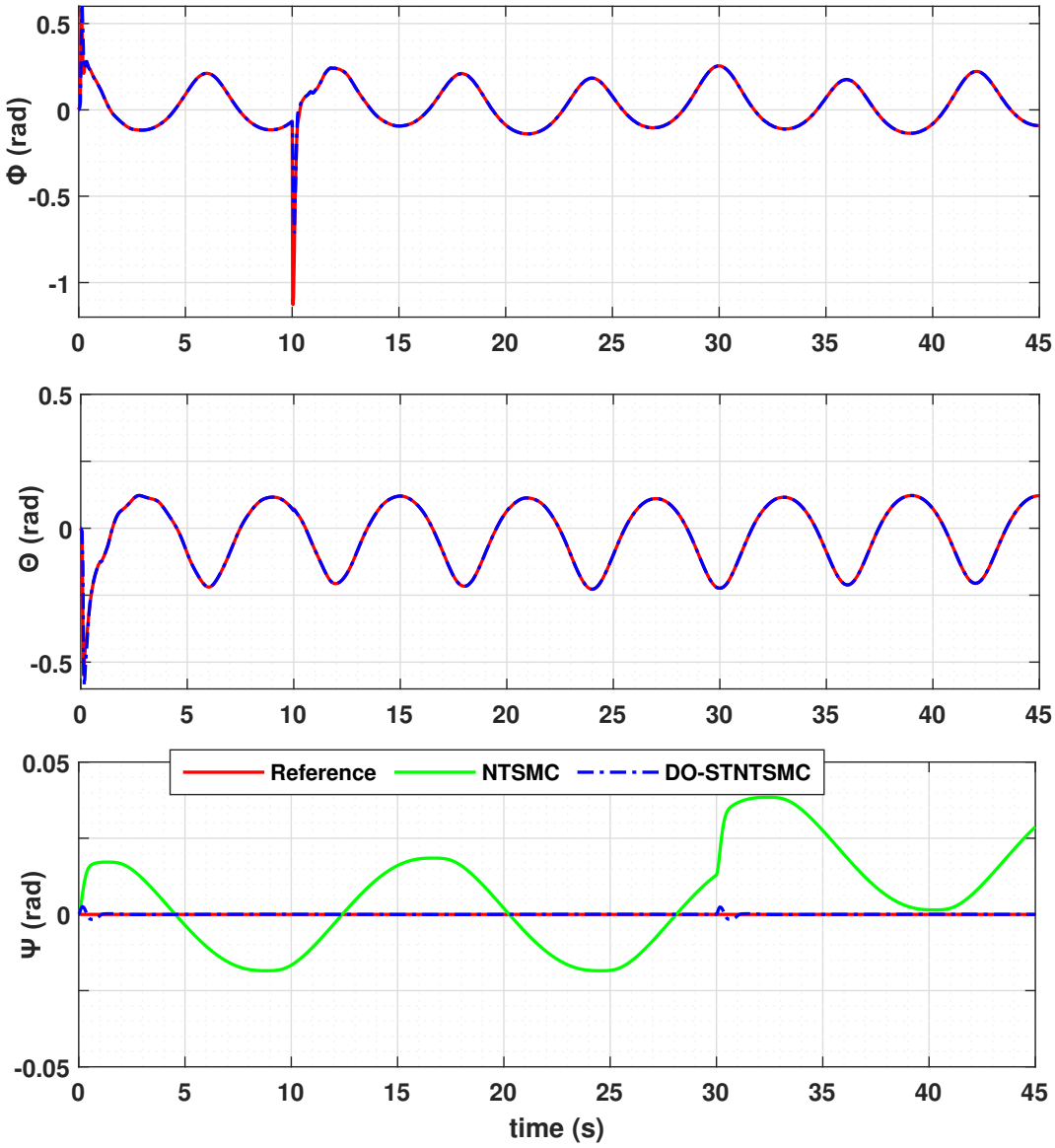

Figure 4.11: Time response evaluation of the quadrotor's attitude (Φ, Θ, Ψ) in the second scenario

Figure 4.12 illustrates the tracking errors resulting from the use of both strategies. It is clear that the tracking errors of the proposed method are smaller than those of the NTSMC method. This improved robustness of the proposed control scheme is due to the integration of the DO, which can provide an accurate estimation of the unknown disturbances during the flight tasks. The profiles of the real and estimated perturbations affecting the position and attitude motions are presented in Figures 4.13 and 4.14, respectively. It is apparent that the external disturbances are precisely estimated. These results confirm the judicious choice and the performances of the adopted DO.

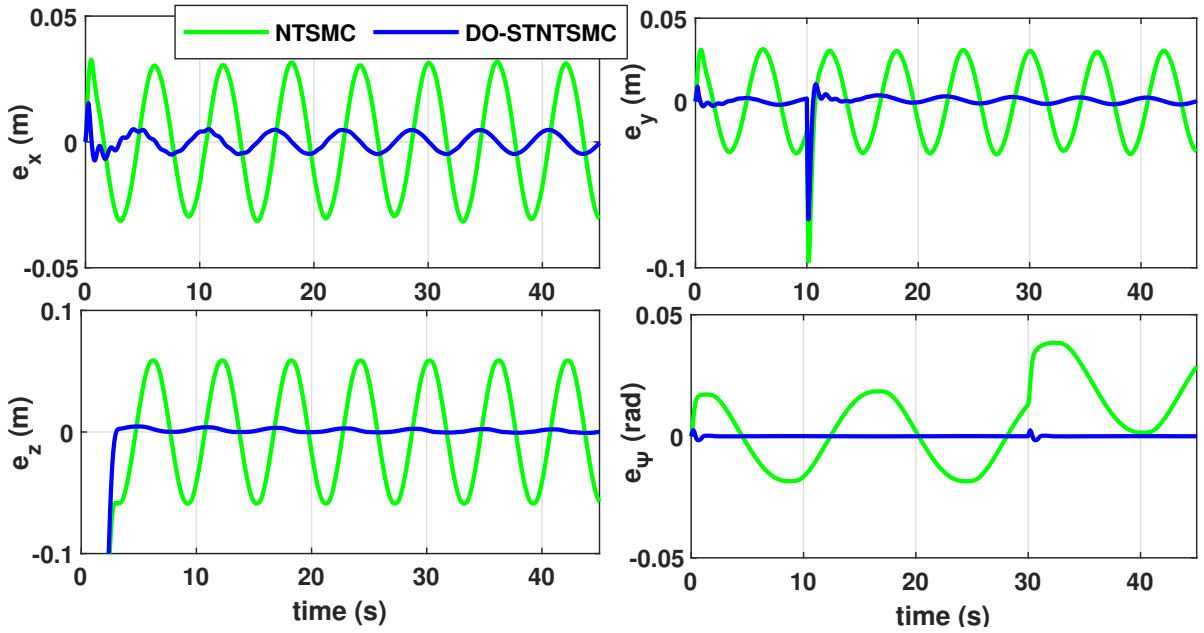

Figure 4.12: Evolution of the tracking errors in the second scenario

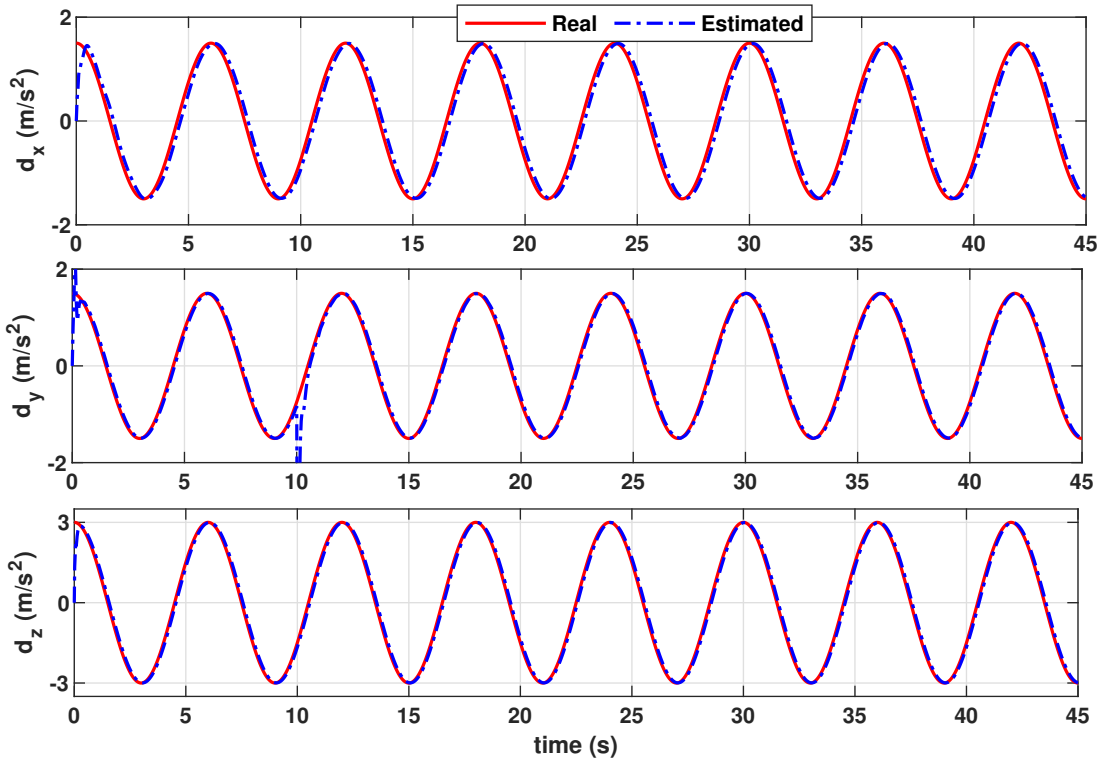

Figure 4.13: Estimation of external disturbances on the quadrotor's position in the second scenario

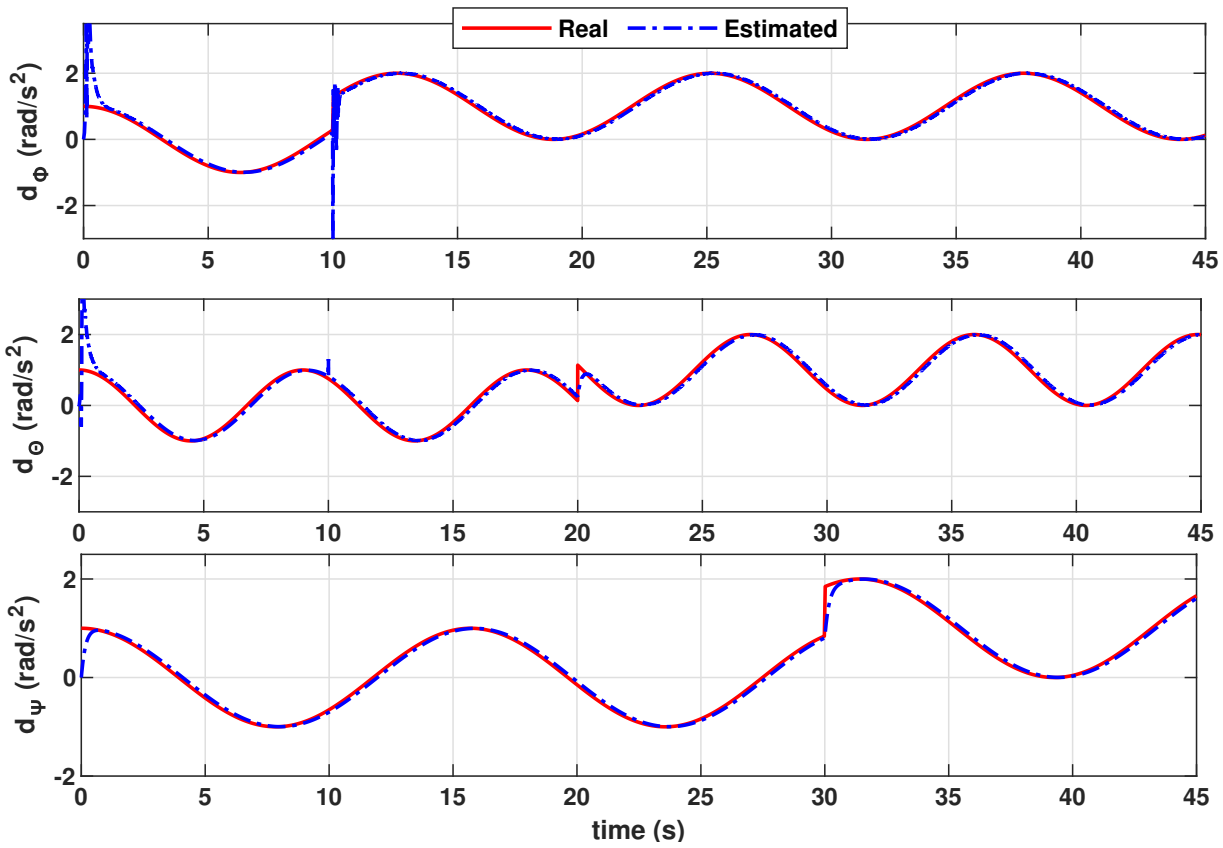

Figure 4.14: Estimation of external disturbances on the quadrotor's attitude in the second scenario

The 3D path following of the eight-shaped trajectory using both controllers is portrayed in Figure 4.15. Similar to the first flight test, it can be seen that the synthesized method is able to overcome the effect of complex uncertain drag coefficients and external disturbances and rather follow the programmed path perfectly compared to the existing strategy.

4.4.3 Comparative analysis

In order to further illustrate the major differences in the flight performance between the investigated controllers, a statistical comparison is suggested in term of the Integral square Error performance index ($ISE = \int_{t_i}^{t_f} e(t)^2 dt$). The findings of this comparative analysis are reported in Table 4.1.

The proposed control scheme provides high performance with better flight accuracy and this can be seen from the smallest value of the ISE in all the conducted tests. Tacking the x movement as example; for the first flight scenario, the offered method is better with the lower value of the ISE ($ISE = 1.8759 \times 10^{-4}$) compared to the NTSMC ($ISE = 0.0532$). Regarding the second test, the proposed controller is the most accurate ($ISE = 5.7318 \times 10^{-4}$)

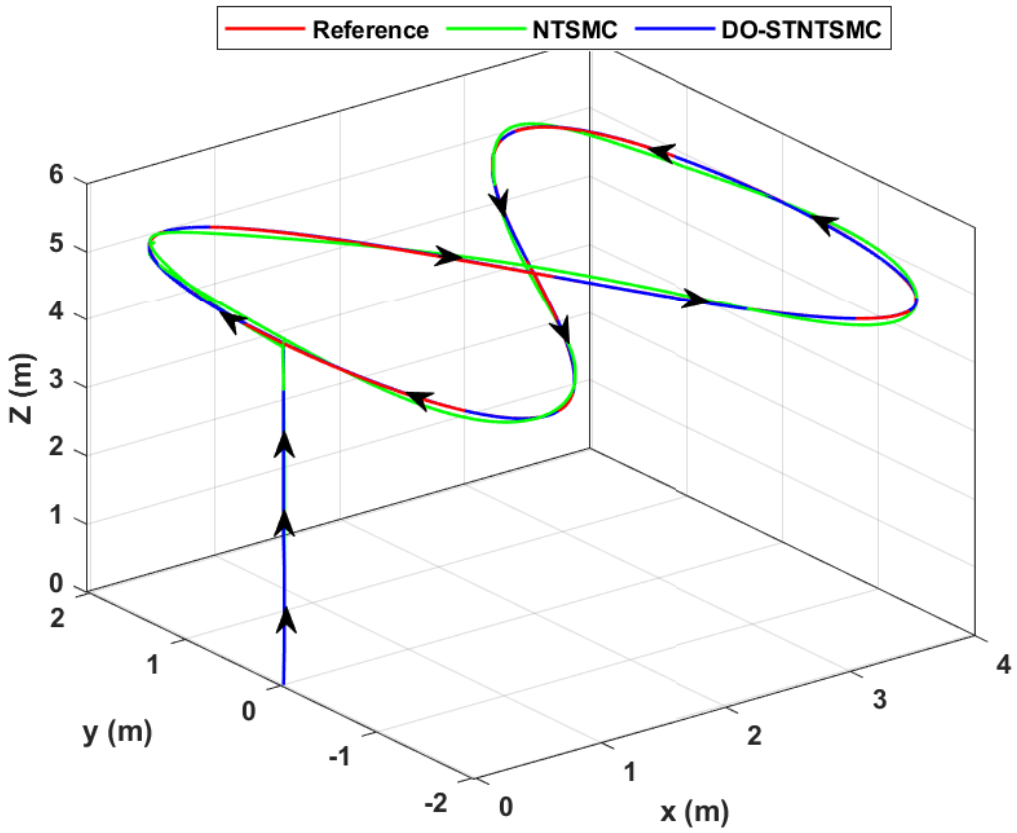

Figure 4.15: Trajectory tracking in the 3D space

compared to the NTSMC ($ISE = 0.0209$).

Table 4.1: Performance's comparisons in terms of the ISE index

Scenario		NTSMC	Proposed method
Scenario 1	x	0.0532	1.8759×10^{-4}
	y	0.0534	3.1898×10^{-5}
	z	0.0332	1.9550×10^{-4}
	Ψ	0.0517	0.0428
Scenario 2	x	0.0209	5.7318×10^{-4}
	y	0.0233	0.0012
	z	12.4712	12.0854
	Ψ	0.0134	4.3565×10^{-6}

To sum up, it has been marked from the presented results that the position and orientation of the quadrotor subject to modeling uncertainties and external disturbances have good tracking performance. Using the RDP introduced in Eq. 3.73, we can conclude that the proposed method provides better accuracy and the total ISE performance index has been decreased by 79.0525% in the first flight test, and by 73.7925% in the second flight test. These results confirm the outperformance of the proposed method compared to the NTSMC method. Finally, the implementation of the suggested method on real hardware can be a strong indication that the proposed method will be successful when used in practice.

4.5 Conclusion

In this chapter, a robust finite-time composite control scheme is designed for a perturbed quadrotor to track multiple desired trajectories under the influence of harsh uncertainties/disturbances. The proposed flight control system consists of a perturbation estimator combined with a finite-time control strategy. A disturbance observer is first conceived to estimate the unknown disturbances, which can effectively remove the negative impact caused by wind gusts. In addition, a supertwisting algorithm combined with a NTSMC is developed with the aims of enhancing the path following accuracy, reducing the tracking errors and improving the system robustness. The proposed control strategy has been successfully implemented on a real autopilot board which validate the feasibility of the proposed method. From the obtained results, it has been asserted that the stability of the proposed method is still maintained even under severe flight conditions. Moreover, the proposed controller remarkably attenuates the impact of uncertain drag coefficients and complex disturbances and tracks precisely the time-varying trajectories.

5 Development of a quadrotor research platform: Experimental validation

Contents

4.1 Introduction 94

4.2 Controller design and stability analysis 94

4.2.1 Disturbance observer 95

4.2.2 Disturbance observer-based nonsingular terminal sliding mode control 96

4.2.3 Disturbance observer-based supertwisting nonsingular terminal sliding mode control 101

4.3 Procedure of the processor-in-the-loop testing 103

4.4 Results and discussion 105

4.4.1 Flight Scenario 1: Robustness against disturbances 105

4.4.2 Flight Scenario 2: Robustness against disturbances and uncertain drag coefficients 110

4.4.3 Comparative analysis 115

4.5 Conclusion 117

5.1 Introduction

The development of a quadrotor aircraft can be difficult, risky, and time-consuming. The procedure for developing a quadrotor vehicle includes modeling, controller design, simulation, and real flight. The simulation step is crucial since it may be used to check whether the controllers are operating correctly or not. This procedure limits the risk of crashes during real flight maneuvers. Although simulations are useful in the development process, it is well known that controller performance in simulation tests may differ completely from that in actual flight due particularly to unmodelled dynamics and external perturbations. For this reason, experimental flying on a test platform can be a good, safe, and efficient solution to verify the controller effectiveness under realistic flight conditions. In this chapter, a quadrotor prototype is constructed to validate the performance of multiple control strategies. Moreover, a step by step validation procedure is followed to explore the advantage of our proposed Supertwisting Nonsingular terminal slidng mode control developed in chapter 5.

The organization of this chapter is given as follows: In section 5.2, the details of the developed quadrotor prototype as well as the proposed vaidation process are presented. In section 5.3, several experimental tests under different flying conditions are performed to validate the outperformance of the proposed controller in comparison of multiple existing strategies. Some conclution remarks are given in section 5.4.

5.2 Experimental setup

In order to practically validate the performance of the suggested flight control system, a low-cost quadrotor prototype has been developed. The software and hardware architecture of the experimental platform is graphically illustrated in Figure 5.1.

In terms of hardware, a custom quadrotor with the DJI F450 frame is built. The quadrotor consists of four brushless DC motors, four Electronic Speed Controllers (ESC), four propellers, a LiPo battery, landing gear, an RC-controller, and a telemetry module. The Pixhawk autopilot is used in the prototype as a flight controller (see section 4.3 for more details). Additionally, the quadrotor's body frame is attached to a 3-DOF spherical joint, allowing the quadrotor to spin around its x, y, and z axes. The mechanism allows the vehicle free yaw motion as well as approximately $\pm 35^\circ$ of roll and pitch. The details of each component are given in Table 5.1.

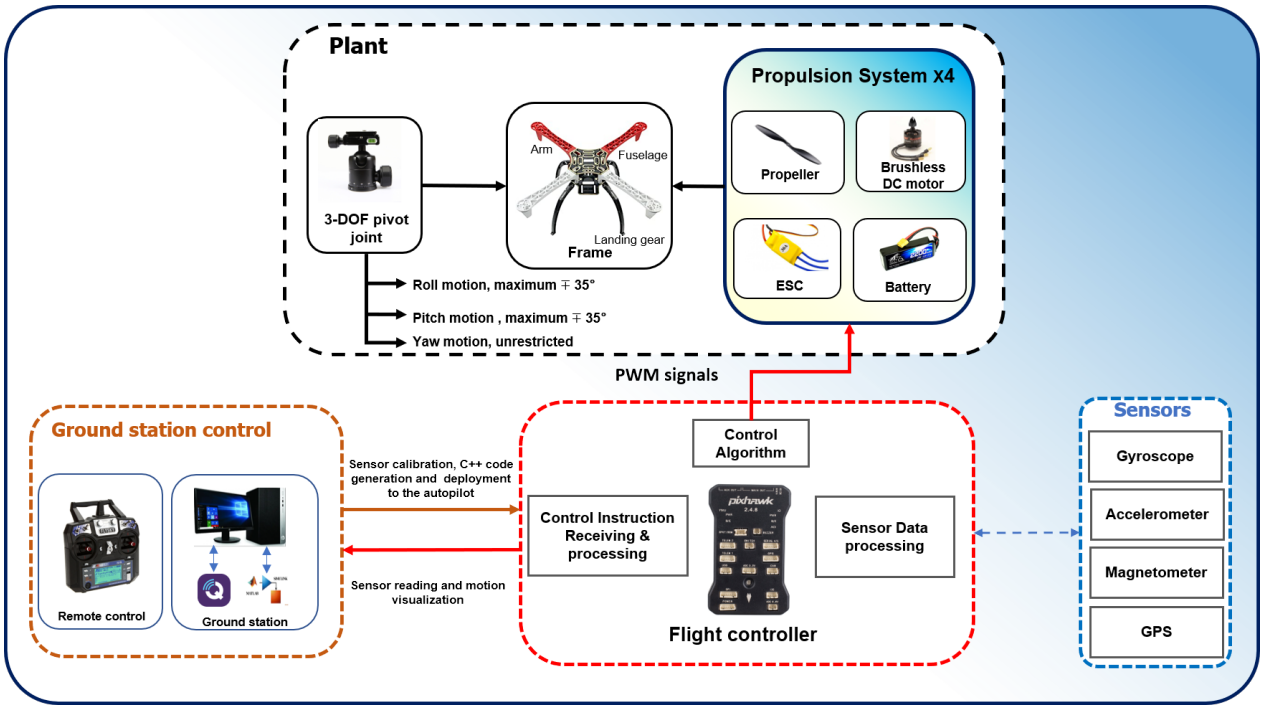

Figure 5.1: Graphical illustration of the experimental platform

Table 5.1: Quadrotor Components

Components	Type	Quantity
Laptop	Intel core i7 processor and 8 GB of RAM	1
Pixhawk	Model 2.4.8	1
GPS/Compass	M8N	1
RC controller	Fly Sky FS-i6 2.4G	1
Radio Telemetry	915 MHz telemetry module	1
Frame	DJI F450	1
Landing gear	DJI landing gear	1
Propellers	1045 DJI propellers	4
Motors	EMAX MT2213-935 KV brushless DC motors	4
ESC	30A BLDC	4
Battery	2200 mAh 30C-11.1 V LiPo battery	1

Figure 5.2 shows the custom quadrotor assembled in our laboratory.

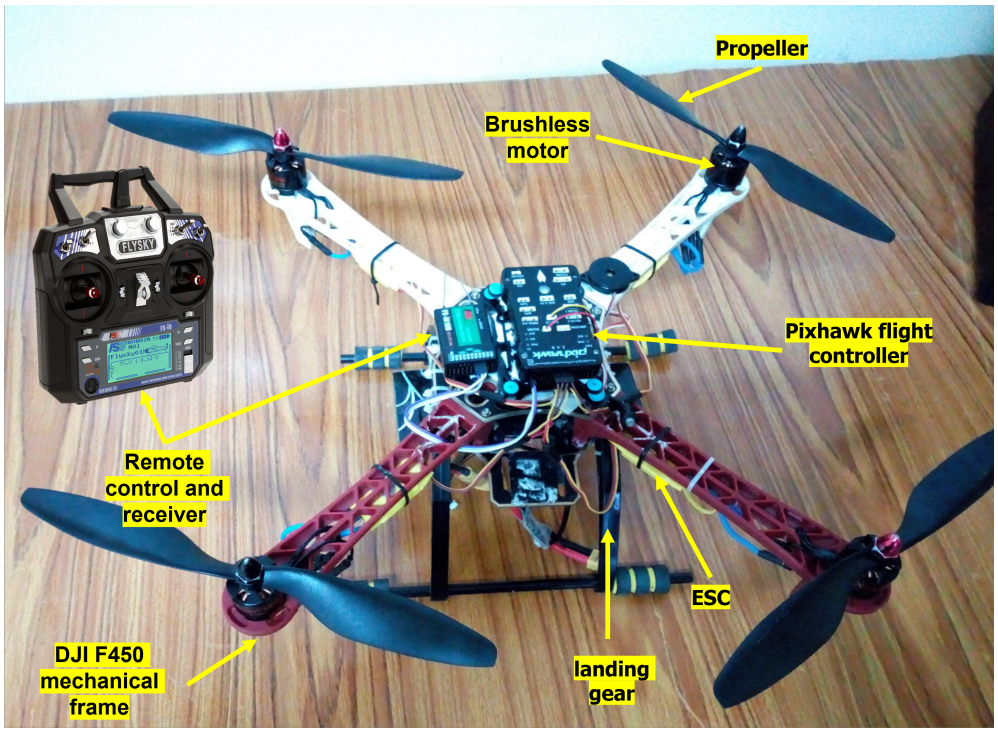

Figure 5.2: Quadrotor vehicle used in the experimental testing

To satisfy the targeted objectives, software is developed using the Matlab/Simulink programming language, which facilitates the integration of the necessary sensors and deployment of the developed control algorithms. The Pixhawk autopilot is used in the developed testbed to benefit from the auto-code generation of matlab/simulink. Particularly, the embedded coder support package for Pixhawk hardware is employed to generate and implement the C^{++} code of the suggested controller to the autopilot hardware [146]. A serial communication, USB wire, is used to connect the autopilot board to the host PC. Then, the experimental tests are performed using the external mode of Simulink®. In this mode, the developed Simulink model serves as a user interface to interact with the implemented code during its execution. The main features of this mode are:

- Visualization of the system's response in real time. A memory card is used to record all signals including attitude, velocities, and control signals.

- Tuning controller parameters during the experiment. The controller's gains are set as global variables, then, they can be modified as the experimentation is running.

The quadrotor model's parameters used in the implementation of the proposed controller have been identified experimentally using the bifilar pendulum experiment [148] illustrated in Figure 5.3. These parameters are given as: $m = 1.23kg, J_x = 0.0217kgm^2, J_y = 0.0221kgm^2, J_z = 0.0352kgm^2, l = 0.225m$.

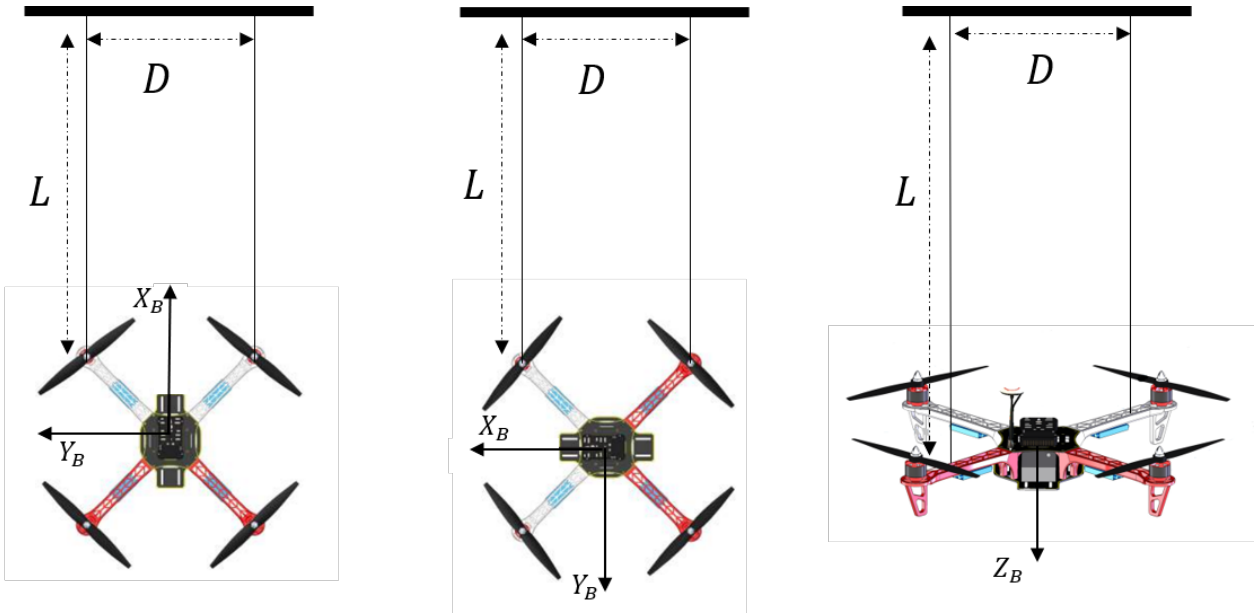

Figure 5.3: Bifilar pendulum setup

The experiment is initiated by suspending the quadrotor by two parallel wires, which allow free rotation around a specific axis. A small moment is exerted on the quadrotor to measure the period of its oscillation denoted by T, which is then used to calculate its angular frequency $w = \frac{2\pi}{T}$. The moments of inertia are computed using the following formula.

$$J_i = \frac{mgD^2}{4Lw^2} = \frac{mgD^2T^2}{16\pi^2 L} \tag{5.1}$$

Where $J_i = (J_x, J_y, J_z)$. $L[m]$ and $D[m]$ denote, respectively, the length of the suspending wires and the distance between the two wires. $T[s]$ is the averaging period of 30 oscillations for 5 trials.

Figure 5.4 shows footage of the developed testbed system. As can be seen, the vehicle is fixed on a 3D spherical joint to examine the attitude control system. An eclectic fan is used to generate wind gusts and evaluate the robustness of the control system in windy conditions. Because of the use of the external mode of Simulink, the results of attitude tracking can be visualized in real time directly on the host PC.The remote control is mainly used to start, or stop the experiment.

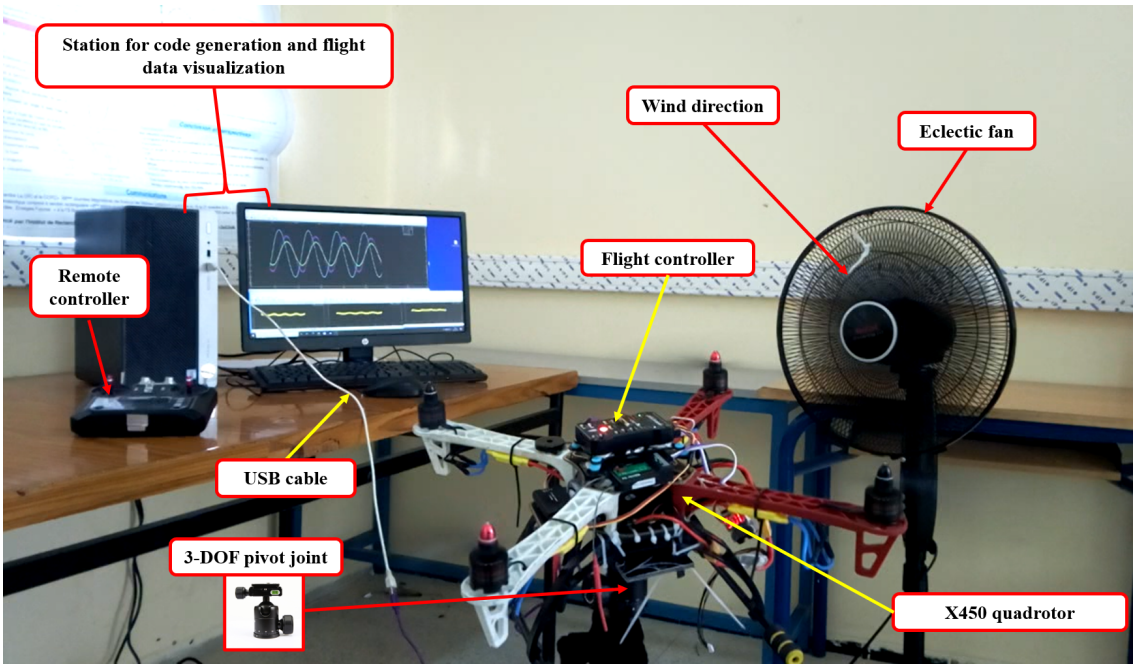

Figure 5.4: Experimental platform developed for real testing under wind disturbances

5.3 Experimental results

Four experimental tests were conducted in order to evaluate the performance of our proposed approach :

- An origin stabilization experiment is first performed. It is regarded as an introductory and simple test that must be conducted as a first step. It seeks to demonstrate the finite-time convergence property and evaluate the effectiveness of the proposed control law in stabilizing the attitude towards the origin from a given random initial configuration.
- A transient response experiment is carried out to measure the speed of the controller.
- Once the controller demonstrates its supremacy in both origin stabilization and transient response experiments, the next step is to assess the controller on a regulation task in which the goal is to evaluate how the controller reacts to multiple abrupt changes in the desired trajectories.
- A tracking experiment is performed to assess the workability and efficiency of the suggested controller in tracking multiple time-varying trajectories in all the three angles.

To evaluate the system robustness and disturbance rejection capability of the suggested strategy, the tracking and regulation tasks are performed under the influence of wind perturbations generated by an eclectic fan. Additionally, unmodeled dynamics are considered disturbances. Also, in a practical implementation, sensor noise and inaccuracies in the rotary

inertia are unavoidable. Certainly, these unknown inaccuracies and disturbances will affect the attitude tracking accuracy. To highlight the superiority of the suggested control algorithm, a comparative study with the commercially available PID controller, the Saturation Integral Backstepping Control (SIBC) [78], the Backstepping Supertwisting SMC control (BSTSMC) [149], and the Backstepping Nonsingular Integral Terminal SMC (BNITSMC) [150] is also presented.

5.3.1 Stabilization experiments

The aim of this experiment is to stabilize the orientation of the aircraft for a stationary flight starting from an arbitrarily initial condition. The desired set points in a stabilization test are equal to zero, which means the controller has to drive the vehicle's orientation to reach 0° i.e. $(\Phi_d, \Theta_d, \Psi_d) = (0, 0, 0)$. Two flying situations are investigated, each with distinct starting conditions for the three angles:

(a) $[\Phi_i, \Theta_i, \Psi_i]^T = [12, 10, -15]^T(\text{deg})$.

(b) $[\Phi_i, \Theta_i, \Psi_i]^T = [-10, -15, 20]^T(\text{deg})$

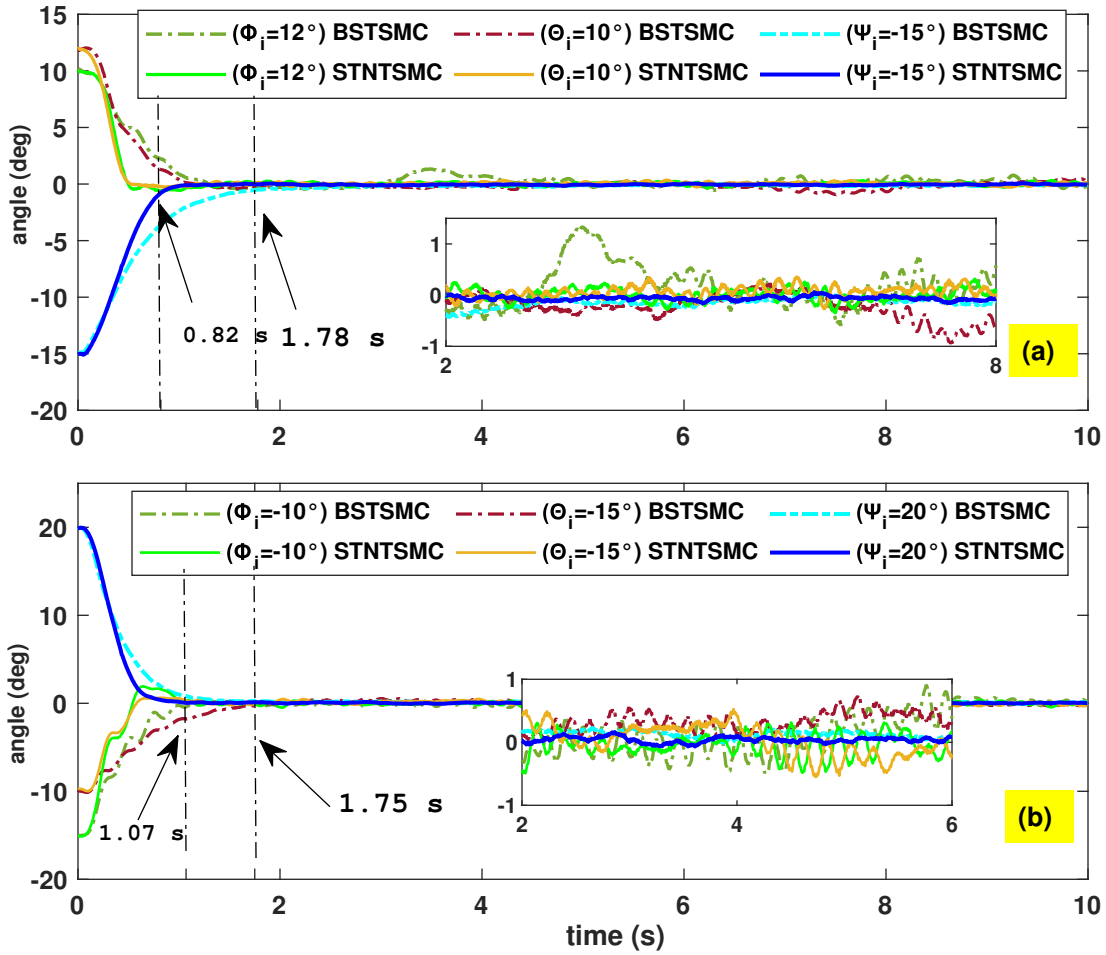

Figure 5.5: Stabilization experiment of the attitude state

Comparisons with the BSTSMC [149] are also performed to evaluate the capabilities of the proposed finite-time controller.

Figure 5.5 shows the time response of the quadrotor's attitude in the origin stabilization experiment. It can be seen how the suggested controller can drive the quadrotor state (Φ, Θ, Ψ) to zero in a short finite-time. Regarding the response of the proposed controller, the roll, pitch, and yaw angles reach their steady $(0, 0, 0)^\circ$ in a short time, $0.82s$ in the first case and $1.07s$ in the the second case, which is significantly better than the response of the BSTSMC controller ($1.78s$ in case (a) and $1.75s$ in case (b)).

Figure 5.6 illustrates the time evolution of the generated control inputs trajectories using the proposed controller and the BSTSMC controller. It is evident that by using the suggested controller, the input signals have lower oscillation and reduced chattering compared to the BSTSMC controller, which means that the quadrotor will be more stable.

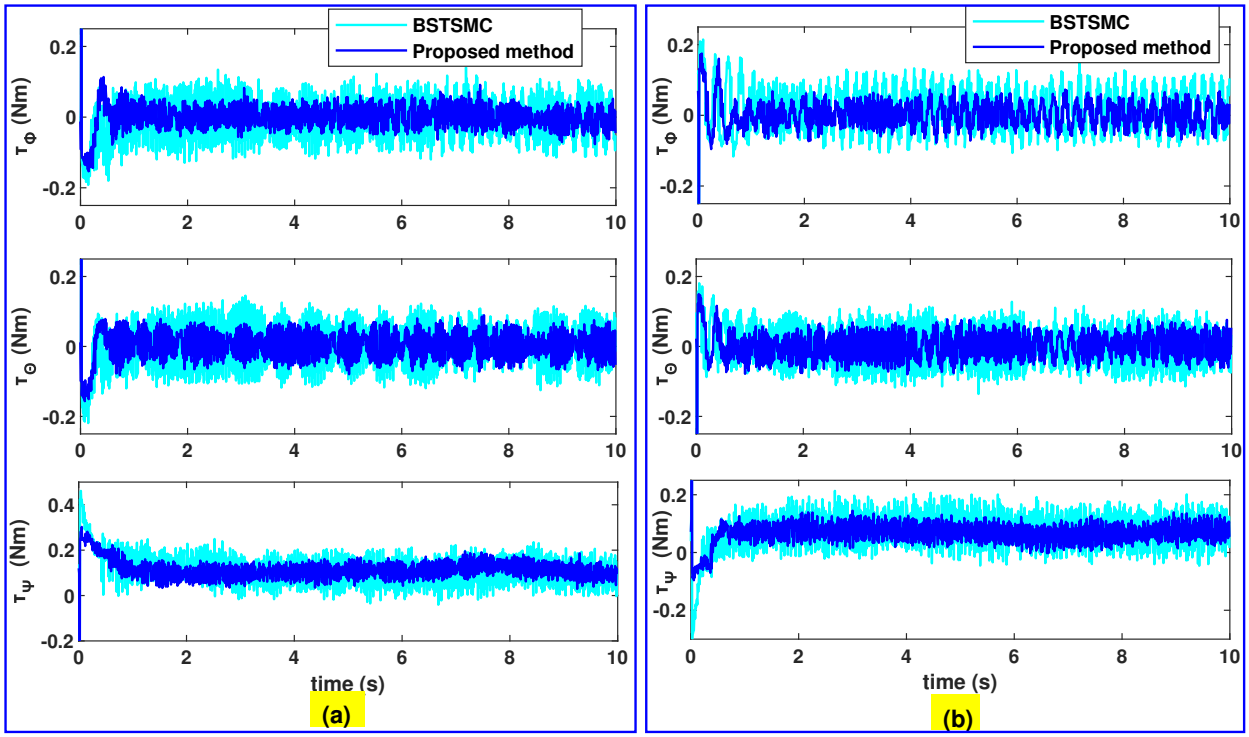

Figure 5.6: Time histories of the control torques in the origin stabilization experiments

5.3.2 Transient response experiment

Transient performance is a key index for most robotic systems during stabilization and tracking tasks. It verifies that the control system can ensure the convergence of the tracking errors within a short time. This characteristic can be evaluated using the settling-time performance

index. This indicator is defined as the duration required to achieve and stabilize the system within a predetermined range of ±5% of the final value ($[9.95°; 10.5°]$ in our case).

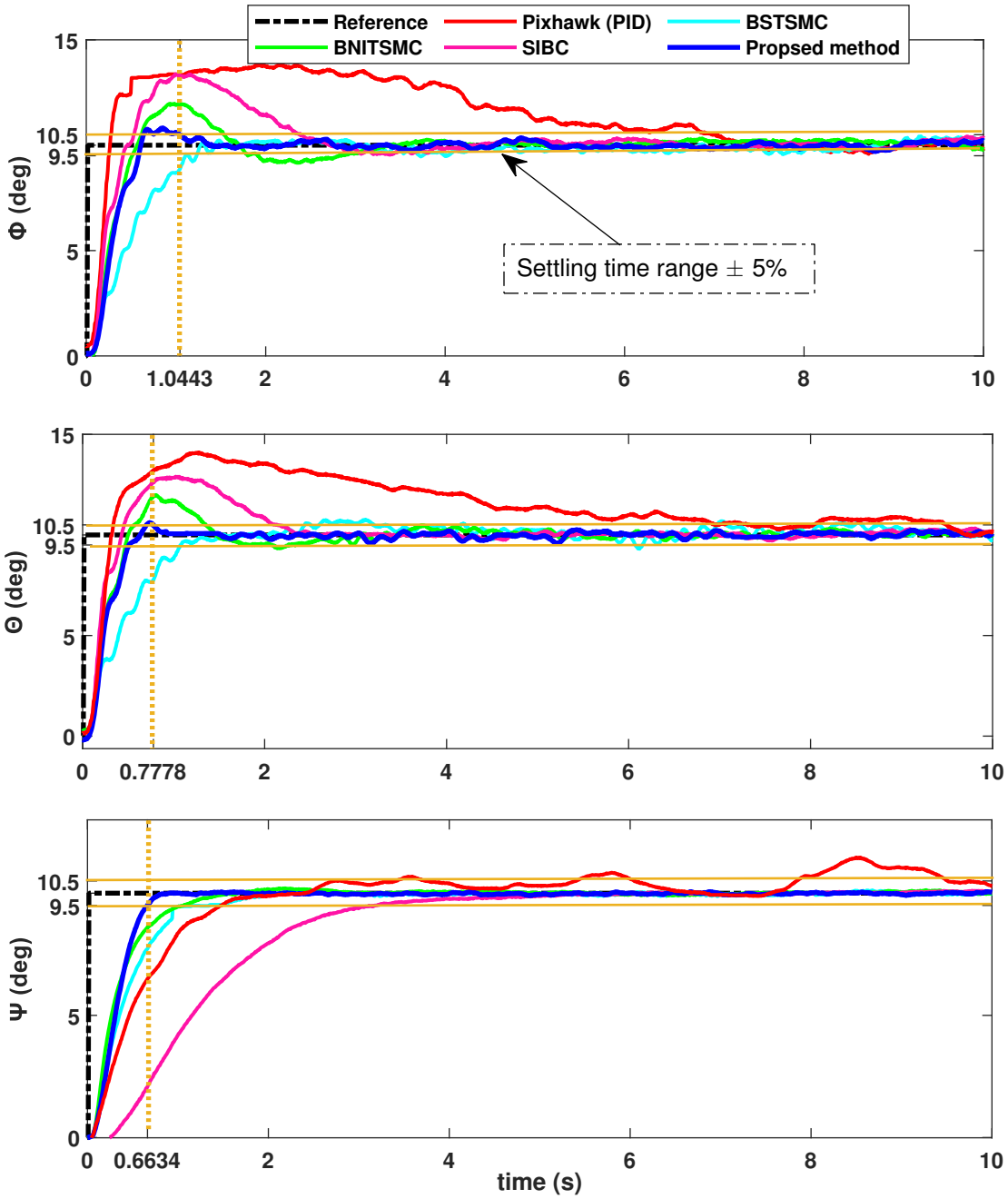

Figure 5.7: Attitude response for the step input

The experimental results for the step reference with 10° of magnitude are illustrated in Figure 5.7. Obviously, the suggested controller provides better and faster response in all the attitude states compared to the existing strategies. For better comparison of these

strategies, the results of the settling-time indicator are compared in Table 5.2. According to these findings, the proposed controller exhibits the best performance for all the three angles ($1.0443s$ for roll, $0.7778s$ for pitch, and $0.6634s$ for yaw). The PID controller, on the other hand, has the longest settling time for all the angles.

Table 5.2: Comparison of the settling-time for the several strategies

Euler angle	Pixhawk(PID)	BSTSMC	BNITSMC	SIBC	Proposed method
Φ	7.0398	4.0250	2.8408	2.3879	**1.0443**
Θ	9.4947	8.7626	3.7308	2.1409	**0.7778**
Ψ	9.5088	1.3473	1.0651	3.1717	**0.6634**

5.3.3 Attitude regulation

In this part, the aircraft is commanded to track and maintain its attitude at some specific values under the influence of wind disturbances. In particular, the main goal of this experiment is to show how the quadrotor aircraft reacts to multiple abrupt changes in all the three angles. To facilitate the evaluation of all the compared controllers, attitude responses, tracking errors, and control signals are displayed.

The experimental results obtained on the quadrotor prototype, with the five compared strategies, are illustrated from Figure 5.8 to 5.10. These findings reveal that all the compared approaches can meet the attitude tracking objectives; however, the accuracy varies from one method to another.

In Figure 5.8, the temporal responses of the attitude trajectories are plotted. Based on this figure, it can be seen that the accurate tracking of the desired attitude trajectories was performed correctly and that the suggested approach showed faster response with respect to the other controllers (see the zoomed area Figure 5.8). It should be mentioned that even though the reference attitude trajectories change all the time, the proposed control strategy is able to drive the aircraft to the new orientations quickly while compensating for the impact of perturbations/uncertainties (introduced from the beginning of the test).

Regarding the disturbance rejection capability, although the quadrotor was subjected to wind disturbances during all the flight tests, it is clear that the proposed control strategy outperformed other techniques and quickly/efficiently rejected the influence of wind disturbances, resulting in a small deviation from the desired trajectories compared to other methods.

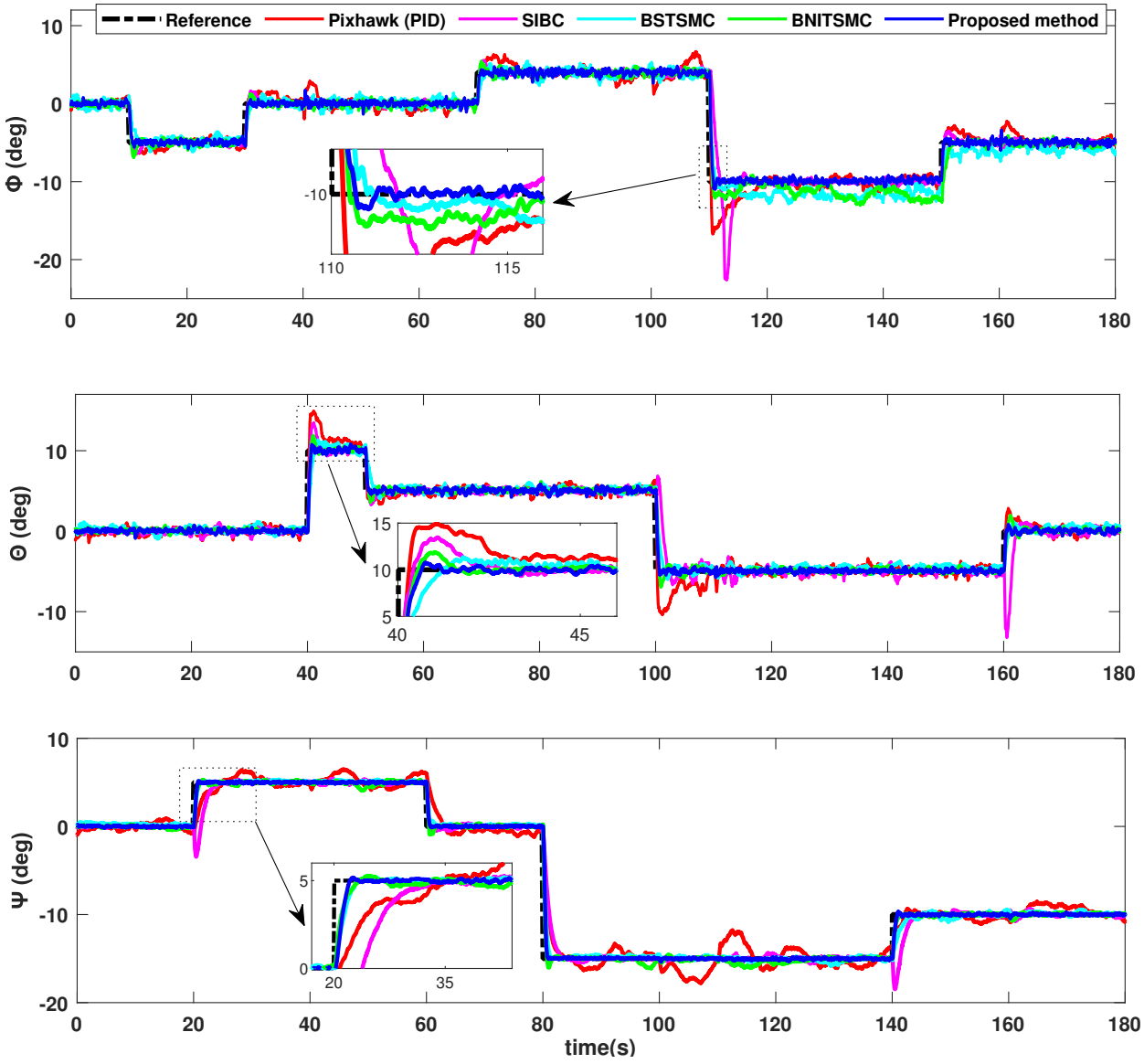

Figure 5.8: Tracking performance for regulation task under wind gust

The time evolution of the orientation tracking errors resulting from the five methods is shown in Figure 5.9. As can be observed, the accuracy of the suggested approach is clear, as its tracking errors quickly drop to small values compared to the other methods (see the zoomed area in Figure 5.9).

To clearly analyze the accuracy of the suggested method, a quantitative comparison with the other strategies in terms of the integral square error (ISE) is suggested.

Table 5.3 summarizes the results of this comparison, where the best results are highlighted in bold text. It is obvious that the ISE of the proposed controller is the smallest compared

to the other controllers, this confirms the accuracy of the proposed techniques. On the other hand, the SIBC has the largest ISE in all the orientations.

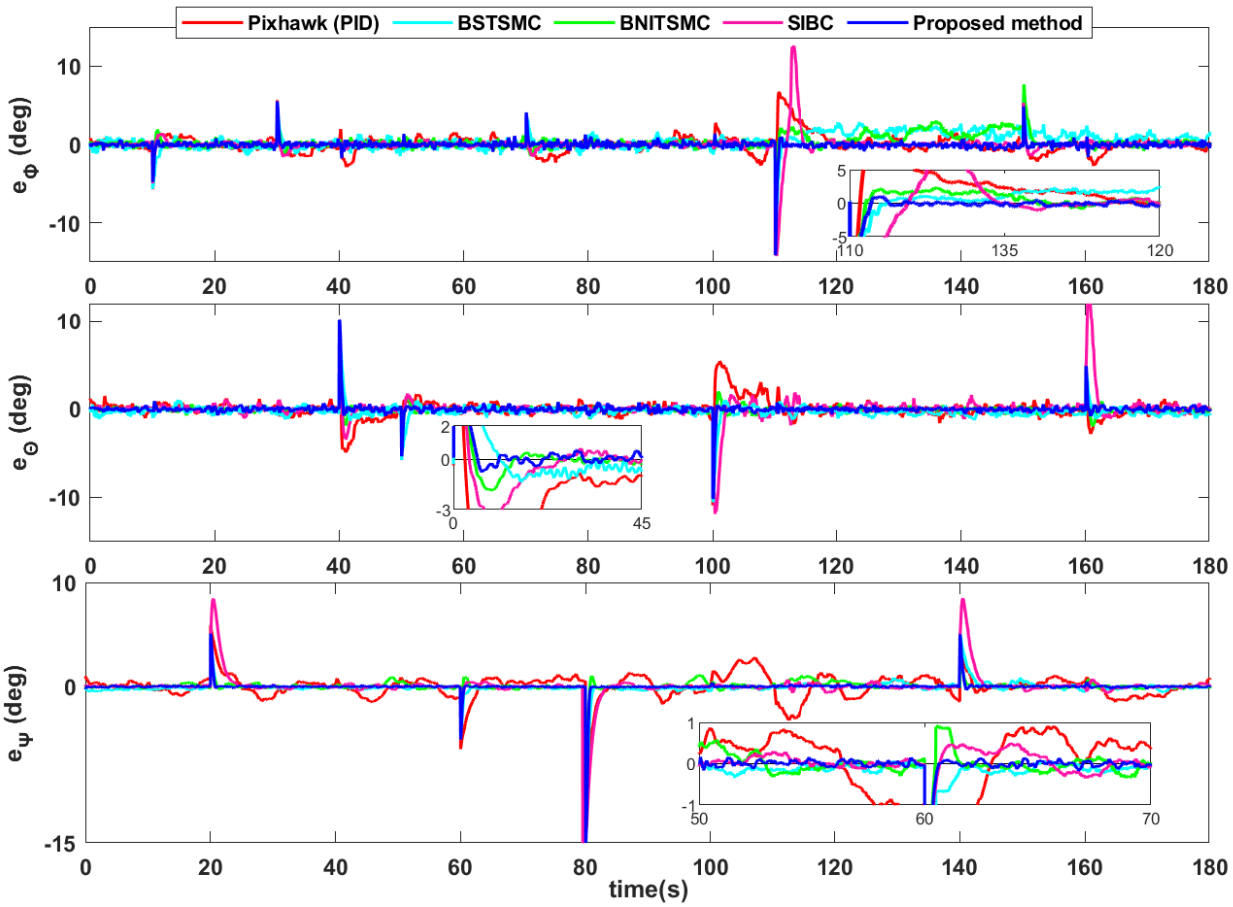

Figure 5.9: Time histories of the attitude tracking errors in the regulation experiment

Table 5.3: Comparison of the ISE performance in the regulation experiment

Euler angle	Pixhawk(PID)	BSTSMC	BNITSMC	SIBC	Proposed method
Φ	0.0802	0.0719	0.0567	0.0987	**0.0234**
Θ	0.0605	0.0374	0.0203	0.0978	**0.0186**
Ψ	0.0845	0.0287	0.0223	0.1173	**0.0218**

In Figure 5.10, control signals obtained using the recommended approach are displayed and compared to control inputs obtained by the other strategies. We can conclude that

the rolling, pitching, and yawing moments $(\tau_\Phi, \tau_\Theta, \tau_\Psi)$ of the proposed method have less chattering compared to those generated by the other controllers. On the other hand, the control signals generated by the other SMC-based controllers are more impacted by the chattering problem.

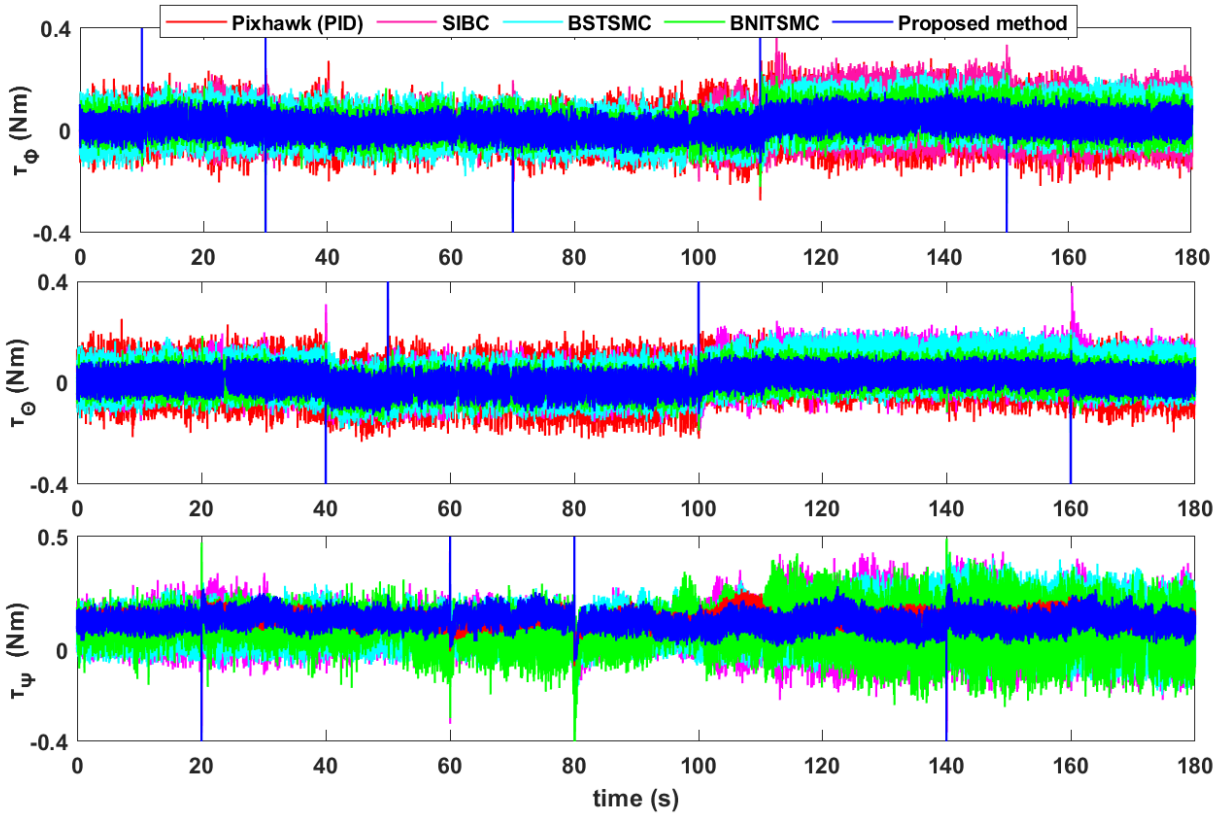

Figure 5.10: Time histories of the generated control signals in the regulation experiment

For the chattering alleviation property, another quantitative comparison is conducted in terms of the performance index "Integral Absolute value of the control inputs Derivative τ_i $(IAD\tau)$" defined as [123]:

$$IAD\tau = \int_{t_i}^{t_f} \left| \frac{d\tau_i(t)}{dt} \right| dt \tag{5.2}$$

This criterion is highly recommended to examine the smoothness of the generated control signals, as it measures the variation of the control signals during the test. The obtained results are summarized in Table 5.4. It can be concluded that the smoothness of the suggested controller is remarkably improved compared to all the other SMC-based controllers.

Table 5.4: Comparison of the $IAD\tau$ index in the regulation experiment

Control signal	Pixhawk(PID)	BSTSMC	BNITSMC	SIBC	Proposed method
τ_Φ	0.1063	0.1035	0.0678	0.1046	**0.0540**
τ_Θ	0.1101	0.1054	0.0639	0.0796	**0.0602**
τ_Ψ	0.0239	0.1610	0.1275	0.1398	**0.0548**

In order to highlight the achieved percentage of chattering reduction by the proposed controller, the relative percentage difference (RPD) introduced in [139] is used, it is defined as:

$$RPD_{\text{method}}\,\% = \frac{|IAD\tau_{\text{method}} - IAD\tau_{\text{proposed}}|}{IAD\tau_{\text{method}}} 100 \tag{5.3}$$

The obtained results are grouped in Table 5.5. Obviously, the amount of chattering in the all control signals has been decreased considerably by the proposed controller. Take for example the roll torque tau_Φ, the chattering in the proposed method is reduced by 47.83% compared to the BSTSMC method, by 48.37% compared to the SIBC strategy, and by 20.35% compared to the BNITSMC method. These quantitative results further confirm the outperformance of the proposed method regarding chattering reduction.

Table 5.5: RDP % for IADτ index in the regulation experiment

Control signal	BSTSMC	SIBC	BNITSMC
τ_Φ	47.83	48.37	20.35
τ_Θ	42.88	24.37	5.79
τ_Ψ	65.96	60.80	57.02

5.3.4 Attitude tracking

To rigorously test our proposed control scheme, an attitude tracking experiment under wind gusts was carried out. The reference attitude trajectories for the roll, pitch and yaw rotations is inspired from [139] and given as:

$$\begin{cases} \Phi_d = 15\sin(2\pi f t) \\ \Theta_d = 10\sin(2\pi f t) \\ \Psi_d = 20\cos(2\pi f t) \end{cases} \tag{5.4}$$

Where $f = \frac{1}{25}$ Hz is the frequency.

The experimental results obtained on the quadrotor prototype with the five compared strategies are illustrated from Figure 5.11 to 5.13. These results clearly illustrate that all control techniques are capable of ensuring reference tracking. In Figure 5.11, the tracking performance of the time-varying attitude trajectories under the impact of wind perturbation is depicted. Enhanced robustness and precision are obtained by the proposed strategy. This can be outlined from the accurate tracking of the targeted attitude trajectories (see the zoomed area in Figure 5.11).

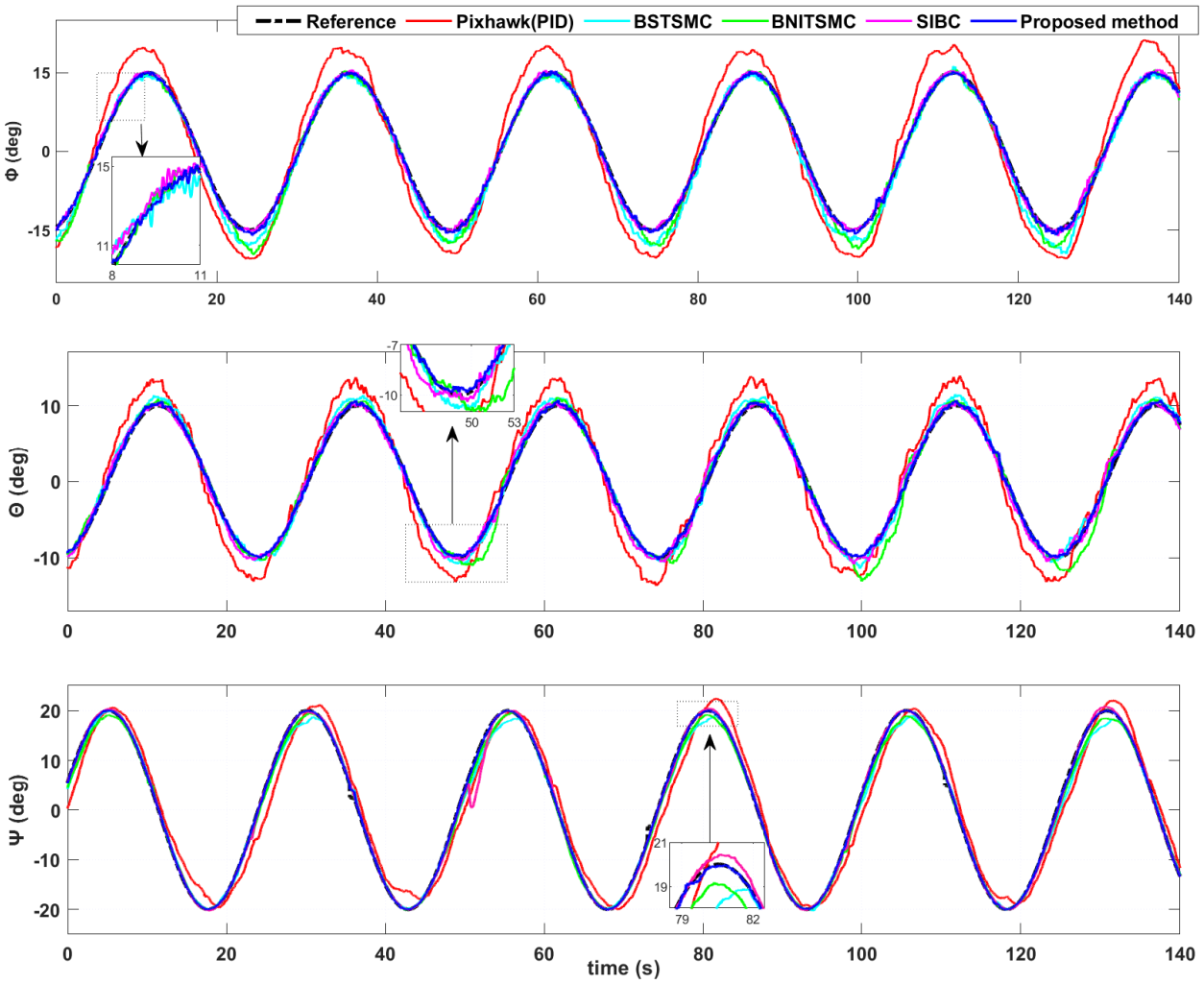

Figure 5.11: Attitude response in the tracking experiment

Figure 5.12 depicts the attitude tracking errors, from which we can conclude that the proposed controller ensures improved tracking performance compared to all the other compared methodologies. On the other hand, the trajectories of the PID controller are far from the targeted trajectories due to the influence of wind perturbations.

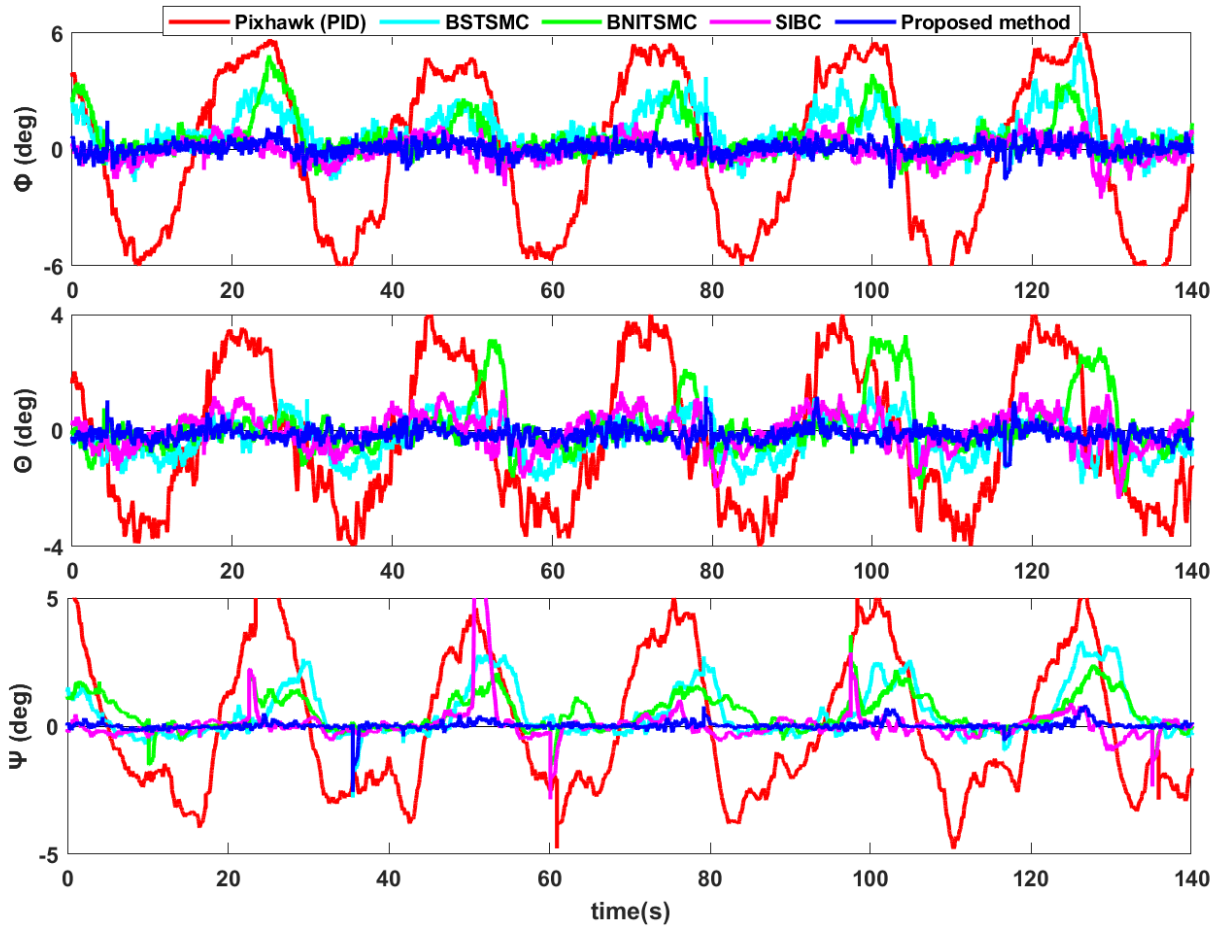

Figure 5.12: Time evolution of the attitude tracking errors in the tracking experiment

Figure 5.13 highlights the generated control signals that permit the accurate tracking of the time-varying trajectories under wind disturbances. Obviously, the control signals of the the proposed strategy have the appropriate amplitude. Moreover, the chattering problem is remarkably reduced compared to the other methods.

Table 5.6 summarizes the comparisons of the tracking performance in terms of the ISE and $IAD\tau$ indicators, the better results are highlighted in bold text.

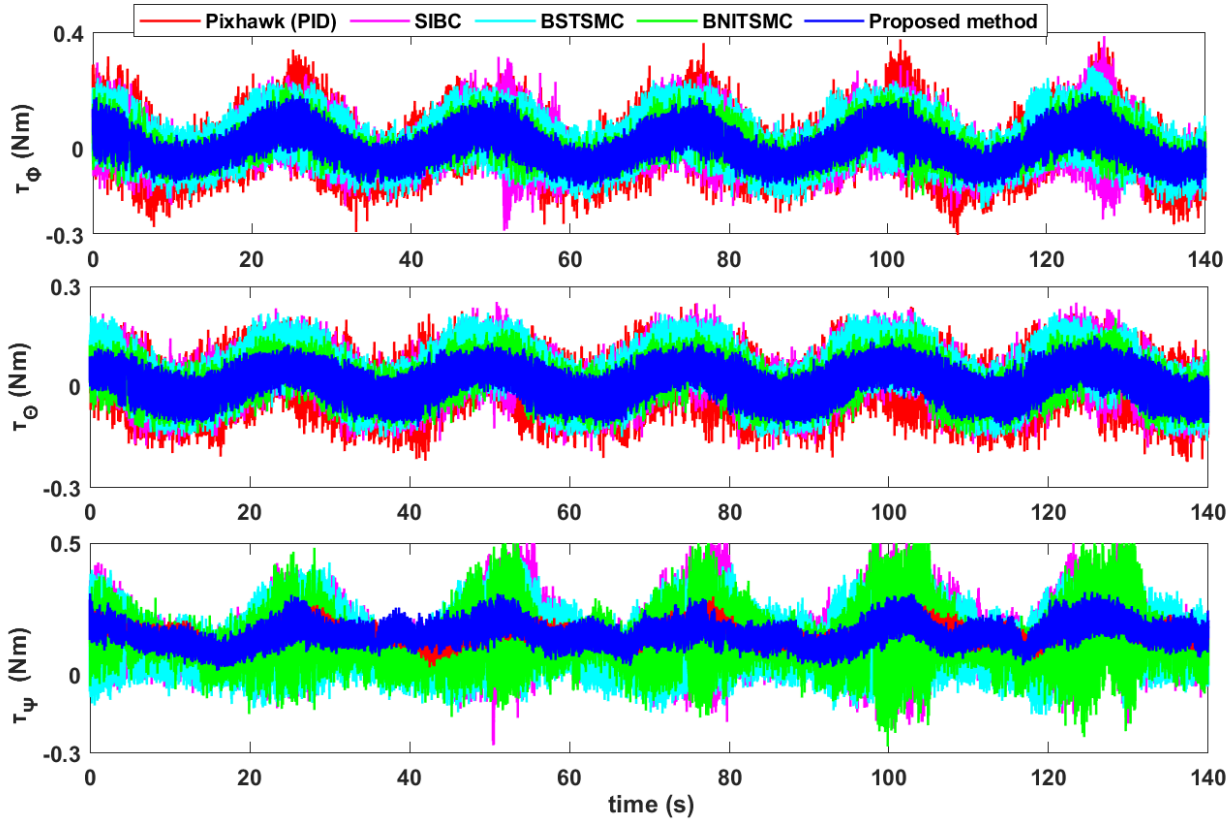

Figure 5.13: Time histories of the generated control signals in the tracking experiment

Table 5.6: Quantitative comparison in the tracking experiment

		Pixhawk (PID)	BSTSMC	BNITSMC	SIBC	Proposed method
ISE	Φ	0.7090	0.0894	0.0659	0.0136	**0.0056**
	Θ	0.2467	0.0245	0.0388	0.0162	**0.0034**
	Ψ	0.3223	0.0529	0.0315	0.0332	**0.0012**
IADτ	τ_Φ	0.0964	0.1017	0.0551	0.0838	**0.0465**
	τ_Θ	0.0883	0.0873	0.0538	0.0685	**0.0512**
	τ_Ψ	0.0227	0.1634	0.1296	0.1299	**0.0507**

It evident that the suggested control scheme has improved the tracking accuracy for the three orientations. Specifically, the ISE of the proposed controller is the smallest among the five strategies. Moreover, the smoothness of the generated inputs $(\tau_\Phi, \tau_\Theta, \tau_\Psi)$ is noticeably enhanced by our controller, which is obvious from the smaller value of the $IAD\tau$ index with

respect to all control signals.

Table 5.7 highlights the percentage reduction of chattering by the proposed method. Here also the chattering has been remarkably decreased, which highlights the chattering alleviation property of the proposed method.

Table 5.7: RDP % for IADτ index in the tracking experiment

Control signal	BSTSMC	SIBC	BNITSMC
τ_Φ	54.28	44.51	15.61
τ_Θ	42.02	25.26	4.83
τ_Ψ	68.97	60.97	60.88

Readers are also encouraged to watch the associated videos for more information on the experimental tests that were conducted (see https://youtu.be/XIFWyxN-IhM and https://youtu.be/-Sty49_HKqw).

5.4 Conclusion

In this chapter, a quadrotor research platform has been developed for the experimental implementation of multiple flight control algorithms. An accurate model-based design approach was used to implement control laws on an autopilot board directly from MATLAB/Simulink software using the embedded coder of the Pixhawk hardware. Multiple experimental scenarios were proposed to scrutinize the performance/advantages of the embedded control strategies. The obtained results indicate that the proposed flight attitude control can effectively stabilize the quadrotor vehicle in both regulation and tracking tasks. Moreover, better robustness against wind disturbances has been observed. Finally, smooth response without chattering or singularity has been achieved by the proposed controller. All these factors demonstrate the high performance of the suggested controller.

6 Conclusions and Scope for Future Works

Conclusions

In this thesis, the problem of finite-time trajectory tracking of a nonlinear underactuated quadrotor system has been addressed. Focusing on improving the robustness and accuracy of the flight control system, multiple enhanced control algorithms have been developed, tested, compared with the existing methodologies, and finally implemented on a real autopilot hardware.

The first goal was to provide an overview of unmanned aerial vehicles (UAVs), with a particular focus on quadrotors aircraft. It investigates the commonly used control algorithms for quadrotors and examines their suitability, as well as their limitations and challenges. By analyzing the advantages and disadvantages of each approach, the overview aims to offer readers a thorough understanding of the cutting-edge advancements in quadrotor control.

The scientific backgrounds of the quadrotor configuration, motion control, and kinematic and dynamic modeling have been discussed. Using the Newton-Euler principle and considering the impact of disturbances on the aircraft, we have presented a step-by-step derivation of the quadrotor model. The obtained model is then rewritten in the state space representation to facilitate control design and performance evaluation of the developed control strategies. An effective hierarchical control architecture has been introduced to solve the problem of underactuation and ensure the full controllability of the quadrotor system.

In order to improve the tracking performance, a robust hybrid control algorithm has been developed and applied for the control of the position and orientation of the quadrotor UAV. The overall control law combines two nonlinear control strategies. A robust backstepping SMC and an adaptive finite-time control law, which are used, respectively, for accurate

tracking of the quadrotor position and robust stabilization of the vehicle's attitude despite the impact of unknown external disturbances and uncertainties. The closed loop stability is ensured and verified using the Lyapunov theory. The performance of the proposed hybrid controller was analyzed and compared to several nonlinear strategies under different flight conditions. Results show robust achievement in terms of accuracy, trajectory tracking, and chattering avoidance. Specifically, the proposed hybrid controller demonstrates faster response time when compared to both the backstepping and integral SMC controllers. Additionally, it exhibits a decreased integral square error performance index, with a reduction of (19.17%) compared to the backstepping control and (15.74%) compared to the integral SMC. The proposed controller also achieves better robustness to disturbances and uncertainties, with a significant reduction in the integral square error of (95.05%) compared to the second-order SMC method and (71.21%) compared to the global fast dynamic SMC method.

To deal with unexpected external disturbances, an efficient control algorithm based on a disturbance observer has also been developed. Firstly, a disturbance observer is used to estimate the unknown external disturbances, and then a nonsingular finite-time controller is used to provide precise path following. Finally, the supertwisting algorithm is introduced to strengthen the system's robustness while reducing the chattering influence. Processor-in-the-loop (PIL) implementations on a real autopilot have been conducted to validate the feasibility of the proposed controller and highlight its improvements compared to the existing methods. The obtained results confirm the outperformance of the suggested control system in terms of accuracy and robustness against disturbances and random variation of the drag coefficients.

Finally, we have adopted and used an effective model-based design approach to implement and evaluate the proposed controllers. In addition, an experimental test bench has been developed. Due to its safety level, it can be used for the practical testing of multiple sophisticated algorithms. The experimental platform allows motion control with a single, two, or three degrees-of-freedom. Moreover, the use of Matlab Simulink software as a user interface simplifies the implementation and allows tuning of the controller's parameters while the experiment is running. A step-by-step validation procedure has also been adopted, in which multiple scenarios in terms of origin stabilization, transient experiment, regulation and tracking experiments are proposed to test the efficiency, workability, and reproducibility of the proposed and developed control strategies. The experimental results on the developed platform reveal that the proposed controller has a fast response time, high trajectory tracking accuracy, improved robustness against wind disturbance, and reduced chattering compared to several linear and nonlinear control algorithms.

Future works

Future research directions based on the design methodologies presented in this thesis are as follows:

- The control strategies developed in this thesis can ensure asymptotic and finite-time convergence of the position and velocity tracking errors, this imply the convergence is initial state dependent. Thus, when the quadrotor is commanded to track some trajectories with large abrupt changes (large angular variations), it may take more time to achieve the new desired trajectories. This point is under investigation for our future work. This can be realized by focusing on fixed-time stabilization.
- The development of a six-DOF research platform for the practical validation of multiple control system during autonomous flight missions will be investigated.
- Within the works developed in this thesis, we have supposed that all the state variables are measurable/available; which is not always possible. In some cases, some state variables are not available or the necessary sensors are expensive. For instance, the sensors usually used for the measurement of the quadrotor position (global positioning system GPS, barometer, etc.) provide only the cartesian position and do not give the vehicle translational velocities. A state estimator will be used to estimate the unmeasured signal as well as the external disturbance, then will be used to enhance the performance of the adopted control systems.
- Another possible extension of this thesis could be to study some strategies to deal with an unexpected failure of the actuators.
- The suggested control strategies may be evaluated on a variety of nonlinear perturbed robotics systems, such as autonomous ground vehicles, underwater vehicles and robot manipulators.
- The obtained results in the finite-time control of one quadrotor can be extended to the finite-time cooperative control of a group of quadrotors.

Appendix

Appendix A: Details of calculations

Detailed proof of the FTSS's convergence time (theorem 3.3.1)

In order to calculate the convergence time of the FTSS, recalling Eq. 3.22 given as,

$$\frac{de_\hbar}{-\alpha_\hbar e_\hbar - \beta_\hbar \left|e_\hbar\right|^{\left(\frac{p_\hbar}{q_\hbar}\right)} sign\left(e_\hbar\right)} = dt \tag{6.1}$$

Eq. 6.1 can be rewriting as:

$$\frac{de_\hbar}{-\alpha_\hbar \left|e_\hbar\right|^{\left(\frac{p_\hbar}{q_\hbar}\right)} sign\left(e_\hbar\right)\left(e_\hbar \left|e_\hbar\right|^{\left(-\frac{p_\hbar}{q_\hbar}\right)} sign\left(e_\hbar\right) + \frac{\beta_\hbar}{\alpha_\hbar}\right)} = dt \tag{6.2}$$

Then after simplification ($\left|e_\hbar\right| = e_\hbar sign\left(e_\hbar\right)$) , we obtain

$$\frac{de_\hbar}{-\alpha_\hbar \left|e_\hbar\right|^{\left(\frac{p_\hbar}{q_\hbar}\right)} sign\left(e_\hbar\right)\left(\left|e_\hbar\right|^{\left(1-\frac{p_\hbar}{q_\hbar}\right)} + \frac{\beta_\hbar}{\alpha_\hbar}\right)} = dt \tag{6.3}$$

Thereafter,

$$\frac{\left|e_\hbar\right|^{\left(-\frac{p_\hbar}{q_\hbar}\right)} sign\left(e_\hbar\right) de_\hbar}{-\alpha_\hbar\left(\left|e_\hbar\right|^{\left(1-\frac{p_\hbar}{q_\hbar}\right)} + \frac{\beta_\hbar}{\alpha_\hbar}\right)} = dt \tag{6.4}$$

The integration of Eq. 6.4 is given as:

$$\frac{1}{-\alpha_\hbar}\int_{e_\hbar(t_0)}^{e_\hbar(t_s)} \frac{\left|e_\hbar\right|^{\left(-\frac{p_\hbar}{q_\hbar}\right)} sign\left(e_\hbar\right) de_\hbar}{\left|e_\hbar\right|^{\left(1-\frac{p_\hbar}{q_\hbar}\right)} + \frac{\beta_\hbar}{\alpha_\hbar}} = \int_{t_0}^{t_s} dt \tag{6.5}$$

Consider $U = \left|e_\hbar\right|$ and known that $\frac{dU}{de_\hbar} = sign\left(e_\hbar\right)$ and $dU = sign\left(e_\hbar\right) de_\hbar$.

Using the new variable U, Eq. 6.5 can be rewriting as follows:

$$\frac{1}{-\alpha_\hbar}\int_{|e_\hbar(t_0)|}^{|e_\hbar(t_s)|}\frac{U^{\left(-\frac{p_\hbar}{q_\hbar}\right)}dU}{U^{\left(1-\frac{p_\hbar}{q_\hbar}\right)}+\frac{\beta_\hbar}{\alpha_\hbar}}=\int_{t_0}^{t_s}dt \tag{6.6}$$

From Eq. 6.6, we obtain

$$\frac{1}{-\alpha_\hbar\left(1-\frac{p_\hbar}{q_\hbar}\right)}\int_{|e_\hbar(t_0)|}^{|e_\hbar(t_s)|}\frac{d(U^{\left(1-\frac{p_\hbar}{q_\hbar}\right)})}{U^{\left(1-\frac{p_\hbar}{q_\hbar}\right)}+\frac{\beta_\hbar}{\alpha_\hbar}}=\int_{t_0}^{t_s}dt \tag{6.7}$$

Consider $X=U^{\left(1-\frac{p_\hbar}{q_\hbar}\right)}$, then Eq. 6.7 can be expressed as:

$$\frac{1}{-\alpha_\hbar\left(1-\frac{p_\hbar}{q_\hbar}\right)}\int_{|e_\hbar(t_0)|^{\left(1-\frac{p_\hbar}{q_\hbar}\right)}}^{|e_\hbar(t_s)|^{\left(1-\frac{p_\hbar}{q_\hbar}\right)}}\frac{dX}{X+\frac{\beta_\hbar}{\alpha_\hbar}}=\int_{t_0}^{t_s}dt \tag{6.8}$$

Known that $\int\frac{dX}{X+c}=\ln(X+c)$, then Eq. 6.8 gives,

$$\frac{1}{-\alpha_\hbar\left(1-\frac{p_\hbar}{q_\hbar}\right)}\left(\ln\left(|e_\hbar(t_0)|^{\left(1-\frac{p_\hbar}{q_\hbar}\right)}+\frac{\beta_\hbar}{\alpha_\hbar}\right)-\ln\left(|e_\hbar(t_s)|^{\left(1-\frac{p_\hbar}{q_\hbar}\right)}+\frac{\beta_\hbar}{\alpha_\hbar}\right)\right)=t_s-t_0 \tag{6.9}$$

Since the terminal state is characterized by $e_\hbar(t_s)=0$, then the convergence time for the FTSS is obtained as:

$$t_s=t_0+\frac{1}{\alpha_\hbar\left(1-\frac{p_\hbar}{q_\hbar}\right)}\ln\frac{\alpha_\hbar\left|e_\hbar(t_0)\right|^{\left(1-\frac{p_\hbar}{q_\hbar}\right)}+\beta_\hbar}{\beta_\hbar} \tag{6.10}$$

Comparison between the TSS and FTSS (Remark 3.3.2)

For the TSS and the FTSS represented by Eq. 3.16 and Eq. 3.20, respectively. if the sliding phase is established, then the convergence time for the FTSS is less than that of TSS.

known that $\exp(a) > 1 + a, \forall a > 0$, we have

$$\exp(\frac{\alpha_\hbar}{\beta_\hbar} |e_\hbar(t_0)|^{\left(1-\frac{p_\hbar}{q_\hbar}\right)}) > 1 + \frac{\alpha_\hbar}{\beta_\hbar} |e_\hbar(t_0)|^{\left(1-\frac{p_\hbar}{q_\hbar}\right)} \tag{6.11}$$

Thereafter,

$$\frac{\alpha_\hbar}{\beta_\hbar} |e_\hbar(t_0)|^{\left(1-\frac{p_\hbar}{q_\hbar}\right)} > \ln(1 + \frac{\alpha_\hbar}{\beta_\hbar} |e_\hbar(t_0)|^{\left(1-\frac{p_\hbar}{q_\hbar}\right)}) \tag{6.12}$$

By multiplying both sides with $\frac{1}{\alpha_\hbar\left(1-\frac{p_\hbar}{q_\hbar}\right)}$, we have:

$$\frac{|e_\hbar(t_0)|^{\left(1-\frac{p_\hbar}{q_\hbar}\right)}}{\beta_\hbar\left(1-\frac{p_\hbar}{q_\hbar}\right)} > \frac{1}{\alpha_\hbar\left(1-\frac{p_\hbar}{q_\hbar}\right)} \ln(1 + \frac{\alpha_\hbar}{\beta_\hbar} |e_\hbar(t_0)|^{\left(1-\frac{p_\hbar}{q_\hbar}\right)}) \tag{6.13}$$

Therefore,

$$t_{TSS} > t_{FTSS} \tag{6.14}$$

We can conclude that the FTSS's convergence time is smaller than the TSS's convergence time.

Appendix B: Quadrotor's parameters && controller's gains

Table 6.1: Physical parameters of the quadrotor used in chapter 3

Parameters	Value	Units
m	0.5	Kg
$J_x = J_y$	0.00485	Kgm^2
J_z	0.00881	Kgm^2
l	0.24	m
$K_{x,y,z}$	5.56710^{-5}	$N/m/s$
$K_{\Phi,\Theta,\Theta}$	5.56710^{-5}	$N/m/s$
k_p	2.9210^{-6}	Ns^2
k_d	1.1210^{-7}	Nms^2
J_r	610^{-5}	Kgm^2
g	9.81	ms^{-2}

Table 6.2: Parameters of the hybrid controller

Parameters	Value	Parameters	Value
$p_\Phi = p_\Theta = p_\Psi$	3	$K_{x1} = K_{y1}$	5.9594
$q_\Phi = q_\Theta = q_\Psi$	5	K_{z1}	20
$\rho_\Phi = \rho_\Theta = \rho_\Psi$	0.05	$K_{x2} = K_{y2}$	0.1642
$\kappa_\Phi = \kappa_\Theta = \kappa_\Psi$	3	K_{z2}	1
$\alpha_\Phi = \alpha_\Theta = \alpha_\Psi$	20.22	$\xi_x = \xi_y$	4.5
$\beta_\Phi = \beta_\Theta = \beta_\Psi$	3.9755	ξ_z	10
$\Gamma_{1i} = \Gamma_{2i}$	0.1	Γ_{3i}	10^{-5}

Table 6.3: Physical parameters of the quadrotor used in chapter 4

Parameters	Value	Units
m	0.74	Kg
$J_x = J_y$	0.004	Kgm^2
J_z	0.0084	Kgm^2
l	0.21	m
$K_{x,y,z}$	5.56710^{-5}	$N/m/s$
$K_{\Phi,\Theta,\Theta}$	5.56710^{-5}	$N/m/s$
k_b	2.910^{-5}	Ns^2
k_d	1.110^{-6}	Nms^2
J_r	2.83810^{-5}	Kgm^2
g	9.81	ms^{-2}

Table 6.4: Parameters of the DO-STNTSMC controller

Parameters	Value	Parameters	Value
$\kappa_{x,y,z}$	0.5	$\kappa_{\Phi,\Theta,\Psi}$	0.01
$\gamma_{x,y,z}$	1.5	$\gamma_{\Phi,\Theta,\Psi}$	1.5
$L_{x,y}$	50	$L_{z,\Phi,\Theta,\Psi}$	6
$b_{1x,y,z}$	50	$b_{2x,y,z}$	0.001
$b_{1\Phi,\Theta,\Psi}$	500	$b_{2\Phi,\Theta,\Psi}$	0.001
$\beta_{1x,y,z,\Phi,\Theta,\Psi}$	3	$\beta_{2x,y,z,\Phi,\Theta,\Psi}$	4

Appendix C: Publications

International journals

H. Hassani, A. Mansouri, and A. Ahaitouf, "Performance Evaluation of an Improved Non-Singular Sliding Mode Attitude Control of a Perturbed Quadrotor: Experimental Validation", **Journal of Vibration and Control**, 2023, doi: 10.1177/10775463231161848.

H. Hassani, A. Mansouri, and A. Ahaitouf, "Optimal Backstepping Controller for Trajectory Tracking of a Quadrotor UAV using Ant colony optimization algorithm", **International Journal of Computer Aided Engineering and Technology**, 2023, vol. 18(1/2/3), pp 39–59, .

H. Hassani, A. Mansouri, and A. Ahaitouf, "Backstepping-based supertwisting sliding mode attitude control for a quadrotor aircraft subjected to wind disturbances: experimental validation," **International Journal of Dynamics and Control**, Aug. 2022, doi: 10.1007/s40435-022-01004-5.

H. Hassani, A. Mansouri, and A. Ahaitouf, "Robust Finite-Time Tracking Control Based on Disturbance Observer for an Uncertain Quadrotor under External Disturbances," **Journal of Robotics**, vol. 2022, p. 4581165, Aug. 2022, doi: 10.1155/2022/4581165.

H. Hassani, A. Mansouri, and A. Ahaitouf, "Robust hybrid controller for quadrotor UAV under disturbances," **International Journal of Modelling, Identification and Control**, vol. 40, no. 3, pp. 195–203, 2022.

H. Hassani, A. Mansouri, and A. Ahaitouf, "Robust autonomous flight for quadrotor UAV based on adaptive nonsingular fast terminal sliding mode control," **International Journal of Dynamics and Control**, vol. 9, no. 2, pp. 619–635, 2021.

H. Hassani, A. Mansouri, and A. Ahaitouf, "Robust Trajectory Tracking Control of an Uncertain Quadrotor via a Novel Adaptive Nonsingular Sliding Mode Control", **Journal of Control**, Under review.

H. Hassani, A. Mansouri, and A. Ahaitouf, "Design and Implementation of a Robust Backstepping Non-singular Integral Terminal Sliding Mode Control for a Quadrotor Aircraft", **International Review of Automatic Control**, Under review.

H. Hassani, A. Mansouri, and A. Ahaitouf, "Model-based robust tracking control of an uncertain quadrotor under disturbances ", being finalized for submission.

Book Chapters

H. Hassani, A. Mansouri, and A. Ahaitouf, "Mechanical Modeling, Control and Simulation of a Quadrotor UAV," in International Conference on Electronic Engineering and Renewable Energy, 2020, pp. 441–449.

H. Hassani, A. Mansouri, and A. Ahaitouf, "Adaptive Fast Terminal Sliding Mode Control for Uncertain Quadrotor Based on Butterfly Optimization Algorithm (BOA)," in WITS 2020, Springer, 2022, pp. 353–364

H. Hassani, A. Mansouri, and A. Ahaitouf, "Modeling and Trajectory Tracking of an Unmanned Quadrotor Using Optimal PID Controller," in WITS 2020, Springer, 2022, pp. 457–467.

H. Hassani, A. Mansouri, and A. Ahaitouf, "Processor in the loop experiments of an adaptive trajectory tracking control for quadrotor UAVs," River Publishers, IEEE, 2022.

International Conferences

H. Hassani, A. Mansouri, and A. Ahaitouf, "A new robust adaptive sliding mode controller for quadrotor UAV flight". In 2020 IEEE 2nd International Conference on Electronics, Control, Optimization and Computer Science (ICECOCS) (pp. 1-6). IEEE.

H. Hassani, A. Mansouri, and A. Ahaitouf, "Modeling and trajectory tracking of an unmanned quadrotor using optimal PID controller". In The 6th International Conference on Wireless Technologies, Embedded and Intelligent Systems (WITS).

H. Hassani, A. Mansouri, and A. Ahaitouf, "Adaptive fast terminal sliding mode control for uncertain quadrotor based on butterfly optimization algorithm (BOA)". In The 6th International Conference on Wireless Technologies, Embedded and Intelligent Systems (WITS).

H. Hassani, A. Mansouri, and A. Ahaitouf, “Modeling and PID controller for quadrotor UAV,” in 1st Mediterranean Conference on Information Technology and its Applications, 2020.

H. Hassani, A. Mansouri, and A. Ahaitouf, "Mechanical Modeling, Control and Simulation of a Quadrotor UAV". In 2nd International Conference on Electronic Engineering and Renewable Energy 2020 (ICEERE).

H. Hassani, A. Mansouri, and A. Ahaitouf, "Control system of a quadrotor UAV with an optimized backstepping controller," in 2019 international conference on intelligent systems and advanced computing sciences (ISACS), 2019, pp. 1–7.IEEE

References

[1] Kimon P Valavanis. Advances in unmanned aerial vehicles: state of the art and the road to autonomy. 2008.

[2] Daniel KD Villa, Alexandre S Brandao, and Mário Sarcinelli-Filho. A survey on load transportation using multirotor uavs. *Journal of Intelligent & Robotic Systems*, 98(2):267–296, 2020.

[3] Nicholas C Coops, Tristan RH Goodbody, and Lin Cao. Four steps to extend drone use in research, 2019.

[4] Brent Skorup and Connor Haaland. How drones can help fight the coronavirus. *Mercatus Center Research Paper Series, Special Edition Policy Brief (2020)*, 2020.

[5] Dan-Marius Dobrea and Monica-Claudia Dobrea. An autonomous uav system for video monitoring of the quarantine zones. *Roman J Inf Sci Technol*, 23:S53, 2020.

[6] Syed Agha Hassnain Mohsan, Muhammad Asghar Khan, Fazal Noor, Insaf Ullah, and Mohammed H Alsharif. Towards the unmanned aerial vehicles (uavs): A comprehensive review. *Drones*, 6(6):147, 2022.

[7] Davide Scaramuzza, Michael C Achtelik, Lefteris Doitsidis, Fraundorfer Friedrich, Elias Kosmatopoulos, Agostino Martinelli, Markus W Achtelik, Margarita Chli, Savvas Chatzichristofis, Laurent Kneip, et al. Vision-controlled micro flying robots: from system design to autonomous navigation and mapping in gps-denied environments. *IEEE Robotics & Automation Magazine*, 21(3):26–40, 2014.

[8] Hazim Shakhatreh, Ahmad H Sawalmeh, Ala Al-Fuqaha, Zuochao Dou, Eyad Almaita, Issa Khalil, Noor Shamsiah Othman, Abdallah Khreishah, and Mohsen Guizani. Unmanned aerial vehicles (uavs): A survey on civil applications and key research challenges. *Ieee Access*, 7:48572–48634, 2019.

[9] Hao Liu, Jianxiang Xi, and Yisheng Zhong. Robust attitude stabilization for nonlinear quadrotor systems with uncertainties and delays. *IEEE Transactions on Industrial Electronics*, 64(7):5585–5594, 2017.

[10] Omid Mofid and Saleh Mobayen. Adaptive sliding mode control for finite-time stability of quad-rotor uavs with parametric uncertainties. *ISA transactions*, 72:1–14, 2018.

[11] Yue Wang, Bin Jiang, Ningyun Lu, and Jun Pan. Hybrid modeling based double-granularity fault detection and diagnosis for quadrotor helicopter. *Nonlinear Analysis: Hybrid Systems*, 21:22–36, 2016.

[12] Tiffany Kelly. The Booming Demand for Commercial Drone Pilots, January 2017. Section: Technology.

[13] Mostafa Hassanalian and Abdessattar Abdelkefi. Classifications, applications, and design challenges of drones: A review. *Progress in Aerospace Sciences*, 91:99–131, 2017.

[14] MA Boon, AP Drijfhout, and Solomon Tesfamichael. Comparison of a fixed-wing and multi-rotor uav for environmental mapping applications: A case study. *The International Archives of Photogrammetry, Remote Sensing and Spatial Information Sciences*, 42:47, 2017.

[15] S Norouzi Ghazbi, Yasaman Aghli, M Alimohammadi, and Ali Akbar Akbari. Quadrotors unmanned aerial vehicles: A review. *International journal on smart sensing and Intelligent Systems*, 9(1), 2016.

[16] Zhen Liu and Jean-Marc Moschetta. Rotary vs. flapping-wing nano air vehicles: Comparing hovering power. In *Proceedings of The European Micro Aerial Vehicle Conference*, pages 21–27, 2009.

[17] Mostafa Hassanalian, Abdessattar Abdelkefi, Mingjun Wei, and Saeed Ziaei-Rad. A novel methodology for wing sizing of bio-inspired flapping wing micro air vehicles: theory and prototype. *Acta Mechanica*, 228(3):1097–1113, 2017.

[18] Farid Kendoul. Survey of advances in guidance, navigation, and control of unmanned rotorcraft systems. *Journal of Field Robotics*, 29(2):315–378, 2012.

[19] Egbert Torenbeek and H Wittenberg. *Flight physics: essentials of aeronautical disciplines and technology, with historical notes*. Springer Science & Business Media, 2009.

[20] Samir Bouabdallah, Pierpaolo Murrieri, and Roland Siegwart. Towards autonomous indoor micro vtol. *Autonomous robots*, 18(2):171–183, 2005.

[21] Ahmad Safaee, Seyed Zeinolabedin Moussavi, and Mohammad Bagher Menhaj. Design and construction of monocopter and its nonlinear control using photo diode array. *U. Porto Journal of Engineering*, 4(2):34–41, 2018.

[22] Farid Kendoul, Zhenyu Yu, and Kenzo Nonami. Guidance and nonlinear control system for autonomous flight of minirotorcraft unmanned aerial vehicles. *Journal of Field Robotics*, 27(3):311–334, 2010.

[23] Gabriel Hugh Elkaim, Fidelis Adhika Pradipta Lie, and Demoz Gebre-Egziabher. Principles of guidance, navigation, and control of uavs. *Handbook of unmanned aerial vehicles*, pages 347–380, 2015.

[24] Kenzo Nonami, Farid Kendoul, Satoshi Suzuki, Wei Wang, and Daisuke Nakazawa. *Autonomous flying robots: unmanned aerial vehicles and micro aerial vehicles*. Springer Science & Business Media, 2010.

[25] Antonios Tsourdos, Brian White, and Madhavan Shanmugavel. *Cooperative path planning of unmanned aerial vehicles*. John Wiley & Sons, 2010.

[26] Karl Johan Åström, Tore Hägglund, and Karl J Astrom. *Advanced PID control*, volume 461. ISA-The Instrumentation, Systems, and Automation Society Research Triangle Park, 2006.

[27] Michael A Johnson and Mohammad H Moradi. *PID control*. Springer, 2005.

[28] Samir Bouabdallah, Andre Noth, and Roland Siegwart. Pid vs lq control techniques applied to an indoor micro quadrotor. In *2004 IEEE/RSJ International Conference on Intelligent Robots and Systems (IROS)(IEEE Cat. No. 04CH37566)*, volume 3, pages 2451–2456. IEEE, 2004.

[29] A Zul Azfar and Desa Hazry. A simple approach on implementing imu sensor fusion in pid controller for stabilizing quadrotor flight control. In *2011 IEEE 7th International Colloquium on Signal Processing and its Applications*, pages 28–32. IEEE, 2011.

[30] Hossein Bolandi, Mohammad Rezaei, Reza Mohsenipour, Hossein Nemati, and Seed Majid Smailzadeh. Attitude control of a quadrotor with optimized pid controller. 2013.

[31] Abdelhamid Tayebi and Stephen McGilvray. Attitude stabilization of a vtol quadrotor aircraft. *IEEE Transactions on control systems technology*, 14(3):562–571, 2006.

[32] Gabriel Hoffmann, Steven Waslander, and Claire Tomlin. Quadrotor helicopter trajectory tracking control. In *AIAA guidance, navigation and control conference and exhibit*, page 7410, 2008.

[33] Grzegorz Szafranski and Roman Czyba. Different approaches of pid control uav type quadrotor. 2011.

[34] Ahmed H Ahmed, Ahmed N Ouda, Ahmed M Kamel, and Yehia Z Elhalwagy. Design and analysis of quadcopter classical controller. In *International Conference on Aerospace Sciences and Aviation Technology*, volume 16, pages 1–17. The Military Technical College, 2015.

[35] Javier Moreno-Valenzuela, Ricardo Pérez-Alcocer, Manuel Guerrero-Medina, and Alejandro Dzul. Nonlinear pid-type controller for quadrotor trajectory tracking. *IEEE/ASME Transactions on Mechatronics*, 23(5):2436–2447, 2018.

[36] Aws Abdulsalam Najm and Ibraheem Kasim Ibraheem. Nonlinear pid controller design for a 6-dof uav quadrotor system. *Engineering Science and Technology, an International Journal*, 22(4):1087–1097, 2019.

[37] Sherif Badr, Omar Mehrez, and AE Kabeel. A design modification for a quadrotor uav: modeling, control and implementation. *Advanced Robotics*, 33(1):13–32, 2019.

[38] Sangram Bharat, Arunangshu Ganguly, Rohit Chatterjee, Biswajit Basak, Deb Kumar Sheet, and Anirban Ganguly. A review on tuning methods for pid controller. *Asian Journal For Convergence In Technology (AJCT) ISSN-2350-1146*, 2019.

[39] Nada El Gmili, Mostafa Mjahed, Abdeljalil El Kari, and Hassan Ayad. Particle swarm optimization and cuckoo search-based approaches for quadrotor control and trajectory tracking. *Applied Sciences*, 9(8):1719, 2019.

[40] Imane Siti, Mostafa Mjahed, Hassan Ayad, and Abdeljalil El Kari. New trajectory tracking approach for a quadcopter using genetic algorithm and reference model methods. *Applied Sciences*, 9(9):1780, 2019.

[41] Hamid Hassani, Anass Mansouri, and Ali Ahaitouf. Modeling and trajectory tracking of an unmanned quadrotor using optimal pid controller. In *WITS 2020*, pages 457–467. Springer, 2022.

[42] Aminurrashid Noordin, MA Mohd Basri, Zaharuddin Mohamed, and AF Zainal Abidin. Modelling and pso fine-tuned pid control of quadrotor uav. *International Journal on Advanced Science, Engineering and Information Technology*, 7(4):1367–1373, 2017.

[43] Andrew Zulu and Samuel John. A review of control algorithms for autonomous quadrotors. *arXiv preprint arXiv:1602.02622*, 2016.

[44] Brian DO Anderson and John B Moore. *Optimal control: linear quadratic methods*. Courier Corporation, 2007.

[45] Samir Bouabdallah. Design and control of quadrotors with application to autonomous flying. Technical report, Epfl, 2007.

[46] Changlong Liu, Jian Pan, and Yufang Chang. Pid and lqr trajectory tracking control for an unmanned quadrotor helicopter: Experimental studies. In *2016 35th Chinese control conference (CCC)*, pages 10845–10850. IEEE, 2016.

[47] Yongbin Sun, Ning Xian, and Haibin Duan. Linear-quadratic regulator controller design for quadrotor based on pigeon-inspired optimization. *Aircraft Engineering and Aerospace Technology*, 88(6):761–770, 2016.

[48] Luís Martins, Carlos Cardeira, and Paulo Oliveira. Linear quadratic regulator for trajectory tracking of a quadrotor. *IFAC-PapersOnLine*, 52(12):176–181, 2019.

[49] Elias Reyes-Valeria, Rogerio Enriquez-Caldera, Sergio Camacho-Lara, and Jose Guichard. Lqr control for a quadrotor using unit quaternions: Modeling and simulation. In *CONIELECOMP 2013, 23rd International Conference on Electronics, Communications and Computing*, pages 172–178. IEEE, 2013.

[50] Zhi Li, Xin Ma, and Yibin Li. Robust trajectory tracking control for a quadrotor subject to disturbances and model uncertainties. *International Journal of Systems Science*, 51(5):839–851, 2020.

[51] Tiago P Nascimento and Martin Saska. Position and attitude control of multi-rotor aerial vehicles: A survey. *Annual Reviews in Control*, 48:129–146, 2019.

[52] Samir Bouabdallah and Roland Siegwart. Backstepping and sliding-mode techniques applied to an indoor micro quadrotor. In *Proceedings of the 2005 IEEE international conference on robotics and automation*, pages 2247–2252. IEEE, 2005.

[53] Orlando García, Patricio Ordaz, Omar-Jacobo Santos-Sánchez, Sergio Salazar, and Rogelio Lozano. Backstepping and robust control for a quadrotor in outdoors environments: An experimental approach. *IEEE Access*, 7:40636–40648, 2019.

[54] Liliam Rodríguez-Guerrero, Alejandro Benítez-Morales, Omar-Jacobo Santos-Sánchez, Orlando García-Pérez, Hugo Romero-Trejo, Mario-Oscar Ordaz-Oliver, and Jesús-Patricio Ordaz-Oliver. Robust backstepping control applied to uavs for pest recognition in maize crops. *Applied Sciences*, 12(18):9075, 2022.

[55] Vibhu Kumar Tripathi, Laxmidher Behera, and Nishchal Verma. Design of sliding mode and backstepping controllers for a quadcopter. In *2015 39th national systems conference (NSC)*, pages 1–6. IEEE, 2015.

[56] Omar Rodríguez-Abreo, Juan Manuel Garcia-Guendulain, Rodrigo Hernández-Alvarado, Alejandro Flores Rangel, and Carlos Fuentes-Silva. Genetic algorithm-based tuning of backstepping controller for a quadrotor-type unmanned aerial vehicle. *Electronics*, 9(10):1735, 2020.

[57] Hamid Hassani, Anass Mansouri, and Ali Ahaitouf. Control system of a quadrotor uav with an optimized backstepping controller. In *2019 international conference on intelligent systems and advanced computing sciences (ISACS)*, pages 1–7. IEEE, 2019.

[58] F Yacef, O Bouhali, M Hamerlain, and A Rezoug. Pso optimization of integral backstepping controller for quadrotor attitude stabilization. In *3rd International Conference on Systems and Control*, pages 462–466. IEEE, 2013.

[59] Mohd Ariffanan Mohd Basri, Abdul Rashid Husain, and Kumeresan A Danapalasingam. Backstepping controller with intelligent parameters selection for stabilization of quadrotor helicopter. *Journal of Engineering Science and Technology Review*, 7(2):66–74, 2014.

[60] MA Basri and A Noordin. Optimal backstepping control of quadrotor uav using gravitational search optimization algorithm. *Bulletin of Electrical Engineering and Informatics*, 9(5):1819–1826, 2020.

[61] Samir Bouabdallah and Roland Siegwart. Full control of a quadrotor. In *2007 IEEE/RSJ international conference on intelligent robots and systems*, pages 153–158. Ieee, 2007.

[62] Nguyen Xuan-Mung and Sung Kyung Hong. Robust backstepping trajectory tracking control of a quadrotor with input saturation via extended state observer. *Applied Sciences*, 9(23):5184, 2019.

[63] Xingling Shao, Jun Liu, and Honglun Wang. Robust back-stepping output feedback trajectory tracking for quadrotors via extended state observer and sigmoid tracking differentiator. *Mechanical Systems and Signal Processing*, 104:631–647, 2018.

[64] Necdet Sinan Özbek, Mert Önkol, and Mehmet Önder Efe. Feedback control strategies for quadrotor-type aerial robots: a survey. *Transactions of the Institute of Measurement and Control*, 38(5):529–554, 2016.

[65] Ashton Roza and Manfredi Maggiore. Path following controller for a quadrotor helicopter. In *2012 American control conference (ACC)*, pages 4655–4660. IEEE, 2012.

[66] Daewon Lee, H Jin Kim, and Shankar Sastry. Feedback linearization vs. adaptive sliding mode control for a quadrotor helicopter. *International Journal of control, Automation and systems*, 7(3):419–428, 2009.

[67] A Benallegue, A Mokhtari, and L Fridman. Feedback linearization and high order sliding mode observer for a quadrotor uav. In *International Workshop on Variable Structure Systems, 2006. VSS'06.*, pages 365–372. IEEE, 2006.

[68] Abdellah Mokhtari, Nacer K M'Sirdi, Kamal Meghriche, and Abdelkader Belaidi. Feedback linearization and linear observer for a quadrotor unmanned aerial vehicle. *Advanced Robotics*, 20(1):71–91, 2006.

[69] Ahmed Aboudonia, Ayman El-Badawy, and Ramy Rashad. Disturbance observer-based feedback linearization control of an unmanned quadrotor helicopter. *Proceedings of the Institution of Mechanical Engineers, Part I: Journal of Systems and Control Engineering*, 230(9):877–891, 2016.

[70] Mohd Fuaad Rahmat, Ahmed Eltayeb, and Mohd Ariffanan Mohd Basri. Adaptive feedback linearization controller for stabilization of quadrotor uav. *International Journal of Integrated Engineering*, 12(4):1–17, 2020.

[71] Bijnan Bandyopadhyay, S Janardhanan, Sarah K Spurgeon, et al. Advances in sliding mode control. *Lecture Notes in Control and Information Sciences*, 440, 2013.

[72] Brahim Brahmi, Mohamed Hamza Laraki, Abdelkrim Brahmi, Maarouf Saad, and Mohammad H Rahman. Improvement of sliding mode controller by using a new adaptive reaching law: Theory and experiment. *ISA transactions*, 97:261–268, 2020.

[73] İ Can Dikmen, Aydemir Arisoy, and Hakan Temeltas. Attitude control of a quadrotor. In *2009 4th International Conference on Recent Advances in Space Technologies*, pages 722–727. Ieee, 2009.

[74] Ariffanan Noordin, MAM Basri, and Z Mohamed. Sliding mode control for altitude and attitude stabilization of quadrotor uav with external disturbance. *Indonesian Journal of Electrical Engineering and Informatics (IJEEI)*, 7(2):203–210, 2019.

[75] Safeer Ullah, Adeel Mehmood, Qudrat Khan, Sakhi Rehman, and Jamshed Iqbal. Robust integral sliding mode control design for stability enhancement of under-actuated quadcopter. *International Journal of Control, Automation and Systems*, 18:1671–1678, 2020.

[76] Iván González, Sergio Salazar, and Rogelio Lozano. Chattering-free sliding mode altitude control for a quad-rotor aircraft: Real-time application. *Journal of Intelligent & Robotic Systems*, 73(1):137–155, 2014.

[77] Zhenyue Jia, Jianqiao Yu, Yuesong Mei, Yongbo Chen, Yuanchuan Shen, and Xiaolin Ai. Integral backstepping sliding mode control for quadrotor helicopter under external uncertain disturbances. *Aerospace Science and Technology*, 68:299–307, 2017.

[78] Laihong Zhou, Juqian Zhang, Houxin She, and Hong Jin. Quadrotor uav flight control via a novel saturation integral backstepping controller. *Automatika*, 60(2):193–206, 2019.

[79] Laloui Derafa, Abdelaziz Benallegue, and L Fridman. Super twisting control algorithm for the attitude tracking of a four rotors uav. *Journal of the Franklin Institute*, 349(2):685–699, 2012.

[80] HJ Jayakrishnan. Position and attitude control of a quadrotor uav using super twisting sliding mode. *IFAC-PapersOnLine*, 49(1):284–289, 2016.

[81] Filiberto Muñoz, Iván González-Hernández, Sergio Salazar, Eduardo S Espinoza, and Rogelio Lozano. Second order sliding mode controllers for altitude control of a quadrotor uas: Real-time implementation in outdoor environments. *Neurocomputing*, 233:61–71, 2017.

[82] José Angel Cano-González, Oscar Salas-Peña, Susana V Gutierrez, De León-Morales, et al. Quadrotor altitude control based on sliding mode control. *Iranian Journal of Science and Technology, Transactions of Electrical Engineering*, 45(2):543–551, 2021.

[83] H Bouadi, M Bouchoucha, and M Tadjine. Modelling and stabilizing control laws design based on backstepping for an uav type-quadrotor. *IFAC Proceedings Volumes*, 40(15):245–250, 2007.

[84] Man Zhihong, Andrew P Paplinski, and Hong Ren Wu. A robust mimo terminal sliding mode control scheme for rigid robotic manipulators. *IEEE transactions on automatic control*, 39(12):2464–2469, 1994.

[85] Saleh Mobayen. Fast terminal sliding mode controller design for nonlinear second-order systems with time-varying uncertainties. *Complexity*, 21(2):239–244, 2015.

[86] Hamid Hassani, Anass Mansouri, and Ali Ahaitouf. Adaptive fast terminal sliding mode control for uncertain quadrotor based on butterfly optimization algorithm (boa). In *WITS 2020*, pages 353–364. Springer, 2022.

[87] Jing-Jing Xiong and Guo-Bao Zhang. Global fast dynamic terminal sliding mode control for a quadrotor uav. *ISA transactions*, 66:233–240, 2017.

[88] Zhiwei Hou, Peng Lu, and Zhangjie Tu. Nonsingular terminal sliding mode control for a quadrotor uav with a total rotor failure. *Aerospace Science and Technology*, 98:105716, 2020.

[89] Liang Yang and Jianying Yang. Nonsingular fast terminal sliding-mode control for nonlinear dynamical systems. *International Journal of Robust and Nonlinear Control*, 21(16):1865–1879, 2011.

[90] Mohamed Boukattaya, Neila Mezghani, and Tarak Damak. Adaptive nonsingular fast terminal sliding-mode control for the tracking problem of uncertain dynamical systems. *Isa Transactions*, 77:1–19, 2018.

[91] Arioberto L Silva and Davi A Santos. Fast nonsingular terminal sliding mode flight control for multirotor aerial vehicles. *IEEE Transactions on Aerospace and Electronic Systems*, 56(6):4288–4299, 2020.

[92] Ha Le Nhu Ngoc Thanh and Sung Kyung Hong. Quadcopter robust adaptive second order sliding mode control based on pid sliding surface. *IEEE Access*, 6:66850–66860, 2018.

[93] Ji-Won Lee, Nguyen Xuan-Mung, Ngoc Phi Nguyen, and Sung Kyung Hong. Adaptive altitude flight control of quadcopter under ground effect and time-varying load: theory and experiments. *Journal of Vibration and Control*, page 10775463211050169, 2021.

[94] Hamid Hassani, Anass Mansouri, and Ali Ahaitouf. A new robust adaptive sliding mode controller for quadrotor uav flight. In *2020 IEEE 2nd International Conference on Electronics, Control, Optimization and Computer Science (ICECOCS)*, pages 1–6. IEEE, 2020.

[95] Mohd Ariffanan Mohd Basri. Design and application of an adaptive backstepping sliding mode controller for a six-dof quadrotor aerial robot. *Robotica*, 36(11):1701–1727, 2018.

[96] Mohsen Vahdanipour and Mahdi Khodabandeh. Adaptive fractional order sliding mode control for a quadrotor with a varying load. *Aerospace Science and Technology*, 86:737–747, 2019.

[97] Omid Mofid, Saleh Mobayen, and Afef Fekih. Adaptive integral-type terminal sliding mode control for unmanned aerial vehicle under model uncertainties and external disturbances. *IEEE Access*, 9:53255–53265, 2021.

[98] Omid Mofid, Saleh Mobayen, Chunwei Zhang, and Balasubramanian Esakki. Desired tracking of delayed quadrotor uav under model uncertainty and wind disturbance using adaptive super-twisting terminal sliding mode control. *ISA transactions*, 123:455–471, 2022.

[99] Karam Eliker and Weidong Zhang. Finite-time adaptive integral backstepping fast terminal sliding mode control application on quadrotor uav. *International Journal of Control, Automation and Systems*, 18(2):415–430, 2020.

[100] Hamid Ghadiri, Maedeh Emami, and Hamed Khodadadi. Adaptive super-twisting non-singular terminal sliding mode control for tracking of quadrotor with bounded disturbances. *Aerospace Science and Technology*, 112:106616, 2021.

[101] Dhafer J Almakhles. Robust backstepping sliding mode control for a quadrotor trajectory tracking application. *IEEE Access*, 8:5515–5525, 2019.

[102] Fuyang Chen, Rongqiang Jiang, Kangkang Zhang, Bin Jiang, and Gang Tao. Robust backstepping sliding-mode control and observer-based fault estimation for a quadrotor uav. *IEEE Transactions on Industrial Electronics*, 63(8):5044–5056, 2016.

[103] Ning Wang, Qi Deng, Guangming Xie, and Xinxiang Pan. Hybrid finite-time trajectory tracking control of a quadrotor. *ISA transactions*, 90:278–286, 2019.

[104] Omar Mechali, Jamshed Iqbal, Xiaomei Xie, Limei Xu, and Abdelkader Senouci. Robust finite-time trajectory tracking control of quadrotor aircraft via terminal sliding mode-based active antidisturbance approach: A pil experiment. *International Journal of Aerospace Engineering*, 2021:1–28, 2021.

[105] Moussa Labbadi and Mohamed Cherkaoui. Robust integral terminal sliding mode control for quadrotor uav with external disturbances. *International Journal of Aerospace Engineering*, 2019, 2019.

[106] Alireza Modirrousta and Mahdi Khodabandeh. Adaptive non-singular terminal sliding mode controller: new design for full control of the quadrotor with external disturbances. *Transactions of the Institute of Measurement and Control*, 39(3):371–383, 2017.

[107] Ö Bingöl and HM Güzey. Neuro sliding mode control of quadrotor uavs carrying suspended payload. *Advanced Robotics*, 35(3-4):255–266, 2021.

[108] Özhan Bingöl and Hacı Mehmet Güzey. Finite-time neuro-sliding-mode controller design for quadrotor uavs carrying suspended payload. *Drones*, 6(10):311, 2022.

[109] Hadi Razmi. Adaptive neural network based sliding mode altitude control for a quadrotor uav. *Journal of Central South University*, 25(11):2654–2663, 2018.

[110] Hadi Razmi and Sima Afshinfar. Neural network-based adaptive sliding mode control design for position and attitude control of a quadrotor uav. *Aerospace Science and technology*, 91:12–27, 2019.

[111] Hugo Yañez-Badillo, Ruben Tapia-Olvera, and Francisco Beltran-Carbajal. Adaptive neural motion control of a quadrotor uav. *Vehicles*, 2(3):468–490, 2020.

[112] Mohd Ariffanan Mohd Basri, Abdul Rashid Husain, and Kumeresan A Danapalasingam. Intelligent adaptive backstepping control for mimo uncertain non-linear quadrotor helicopter systems. *Transactions of the Institute of Measurement and Control*, 37(3):345–361, 2015.

[113] Rakesh Goswami and Dheeraj Joshi. Performance review of fuzzy logic based controllers employed in brushless dc motor. *Procedia computer science*, 132:623–631, 2018.

[114] Ayad Al-Mahturi, Fendy Santoso, Matthew A Garratt, and Sreenatha G Anavatti. Modeling and control of a quadrotor unmanned aerial vehicle using type-2 fuzzy systems. In *Unmanned Aerial Systems*, pages 25–46. Elsevier, 2021.

[115] Xiaorong Huang, Anca L Ralescu, Hongli Gao, and Haibo Huang. A survey on the application of fuzzy systems for underactuated systems. *Proceedings of the Institution of Mechanical Engineers, Part I: Journal of Systems and Control Engineering*, 233(3):217–244, 2019.

[116] Vahab Nekoukar and Nima Mahdian Dehkordi. Robust path tracking of a quadrotor using adaptive fuzzy terminal sliding mode control. *Control Engineering Practice*, 110:104763, 2021.

[117] Edwar Yazid, Matthew Garratt, and Fendy Santoso. Position control of a quadcopter drone using evolutionary algorithms-based self-tuning for first-order takagi–sugeno–kang fuzzy logic autopilots. *Applied Soft Computing*, 78:373–392, 2019.

[118] Rupal Roy, Maidul Islam, Nafiz Sadman, MA Mahmud, Kishor Datta Gupta, and Md Manjurul Ahsan. A review on comparative remarks, performance evaluation and improvement strategies of quadrotor controllers. *Technologies*, 9(2):37, 2021.

[119] Jinho Kim, S Andrew Gadsden, and Stephen A Wilkerson. A comprehensive survey of control strategies for autonomous quadrotors. *Canadian Journal of Electrical and Computer Engineering*, 43(1):3–16, 2019.

[120] Hongwei Mo and Ghulam Farid. Nonlinear and adaptive intelligent control techniques for quadrotor uav–a survey. *Asian Journal of Control*, 21(2):989–1008, 2019.

[121] Paul Pounds, Robert Mahony, Joel Gresham, Peter Corke, and Jonathan Roberts. Towards dynamically-favourable quad-rotor aerial robots. In *Proceedings of the 2004 Australasian Conference on Robotics and Automation*, pages 1–10. Australian Robotics and Automation Association (ARAA), 2004.

[122] Robert Niemiec and Farhan Gandhi. A comparison between quadrotor flight configurations. 2016.

[123] Guilherme V Raffo, Manuel G Ortega, and Francisco R Rubio. An integral predictive/nonlinear h∞ control structure for a quadrotor helicopter. *Automatica*, 46(1):29–39, 2010.

[124] Teppo Luukkonen. Modelling and control of quadcopter. *Independent research project in applied mathematics, Espoo*, 22:22, 2011.

[125] Yogianandh Naidoo, Riaan Stopforth, and Glen Bright. Quad-rotor unmanned aerial vehicle helicopter modelling & control. *International Journal of Advanced Robotic Systems*, 8(4):45, 2011.

[126] CH Kuo, CM Kuo, A Leber, and C Boller. Vector thrust multi-rotor copter and its application for building inspection. *IMAV2013 Toulouse, France*, 2013.

[127] Tarek N Dief and Shigeo Yoshida. Modeling and classical controller of quad-rotor. *arXiv preprint arXiv:1707.04173*, 2017.

[128] Tammaso Bresciani. Modelling, identification and control of a quadrotor helicopter. *MSc theses*, 2008.

[129] Robert Mahony, Vijay Kumar, and Peter Corke. Multirotor aerial vehicles: Modeling, estimation, and control of quadrotor. *IEEE Robotics and Automation magazine*, 19(3):20–32, 2012.

[130] Bara J Emran and Homayoun Najjaran. A review of quadrotor: An underactuated mechanical system. *Annual Reviews in Control*, 46:165–180, 2018.

[131] SJ Gambhire, D Ravi Kishore, PS Londhe, and SN Pawar. Review of sliding mode based control techniques for control system applications. *International Journal of Dynamics and Control*, 9(1):363–378, 2021.

[132] Weibing Gao and James C Hung. Variable structure control of nonlinear systems: A new approach. *IEEE transactions on Industrial Electronics*, 40(1):45–55, 1993.

[133] Shanchao Yi and Junyong Zhai. Adaptive second-order fast nonsingular terminal sliding mode control for robotic manipulators. *ISA transactions*, 90:41–51, 2019.

[134] Liangyong Wang, Tianyou Chai, and Lianfei Zhai. Neural-network-based terminal sliding-mode control of robotic manipulators including actuator dynamics. *IEEE Transactions on Industrial Electronics*, 56(9):3296–3304, 2009.

[135] Mathworks advisory board (mab) guidelines:https:www.mathworks.com/solutions/mab-guidelines.html.

[136] Iván González-Hernández, Sergio Salazar, Abraham Efraim Rodriguez-Mata, Filiberto Muñoz-Palacios, Ricardo López, and Rogelio Lozano. Enhanced robust altitude controller via integral sliding modes approach for a quad-rotor aircraft: Simulations and real-time results. *Journal of Intelligent & Robotic Systems*, 88(2):313–327, 2017.

[137] Mohd Ariffanan Mohd Basri, Mohamad Shukri Zainal Abidin, and Nurul Adilla Mohd Subha. Simulation of backstepping-based nonlinear control for quadrotor helicopter. *Applications of Modelling and Simulation*, 2(1):34–40, 2018.

[138] En-Hui Zheng, Jing-Jing Xiong, and Ji-Liang Luo. Second order sliding mode control for a quadrotor uav. *ISA transactions*, 53(4):1350–1356, 2014.

[139] Omar Mechali, Limei Xu, Ya Huang, Mengji Shi, and Xiaomei Xie. Observer-based fixed-time continuous nonsingular terminal sliding mode control of quadrotor aircraft under uncertainties and disturbances for robust trajectory tracking: Theory and experiment. *Control Engineering Practice*, 111:104806, 2021.

[140] Wen-Hua Chen, Donald J Ballance, Peter J Gawthrop, and John O'Reilly. A nonlinear disturbance observer for robotic manipulators. *IEEE Transactions on industrial Electronics*, 47(4):932–938, 2000.

[141] Jun Yang, Wen-Hua Chen, and Shihua Li. Autopilot design of bank-to-turn missiles using state-space disturbance observers. 2010.

[142] Wen-Hua Chen. Nonlinear disturbance observer-enhanced dynamic inversion control of missiles. *Journal of Guidance, Control, and Dynamics*, 26(1):161–166, 2003.

[143] Xuerui Wang, Erik-Jan van Kampen, and Qiping Chu. Quadrotor fault-tolerant incremental nonsingular terminal sliding mode control. *Aerospace Science and Technology*, 95:105514, 2019.

[144] Jaime A Moreno and Marisol Osorio. Strict lyapunov functions for the super-twisting algorithm. *IEEE transactions on automatic control*, 57(4):1035–1040, 2012.

[145] Nasim Ullah, Irfan Sami, Abdulrahman Jamal Babqi, Hend I Alkhammash, Youcef Belkhier, Ahmed Althobaiti, and Asier Ibeas. Processor in the loop verification of fault tolerant control for a three phase inverter in grid connected pv system. *Energy Sources, Part A: Recovery, Utilization, and Environmental Effects*, pages 1–17, 2021.

[146] Px4 autopilots support from uav toolbox - matlab:https://www.mathworks.com/hardware-support/px4-autopilots.html.

[147] Pixhawk overview — copter documentation:https://ardupilot.org/copter/docs/common-pixhawk-overview.html.

[148] Quan Quan. *Modeling and Evaluation of Propulsion System*, pages 73–95. Springer Singapore, Singapore, 2017.

[149] Hamid Hassani, Anass Mansouri, and Ali Ahaitouf. Backstepping-based supertwisting sliding mode attitude control for a quadrotor aircraft subjected to wind disturbances: experimental validation. *International Journal of Dynamics and Control*, pages 1–12, 2022.

[150] Tong Li, Xudong Liu, and Haisheng Yu. Backstepping nonsingular terminal sliding mode control for pmsm with finite-time disturbance observer. *IEEE Access*, 9:135496–135507, 2021.